PB84-158856

# Volatilization of Organic Pollutants in Wastewater Treatment: Model Studies

Stanford Univ., CA

Prepared for

Municipal Environmental Research Lab.
Cincinnati, OH

Feb 84

U.S. Department of Commerce
National Technical Information Service
NTIS

## TECHNICAL REPORT DATA

*(Please read Instructions on the reverse before completing)*

| | | |
|---|---|---|
| 1. REPORT NO.<br>EPA-600/2-84-047 | 2. | 3. RECIPIENT'S ACCESSION NO.<br>PB84 158856 |

| | |
|---|---|
| 4. TITLE AND SUBTITLE<br>Volatilization of Organic Pollutants in Wastewater Treatment--Model Studies | 5. REPORT DATE<br>February 1984<br>6. PERFORMING ORGANIZATION CODE |
| 7. AUTHOR(S)<br>Paul V. Roberts<br>Christoph Munz<br>Paul Dändliker<br>Christine Matter-Müller | 8. PERFORMING ORGANIZATION REPORT NO. |
| 9. PERFORMING ORGANIZATION NAME AND ADDRESS<br>Department of Civil Engineering<br>Stanford University<br>Stanford, California 94305 | 10. PROGRAM ELEMENT NO.<br>11. CONTRACT/GRANT NO.<br>R-806631 |
| 12. SPONSORING AGENCY NAME AND ADDRESS<br>Municipal Environmental Research Laboratory-Cin.,OH<br>Office of Research and Development<br>U. S. Environmental Protection Agency<br>Cincinnati, Ohio 45268 | 13. TYPE OF REPORT AND PERIOD COVERED<br>14. SPONSORING AGENCY CODE<br>EPA/600/14 |

15. SUPPLEMENTARY NOTES
Project Officer: H. Paul Warner 513 684 2621

16. ABSTRACT

Methods are presented for simulating the transfer of volatile organic contaminants to the atmosphere during surface and bubble aeration. Suitable values of the input parameters for conditions representative of activated sludge treatment are suggested, and model calculations are presented. The effects of important variables such as oxygen transfer requirement, the solute's Henry coefficient, and the oxygen transfer efficiency are illustrated by the calculations. Transfer of volatile organics to the atmosphere is to predicted to be substantially greater in surface aeration than in bubble aeration for a given oxygen transfer rate under conditions of practical interest. This difference is attributed to greater saturation of the gas phase in bubble aeration, compared to surface aeration. The transfer of organic solutes to the atmosphere in bubble aeration decreases with increasing oxygen transfer efficiency, if the oxygen transfer requirement is held constant, as a consequence of the concomitant decrease in the required air flow rate.

17. KEY WORDS AND DOCUMENT ANALYSIS

| a. DESCRIPTORS | b. IDENTIFIERS/OPEN ENDED TERMS | c. COSATI Field/Group |
|---|---|---|
| Aeration, Atmosphere, Organics, Oxygen Prediction, Transfer, Volatilization, Wastewater | Activated Sludge | |

| | | |
|---|---|---|
| 18. DISTRIBUTION STATEMENT<br>Release to Public | 19. SECURITY CLASS *(This Report)*<br>Unclassified | 21. NO. OF PAGES<br>172 |
| | 20. SECURITY CLASS *(This page)*<br>Unclassified | 22. PRICE |

EPA Form 2220-1 (Rev. 4-77) PREVIOUS EDITION IS OBSOLETE

EPA-600/2-84-047
February 1984

PB84-158856

# VOLATILIZATION OF ORGANIC POLLUTANTS IN WASTEWATER TREATMENT--MODEL STUDIES

by

Paul V. Roberts, Christoph Munz
Paul Dändliker, Christine Matter-Müller
Stanford University
Stanford, California 94305

Cooperative Agreement #EPA-R-806631

Project Officer

H. Paul Warner
Wastewater Research Division
Municipal Environmental Research Laboratory
U.S. Environmental Protection Agency
Cincinnati, Ohio 45268

MUNICIPAL ENVIRONMENTAL RESEARCH LABORATORY
OFFICE OF RESEARCH AND DEVELOPMENT
U.S. ENVIRONMENTAL PROTECTION AGENCY
CINCINNATI, OHIO 45268

REPRODUCED BY
NATIONAL TECHNICAL
INFORMATION SERVICE
U.S. DEPARTMENT OF COMMERCE
SPRINGFIELD, VA. 22161

# DISCLAIMER

The information in this document has been funded wholly or in part by the United States Environmental Protection Agency under assistance agreement number R-806631 to Stanford University. It has been subject to the Agency's peer and administrative review, and it has been approved for publication as an EPA document. Mention of trade names or commercial products does not constitute endorsement or recommendation for use.

# FOREWORD

The U.S. Environmental Protection Agency was created because of increasing public and government concern about the dangers of pollution to the health and welfare of the American people. Noxious air, foul water, and spoiled land are tragic testimonies to the deterioration of our natural environment. The complexity of that environment and the interplay of its components require a concentrated and integrated attack on the problem.

Research and development is that necessary first step in problem solution, and it involves defining the problem, measuring its impact, and searching for solutions. The Municipal Environmental Research Laboratory develops new and improved technology and systems to prevent, treat, and manage wastewater and solid and hazardous waste pollutant discharges from municipal and community sources, to preserve and treat public drinking water supplies, and to minimize the adverse economic, social, health, and aesthetic effects of pollution. This publication is one of the products of that research and is a most vital communication link between the researcher and the user community.

This report explains and demonstrates the principles governing the transfer of volatile, hazardous organic solutes to the atmosphere during aerobic treatment as practiced in publicly owned treatment works. The goal is to demonstrate that such transfer of organic pollutants can be appreciable wherever air-water contact is practiced to enhance oxygen transfer, and to describe a methodology for predicting its extent if the oxygen transfer rate is known.

Francis T. Mayo
Director
Municipal Environmental Research
Laboratory

# ABSTRACT

Research was undertaken to improve understanding of the factors governing the transfer of volatile organic contaminants from water to air during wastewater treatment. The work focused on surface and bubble aeration, the two types of air-water contacting most widely used in publicly owned treatment works to achieve oxygen transfer.

The basic hypothesis of this work is that the transfer rate of organic compounds is controlled by the liquid-phase resistance if the compounds are sufficiently volatile, and that the gas-phase resistance can be neglected. Hence the factors governing the mass transfer rate are the liquid-phase mass transfer coefficient, the specific interfacial contact area, and the Henry coefficient (i.e., the gas-liquid partition coefficient). A corollary of the basic hypothesis is that the mass transfer rates of volatile compounds vary proportionally with changes in mixing conditions. In particular, the transfer rates of volatile organic compounds should be proportional to that of oxygen.

The basic hypothesis described above was tested by conducting model experiments to simulate surface and bubble aeration. The rates of transfer of oxygen and six organic compounds--dichlorodifluoromethane ($CCl_2F_2$), chloroform ($CHCl_3$), 1,1,1-trichloroethane ($CH_3CCl_3$), carbon tetrachloride ($CCl_4$), trichloroethylene ($CHCl{=}CCl_2$), and tetrachloroethylene ($CCl_2{=}CCl_2$). These compounds differ over a range of three orders of magnitude of the Henry coefficient.

The model experiments demonstrated that the mass transfer rate of volatile organic compounds indeed depends only on the liquid-phase mass transfer constant under surface aeration conditions. Moreover, the mass transfer rate constants for all six volatile compounds were approximately equal to 60% of the oxygen-transfer rate constant over a wide range of energy inputs (0.76 to 350 $W/m^3$). The mass transfer rate constants were proportional to the energy input in the fully turbulent region ($Re > 10^4$).

Analysis of mass transfer from the aqueous phase to a gas phase during bubble aeration is complicated by the saturation of the gas bubbles as they rise upward through the liquid column. In this work, air bubbles of approximately 1 mm diameter contacted the aqueous phase while rising through a water column 35 to 60 cm deep. Under those conditions, gas phase saturation was negligible only for $O_2$ and $CCl_2F_2$ among the compounds studied; the gas phase was saturated substantially for the other five organic compounds. A mathematical model is proposed that permits estimation of (1) the mass transfer rate constant $K_La$ when gas-phase saturation is negligible, (2) the Henry coefficient $H_c$ when gas-phase saturation is complete, and (3) either $K_L$ or $H_c$ (if the other is known *a priori*) in the intermediate range of gas-phase saturation. The value of $K_La$ for $CCl_2F_2$ in bubble aeration was approximately 60% that of oxygen, which agrees with the surface-aeration result. The Henry coefficient determined with the bubble column experiments generally agreed in order of magnitude with those predicted from vapor pressure and solubility data, but deviations as large as a factor of three were observed.

This report was submitted in fulfillment of Cooperative Agreement No. R-806631 by Stanford University under the sponsorship of the U.S. Environmental Protection Agency. This report covers the period September 1, 1979 to January 31, 1982, and work was completed as of January 31, 1982.

# CONTENTS

Foreword . . . . . . . . . . iii
Abstract . . . . . . . . . . iv
Figures . . . . . . . . . . ix
Tables . . . . . . . . . . xi
Abbreviations and Symbols . . . . . . . . . . xii

1. Introduction . . . . . . . . . . 1
2. Conclusions . . . . . . . . . . 3
3. Recommendations . . . . . . . . . . 6
4. Theory . . . . . . . . . . 7
    - Vapor liquid equilibria for dilute solutions . . . . . . . . . 7
    - Models of mass transfer . . . . . . . . . . 12
    - Diffusion coefficients . . . . . . . . . . 20
    - Relation of mass transfer coefficient to diffusion coefficient . . . . . . . . . . 22
    - Mixing in a surface-aeration contactor . . . . . . . . . . 23
    - Mass transfer in a bubble column . . . . . . . . . . 25
5. Experimental Methods . . . . . . . . . . 43
    - Surface-aeration experiments . . . . . . . . . . 43
    - Bubble-column experiments . . . . . . . . . . 47
    - Vapor liquid equilibrium (VLE) measurements . . . . . . . . . . 52
    - Preparation of water . . . . . . . . . . 52
    - Analytical procedures . . . . . . . . . . 54
    - Power measurements . . . . . . . . . . 57
6. Results of Surface-Aeration Experiments . . . . . . . . . . 58
    - Data evaluation . . . . . . . . . . 58
    - Values of the mass transfer coefficient ratio $\Psi$ from preliminary experiments . . . . . . . . . . 61
    - Statistical analyses of preliminary data . . . . . . . . . . 67
    - Design of the main series of experiments . . . . . . . . . . 68
    - Results of main set of experiments . . . . . . . . . . 69
7. Results of Bubble-Column and Equilibrium Experiments . . . . . . . . 75
    - Data analysis . . . . . . . . . . 75
    - Experiments varying the ratio $Q_G/V_L$ . . . . . . . . . . 83
    - Influence of methanol on $H_{ci}$ and $\Psi_{CCl_2F_2}$ . . . . . . . . . . 88
    - Closed-system vapor-liquid equilibrium experiments . . . . . . 89
    - Filtered secondary effluent . . . . . . . . . . 90
    - Summary of observed Henry coefficients . . . . . . . . . . 91
    - Bubble characteristics and flow regime . . . . . . . . . . 92
8. Discussion . . . . . . . . . . 97
    - Surface-aeration experiments . . . . . . . . . . 97
    - Bubble-column experiments . . . . . . . . . . 111

9. Engineering Application . . . . . . . . . . . . . . . . . . . . . . 125
  Surface aeration in activated sludge treatment--example . . . 125
  Bubble aeration--examples . . . . . . . . . . . . . . . . . . 128

References . . . . . . . . . . . . . . . . . . . . . . . . . . . . . 132

Appendices

A. Properties of solutes studied . . . . . . . . . . . . . . . . . . 139
B. Power measurement . . . . . . . . . . . . . . . . . . . . . . . . 142
  Procedure . . . . . . . . . . . . . . . . . . . . . . . . . . 142
  Results . . . . . . . . . . . . . . . . . . . . . . . . . . . 143
  Calculation of oxygen-transfer:energy ratio . . . . . . . . . 145
C. Results of main set of surface-aeration experiments . . . . . . . 146
D. Results of bubble-column experiments . . . . . . . . . . . . . . 147
E. Activated sludge examples . . . . . . . . . . . . . . . . . . . . 148
  General approach . . . . . . . . . . . . . . . . . . . . . . . 148
  Bubble-aeration calculations . . . . . . . . . . . . . . . . . 151

## FIGURES

Number / Page

1 Concentration profiles according to the two-film model . . . . . 13

2 Distribution of turbulent eddies in the surface layer according to the penetration and surface-renewal theories . . . . . . . . . 17

3 Mean transfer rates as a function of time of exposure . . . . . . 19

4 Power curve for standard tank configuration . . . . . . . . . . . . 25

5 Gas-phase mass balance for bubble column . . . . . . . . . . . . . 29

6 Shape regimes for bubbles and drops in unhindered gravitational motion through liquids . . . . . . . . . . . . . . 35

7 Terminal velocity of air bubbles in water at 20°C . . . . . . . . . 36

8 Transition from "large" bubble to "small" bubble mass transfer coefficients . . . . . . . . . . . . . . . . . . . . . . . . . 37

9 Correlation of heat and mass transfer coefficients for dispersions of bubbles and spheres . . . . . . . . . . . . . . . 42

10 Surface-aeration contactor used in preliminary experiments . . . 44

11 Modified surface-aeration contactor . . . . . . . . . . . . . . . . 45

12 Schematic diagram of bubble column and appurtenances . . . . . . 48

13 Bubble column . . . . . . . . . . . . . . . . . . . . . . . . . . . 49

14 Milli-Q water system . . . . . . . . . . . . . . . . . . . . . . . . 53

15 Filtration unit . . . . . . . . . . . . . . . . . . . . . . . . . . 53

16 Calibration of oxygen probe . . . . . . . . . . . . . . . . . . . . 54

17 Sample data plot for stripping of an organic solute during surface aeration . . . . . . . . . . . . . . . . . . . . . . . 59

18 $\Psi$-values for Freon-12 from preliminary surface-aeration experiments . . . . . . . . . . . . . . . . . . . . . . . . . . . 62

Number Page

19 Ψ-values for chloroform from preliminary surface-aeration experiments . . . . . . . . . . . . . . . . . . . . . . . . . . 63

20 Ψ-values for 1,1,1-trichloroethane from preliminary surface-aeration experiments . . . . . . . . . . . . . . . . . . 63

21 Ψ-values for carbon tetrachloride from preliminary surface-aeration experiments . . . . . . . . . . . . . . . . . . 64

22 Ψ-values for trichloroethylene from preliminary surface-aeration experiments . . . . . . . . . . . . . . . . . . 64

23 Ψ-values for tetrachloroethylene from preliminary surface-aeration experiments . . . . . . . . . . . . . . . . . . 65

24 Average values of Ψ with 95% confidence interval measured in preliminary surface-aeration experiments . . . . . . . . . . 67

25 Comparison of values of Ψ for Milli-Q and PASE . . . . . . . . . . 70

26 Relation between Ψ for Freon and the oxygen mass transfer coefficient . . . . . . . . . . . . . . . . . . . . . . . . . . 72

27 Relation between Ψ for chloroform and the oxygen mass transfer coefficient . . . . . . . . . . . . . . . . . . . . . 72

28 Relation between Ψ for trichloroethane and the oxygen mass transfer coefficient . . . . . . . . . . . . . . . . . . . 73

29 Relation between Ψ for carbon tetrachloride and the oxygen mass transfer coefficient . . . . . . . . . . . . . . . . . . . 73

30 Relation between Ψ for trichloroethylene and the oxygen mass transfer coefficient . . . . . . . . . . . . . . . . . . . 74

31 Relation between Ψ for tetrachloroethylene and the oxygen mass transfer coefficient . . . . . . . . . . . . . . . . . . . 74

32 Linear regression of bubble-column stripping data . . . . . . . . . 77

33 Non-linear regression of bubble-column stripping data . . . . . . 77

34 Residual plot of linear regression . . . . . . . . . . . . . . . 79

35 Residual plot of non-linear regression . . . . . . . . . . . . . . 80

36 Change in gas-phase concentration with submergence at different hydrodynamic conditions . . . . . . . . . . . . . . . . 80

37 Regression of $H_{c,CHCl_3}$ versus $K_{L,O_2}a$ from bubble-column data . . 85

Number Page

38 Regression of $H_{c,CH_3CCl_3}$ versus $K_{L,O_2}a$ from bubble-column data . 85

39 Regression of $H_{c,CCl_4}$ versus $K_{L,O_2}a$ from bubble-column data . . . 86

40 Regression of $H_{c,CHCl=CCl_2}$ versus $K_{L,O_2}a$ from bubble-column data 86

41 Regression of $H_{c,CCl_2=CCl_2}$ versus $K_{L,O_2}a$ from bubble-column data 87

42 Regression of $\Psi_{CCl_2F_2}$ versus $K_{L,O_2}a$ from bubble-column data . . 87

43 Average values of $H_{c,i}$ and $\Psi_{CCl_2F_2}$ obtained in bubble-column experiments with variable methanol concentration . . . . . . . 88

44 Rising bubble swarm at a gas flow rate of 0.47 ℓ/min . . . . . . 93

45 Rising bubble swarm at a gas flow rate of 1.2 ℓ/min . . . . . . . . 94

46 Rising bubble swarm at a gas flow rate of 2.3 ℓ/min . . . . . . . . 95

47 Power curve for impeller used in the main set of surface-aeration experiments . . . . . . . . . . . . . . . . . . 100

48 Effect of impeller speed on power input . . . . . . . . . . . . . 101

49 Effect of impeller speed on the oxygen mass transfer rate constants . . . . . . . . . . . . . . . . . . . . . . . . 101

50 Dependence of $K_{L,O_2}a$ $[s^{-1}]$ on power input [W] to surface aerator . . . . . . . . . . . . . . . . . . . . . . . . . . . 102

51 Summary of regressions of $\Psi$ vs $K_{L,O_2}a$ from surface-aeration experiments . . . . . . . . . . . . . . . . . . . . . . . . . 104

52 Comparison of mass transfer models for describing the relation between $\Psi$-values and diffusion coefficients . . . . . 106

53 Removal of organic compounds by volatilization in standard cases of bubble aeration and surface aeration . . . . . . . . . . 130

# TABLES

| Number | | Page |
|---|---|---|
| 1 | Order of Preliminary Surface-Aeration Experiments . . . . . . . . . | 45 |
| 2 | Order of Main Series of Surface-Aeration Experiments . . . . . . | 46 |
| 3 | Order of Bubble-Column Experiments with Differing Initial Liquid Volumes and Gas Flow Rates . . . . . . . . . . . . . . . | 50 |
| 4 | Order of Bubble-Column Experiments with Differing Methanol Concentration . . . . . . . . . . . . . . . . . . . . . . . . . | 51 |
| 5 | Water Characteristics . . . . . . . . . . . . . . . . . . . . . . . | 53 |
| 6 | Oxygen Mass Transfer Rate Constants Measured at Top and Bottom of Bubble Column and with DO-Probe and Winkler Titration . . . | 55 |
| 7 | Response Factors for VOA Analysis . . . . . . . . . . . . . . . . | 56 |
| 8 | Response Factors for Chlorinated Benzene Analysis . . . . . . . . . | 57 |
| 9 | Sample of MINITAB Output . . . . . . . . . . . . . . . . . . . . | 60 |
| 10 | Average of All Values of $\Psi$ Measured in Surface-Aeration Experiments . . . . . . . . . . . . . . . . . . . . . . . . . | 61 |
| 11 | Average Values of $\Psi$ Measured at 190 rpm . . . . . . . . . . . . . . | 62 |
| 12 | Overall Average Values of $\Psi$ in Milli-Q Water at 20°C . . . . . . | 62 |
| 13 | Mass Transfer Rate Constant for Oxygen at 230 rpm . . . . . . . . . | 65 |
| 14 | Results of Surface-Aeration Experiments with Chlorinated Benzenes at 190 RPM . . . . . . . . . . . . . . . . . . . . . . | 66 |
| 15 | Regression of $\Psi$ vs $K_{L,O_2}a$ for Milli-Q Water at 20°C . . . . . . . | 68 |
| 16 | Average Values of $\Psi$ from the Main Series of Surface-Aeration Experiments . . . . . . . . . . . . . . . . . . . . . . . . . | 69 |
| 17 | Values of $K_La$ and $\alpha$ for PASE at 172 rpm and 281 rpm . . . . . . . | 71 |
| 18 | Regression of $\Psi$ vs $K_{L,O_2}a$ . . . . . . . . . . . . . . . . . . . . . | 71 |

| Number | | Page |
|---|---|---|
| 19 | Experimental Gas-Phase Saturation Values, $\Phi Z_s$ | 79 |
| 20 | Average Values of $H_{c,i}$ and $\Psi_i$ from Bubble-Column Experiments | 84 |
| 21 | Regression Equations of $H_{c,i}$ and $\Psi_i$ versus $K_{L,O_2}a$ for Bubble-Column Experiments | 84 |
| 22 | Average Values of $H_c$ and $\Psi$ from Bubble-Column Experiments with Variable Methanol Concentration | 89 |
| 23 | Results of Bubble-Column Experiments with Methanol Addition at Midpoint | 89 |
| 24 | Average Values of $H_{c,i}$ from Closed-System VLE Experiments | 90 |
| 25 | Results of Bubble-Column Experiments Comparing Milli-Q and PASE | 91 |
| 26 | Experimental and Previously Reported Values of $H_c$ | 91 |
| 27 | Bubble Diameters | 96 |
| 28 | Ratio of Mass Transfer Rate Coefficients and Diffusivities | 106 |
| 29 | Estimated Values of $\Omega$ | 107 |
| 30 | Values of $\alpha$ Inferred from Surface-Aeration Experiments | 109 |
| 31 | Recommended Values of $\Psi$ for Wastewater Engineering Purposes | 110 |
| 32 | Estimated Values of the Specific Interfacial Area | 119 |
| 33 | Predicted and Measured $K_{L,O_2}a$-Values | 121 |
| 34 | Fractional Removal and Fractional Bubble Saturation in the Standard Case of Fine-Bubble Aeration | 129 |
| 35 | Fractional Removal and Fractional Bubble Saturation in the Standard Case of Coarse-Bubble Aeration | 129 |

## ABBREVIATIONS AND SYMBOLS

### ABBREVIATIONS

| | |
|---|---|
| Eo | Eotvos number = $(g \cdot \Delta\rho \cdot d^2 \cdot \sigma^{-1})$ [dimensionless] |
| Fr | Froude number = $(\mu \cdot g^{-1/2} \cdot d^{-1/2})$ [dimensionless] |
| int | interface |
| Mo | Morton number = $(g \cdot \mu^4 \cdot \Delta\rho \cdot \rho^{-2} \cdot \sigma^{-3})$ [dimensionless] |
| Pe | Peclet number = Re•Sc [dimensionless] |
| Po | power number = $P \cdot \rho^{-1} \cdot N^{-3} \cdot D^{-5}$ |
| Re | Reynolds number = $(ud/\nu)$ [dimensionless] |
| Sc | Schmidt number = $(\nu/D)$ [dimensionless] |
| Sh | Sherwood number = $(kd/D)$ [dimensionless] |

### SYMBOLS

| | |
|---|---|
| A | interfacial area [$m^2$] |
| $\underset{\wedge}{a}$ | specific interfacial area [$m^2/m^3$] |
| a | activity of solute |
| B | coefficient in Margules expression |
| C | mass concentration [$g \cdot m^3$] |
| c | constant |
| D | diffusion coefficient [$m^2 \cdot s^{-1}$] |
| d | distance or diameter [m] |
| e | base of natural logarithms |
| f | fugacity |
| G | Gibbs free energy |
| H | Henry coefficient [$atm \cdot mol^{-1} \cdot m^3$] |
| $H_c$ | Henry coefficient [$g \cdot m^{-3}/g \cdot m^{-3}$] |
| $K_G$ | overall mass transfer coefficient based on gas phase [m/s] |
| $K_L$ | overall mass transfer coefficient based on liquid phase [m/s] |
| $k_G$ | individual mass transfer coefficient for gas phase [m/s] |
| $k_L$ | individual mass transfer coefficient for liquid phase [m/s] |
| $K_Ga$ | overall mass transfer rate constant based on gas phase [$s^{-1}$] |
| $K_La$ | overall mass transfer rate constant based on liquid phase [$s^{-1}$] |
| $\underline{k}$ | Boltzmann's constant |
| M | molecular weight [amu] |
| m | mass [g] |
| n | number of moles; or index in series |
| N | rotational speed [$s^{-1}$] or [rpm] |
| P | power [watt] |
| p | partial pressure [atm] |
| P' | vapor pressure [atm] |
| R | universal gas constant = $8.2 \times 10^{-5}$ [$atm \cdot m^3 \cdot mol^{-1} \cdot K^{-1}$] |
| r | radius [m] |
| S | slope [dimensionless] |
| s | standard deviation, fractional rate of surface renewal, or sec. |
| t | time [s], or t-statistic [dimensionless] only in Table 18 |
| T | absolute temperature [K] |
| u | velocity [m/s] |
| V | volume [$m^3$] |
| x | mol fraction in liquid phase [dimensionless] |
| $V_A$ | molal volume of solute at its normal boiling point [$cm^3/mol$] |
| $V_c$ | critical volume [$cm^3/mol$] |
| y | mol fraction in gas phase [dimensionless] |
| Z | submergence depth [m] |

## GREEK SYMBOLS

| | |
|---|---|
| $\alpha$ | ratio of mass transfer rate constants, between contaminated and clean water |
| $\Psi$ | ratio of mass-transfer coefficients [dimensionless] |
| $\gamma$ | activity coefficient [dimensionless] |
| $\delta$ | film thickness [m] |
| $\varepsilon$ | exponent for dependence of diffusivity on critical volume [dimensionless] |
| $\varepsilon_b$ | volume fraction occupied by bubble phase [dimensionless] |
| $\mu$ | viscosity [$kg\cdot m^{-1}\cdot s^{-1}$] |
| $\nu$ | kinematic viscosity [$m^2/s$] |
| $\varphi$ | surface age distribution function (surface-renewal theory), or association parameter for estimating diffusion coefficients |
| $\rho$ | density [$g/m^3$] |
| $\sigma$ | surface tension [$kg/s^2$] |
| $\tau$ | torque [$kg\cdot m^2\cdot s^{-2}$] or [inch•ounces] |
| $\tau_b$ | average bubble residence time [s] |
| $\omega$ | exponent for dependence of $k_L$ on $D_L$ |
| $\Omega_d$ | diffusion collision integral |
| $\xi$ | viscosity ratio |

## Subscripts

| | |
|---|---|
| A | solute |
| a | agitator or impeller |
| av | average |
| B | solvent |
| b | bubble |
| c | concentration |
| E | effluent |
| G | gas phase |
| I | influent |
| i | component i |
| L | liquid phase |
| o | initial condition |
| s | total submersion depth |
| w | water |

## Superscripts

| | |
|---|---|
| E | excess free energy |
| s | solubility limit |
| o | infinite dilution |
| * | equilibrium |
| ' | standard state, or pure solute |

# SECTION 1

# INTRODUCTION

Current estimates show that more than 50,000 chemicals are used in commerce (1), and an additional 500 to 1000 new compounds are introduced every year (2). Most of them are petroleum derivatives. The toxicological and ecological effects of these compounds are difficult to quantify. Many of these substances are persistent--that is, they are virtually nonbiodegradable. Some substances such as chlorinated hydrocarbons are of particular concern because they tend to accumulate in the environment, owing to their lipophilicity. Moreover, many of them are suspected carcinogens, mutagens, and/or teratogens (3). These compounds find their way into the environment through industrial wastewater discharges, accidental spills, dumpsites leaking into ground water aquifers, and municipal wastewater effluents.

Controlling organic priority pollutants recently has emerged as an important objective of water pollution control and water supply. The U.S. Environmental Protection Agency (4) has formulated a list of more than 300 compounds of hazardous chemicals discovered in drinking water. Many of these compounds are suspected carcinogens. Various alternatives for removing them from the water should therefore be considered.

One method of removing an important class of organic pollutants is by transfer to the atmosphere (volatilization). This seems promising for volatile compounds such as chloroform and other trihalomethanes, carbon tetrachloride, and trichloroethylene. Some of these compounds are difficult to remove by other methods such as biodegradation, adsorption, and reverse osmosis. Hence volatilization may be cost-effective in controlling particular pollutants.

The objective of the work reported here was to investigate the mass transfer behavior of volatile compounds. The choice of pollutants treated in this research was made on the basis of their volatility, as represented by the Henry coefficient. Compounds with Henry coefficients exceeding $10^{-3}$ $[\mathrm{atm \cdot m^3 \cdot mol^{-1}}]$ were taken into consideration. The ten compounds chosen represent a region of Henry coefficients from 1.5 $[\mathrm{atm \cdot m^3 \cdot mol^{-1}}]$ to $1.5 \times 10^{-3}$ $[\mathrm{atm \cdot m^3 \cdot mol^{-1}}]$, as shown in Appendix A.

Mass transfer coefficients were determined in a bench-scale reactor, simulating surface aeration in the activated sludge process. The mass transfer rate constants of the organic compounds are compared with that of oxygen. The underlying hypothesis is that the transfer rates of these volatile organic pollutants can be related directly to a more easily measurable quantity--namely, oxygen transfer. Such a methodology would be useful for estimating pollutant removals by volatilization not only in surface aeration during waste treatment, but also in natural streams, provided that the oxygen transfer rate is known.

In a bubble column contactor, both mass transfer and phase equilibria can be studied. The bubble column contactor was used in this study to determine mass transfer rate constants for highly volatile compounds and Henry coefficients for less volatile compounds; it was also used to simulate submerged aeration as used in publicly owned treatment works.

## SECTION 2

## CONCLUSIONS

Mass transfer rates for oxygen and highly volatile organic compounds were measured in a bench-scale surface aerator. With these data, a ratio of mass transfer coefficients defined as $\Psi = K_{L,i}\,a/K_{L,O_2}a$ was determined for a wide range of hydraulic conditions. In addition, the behavior of $\Psi$ was investigated for filtered secondary effluent. The following conclusions were drawn:

1. With increasing turbulence, the mass transfer rates for oxygen and for the organic compounds behave quite similarly. The rates for organic compounds increase slightly faster than those for oxygen and therefore the $\Psi$-value increases slightly with increasing turbulence. In the measured range of mixing intensity, the increase is less than 10%. Thus an average $\Psi$-value is applicable for engineering purposes.

2. In filtered secondary effluent, the rate of mass transfer is slightly lower than in clean water. The constituents in the wastewater inhibit the transfer of oxygen slightly more strongly than that of the organic compounds; but the differences are not significant. All the organic compounds were influenced to the same degree. Hence for engineering calculations it appears justified to use values of the $\Psi$ ratio obtained in experiments conducted with clean water.

3. The mass transfer data indicate that the transfer rate constant $K_La$ depends on the solute's diffusivity to the $^2/_3$-power. This agrees with the predictions of the boundary-layer and film-penetration theories, but differs significantly from the simple film theory.

4. Changing temperature affects the mass transfer coefficients of the organic solutes in the same manner as that of oxygen.

5. In the fully turbulent region, the oxygen mass transfer coefficient is proportional to the power input.

Stripping rates of highly volatile organic compounds and the absorption rate of oxygen were measured simultaneously in a bubble column, representative of subsurface (diffused) aeration. From these measurements and depending on the compound's volatility, either the Henry coefficients (i.e., air-water partition coefficient) or the ratio of mass transfer rate constants (defined as $\Psi = K_{L,i}a/K_{L,O_2}a$) was determined. Theoretical considerations indicate that for gas-liquid dispersions, the boundary-layer modification of the two-film theory predicts a dependence of the mass transfer coefficient, $k_L$, on the diffusion coefficient raised to the power of $1/2$ to $2/3$, depending on the degree of internal circulation of the bubbles or purity of the system. This narrows considerably the differences between the simple two-film theory (which predicts a first-power dependence) and the penetration or surface-renewal theories (which predict a square-root dependence of mass transfer coefficients on diffusion coefficients). Based on the results of the bubble-column experiments, the following conclusions were drawn:

1. The value of $\Psi$ increases with increasing turbulence as predicted by theory. Since $\Psi$-values could be estimated only for one compound ($CCl_2F_2$), no final conclusion can be made regarding the validity of the theory described above. For this compound, the exponent of the diffusion coefficient ratio was found to range between $0.67 \leq \Omega \leq 0.91$, thus approaching the prediction of the two-film theory (i.e., $k_L \propto D_L$). But the discrepancy could be due to the error in estimating diffusion coefficients.

2. The observed air bubble sizes and shapes were in accordance with published empirical correlations. The observed oxygen mass transfer coefficient agreed approximately with predictions based on published, generalized correlations.

3. For the other five compounds studied ($CHCl_3$, $CH_3CCl_3$, $CCl_4$, $CHCl{=}CCl_2$ and $CCl_2{=}CCl_2$), Henry coefficients ($H_c$) were estimated. Unexpectedly, values of $H_c$ depended inversely on the turbulence as measured by the oxygen mass transfer coefficient. No reasonable explanation was found to account for this behavior. However, the variability was slight--less than ± 10% of the average value for all five compounds. Hence the average values found (with relatively small standard deviations) are useful in view of the large variability of Henry coefficients found in the literature predicted from solubility and vapor pressure data.

4. The Henry coefficients measured in filtered secondary effluent were 5 to 30% greater than in purified water. This difference was significant for six of seven organic compounds observed.

5. The presence of methanol (used to dissolve the organic solutes in water) does not influence the measurement of Henry coefficients and $\Psi$-values when used at low concentrations ($x \leq 10^{-3}$). This fact was shown both theoretically and experimentally.

For a typical case of activated sludge treatment, example calculations based on the mass transfer models developed in this work show that the fractional removal of organic contaminants by volatilization is likely to be greater with surface aeration than with bubble aeration. The removal by volatilization is more strongly dependent on the Henry coefficient of the solute in the case of bubble aeration than in surface aeration. The calculations also indicate that, for a given oxygen transfer rate (mass/time), the removal of organics by volatilization is greater for a case of low oxygen transfer efficiency (coarse bubbles) than for one of high oxygen transfer efficiency (fine bubbles). All of these phenomena are explained by the relative importance of gas-phase saturation in bubble aeration compared with its unimportance in surface aeration.

# SECTION 3

# RECOMMENDATIONS

The work reported here represents only a beginning of the quest to understand the factors that determine the volatilization rates of organic compounds in treatment and natural environments. The analogy to oxygen mass transfer works satisfactorily as a first approximation, but there are noticeable deviations.

More research is needed to understand what governs mass transfer in a liquid-gas-phase system. This suggests that further laboratory experiments should be undertaken under extremely well controlled conditions. Probably a wetted-wall column would better assure a well defined flow pattern than does the kind of surface aerator used in the present work. Possible influences of the flow regime could be better accounted for.

Further laboratory-scale experiments with surface aerators should characterize more rigorously the flow patterns, as well as the scale and the intensity of turbulence. Continuous power measurements during the experimental runs and widening the hydraulic range from laminar to turbulent might give more insight into the importance of hydraulic conditions. Additional laboratory studies are necessary to determine the influence of surfactants, ionic strength, and suspended solids on the rates of mass transfer. Improved understanding of those effects might lead to better insight into the mechanisms of mass transfer.

Additional mass transfer studies with bubble columns are necessary for several purposes. The $\Psi$ values have to be measured for additional compounds to prove the validity of the theory proposed in this report and to allow generalizations for diverse compounds. Additional experiments are necessary to confirm the apparent dependence of the Henry coefficient on turbulence and to explain this behavior. Also, similar studies should be conducted with natural and contaminated waters (rivers, lakes, sea, wastewater, leachates) quantifying the influence of several parameters such as suspended solids, ionic strength, etc. to make the results more representative and applicable to environmental conditions.

All results should be verified in large-scale field studies to investigate possible difficulties in scale-up.

# SECTION 4

# THEORY

## VAPOR-LIQUID EQUILIBRIA FOR DILUTE SOLUTIONS

To derive a useful model for mass transfer, the relation between the compositions of the gas and liquid phases at equilibrium should be known. For dilute solutions, Henry's law is the most convenient way to relate the equilibrium between these two phases. Henry's law states that, at low concentrations, the phase equilibrium can be represented by a linear relationship. This can be confirmed by considering the principle of phase equilibria as follows.

### Binary Solutions

A component i is in equilibrium between two phases when the fugacities $\hat{f}$ of the component in the phases are equal

$$\hat{f}_i^{L} = \hat{f}_i^{G} \tag{1}$$

where $\hat{f}_i^{L}$ = fugacity of component i in the liquid phase

$\hat{f}_i^{G}$ = fugacity of component i in the gas phase.

The fugacity is a measure of the escaping tendency of a compound from a phase (5). It is defined in units of pressure, and may be thought of as the partial pressure of the compound in a vapor phase in equilibrium with the phase of interest.

The gas phase normally behaves nearly ideally, because the intermolecular interactions are negligible. In this case, the fugacity of the gas phase can be written as

$$\hat{f}_i^{G} = p_i = y_i P \tag{2}$$

where $p_i$ = partial pressure of component i

$P$ = total pressure

$y_i$ = mole fraction of component i in the gas phase.

For the liquid phase, which seldom behaves ideally, the fugacity is defined by the following relation (6, p. 266):

$$\hat{f}_i^L = x_i \gamma_i f_i' \qquad (3)$$

where $x_i$ = mole fraction of component i in the liquid phase

$\gamma_i$ = activity coefficient

$f_i'$ = fugacity of component i at a given standard state.

Equating (2) and (3) gives

$$p_i = x_i \gamma_i f_i' \qquad (4)$$

The standard state usually is chosen as pure liquid i, and $f_i'$ is a constant equal to the vapor pressure $p_i'$ of pure i. However, $\gamma_i$ is dependent on $x_i$. Therefore, it is important to know how $\gamma_i$ changes with $x_i$.

From thermodynamic principles (6, p. 267) the activity coefficient $\gamma_i$ is defined as

$$\ell n\ \gamma_i = \left[\frac{\partial(nG^E/RT)}{\partial n_i}\right]_{T,p,n_j} \qquad (5)$$

For a binary liquid solution of components that are chemically not too dissimilar, the excess Gibbs free energy is well represented by (6, pp. 48,86,617):

$$\frac{G^E}{RT} = \frac{c}{RT} x_1 x_2 = \frac{c}{RT} \frac{n_1 n_2}{n^2} \qquad (6)$$

where c is a constant independent of x.

Substituting Eq. 6 into Eq. 5 yields

$$\ell n\ \gamma_1 = \frac{\partial}{\partial n_1}\left[\frac{c}{RT} \frac{n_1 n_2}{n}\right] = \frac{c}{RT} n_2\left(\frac{1}{n} - \frac{n_1}{n_2}\right) = \frac{c}{RT} \frac{n_2}{n}\left(1 - \frac{n_1}{n}\right) \qquad (7a)$$

$$\ell n\ \gamma_1 = \frac{c}{RT} x_2(1 - x_1) = \frac{c}{RT} (1 - x_1)^2 \qquad (7b)$$

The solubility limit $x_1^s$ is reached when the slope of the free energy of the mixing curve (i.e., excess free energy plus ideal free energy), (6, p. 266) becomes zero:

$$\frac{\partial \Delta G}{\partial x_1} = \frac{\partial}{\partial x_1}\left[x_1 x_2 c + RT(x_1\ \ell n\ x_1 + x_2\ \ell n\ x_2)\right] = 0$$

$$= (1 - 2x_1) \frac{c}{RT} + \ell n\ x_1 - \ell n(1 - x_1) = 0 \qquad (8)$$

For slightly soluble compounds, $x_1$ must be << 1; hence, Eq. 8 can be approximated by

$$\lim_{x_1 \to 0} \frac{\partial \Delta G}{\partial x_1} = \ln x_i^s + \frac{c}{RT} = 0 \qquad (9a)$$

or

$$\ln x_i^s = - \frac{c}{RT} \qquad (9b)$$

where $x_i^s$ = the solubility limit.

Solving Eq. 9b for c and substituting into Eq. 7b gives

$$\ln \gamma = - (1 - x_1)^2 \ln x_i^s = (1 - x_1)^2 \ln \frac{1}{x_i^s} \qquad (10).$$

For small values of $x_i$ this leads to

$$\gamma_i \simeq \frac{1}{x_i^s} = \text{constant} \qquad (11)$$

Using this result in Eq. 4 we can write

$$p_i = H_i x_i \qquad (12)$$

$$H_i = \gamma_i f_i' = \text{constant}$$

Equation 12 is one form of Henry's law with $H_i$ as the Henry coefficient. Mackay and coworkers (7-9) have shown that H can be calculated as

$$H_i = \frac{p_i'}{x_i^s} \qquad (13)$$

where $p_i'$ = vapor pressure of pure component i

$x_i^s$ = solubility of component i.

This suggests that for dilute solutions ($x_i < 0.01$) Henry's law describes the phase equilibrium within a few percent, and that the value of the Henry coefficient can be estimated from the vapor pressure of the pure solute and its solubility. Depending on the available data, different variations of Henry's law are convenient. For convenience in mass transfer calculations, the Henry coefficient is defined as

$$H_c = \frac{C_G^* \ [\mathrm{g \cdot m^{-3}}]}{C_L \ [\mathrm{g \cdot m^{-3}}]} \qquad (14)$$

where $C_G^*$ is the equilibrium concentration in the gas phase for the liquid concentration, $C_L$.

In the literature the Henry coefficient is often defined as

$$H = \frac{p_i'}{C_L^s} \frac{[\text{atm}]}{[\text{mol} \cdot \text{m}^{-3}]} \tag{15}$$

where $C_L^s$ is the concentration of solute in the liquid phase at its solubility limit. The relation between the two forms of the Henry coefficient, $H_c$ and H, is given by

$$H = H_c \; RT \tag{16}$$

where R = universal gas constant = $8.2 \times 10^{-5}$ $[\text{atm} \cdot \text{m}^3 \cdot \text{mol}^{-1} \cdot \text{K}^{-1}]$

T = temperature [K].

Influence of a Second Solvent on Henry Coefficient (Ternary System)

Often when studying a binary system a third component is introduced because of experimental convenience, e.g. to facilitate dissolution of the solutes of interest in the aqueous phase. When this is done, one has to be sure that the additional component does not influence the binary system. We define the components as follows:

(1): solvent 1 (= $H_2O$)

(2): solute

(3): solvent 3 (= $CH_3OH$)

If each binary system is well represented by a one-parameter Margules expansion (10), we may write

$$\frac{G^E_{12}}{RT} = B_{12} \cdot x_1 \cdot x_2 \tag{17}$$

$$\frac{G^E_{13}}{RT} = B_{13} \cdot x_1 \cdot x_3 \tag{18}$$

$$\frac{G^E_{23}}{RT} = B_{23} \cdot x_2 \cdot x_3 \tag{19}$$

where the $B_{ij}$ are empirical coefficients independent of composition. The molar excess free energy for the ternary system is then assumed to be

$$\frac{G^E_{123}}{RT} = B_{12} \cdot x_1 \cdot x_2 + B_{13} \cdot x_1 \cdot x_3 + B_{23} \cdot x_2 \cdot x_3 \tag{20}$$

If Eq. 20 applies, then the Henry coefficient for the mixture can be expressed as (6,11)

$$\ln H_{2m} = x_1 \cdot \ln H_{21} + x_3 \cdot \ln H_{23} - B_{13} \cdot x_1 \cdot x_3 \qquad (21)$$

where $H_{2m}$ = Henry coefficient of solute 2 in mixed solvent

$H_{21}$ = Henry coefficient of solute 2 in solvent 1

$H_{23}$ = Henry coefficient of solute 2 in solvent 3

In order to use Eq. 21 we need to know $B_{13}$, $H_{21}$, and $H_{23}$. In the previous section we saw that $H_{21}$ may be estimated from the vapor pressure and solubility if the solute is only slightly soluble in solvent 1. We will now assume $x_1 \simeq 1$. More specifically, we assume that components 2 and 3 are infinitely dilute in solvent 1, and component 2 is also infinitely dilute in solvent 3. The implications and need for this assumption will be explained at the end of this section.

Applying Eq. 5 to each binary system we obtain:

system 1-2 $\quad \ln \gamma_1 = B_{12} \cdot x_2^2 \quad \ln \gamma_2 = B_{12} \cdot x_1^2 \quad$ (22a,b)

system 1-3 $\quad \ln \gamma_1 = B_{13} \cdot x_3^2 \quad \ln \gamma_3 = B_{13} \cdot x_1^2 \quad$ (23a,b)

system 2-3 $\quad \ln \gamma_2 = B_{23} \cdot x_3^2 \quad \ln \gamma_3 = B_{23} \cdot x_2^2 \quad$ (24a,b)

The infinite dilution assumption made above allows us to simplify Eqs. 22, 23, and 24:

$$x_2 << 1 \; , \; x_1 \simeq 1 \qquad \ln \gamma_{21}^{o} \simeq B_{12} \qquad (22c)$$

$$x_3 << 1 \; , \; x_1 \simeq 1 \qquad \ln \gamma_{31}^{o} \simeq B_{13} \qquad (23c)$$

$$x_2 << 1 \; , \; x_3 \simeq 1 \qquad \ln \gamma_{23}^{o} \simeq B_{23} \qquad (24c)$$

where $\gamma_{ij}^{o}$ = activity coefficient at infinite dilution of component i in solvent j.

O'Connell and Prausnitz (11) show that

$$B_{23} = B_{12} + \ln \left[\frac{H_{23}}{H_{21}}\right] \qquad (25)$$

based on the relationship between symmetric and unsymmetric activity coefficients. The reference vapor pressures in Eq. 25 differ slightly from those used in the original paper (11), but this has no influence on the outcome.

Next we need to estimate the activity coefficients at infinite dilution in order to calculate the $B_{ij}$, Eqs. 22c, 23c, and 24c. Then, using Eq. 25, we can estimate $H_{23}$, which upon substitution into Eq. 21 will yield $H_{2m}$. For slightly soluble compounds the activity coefficient can be estimated from its solubility, as was shown in the preceding section (Eq. 11). Alternatively, a general correlation such as that proposed by Pierroti et al. (12) can be used. This correlation is not restricted to low solubility compounds, and is based on contributions from individual interactions between pairs of structural groups in the solute and solvent molecules which depend solely on the number, type, and configuration of the groups in the respective structures. However, if available, actual experimental data are preferred over any other estimation method.

It is important to recognize the restrictions to which this section is subject. The analysis presented here applies strictly only to simple, nonpolar solutions (11). For this reason the simple one-term Margules equation, $G^E/RT = B_{ij}x_ix_j$, could be used, implying that a graph of $G^E/RT$ vs $x_i$ is symmetrical with respect to $x_i = 0.5$ because $B_{ij}$ is constant. However, few systems, if any, will behave in this manner. Nevertheless, for an unsymmetrical system a constant $B_{ij}$ independent of composition can be defined, if only a small composition range, say $\Delta x_i < 0.1$, is considered. But if data for binary systems are used to obtain data for ternary systems, as was done here, this composition range has to be the same in the binary systems as in the ternary system. This restriction is only satisfied when the following conditions apply simultaneously:

for the ternary system: $$x_2 \ll 1 \, , \quad x_3 \ll 1 \, , \quad x_1 \approx 1 \tag{26}$$

and

for the binary systems: $$x_2 \ll 1 \, , \quad x_1 \approx 1 \tag{27a}$$

$$x_3 \ll 1 \, , \quad x_1 \approx 1 \tag{27b}$$

$$x_2 \ll 1 \, , \quad x_3 \approx 1 \tag{27c}$$

where $x_i \ll 1$ means $x_i < 0.01$.

In dealing with organic solutes under the conditions of the present work, it has been found possible to satisfy the conditions 26 and 27a,b,c. Hence, the estimation of Henry coefficients for ternary systems can be carried out with confidence using Eq. 21.

## MODELS OF MASS TRANSFER

### Two-Film Theory

This model describes the mass transfer at an interface in a turbulent system (Fig. 1). The solute is transported from the bulk of one phase to the phase boundary, and then from the interface to the bulk of the second phase.

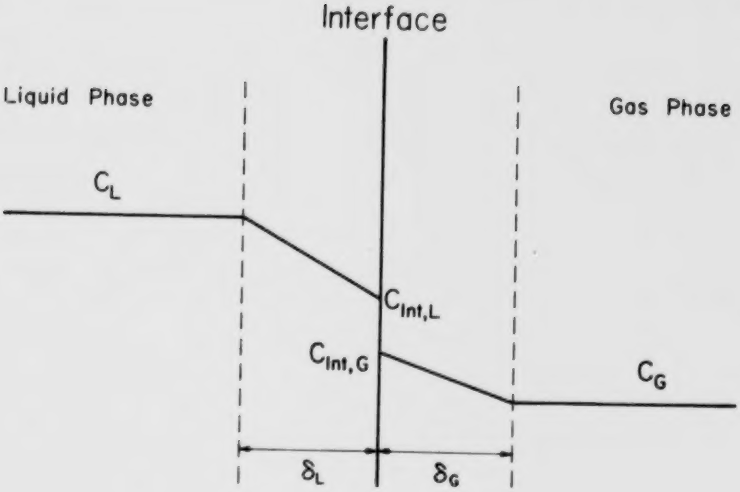

Figure 1. Concentration profiles according to the two-film model.

The mass transport to the interface can be written, in the form of Fick's first law, as

$$-\frac{dm}{dt} = D\ A\ \frac{\partial C}{\partial x} = A\ \frac{D_L}{\delta_L}(C_L - C_{int,L}) \tag{28}$$

and the mass transport from the interface can be written as

$$-\frac{dm}{dt} = D\ A\ \frac{\partial C}{\partial x} = A\ \frac{D_G}{\delta_G}(C_{int,G} - C_G) \tag{29}$$

where D = diffusion coefficient [$m^2/s$]

$\delta$ = film thickness [m]

m = mass [g]

A = interfacial area [$m^2$]

C = concentration [$g \cdot m^{-3}$].

$D/\delta$ is known as the mass transfer coefficient k. For the liquid film

$$k_L = \frac{D_L}{\delta_L} \tag{30}$$

and for the gas film

$$k_G = \frac{D_G}{\delta_G} \tag{31}$$

In laboratory experiments, $C_L$ and $C_G$ are determined easily, whereas the determination of $C_{int,L}$ and $C_{int,G}$ is almost impossible. For convenience one may define overall mass transfer coefficients based on an overall concentration difference

$$-\frac{dm}{dt} = K_G\ A(C_G{}^* - C_G) \tag{32}$$

$$= K_L\ A(C_L - C_L{}^*) \tag{33}$$

$C_G{}^*$ is the gas-phase concentration in equilibrium with the liquid. Using Henry's law in the form of a mass concentration ratio (Eq. 14).

$$C_G{}^* = C_L\ H_c \tag{34}$$

$C_L{}^*$ is the liquid-phase concentration corresponding to equilibrium with the gas. Using Henry's law

$$C_L{}^* = \frac{C_G}{H_c} \tag{35}$$

We assume that at the interface the gas and the liquid are at equilibrium, so that Henry's law will yield

$$C_{int,G} = C_{int,L}\ H_c \tag{36}$$

Expanding Eq. 32 with ± $C_{int,G}$ and substituting Eq. 34 and Eq. 36 into Eq. 32 gives

$$-\frac{dm}{dt} = K_G\ A[(C_{int,G} - C_G) + (C_G{}^* - C_{int,G})] \tag{37}$$

$$-\frac{dm}{dt} = K_G\ A[(C_{int,G} - C_G) + H_c(C_L - C_{int,L})] \tag{38}$$

Substituting Eq. 28 and Eq. 29 into 38 gives for the gas film

$$\frac{1}{K_G} = \frac{1}{k_G} + \frac{H_c}{k_L} \tag{39}$$

Similarly for the liquid film

$$\frac{1}{K_L} = \frac{1}{k_L} + \frac{1}{H_c k_G} \tag{40}$$

Substituting H, as defined by Eq. 16, for $H_c$ gives

$$\frac{1}{K_G} = \frac{1}{k_G} + \frac{H}{RT\,k_L} \tag{41}$$

and

$$\frac{1}{K_L} = \frac{1}{k_L} + \frac{RT}{H\,k_G} \tag{42}$$

Equations 39-42 suggest that the relationship among the individual-phase transfer coefficients and the overall transfer coefficients can be expressed by summing the individual resistances:

$$R_T = R_G + R_L \tag{43}$$

$$\text{liquid-phase resistance} \qquad R_L = \frac{1}{k_L} \tag{44}$$

$$\text{gas-phase resistance} \qquad R_G = \frac{RT}{H\,k_G} \tag{45}$$

Dividing Eq. 44 by Eq. 45 we obtain

$$\frac{R_L}{R_G} = \frac{H}{RT}\,\frac{k_G}{k_L} = \frac{H_c k_G}{k_L} \tag{46}$$

Leinonen et al. (7) state that the resistances of the two phases are equally important ($R_L = R_G$) when the value of H equals $1.6 \times 10^{-4}$ [$\text{atm}\cdot\text{m}^3\cdot\text{mol}^{-1}$] assuming that $k_G/k_L = 150$. This criterion is based on measurements of $k_G$ for water and $k_L$ for $CO_2$ at the air-sea interface (13-15), corrected for other compounds as suggested by Liss and Slater (14).

For example, substituting values for chloroform at 20°C into Eq. 46 yields

$$\frac{R_L}{R_G} = \frac{3.2 \times 10^{-3}\ [\text{atm}\cdot\text{m}^3/\text{mol}^{-1}]}{8.2 \times 10^{-5}\ [\text{atm}\cdot\text{m}^3\cdot\text{mol}^{-1}\cdot\text{K}]\ 293\ [\text{K}]} \times 150 \simeq 20 \tag{47}$$

This means that for chloroform the gas-phase resistance will approximately be 5% of the liquid-phase resistance. Hence, for highly volatile compounds such as chloroform, the liquid-phase resistance will control the rate of mass transfer, the gas-phase resistance should have little influence, and $K_L \simeq k_L$.

Due to this aspect of the mass transfer behavior, the criterion for choosing the compounds to be studied in the present work was $H \geq 3 \times 10^{-3}$ [$\text{atm}\cdot\text{m}^3\cdot\text{mol}^{-1}$], or equivalently $H_c \geq 0.13$. When this criterion is satisfied, we can feel reasonably certain that the liquid-phase resistance limits the mass transfer rate, and therefore that the gas-phase resistance can be neglected; the above assumption is implicit in the following derivations. However, it is clear that this widely accepted criterion is based upon the probably simplistic assumption that the ratio of the individual mass transfer coefficients in the system of interest is equal to that at the air-sea interface.

### The Penetration Theory

The penetration theory, first proposed by Higbie (16), pictures small turbulent eddies from the bulk phase reaching the interface, where they remain for a short but constant time (too short to attain steady-state) before being displaced back into the bulk fluid. Solute molecules are assumed to penetrate into a given eddy during its stay at the interface by a process of unsteady-state or transient molecular diffusion. The concentrations at the interface $C_{int}$ and in the bulk liquid phase $C_L$ under consideration are assumed to remain constant. Fick's second law describes such processes:

$$\frac{\partial C}{\partial t} = D \cdot \frac{\partial^2 C}{\partial x^2} \tag{48}$$

With initial condition condition

$$t = 0 \ , \quad 0 \leq x \leq \infty \ , \quad C = C_L \tag{49}$$

and boundary conditions

$$t > 0 \ , \quad x = 0 \ , \quad C = C_{int,L} \tag{50}$$

$$t > 0 \ , \quad x = \infty \ , \quad C = C_L \tag{51}$$

the expression obtained for the average mass transfer over the exposure time $t_e$ of any eddy is

$$\frac{dm}{dt} = 2\left(\frac{D_L}{\pi t_e}\right)^{1/2} \cdot A \cdot (C_{int,L} - C_L) \tag{52}$$

The mass transfer coefficient is

$$k_L = 2\left(\frac{D_L}{\pi t_e}\right)^{1/2} \tag{53}$$

The penetration theory predicts a square-root dependence of $k_L$ on the diffusion coefficient of the solute, in contrast to the film theory which predicts a first-power dependence.

### The Surface-Renewal Theory

Danckwerts' (17) surface-renewal theory is an extension of the penetration theory. The residence time t of an eddy at the interface is assumed to vary from zero to infinity, in contrast to the constant time of exposure assumed according to the penetration theory (16), as shown in Fig. 2.

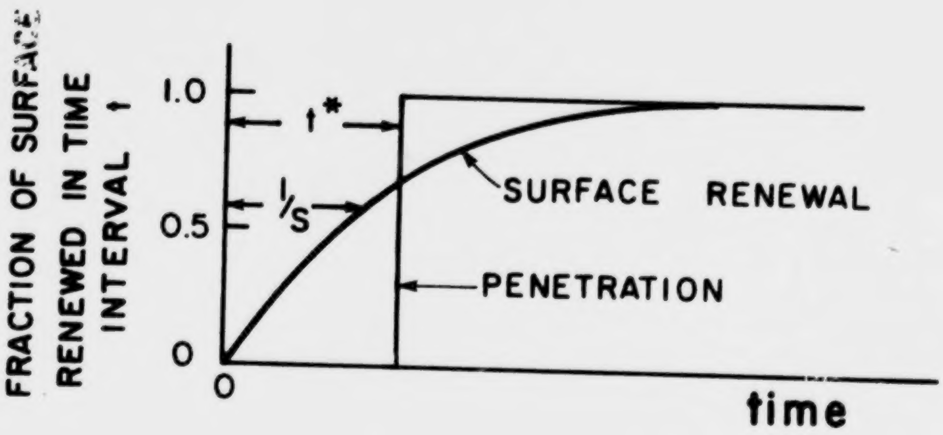

Figure 2. Distribution of turbulent eddies in the surface layer according to the penetration and surface-renewal theories (from 18).

A surface age distribution function $\phi(t)$ is introduced. If the probability of replacement of a surface element is independent of its age, Danckwerts (17) showed that

$$\phi(t) = s \cdot e^{-t} \qquad (54)$$

where s, the fractional rate of surface renewal of the area exposed to penetration, is assumed to remain constant. From this analysis, the average mass transfer normal to the phase boundary is

$$\frac{dm}{dt} = a \cdot (C_{int,L} - C_L) \cdot \sqrt{D} \cdot \int_0^\infty \frac{s \cdot e^{-t}}{\sqrt{\pi \cdot t}} dt = A \cdot (C_{int,L} - C_L) \cdot \sqrt{Ds}$$

$$= k_L \cdot A \cdot (C_{int,L} - C_L) \qquad (55)$$

where $k_L = \sqrt{Ds}$ (56)

According to Eq. 56 the mass transfer coefficient is proportional to the square root of the molecular diffusivity, as is the case for the penetration theory (Eq. 53). The fractional rate of renewal, s, when compared to the penetration theory, Eq. 53, corresponds to

$$s = \frac{4}{\pi} \cdot \frac{1}{t_e} \qquad (57)$$

Some alternative surface age distribution functions have been proposed by Perlmutter (19).

## The Film-Penetration Theory

The film-penetration model, presented by Toor and Marchello (20), represents a combination of the three theories described earlier. The entire resistance to mass transfer is assumed to lie in a laminar surface layer of thickness $\delta$. Surface renewal occurs by eddies which penetrate the surface from the bulk of the phase. Thus transfer through young elements of surface obeys the penetration theory ($k \propto D^{1/2}$); transfer through old elements obeys the film theory ($k \propto D$); and transfer through elements of intermediate age combines both mechanisms. The bulk concentration is assumed to be uniform. The transfer equation is again Fick's second law

$$\frac{\partial C}{\partial t} = D \cdot \frac{\partial^2 C}{\partial x^2} \qquad (48)$$

with initial condition $\quad t = 0 \ , \quad 0 \leq x \leq \infty \ , \quad C = C_L \qquad (58)$

and boundary conditions $\quad t > 0 \ , \quad x > 0 \ , \quad C = C_{int} \qquad (59)$

$t > 0 \ , \quad x = \delta \ , \quad C = C_L \qquad (60)$

The key difference from the penetration theory lies in the second boundary condition, Eq. 60 (compare with Eq. 51). After solving the above equations for the instantaneous mass transfer rates, an appropriate surface age distribution $\phi(t)$ has to be assumed. We will assume Danckwerts' distribution (17), as thought to be more realistic than Higbie's constant exposure time (16).

The resulting mass transfer equations are:

- for short average element life

$$\frac{dm}{dt} = (C_{int} - C_L) \cdot A \cdot \sqrt{D \cdot s} \cdot \left(1 + 2 \cdot \sum_{n=1}^{\infty} \exp(-2n\delta \cdot \sqrt{s/D})\right) \qquad (61)$$

- and for long average element life

$$\frac{dm}{dt} = (C_{int} - C_L) \cdot A \cdot \frac{D}{s} \left(1 + 2 \cdot \sum_{n=1}^{\infty} \frac{1}{1 + n^2 \cdot \pi^2 \cdot (D/s\delta^2)}\right) \qquad (62)$$

When the rate of surface renewal is high (large $s\delta^2/D$), Eq. 61 reduces to Danckwerts' (17) equation, Eq. 55. Conversely, when $s\delta^2/D$ is small, Eq. 62 reduces to the film theory, Eq. 28.

The resulting equations when using Higbie's constant time of exposure may be found elsewhere (20,21).

Figure 3 shows that the two-film and penetration theories are asymptotes of the film-penetration model. Both coordinates in Fig. 3 are dimensionless:

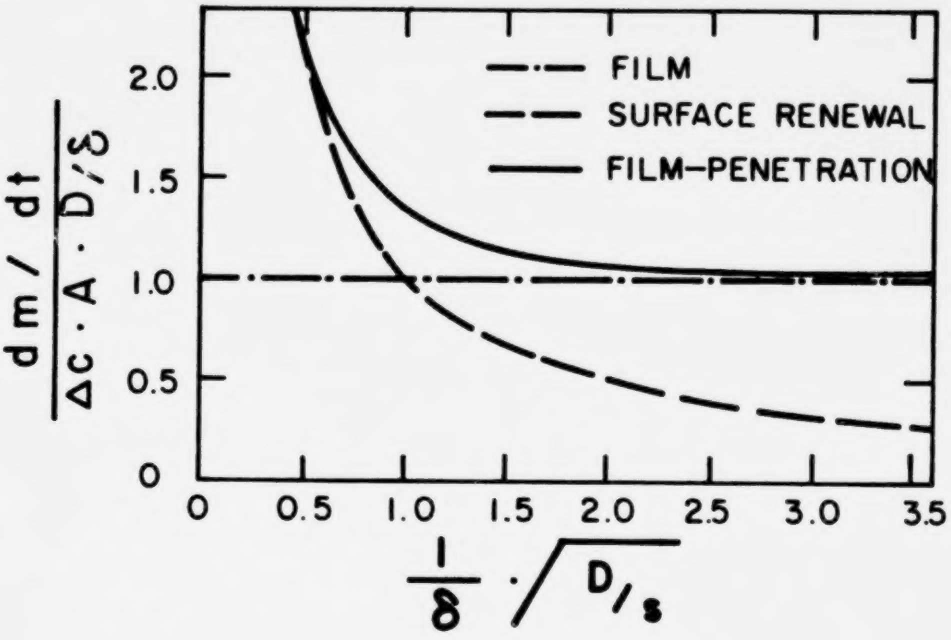

Figure 3. Mean transfer rates as a function of time of exposure (20).

the ordinate is the ratio of the mass transfer rate to the mass transfer rate according to the film theory; the abscissa is a dimensionless time parameter related to the age of fluid elements in the film ($\delta$) that controls the rate of mass transfer.

## Summary of Mass Transfer Models

Several other theories have been proposed, but those discussed above are the most widely used to describe mass transfer between fluid phases. The application of these theories presents practical difficulties: it is difficult to measure the film thickness $\delta$, the exposure time $t_e$, or the fractional rate of surface renewal s. Since the film-penetration model includes always two of these parameters, it is virtually impossible to make analytical use of it other than by fitting the quantities $\delta$ and s and the exponent of the diffusion coefficient in Eqs. 61 and 62. The differences between the penetration and the surface-renewal theories are slight (see Eq. 57), but it is essential to recognize the square-root dependence of the mass transfer coefficient on the diffusion coefficient in contrast to the film theory, which predicts a linear dependence.

The principal merit of the two-film theory is probably the concept of additivity of the resistances. Using this concept, assurance of dominance by the resistance in either film and close control of the surface area A available to transfer, some researchers have been able to measure single-phase resistances and thereby to estimate the magnitude of $\delta$ or s. Notably, Liss

(13) and Schooley (15) were able to estimate the effective gas film thickness $\delta_G$ based on measurements of the evaporation rate of water (gas-phase controlled) at different wind velocities. Tsao and Lee (22) and Bungay et al. (23) measured surface oxygen absorption (liquid-phase controlled) with microelectrodes, and were able to estimate a surface renewal rate s when using the surface renewal theory.

Goodgame and Sherwood (24) tested the concept of additivity of resistances while using the surface-renewal theory as their mass transfer model. Their work compared the observed overall coefficients for the absorption of ammonia and acetone in water (the resistances of both phases affect the transfer rate) with values predicted from the individual mass transfer coefficients obtained from experiments on water evaporation (gas-phase controlled) and carbon dioxide absorption in water (liquid-phase controlled). Excellent agreement was found, indicating that the concept of additivity of resistances is indeed very likely to be valid, whether used in the original context of the two-film theory or with the surface renewal theory.

## DIFFUSION COEFFICIENTS

The elementary concepts of classical kinetic theory provide a basis for the development of an approximate theory of diffusion. Molecular diffusion in binary systems has been the subject of theoretical and experimental investigation for nearly a century. The Stokes-Einstein equation (25, p. 25), based on a model in which a spherical solute molecule is considered to move through a continuum of the solvent, is

$$D_{AB} = \frac{\bar{k}T}{6\pi\gamma_o \mu} \tag{63}$$

where $\gamma_o$ is the sphere radius and $\bar{k}$ is Boltzmann's constant. This was modified by Wilke and Chang (26), as follows:

$$D_{AB}^{o} = 7.4 \times 10^{-15} \left[ (\phi\, M_B)^{1/2} \frac{T}{\mu_B\, V_A^{0.6}} \right] \tag{64}$$

where $D_{AB}^{o}$ = mutual diffusion coefficient of solute A at very low concentrations in solvent B $[m^2 \cdot s^{-1}]$

$\phi$ = association parameter of B usually taken as 2.6 for water

$M_B$ = molecular weight of the solvent [g/mol]

T = temperature [K]

$\mu_B$ = viscosity of the solvent $[kg \cdot m^{-1} \cdot s^{-1}]$

$V_A$ = molal volume of the solute at its normal boiling point $[cm^3/mol]$.

It is to be noted that Eq. 64 is not dimensionally consistent, and hence the value of the constant depends on the units chosen.

For dilute aqueous systems Othmer and Thakar (27) developed an equation that correlates experimental data very well

$$D_{AB}^{o} = 5.57 \times 10^{-4} \mu_B V_A^{-0.6} \qquad (65)$$

where $V_A$ = molal volume of solute A [cm$^3$/mol]

$\mu_B$ = viscosity of water [kg$\cdot$m$^{-1}\cdot$s$^{-1}$].

A relationship between the diffusion coefficient and the critical volume $V_C$ can be shown

$$D_L = f V_C^{\varepsilon} \qquad (66)$$

Matter (28) proposed that $\varepsilon$ can vary between $-1/3$ and $-2/3$, depending on the size and shape of the diffusing molecule.

In contrast to the situation in gases, the diffusivity $D_{AB}$ in the liquid phase shows a variation with concentration (25, p. 31). $D_{AB}$ can vary considerably with concentration, often passing through a maximum or minimum, with the extreme values for infinite dilution and pure solute sometimes differing several fold. However, this phenomenon is unlikely to be important in the very dilute range studied in this work.

Because the mass transfer coefficient is defined as $k_L = D_{AB}/\delta$ this suggests that $k_L$ also can vary with concentration. But in Eqs. 37-46 the assumption is made that $k_L$ does not vary with concentration; therefore, the experimental data have to be checked for variability of the mass transfer coefficient.

## Gas Phase

The kinetic theory of gases, in which molecules are regarded as rigid spheres experiencing elastic collisions, is well developed. For binary gas systems at low pressure a widely used expression (29) is:

$$D_{AB} = \frac{1.858 \cdot 10^{-3} \cdot T^{3/2}}{P \cdot \sigma_{AB}^{2} \cdot \Omega_d} \cdot \left(\frac{1}{M_A} + \frac{1}{M_B}\right)^{1/2} \qquad (67)$$

where $D_{AB}$ = diffusion coefficient [cm$^2$/s]

$T$ = absolute temperature [K]

$P$ = pressure [atm]

$\sigma$ = characteristic length [Å]

$\Omega_d$ = diffusion collision integral [dimensionless]

To use Eq. 67, an intermolecular force law must be chosen and the constants $\sigma_{AB}$ and $\Omega_d$ must be evaluated. Usually the Lennard-Jones potential is used to estimate these quantities.

Several proposed semiempirical correlations for estimating $D_{AB}$ in low pressure binary gas systems retain the general form of Eq. 67, with empirical constants based on experimental data. Lugg (30), in an extensive study of 147 gases in air, finds the Wilke and Lee (31) and Chen and Othmer (32) correlations to fit the data best. Since the latter employs critical constants not available for all compounds, the Wilke and Lee correlation (31) is preferred:

$$D_{AB} = \left\{0.00217 - 0.00050 \cdot \left(\frac{1}{M_A} + \frac{1}{M_B}\right)^{1/2}\right\} \cdot \frac{T^{3/2}}{P \cdot \sigma_{AB}^{2} \cdot \Omega_d} \cdot \left(\frac{1}{M_A} + \frac{1}{M_B}\right)^{1/2} \quad (68)$$

Elliott and Watts (33) also find Eq. 68 better than any alternative and note that: "... if good data for its use were available, the kinetic theory equation (Eq. 67) should be superior to the other equations because of its sound theoretical basis."

## RELATION OF MASS TRANSFER COEFFICIENT TO DIFFUSION COEFFICIENT

From dimensional analysis, the functional equation for forced-convection mass transfer (34, p. 564) is

$$Sh = c_1 \, Re^{c_2} \, Sc^{c_3} \quad (69)$$

where $Sh = k_L d/D_{AB}$; Sherwood number [dimensionless]

$Re = ud/\nu$; Reynolds number [dimensionless]

$Sc = \nu/D_{AB}$; Schmidt number [dimensionless].

Solving for $k_L$ yields

$$k_L = c_1 \, u^{c_2} \, d^{(c_2-1)} \, \nu^{(c_3-c_2)} \, D_{AB}^{(1-c_3)} \quad (70)$$

where $c_1, c_2, c_3$ = constants

$d$ = characteristic length [m]

$u$ = characteristic velocity [$m \cdot s^{-1}$]

$\nu$ = kinematic viscosity of water [$m^2 \cdot s^{-1}$].

Equation 70 shows that the mass transfer coefficient is a function of turbulence, the kinematic viscosity, and the diffusion coefficient. Depending on which model is used, the exponent of the diffusion coefficient $(1 - c_3)$ will change from 1 for the film model to 0.5 for the penetration model. Because the characteristic length, the turbulence, and the kinematic viscosity of water will not change for different organic compounds, it is convenient to define a mass transfer ratio (29,35,36)

$$\Psi = \frac{k_{L,j}}{k_{L,i}} \simeq \frac{K_{L,j}}{K_{L,i}} \tag{71}$$

where $k_{L,i}$ = mass transfer coefficient of compound i [m/s]

$k_{L,j}$ = mass transfer coefficient of compound j [m/s].

Substituting Eq. 70 into Eq. 71 gives

$$\Psi = \frac{k_{L,i}}{k_{L,j}} = \left(\frac{D_{A,i}}{D_{A,j}}\right)^{(1-c_3)} \equiv \left(\frac{D_{A,i}}{D_{A,j}}\right)^{\Omega} \tag{72}$$

Further, if the diffusion coefficient is replaced by the critical volume $V_C$, the expression for $\Psi$ becomes (28)

$$\Psi = \left(\frac{D_{A,i}}{D_{A,j}}\right)^{\Omega} = \left(\frac{V_{C,i}}{V_{C,j}}\right)^{\Omega\varepsilon} \tag{73}$$

The exponent $\Omega$ in Eqs. 72 and 73 depends on the mechanism of mass transfer. The value of $\Omega$ may range from $1/2$ to 1, according to the film-penetration theory. The exponent $\varepsilon$ in Eq. 73 depends on shape and size of the diffusing molecule and can vary from $-1/3$ to $-2/3$. These two exponents are related to the shape of the diffusing molecule (28). If the molecule has a spherical shape, $\varepsilon = -1/3$, whereas if the molecule has a planar shape, $\varepsilon = -2/3$, according to the Stokes Einstein relation (Eq. 63).

Equation 72 promises to be extremely useful for engineering applications; it enables us to estimate the mass transfer coefficient for a given compound i from that of a reference compound j, if the diffusivities or critical volumes of both are known. For example, the reference compound may be chosen as oxygen, a compound for which mass transfer data are ample and measurements are easily made. If the mass transfer coefficient for oxygen is known for a given situation, the mass transfer coefficients for volatile organic contaminants can be estimated approximately using Eq. 73. It is one of the principal objectives of the present work to demonstrate the efficacy of this approach, and to determine the proper value of the exponent $\Omega$ for use in Eq. 73.

## MIXING IN A SURFACE AERATION CONTACTOR

The mass transfer equations derived so far hold only for a completely mixed system. Therefore, the surface-aeration contactor has to be checked for its mixing properties. This can be done by interpreting power consumption measurements for the mixing system. Moreover, it can be anticipated that the mass transfer rate will increase with increasing power input.

## Power Number

Power measurements at various mixer speeds are necessary to provide the data required to draw power curves for a reactor. At a specific value of liquid density $\rho$, agitator speed N, and agitator diameter $d_a$, the power P must be measured in order to evaluate the power number (37)

$$Po = \frac{P}{\rho N^3 d_a^5} \text{ [dimensionless]} \tag{74}$$

The easiest and most accurate way to measure the power is to measure the torque produced by the rotating agitator. Knowing the torque, the power can be calculated by

$$P = \tau \times \omega$$

where $\omega$ = rotational velocity [radians/s] = $2\pi N/60$ [rpm], or

$$P = \tau \frac{\pi \times \text{revolutions per minute [rpm]}}{30} \tag{75}$$

In order to convert P to units of watts [$kg \cdot m^2 \cdot s^{-3}$], when the units of $\tau$ are [in.oz], Eq. 75 has to be modified to

$$P\left[\frac{kg \cdot m^2}{s^3}\right] = \frac{\tau \text{ [in}\cdot\text{oz]} \times \text{rpm}}{1.352 \times 10^3} \tag{76}$$

## Power Curve

The power drawn by an agitator in a liquid mixing system is determined by its rotational speed and geometry, as well as by the environment in which it operates. Using dimensional analysis (37, p. 30) one obtains

$$Po = c_1 (Re)^{c_2} (Fr)^{c_3} \tag{77}$$

Equation 72 relates the dimensionless power number Po to the dimensionless Reynolds number, Re; the dimensionless Froude number, Fr; and a dimensionless shape factor, $c_1$. For nonvortexing systems, gravitational forces have a negligible effect, and the exponent $c_3$ of the Froude number is zero. Therefore, $Fr^{c_3} = 1$ and Eq. 72 becomes

$$Po = c_1 (Re)^{c_2} \tag{78}$$

A plot of Po vs Re on log-log coordinates is commonly called a power curve. An individual power curve is valid only for a particular geometrical configuration, but is independent of vessel size. Figure 4 illustrates the power curve for a standard tank configuration (37, p. 12). The geometry of the impeller on which the data in Fig. 4 are based differs from that used in this

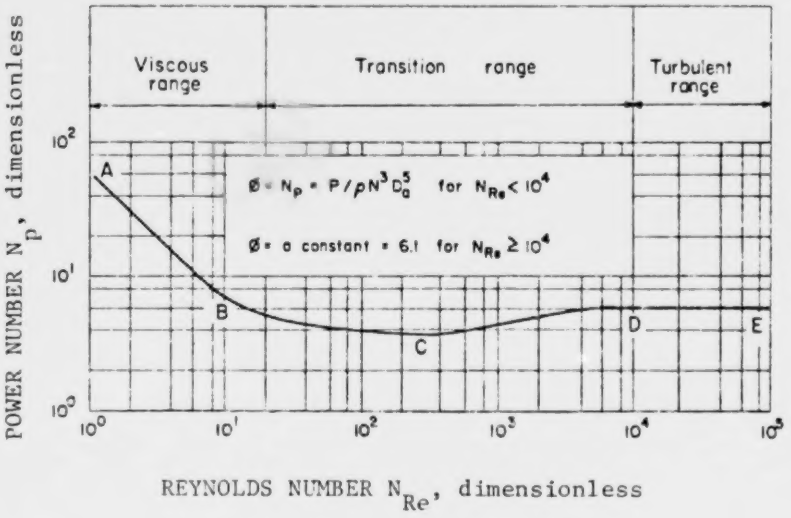

Figure 4. Power curve for standard tank configuration (37).

work, but the example nonetheless provides a useful illustration of how Po depends on Re. This power curve illustrates some general principles. At low Reynolds numbers (between point A and B), the plot is linear with a slope of -1. This is typical for laminar flow. As the Reynolds number increases, the flow turns from laminar to turbulent (segment B-D). When the flow becomes fully turbulent, the power curve becomes horizontal (segment D-E). In the latter segment, the flow is independent of the Reynolds number and the power number is constant.

## MASS TRANSFER IN A BUBBLE COLUMN

### Accounting for Variable Gas-Phase Concentration

In a previous section the basic mass transfer equations (Eqs. 32 or 33) were described. Because usually concentrations are measured instead of mass, it is convenient to rearrange those equations by dividing on each side by the total liquid volume, $V_L$, i.e.,

$$\frac{dm}{dt} = - K_L \cdot A \cdot (C_L - C_L^*) \qquad (33)$$

becomes

$$\frac{dC}{dt} = K_L \cdot a \cdot (C_L^* - C_L) \qquad (79)$$

where

$$a = A/V_L = \text{specific interfacial surface area } [m^{-1}]. \qquad (80)$$

Equation 80 is appropriate for describing surface aeration where $C_L^* =$ constant, but not for bubble aeration where $C_L^*$ varies as the bubbles rise through the liquid. Therefore, we need to develop an expression which describes the variation of $C_L^*$ in order to be able to use Eq. 79.

The following assumptions are made: the process is isothermal; the liquid-film resistance controls mass transfer; the overall mass transfer coefficient, $K_L$, is considered constant during an experiment and depends only on liquid temperature, i.e., $K_L$ is independent of time and position of bubbles; equilibrium holds at the interface and is described by Henry's law; only one solute is transferred; the gas flow rate is constant; the rising bubbles are distributed uniformly across the tank section; the reactor is well mixed, i.e., liquid-phase concentration is time-dependent but spatially invariant during an experiment; and the gas-phase concentration is dependent on bubble residence time and vertical position.

The gas-phase concentration in a rising gas bubble can be described with the continuity equation, as shown by Lakin and Salzmann (38):

$$\frac{\partial}{\partial t}\left(\frac{pV_b}{RT} \cdot y\right) + u_b \cdot \frac{\partial}{\partial Z}\left(\frac{pV_b}{RT} \cdot y\right) = -K_G \cdot \left(\frac{A_b}{V_b}\right) \cdot pV_b\left(y - \frac{C_L \cdot H}{p}\right) \qquad (81)$$

where $A_b$ = bubble surface area [m$^2$]

$C_L$ = solute liquid-phase concentration [mol$\cdot$m$^{-3}$]

$H$ = Henry coefficient [atm$\cdot$m$^3\cdot$mol$^{-1}$]

$K_G$ = overall gas-phase mass transfer coefficient [mole/atm$\cdot$m$^2\cdot$s]

$p$ = pressure [atm]

$R$ = universal gas constant = $8.206 \times 10^{-5}$ [atm$\cdot$m$^3\cdot$mol$^{-1}\cdot$K$^{-1}$]

$T$ = absolute temperature [K]

$t$ = time [s]

$V_b$ = bubble volume [m$^3$]

$u_b$ = bubble rise velocity [m/s]

$y$ = mole fraction of solute in gas phase [dimensionless]

$Z$ = submergence [m]

It can be assumed that the local time rate of change in gas-phase mass transfer is negligible: the changes that occur in the liquid phase during the bubble residence time are insignificant when compared with changes that take place in the vertical direction in the gas phase. Therefore Eq. 81 becomes:

$$u_b \cdot \frac{\partial}{\partial Z}\left(\frac{pV_b}{RT} \cdot y\right) = -K_G \cdot \left(\frac{A_b}{V_b}\right) \cdot pV_b \cdot \left(y - \frac{C_L \cdot H}{p}\right) \qquad (82)$$

This does not make Eq. 82 time-independent, since $C_L = f(t)$. On the other hand, $u_b$, $A_b$, and $V_b$ are position-dependent and need to be averaged in order to solve Eq. 82. The average bubble volume is defined as

$$(V_b)_{av} = \frac{1}{Z_s} \int_0^{Z_s} V_b \cdot dZ \qquad (83)$$

where $Z_s$ = total submergence, from liquid free surface to gas inlet [m]. The bubble area, $A_b$, and bubble rise velocity, $u_b$, are now dependent only on this quantity, $V_{b(av)}$, and can themselves be represented as average values (38). Recognizing that $K_G = K_L/H$, and rearranging, Eq. 82 becomes

$$\frac{\partial y}{\partial Z} + y \cdot \frac{\partial(\ln p)}{\partial Z} = -K_L \cdot \frac{1}{u_{b(av)}} \cdot \left(\frac{A}{V_b}\right) \cdot \frac{RT}{H} \cdot \left(y - \frac{C_L \cdot H}{p}\right) \qquad (84)$$

The following relationships hold (after averaging the bubble volume, $V_b$):

$$\bar{t}_b = \frac{V_{G(av)}}{Q_G} \qquad (85)$$

$$u_{b(av)} = -\frac{Z_s}{\bar{t}_b} \qquad (86)$$

and consequently

$$u_{b(av)} = -\frac{Z_s \cdot Q_G}{V_{G(av)}} \qquad (87)$$

and

$$\left(\frac{A_b}{V_b}\right) = \frac{A}{V_{G(av)}} \cdot \left(\frac{V_L}{V_L}\right) \qquad (88)$$

with $a = A/V_L$

$$\left(\frac{A_b}{V_b}\right) = a \cdot \frac{V_L}{V_{G(av)}} \qquad (89)$$

where $A$ = total surface area available for transfer [$m^2$], i.e., surface area of all bubbles at any given time)

$a$ = specific interfacial surface area [$m^{-1}$]

$Q_G$ = volumetric gas flow rate evaluated at a pressure corresponding to $Z_s/2$ [$m^3/s$]

$\bar{t}_b$ = average bubble residence time [s]

$V_G$ = gas volume in reactor at any given time [$m^3$]

$V_L$ = liquid volume of reactor [$m^3$]

Upon substitution of Eqs. 87 and 89 into Eq. 84 we obtain

$$\frac{\partial y}{\partial Z} + y \cdot \frac{\partial(\ell n\ p)}{\partial Z} = \frac{K_L a \cdot V_L}{Q_G \cdot Z_s} \cdot \frac{RT}{H} \cdot \left(y - \frac{C_L \cdot H}{p}\right) \tag{90}$$

Substituting $H = H_c RT$ and defining

$$\Phi = \frac{K_L a \cdot V_L}{H_c \cdot Q_G \cdot Z_s}\ [m^{-1}] \tag{91}$$

where $\Phi$ is constant for any experiment, we obtain

$$\frac{\partial y}{\partial Z} + y \cdot \frac{\partial(\ell n\ p)}{\partial Z} = \Phi \cdot \left(y - \frac{C_L}{p} \cdot H_c \cdot RT\right) \tag{92}$$

Since we know the dependence of pressure on liquid depth, Z, we may readily evaluate the term $\partial(\ell n\ p)/\partial Z$, and Eq. 92 reduces to

$$\frac{\partial y}{\partial Z} + y \cdot \left(\frac{\rho g}{p} - \Phi\right) = - \frac{C_L \cdot H_c \cdot \Phi \cdot RT}{p} \tag{93}$$

Integrating Eq. 93, we obtain a general expression which describes the gas-phase mole fraction, y, as a function of submergence, Z,

$$y(Z) = \frac{1}{p \cdot \exp(-\Phi Z)} \cdot \left(C_L \cdot H_c \cdot RT \cdot \exp(-\Phi Z) + \text{constant}\right) \tag{94}$$

So far, the analysis has been general: it applies to the process of absorption as well as to that of desorption or stripping. Although the further development is similar for both processes, it is useful to distinguish between them to avoid confusion.

Oxygen Absorption--

First we need to evaluate the constant of integration in Eq. 94 by use of an appropriate boundary condition. This is:

$$\text{at} \quad Z = Z_s \ , \quad p = p_s \ , \quad y = y_I \tag{95}$$

where $y_I$ = inlet oxygen mole fraction of air (≈ 0.21), from which we obtain

$$\text{constant} = \exp(-\Phi Z_s) \cdot (y_I \cdot p_s - C_L \cdot H_c \cdot RT) \tag{96}$$

Therefore, the oxygen mole fraction as a function of submergence Z is described by

$$y(Z) = C_L \cdot H_c \cdot \frac{RT}{p} + \left(y_I - C_L \cdot H_c \cdot \frac{RT}{p_s}\right) \cdot \frac{p_s}{p} \cdot \exp\left(-\Phi(Z_s - Z)\right) \qquad (97)$$

If we expand Eq. 97 with p/RT we obtain an analogous expression in terms of a gas-phase concentration

$$C_G = C_L \cdot H_c + (C_{GI} - C_L \cdot H_c) \cdot \exp\left(-\Phi(Z_s - Z)\right) \qquad (98)$$

where

$$C_G = \frac{y \cdot p}{RT} \text{ [moles/m}^3\text{]} \qquad (99)$$

and

$$C_{GI} = \frac{y_I \cdot p_s}{RT} \text{ [moles/m}^3\text{]} \qquad (99a)$$

Finally, we will use a mass balance assuming $Q_{GI} = Q_{GE}$ (Fig. 5) in conjunction with Eq. 98 to describe the transfer of oxygen into the liquid phase:

$$Q_G \cdot C_{GI} - Q_G \cdot C_{GE} = V_L \cdot \frac{dC_L}{dt} \qquad (100)$$

The exit oxygen gas-phase concentration, $C_{GE}$, is obtained by evaluating Eq. 98 at $Z = 0$. Substituting the expression for $C_{GE}$ into Eq. 100 and integrating

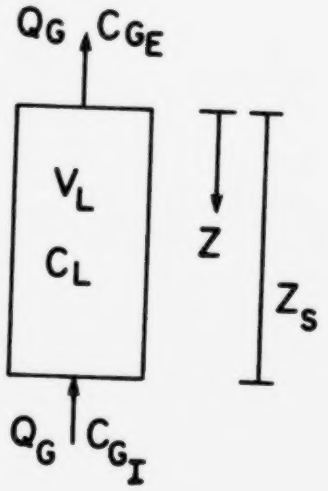

Figure 5. Gas-phase mass balance for bubble column.

from $t = t_o$ to $t = t$ and $C_L = C_{Lo}$ to $C_L = C_L$, we obtain

$$-\ln \left(\frac{(C_{GI}/H_c) - c_L}{(C_{GI}/H_c) - C_{Lo}}\right) = \frac{Q_G \cdot H_c}{V_L} \cdot \left[1 - \exp(-\Phi Z_s)\right] \cdot (t - t_o) \qquad (101)$$

We know that as $t \to \infty$, $C_L \to C_L^*$, where $C_L^*$ = oxygen saturation concentration. Applying this criterion in Eq. 101, we obtain

$$C_{GI}/H_c = C_L^* \qquad (102)$$

Therefore,

$$-\ln \left(\frac{1 - (C_L/C_L^*)}{1 - (C_{Lo}/C_L^*)}\right) = \frac{Q_G \cdot H_c}{V_L} \cdot \left[1 - \exp(-\Phi Z_s)\right] \cdot (t - t_o) \qquad (103)$$

is the expression which describes the process of oxygen absorption in a bubble column.

From a linear regression of Eq. 103, which may be rewritten as

$$f(C) = \text{slope} \cdot (t - t_o) \qquad (104)$$

we obtain the slope ($\equiv S$)

$$S = \frac{f(C)}{dt} = \frac{Q_G \cdot H_c}{V_L} \cdot \left[1 - \exp(-\Phi Z_s)\right] \qquad (105)$$

from which the average oxygen mass transfer coefficient, $K_{LO_2}a$, may be calculated:

$$K_{L,O_2}a = -\frac{Q_G \cdot H_c}{V_L} \cdot \ln \left(1 - \frac{S \cdot V_L}{Q_G \cdot H_c}\right) \qquad (106)$$

Stripping of Organics--

The appropriate boundary condition to evaluate the constant of integration in Eq. 94 is in this case,

$$\text{at} \quad Z = Z_s \;, \quad y_I = 0 \;, \quad p = p_s \qquad (107)$$

assuming that the inlet gas is free of organics. We obtain:

$$\text{constant} = C_L \cdot H_c \cdot RT \cdot \exp(-\Phi Z_s) \qquad (108)$$

which substituted back into Eq. 94 yields

$$y(Z) = \frac{C_L \cdot H_c \cdot RT}{P} \cdot \left[1 - \exp\left\{-\Phi(Z_s - Z)\right\}\right] \qquad (109)$$

Noting that $y(Z) \cdot P/RT = C_G$ [mole/m$^3$], we get

$$\frac{C_G}{C_G^*} = \frac{C_G}{C_L H_c} \left[1 - \exp\left\{-\Phi(Z_s - Z)\right\}\right] \qquad (110)$$

which describes the change in gas-phase concentration of the organic solutes, as well as the fractional gas-phase saturation ($C_G/C_G^*$), with submergence Z. Now, we use again the mass balance and, as before, evaluate $C_{GE}$, the exit gas-phase concentration, from Eq. 110 by substituting $Z = 0$. We also note that $C_{GI}$, the inlet gas-phase concentration, is zero, and integrate from $t_o$ to t and from $C_L = C_{Lo}$ to $C_L = C_L$ and obtain

$$-\ln\left(\frac{C_L}{C_{Lo}}\right) = \frac{Q_G \cdot H_c}{V_L} \cdot \left[1 - \exp(-\Phi Z_s)\right] \cdot (t - t_o) \qquad (111)$$

Equation 111 is the integrated rate equation for the stripping process in a bubble column. From a linear regression of Eq. 111, which may be rewritten as

$$f(C) = \text{slope} \cdot (t - t_o) \qquad (104)$$

we obtain the slope ($\equiv$ S) which is given by

$$S = \frac{df(C)}{dt} = \frac{Q_G \cdot H_c}{V_L} \cdot \left[1 - \exp(-\Phi Z_s)\right] \qquad (112)$$

In contrast to the case of gas absorption, where the gas-phase concentration decreases as the bubbles rise, during volatilization the gas-phase concentration increases, eventually reaching the value corresponding to the equilibrium between liquid and gas phase if the bubble column is sufficiently long.

This suggests that Eq. 111 has two limiting cases (39). In the first case

1.) $$\Phi Z_s = \frac{K_L a \cdot V_L}{Q_G \cdot H_c} \gg 1 \qquad (113)$$

the exponential term becomes zero and therefore Eqs. 111 and 112 become, respectively,

$$-\ln\left(\frac{C_L}{C_{Lo}}\right) = \frac{Q_G \cdot H_c}{V_L} \cdot (t - t_o) \qquad (114)$$

and

$$S = \frac{Q_G \cdot H_c}{V_L} \tag{115}$$

This represents the case where the exit gas is saturated with the organic compound. Under these circumstances Eqs. 114 and 115 may be used to determine the Henry coefficient, $H_c$, as proposed by Mackay et al. (9). The criterion used in this study to measure Henry coefficients is $\Phi Z_s \geq 5$, which corresponds to $\geq 99.33\%$ gas-phase saturation. In the second case, where

2.) $$\Phi Z_s = \frac{K_L a \cdot V_L}{Q_G \cdot H_c} << 1 \tag{116}$$

the exponential term can be expanded and Eqs. 111 and 112 reduce, respectively, to

$$-\ln \left(\frac{C_L}{C_{Lo}}\right) = K_L a \cdot (t - t_o) \tag{117}$$

$$S = K_L a \tag{118}$$

This represents the case where the exit gas is far from saturation. This situation is encountered where $H_c$ is large, or where $Q_G$ is large, as in surface aeration. The criterion for this case is $\Phi Z_s < 0.1$ (39).

For the intermediate range ($0.1 < \Phi Z_s < 5$) Eqs. 111 and 112 have to be used. Here, the need arises to know _a priori_ either $H_c$ or $K_L a$. However, having reasonable estimates of $H_c$ for the compound under consideration, it is possible to calculate a $K_L a$-value by transforming Eq. 112 to the following form

$$K_L a = -\frac{Q_G \cdot H_c}{V_L} \cdot \ln \left(1 - \frac{S \cdot V_L}{Q_G \cdot H_c}\right) \tag{119}$$

which is identical to Eq. 106 derived for absorption.

Units of Concentration--

Throughout the development of Eqs. 103 and 111 the gas- and liquid-phase concentrations were expressed in units of [moles/m$^3$]. These equations, however, suggest that $C_L$ could be expressed in any customary units, since always a ratio of concentrations appears. This is true if $C_L$ is expressed as a volumetric concentration, i.e., g/m$^3$ or mg/m$^3$, but false if $C_L$ is expressed as a mass concentration, i.e., mole fraction. The reason for this difference is the Henry coefficient. $H_c$ [dimensionless] takes the same value when $C_L$ is expressed in moles/m$^3$, g/m$^3$, or mg/m$^3$, but is different when $C_L$ is expressed in mole fractions, although $H_c$ remains dimensionless.

The units chosen in this work for the variables of Eqs. 103 and 111 are as follows:

$C_L$ = $[g/m^3]$ for oxygen

$C_L$ = $[mg/m^3]$ for organic solutes

$Q_G$ = $[m^3/s]$

$V_L$ = $[m^3]$

$H_c$ = [dimensionless] = $[(g/m^3)_G/(g/m^3)_L]$

$t$ = $[s]$

$K_La$ = $[s^{-1}]$.

However, the unit of time is chosen as minutes for convenience of expression in some graphs and tables.

Summary of Absorption and Stripping in a Bubble Column--

Oxygen absorption in a bubble column is described by:

$$-\ln\left(\frac{1-(C_L/C_L^*)}{1-(C_{Lo}/C_L^*)}\right) = \frac{Q_G \cdot H_c}{V_L} \cdot \left[1-\exp(-\phi Z_s)\right] \cdot (t-t_o) \qquad (103)$$

from which the average mass transfer coefficient, $K_{L,O_2}a$, may be calculated using a linear regression.

Stripping (or volatilization) of organics in a bubble column is described by

$$-\ln\left(\frac{C_L}{C_{Lo}}\right) = \frac{Q_G \cdot H_c}{V_L} \cdot \left[1-\exp(-\phi Z_s)\right] \cdot (t-t_o) \qquad (111)$$

from which, depending on the degree of gas-phase saturation, either the Henry coefficient, $H_c$, or the average mass transfer coefficient, $K_La$, of the compound under consideration can be estimated using a linear regression if the other of the two variables is known a priori.

## Gas Bubbles Dispersed in a Liquid Phase

We define the material forming the particulate phase, i.e. the gas in the case of bubbles, as the dispersed phase. The fluid surrounding the particulates, i.e. liquid, is termed the continuous phase. In this work the gas is air, and the liquid is water. When referring to particles it must be recognized that bubbles are simply a special kind of particles.

Many workers (40-47) have attempted to characterize gas-liquid dispersions, including parameters such as the following: equivalent bubble diameter, d; volumetric gas holdup ratio, $\varepsilon_G$; bubble rise velocity, $u_b$; superficial gas velocity, $V_s$; fluid properties; geometry; etc. Similarly, numerous studies have tried to correlate the mass transfer coefficient, $k_L$, with combinations of the above mentioned parameters. The multiplicity of factors and interactions make a single general correlation virtually impossible to achieve (48).

Flow Regime and Bubble Characterization--

Shapes of bubbles in free rise or fall in infinite media under the influence of gravity are generally grouped under the following categories: spherical, ellipsoidal, and spherical cap.

Clift et al. (49) produced a generalized graphical correlation for shape regimes of bubbles and drops in terms of dimensionless parameters. The correlation is shown in Fig. 6, where the dimensionless parameters are defined as follows:

$$Eo = \frac{g \cdot \Delta\rho \cdot d_b^2}{\sigma} = \text{Eotvos number} \tag{120}$$

$$Mo = \frac{g \cdot \mu^4 \cdot \Delta\rho}{\rho^2 \cdot \sigma^3} = \text{Morton number} \tag{121}$$

$$Re = \frac{\rho \cdot d_b \cdot u}{\mu} = \text{particle Reynolds number} \tag{122}$$

where $g$ = gravitational acceleration [$m/s^2$]

$\Delta\rho$ = $|\rho_p - \rho|$, absolute density difference between particle and continuous phase [$kg/m^3$]

$d_b$ = equivalent bubble diameter = $[(6 \cdot V_b)/\pi]^{1/3}$

$r$ = bubble radius ($d_b/2$)

$\sigma$ = surface tension in continuous phase [$kg \cdot m^{-1} \cdot s^{-2}$]

$\mu$ = viscosity of continuous phase [$kg \cdot m \cdot s^{-1}$]

$u$ = velocity of particle relative to remote continuous phase [m/s]
$\equiv$ terminal bubble rise velocity = $u_b$

The Eotvos number is the ratio of the Weber number to the Froude number, that is:

$$Eo = \frac{\text{gravity forces}}{\text{interfacial tension forces}} \tag{120a}$$

In the literature, the Morton number (44) is often simply referred to as the M-group, and its inverse as the P-group.

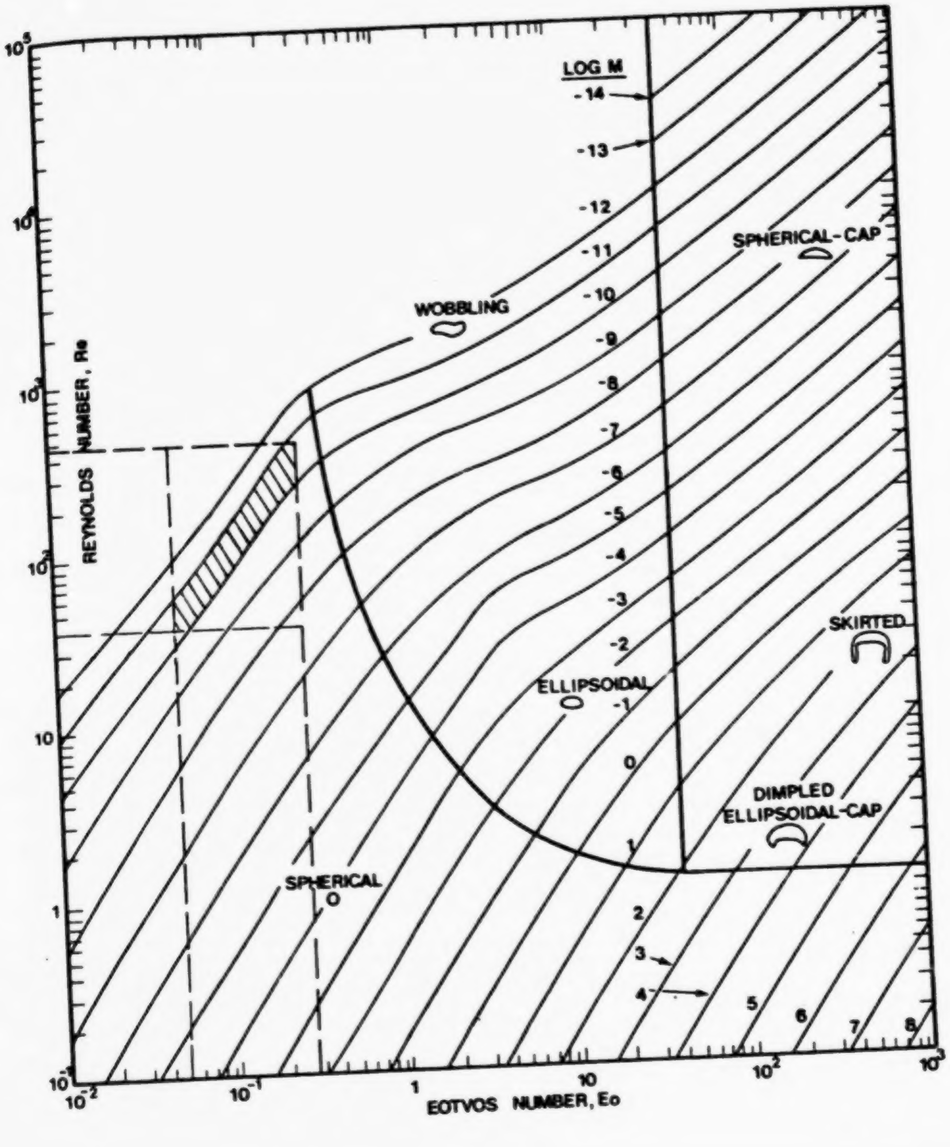

Figure 6. Shape regimes for bubbles and drops in unhindered gravitational motion through liquids (from 49).

The Morton number for pure water at 20°C as the continuous phase is $Mo \approx 2.56 * 10^{-11}$ or $\log Mo = -10.6$. According to Fig. 6, the transition from spherical to ellipsoidal shape occurs at $Eo \approx 0.35$, corresponding to a bubble diameter of approximately 1.6 mm. Small bubbles, $d_b \leq 1.2$ mm ($Eo \leq 0.20$), act like rigid spheres, and their path of rise is virtually rectlinear, whereas larger bubbles, $1.2 \leq d_b \leq 17$ mm ($0.2 \leq Eo \leq 40$), with increasing diameter show increasingly an ellipsoidal shape and rise in a helical or zig-zag manner. This is equivalent to an increasing internal circulation; spherical bubbles have little internal circulation, while larger bubbles show a vigorous (toroidal) internal circulation (49,50). The Reynolds number for which bubbles still can be considered spherical is approximately $Re < 300$ (49,51).

The effect of surface-active contaminants is to lower the surface tension, $\sigma$. In this situation log Mo becomes larger, and the internal circulation may be reduced markedly, causing the bubbles to act more like rigid spheres even at larger diameters.

Bubble Rise Velocity--

Good agreement is found in the literature in regard to bubble rise velocity of single bubbles, as is shown in Fig. 7.

From Fig. 7 the great effect of contaminants on the terminal velocity is also evident, particularly for $0.8 \leq d_b \leq 10$ mm. The rising velocity of a swarm of bubbles will be lower than for single bubbles, the deviations being larger with increasing gas holdup (51-53).

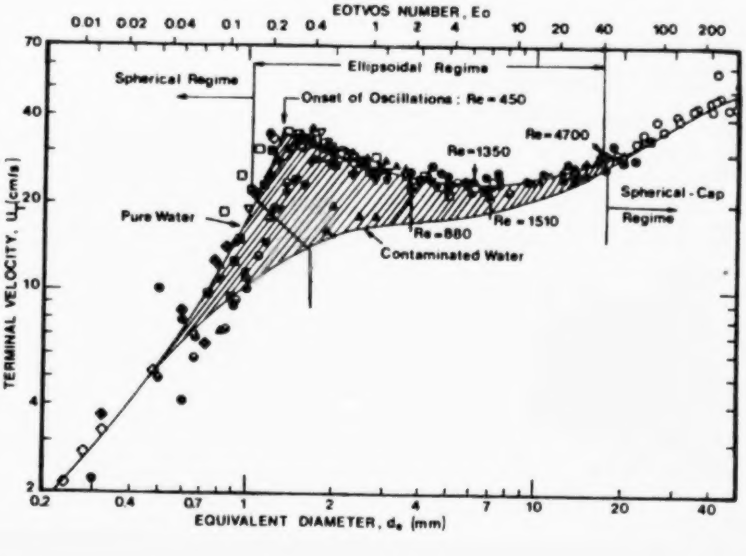

Figure 7. Terminal velocity of air bubbles in water at 20°C (49).

Gas Holdup--

The volumetric gas holdup ratio, $\varepsilon_G$, is strongly dependent on the configuration of the bubbling device (40,42,46,47). Nevertheless, all correlations show a linear dependence of $\varepsilon_G$ on the superficial gas velocity, for $\varepsilon_G \leq 0.15$. Only Akita and Yoshida (40), however, give an explicit correlation in terms of dimensionless groups.

Another parameter of interest is the specific area of the gas bubbles, a, which is equivalent to the available area for mass transfer. Although this parameter has also been correlated, it is defined explicitly by:

$$a = \frac{6 \cdot \varepsilon_G}{d_b} \tag{123}$$

Therefore, if $\varepsilon_G$ is known or estimated with an appropriate correlation, the specific interfacial area can be calculated using Eq. 123.

Mass Transfer Coefficient--

The mass transfer coefficient, $k_L$, has been related to the bubble diameter by several workers (40,41,50,54,55). When large bubbles were studied (40,55) a linear relationship of $k_L$ vs $d_b$ was found. However, when small bubbles were involved, Calderbank et al. (54) found two distinct regions for $k_L$ (Fig. 8). For small bubbles, $d_b \leq 0.8$ mm, and for large bubbles, $d_b \geq 2$ mm, $k_L$-values were independent of $d_b$, while for the intermediate size a rather sharp transition was observed.

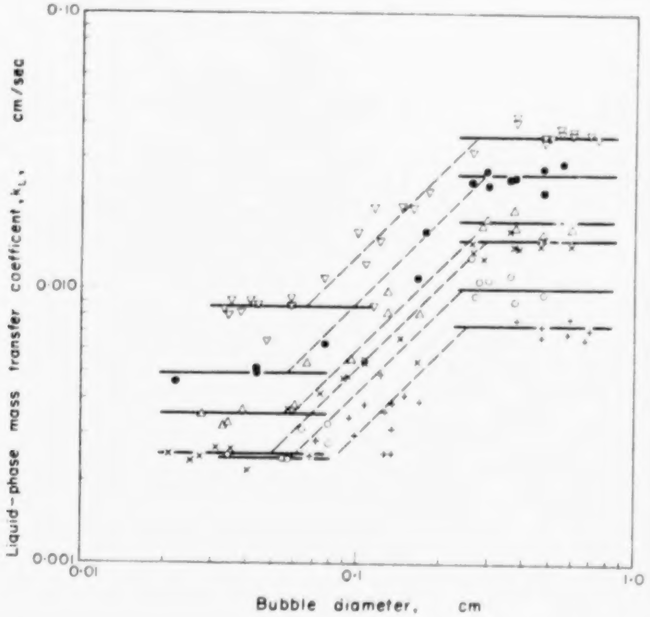

Figure 8. Transition from "large" bubble to "small" bubble mass transfer coefficients (from 54).

Similar results have been observed by Garner et al. (50) and by Schulman et al. (46) for the dependence of $k_L$ on the gas flow rate. The former authors also show that the transition region can be shifted towards larger diameters by addition of small quantities of surface-active materials.

## Boundary-Layer Theory and Mass Transfer Coefficients

The physical basis of the boundary-layer theory is that irreversible transport processes occur nearly exclusively within a thin layer of fluid. This is the same basis as used previously for the two-film theory.

Many correlations which employ dimensionless groups can be found in the literature, as reviewed by Griffith (56) and Yaron and Gal-Or (57). If the film thickness $\delta$ has any physical meaning, it must depend on the hydrodynamics of the system under consideration, and hence on the Reynolds number. Moreover, the fluid characteristics are also expected to play a major role; the Schmidt number accounts for these factors. The third dimensionless group, the Sherwood number, incorporates the mass transfer coefficient. Hence, the functional equation for forced-convection mass transfer (34) is

$$Sh = c_1 \cdot Re^{c_2} \cdot Sc^{c_3} \qquad (124)$$

where

$$Sh = \frac{k \cdot d}{D_{AB}} \equiv \text{Sherwood number [dimensionless]} \qquad (125)$$

$$Re = \frac{u \cdot d}{\nu} \equiv \text{Reynolds number [dimensionless]} \qquad (126)$$

$$Sc = \frac{\nu}{D_{AB}} \equiv \text{Schmidt number [dimensionless]} \qquad (127)$$

$$Pe = Re \cdot Sc \equiv \text{Peclet number [dimensionless]} \qquad (128)$$

It is understandable that a large array of values for $c_1$, $c_2$, and $c_3$ have been reported in the literature, if one only considers the complexity of the hydrodynamics of an ensemble of gas bubbles rising through a liquid column, as in the bubble column experiments in this work.

### Liquid Phase--

The fluid dynamics of viscous flow through assemblages consisting of a large number of spherical solid particles, drops and bubbles in the presence or absence of surfactants has been formulated by Gal-Or and Waslo (58) and Gal-Or (52). Although the analytical treatment accounts only for viscous forces, i.e. low bubble Re, it will apply to systems with considerably higher Re, since at higher particle concentration the boundary-layer separation (especially for particles with strong internal circulation) is less pronounced. The validity of this assumption has been demonstrated by Pfeffer (59) and LeClair and Hamielec (60). In a subsequent article, Waslo and Gal-Or

(53) treated the problem of convective heat and mass transfer employing principles of the boundary-layer theory described above (52,58). A second constraint in Waslo and Gal-Or's solution, besides low particle Re, is Pe >> 1, or since $Pe = Re \cdot Sc$, $Sc >> 1$, i.e., most Newtonian liquids. Waslo and Gal-Or (53) claimed to have solved the controversy regarding the correct exponents to which the Re and Sc numbers should be raised, $c_2$ and $c_3$ in Eq. 124, by considering different degrees of internal circulation within the bubbles. They found

$$Sh \propto Re^{1/3} \cdot Sc^{1/3} \tag{129}$$

for particles with no internal circulation, e.g. solid particles. Small bubbles or bubbles contaminated with surface-active materials behave approximately like solid particles, in that the tangential velocity at the interface is nearly zero (no slip condition). For drop or bubble assemblages where strong internal circulation occurs, i.e., in highly purified systems, Waslo and Gal-Or (53) found

$$Sh \propto Re^{1/2} \cdot Sc^{1/2} \tag{130}$$

Since these correlations refer to the continuous phase, i.e., in our case the liquid phase surrounding the gas bubbles, in terms of mass transfer coefficients Eqs. 129 and 130, respectively, translate into

$$k_L \propto D_L^{2/3} \quad \text{(no internal circulation)} \tag{131}$$

and

$$k_L \propto D_L^{1/2} \quad \text{(strong internal circulation)} \tag{132}$$

While the above analysis is strictly valid only for ensembles of particles of uniform size, Yaron and Gal-Or (57) extended it for total average convective transfer in size-distributed populations. Their equations 37 and 38 show the same dependence as those of Eqs. 131 and 132. In their analytical development Yaron and Gal-Or (57) give explicit solutions for the thin concentration boundary-layer thickness $\delta$.[†] When substituting these expressions directly into the two-film model mass transfer coefficient, $k_L = D_L/\delta_L$, again the same dependence of Eqs. 126 and 127 appear.

For intermediate levels of internal circulation the analytical solution, as given by Yaron and Gal-Or (57), takes the form

$$c_1 \cdot Sh^{-2} + c_2 \cdot Sh^{-3} = Pe^{-1} \tag{133}$$

---

[†] In the original paper (57), Pe is erroneously shown as being raised to the $-1/2$ power. Instead Pe should be raised to the $-1/3$ power (p. 732, right column, third expression from top). This can easily be verified by analyzing the prior expressions in that paper, and is consistent with a subsequent paper by the same authors (61).

Equation 133 reduces to Eqs. 130 and 131 evaluated at each limit, and gives

$$k_L \propto D_L^{1/2} \text{ to } D_L^{2/3} \quad \text{(for intermediate internal circulation)} \tag{134}$$

The approach of mass transfer from and into assemblages of freely rising bubbles by means of boundary-layer theory provides some very interesting results. That is, the controversy whether the mass transfer coefficient is linearly proportional to the diffusion coefficient, as proposed in the film theory, or whether proportional to the square root of the diffusion coefficient, as proposed in the penetration and surface-renewal theories, is resolved to a certain extent. We have shown that also the boundary-layer theory predicts $k_L \propto D_L^{1/2}$ for clean systems according to Eq. 130, while for contaminated systems (or small, clean bubbles) it predicts $k_L \propto D_L^{2/3}$ according to Eq. 129. Therefore, it appears that the exponent of the diffusion coefficient ought to lie between $1/2$ and $2/3$, instead of between $1/2$ and 1, thus narrowing the difference considerably.

It must be emphasized that the above discussion is strictly applicable for systems with $Pe \gg 1$ and low bubble Re, implying $Sc \gg 1$, i.e., the liquid phase ($Sc \simeq 10^3$) in our case. It would be of interest to know if the developed relations hold also for large bubble Re. Ruckenstein (62) made a similar analysis for single bubbles for $Re \ll 1$ and $Re \gg 1$. His results give the same dependencies for all three cases of internal circulation as found above, suggesting that these are valid for the entire range $0 < Re < \infty$ when $Pe \gg 1$.

Gas Phase--

In order to make the analysis complete, a similar approach would be useful for the gas phase. This appears to be considerably more difficult, because the velocity field inside a gas bubble remains to be described. Since no attempts to solve or quantify this task are known to exist in the literature, perhaps the analogy of liquid drops falling through gases might give some insights. In this case the continuous phase is the gas. Such systems have the characteristics of low Schmidt numbers, i.e., $Sc \simeq 1$. Of particular interest would be the evaporation of water drops. As this process is virtually completely gas-film-controlled, we can be assured that the gas-phase mass transfer coefficient is under consideration.

Griffith (56) lists a table with several correlations based on boundary-layer theory for systems with $Sc \simeq 1$ and Re from 0 to 2500, including three for evaporating water drops. Notably, all these correlations take the form

$$Sh \propto c_1 + c_2 \cdot Re^{1/2} \cdot Sc^{1/3} \tag{135}$$

which indicates

$$k_G \propto D_G^{2/3} \tag{136}$$

if the first term on the right-hand side of Eq. 135 is negligible, i.e., in turbulent flow. Kinzer and Gunn (63) derived an equation for the rate of evaporation of free-falling water drops of the form

$$\frac{dm}{dt} \propto r \cdot \Delta\rho \cdot \left(D_G + f \cdot D_G^{1/2}\right) \qquad (137)$$

where r is the drop radius. When this expression is rearranged to

$$\frac{dm}{dt} \propto r \cdot \Delta\rho \cdot \left(g \cdot D_G^{\Omega}\right) \qquad (138)$$

fitting the experimental results, as was done by Stewart (64), the exponent $\Omega$ is found to be $\Omega = 0.59$ for $r = 0.7$ mm and $\Omega = 0.56$ for $r = 1.5$ mm, i.e., $1/2 \leq \Omega \leq 2/3$.

Moreover, Toor and Marchello (20) note that: "at low Schmidt numbers the steady (concentration) gradient is set up very rapidly in any new surface element, so that unless the rate of renewal is high enough to remove a large fraction of surface elements before they are penetrated, most of the surface is old. Steady state transfer then takes place through what is essentially a film and the effect of surface renewal is negligible." This means that unless the rate of surface renewal is very high, systems with low Sc would follow the boundary-layer modification of the two-film theory, i.e., $1/2 \leq \Omega \leq 2/3$.

Also, Clift et al. (49) state: "... the thin concentration boundary layer approximation formally requires $Pe \to \infty$, which for most practical situations means $Sc \to \infty$ for any finite Re. Surprisingly, this approximation is often reasonable down to Sc of order unity." This was confirmed by Calderbank and Moo-Young (54). Figure 9 clearly shows that mass transfer coefficients for "large" and "small" bubbles approach each other at low values of Sc. Moreover, their work also give strong support to the earlier analysis of liquid-phase mass transfer. Although the authors generally refer to liquid- (continuous) phase mass transfer coefficients, they include the data of Kinzer and Gunn (63), which, as mentioned earlier, refers to the gas phase. Therefore, Calderbank and Moo-Young's work (54) also leads to expressions analogous to Eqs. 131 and 132:

$$k_G \propto D_G^{1/2} \qquad \text{for strong internal circulation ("large" drops and bubbles)} \qquad (139)$$

and

$$k_G \propto D_G^{2/3} \qquad \text{for no internal circulation ("small" drops and bubbles)} \qquad (140)$$

It is hard to draw any definitive conclusion on the correct exponent of the diffusion coefficient for gas-phase controlled mass transfer. Although most correlations given by Griffith (56) give $Sh \propto Sc^{1/3}$, it is fair to point out that since $Sc \simeq 1$, this quantity is very insensitive when comparing it raised to the $1/3$ and $1/2$ powers, suggesting that some data might be fitted as well with

$$Sh \propto b + a' \cdot Re^{1/2} \cdot Sc^{1/2} \qquad (141)$$

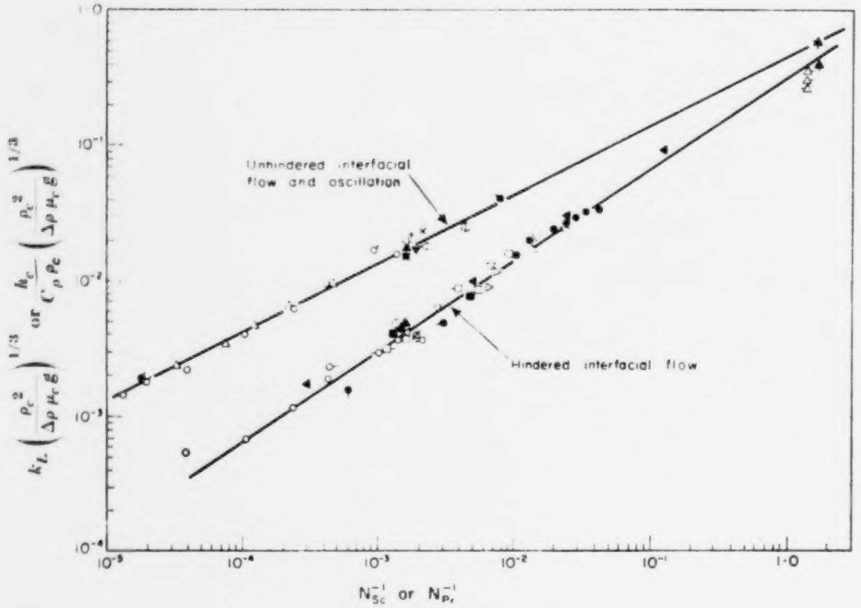

Figure 9. Correlation of heat and mass transfer coefficients for dispersions of bubbles and spheres (54). Lower line--small bubbles and rigid spheres; upper line--large bubbles.

as with Eq. 135. This is confirmed by Calderbank and Moo-Young (54) and is evident from Fig. 9. In view of the analogy of falling water drops in air with rising air bubbles in water, one is tempted to conclude that the gas-phase relationships should be similar to the liquid-phase relationships (Eqs. 131 and 132). That is,

$$k_G \propto D_G^{1/2} \qquad \text{for strong internal circulation} \qquad (142)$$

$$k_G \propto D_G^{2/3} \qquad \text{for no internal circulation} \qquad (143)$$

and

$$k_G \propto D_G^{1/2} \text{ to } D_G^{2/3} \qquad \text{for intermediate internal circulation} \qquad (144)$$

# SECTION 5

# EXPERIMENTAL METHODS

## SURFACE AERATION EXPERIMENTS

### Reactor for Preliminary Experiments

The aeration device consisted of a cylindrical glass vessel with an open top (Fig. 10). To assure adequate mixing, four stainless steel baffles were inserted into the tank, with a baffle width of $^1/_8$ the tank diameter. The vessel height and width were both 28 cm; the total volume was 14 liters. Two baffles were used as supports for diffusers to purge oxygen from the water prior to the experiment. The oxygen probe was attached to a third baffle in such a manner that the height of the probe could be adjusted to different water levels. The reactor volume was 12 liters, which is equivalent to a water depth of 210 mm. The stirrer was a pitched, two-blade impeller with a diameter of 135 mm and a width of 37 mm.

### Modified Reactor

For the main block of surface-aeration experiments, the reactor vessel and baffles were the same as in the preliminary experiments (Fig. 10), but the impeller was exchanged and the reactor volume reduced (Fig. 11). These changes were undertaken to permit operation over a wider range of mixing conditions, while minimizing problems of poor bulk mixing at the one extreme and of vortex formation at the other extreme. The reactor volume in these experiments was 7.3 liters, which is equivalent to a water depth of 120 mm. This reduction of the water level below the maximum volume was necessary to assure adequate freeboard.

The stirrer was a hybrid of a ring-guarded surface turbine with three pitched blades (diameter 75 mm) and a single flat-bladed subsurface impeller (diameter 90 mm). The latter was installed to assure adequate mixing of the bulk liquid at low speeds. The stirrer speed was adjusted by means of a voltage regulator, and monitored by an electronic counter connected to a reed switch fitted onto the stirrer shaft.

### Exhausting of Surrounding Air

All of the surface aeration experiments were conducted in a fume hood with forced exhaust. The hood was rated at 0.4 $m^3$/min air exhaust rate. This corresponds to linear air velocities on the order of 0.8 m/s in the vicinity of the surface aeration contactor.

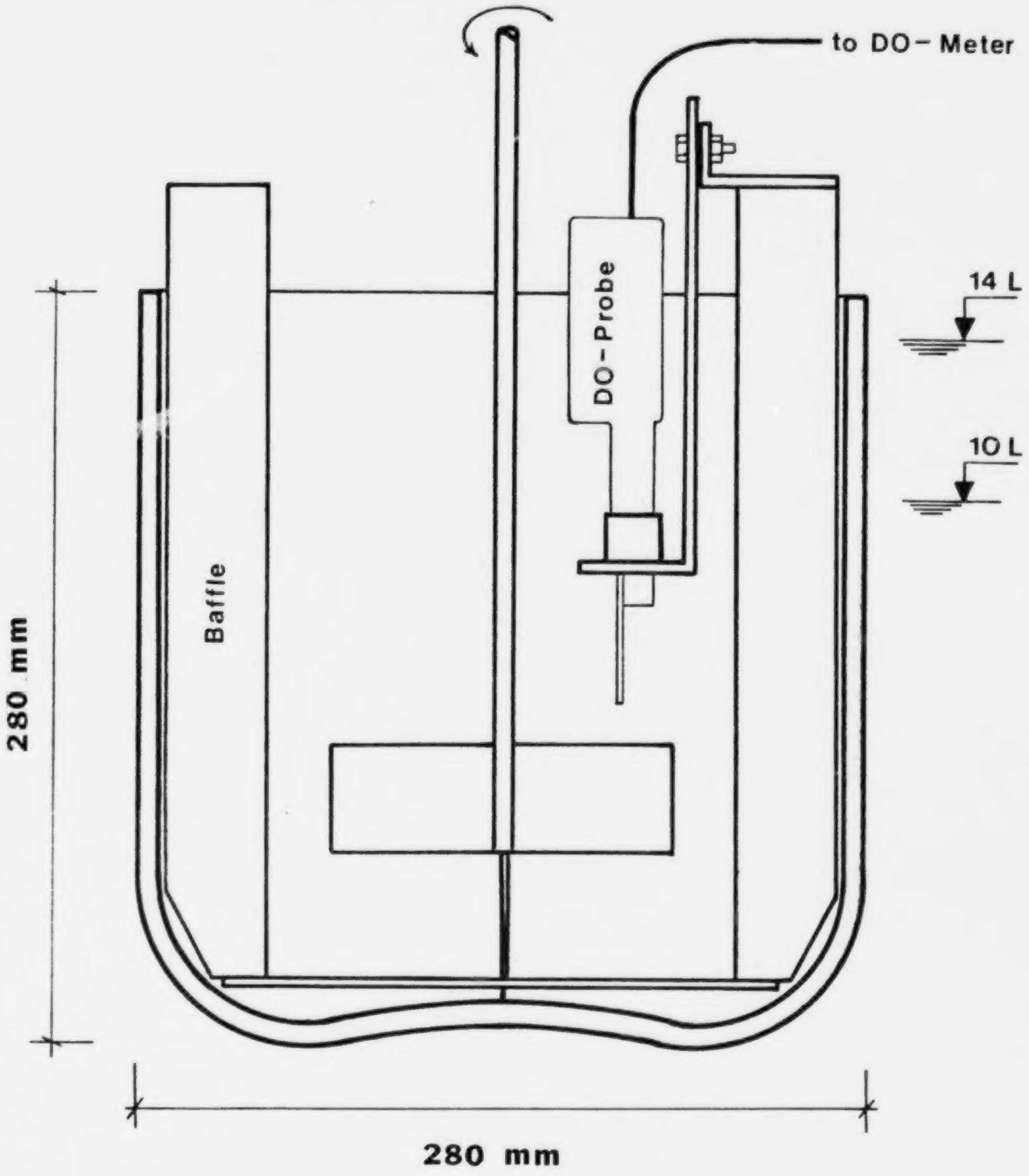
to DO- Meter
DO-Probe
14 L
10 L
Baffle
280 mm
280 mm

Figure 10. Surface aeration contactor used in preliminary experiments.

Preliminary Experiments

The series consisted of a set of six experiments with halogenated aliphatic compounds, conducted in triplicate. In five experiments Milli-Q water was used; for the remaining experiment Palo Alto secondary effluent (PASE) was taken. The stirring speed ranged from 65 rpm to 230 rpm (Table 1).

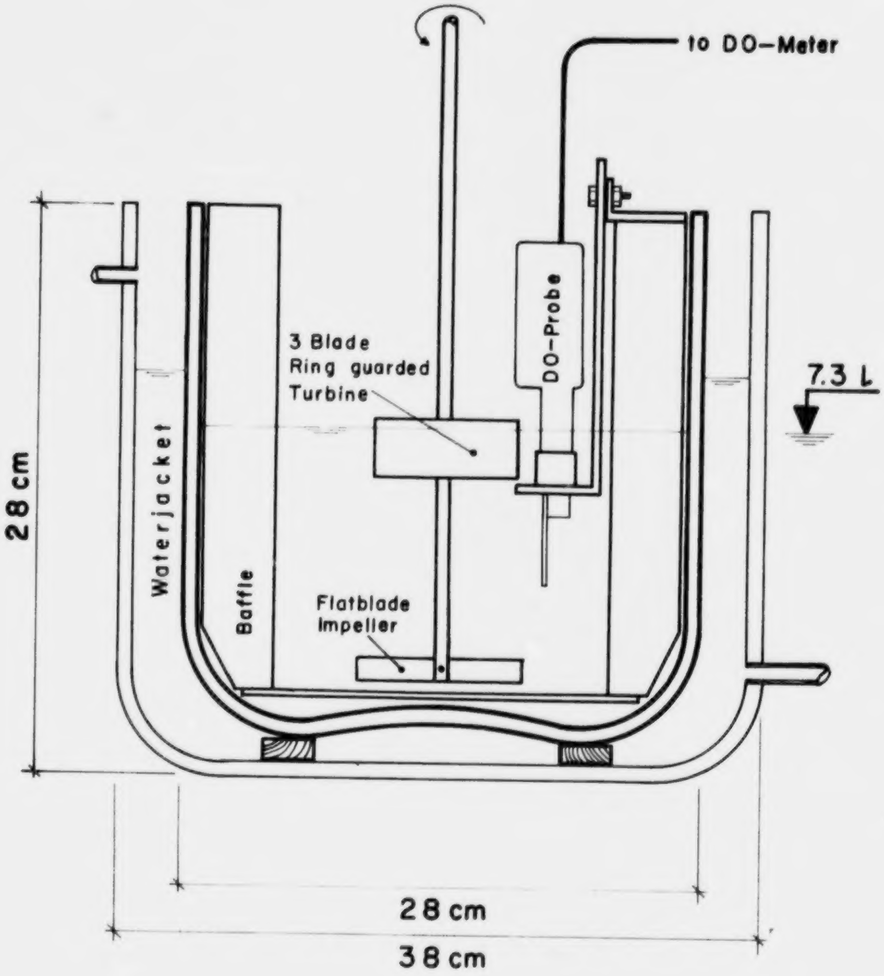
to DO–Meter
DO–Probe
3 Blade
Ring guarded
Turbine
7.3 L
28 cm
Waterjacket
Baffle
Flatblade
Impeller
28 cm
38 cm

Figure 11. Modified surface aeration contactor.

TABLE 1. ORDER OF PRELIMINARY SURFACE AERATION EXPERIMENTS

| rpm | 65 | 140 | 190 | | 230 |
|---|---|---|---|---|---|
| Temp. | 20°C | 20°C | 20°C | 7°C | 20°C |
| Solvent: | | | | | |
| Milli-Q | 8<br>9<br>15 | 5<br>6<br>17 | 4<br>7<br>13 | 12<br>14<br>16 | 1<br>2<br>3 |
| PASE | | | 10<br>11<br>18 | | |

It was not possible to do any experiments with sea water because of erratic oxygen data, probably owing to the influence of the high ionic strength on the oxygen probe. Besides the initial 18 experiments, two more were conducted with chlorinated benzenes at 20°C and 190 rpm.

## Main Set of Experiments

The entire series consisted of a set of ten experiments conducted in duplicate. In eight experiments Milli-Q water was used; for the other two experiments Palo Alto secondary effluent (PASE) was taken. The experiments were conducted in random order to avoid bias. The stirring speed ranged from 65 rpm to 375 rpm. Below 65 rpm complete mixing could not be guaranteed. At speeds higher than 375 rpm large amounts of air bubbles were present in the water, i.e., there was a mixed mode of surface and bubble aeration. Table 2 shows the range of speeds and the order in which the experiments were run.

TABLE 2. ORDER OF MAIN SERIES OF SURFACE AERATION EXPERIMENTS

| rpm | 65 | 135 | 180 | 250 | 280 | 315 | 350 | 375 |
|---|---|---|---|---|---|---|---|---|
| Type of Water: | | | | | | | | |
| MILLI-Q | 2 | 8 | 10 | 3 | 7 | 12 | 5 | 1 |
| | 4 | 17 | 15 | 14 | 18 | 16 | 19 | 11 |
| PASE | | | 6 | | 13 | | | |
| | | | 9 | | 20 | | | |

## Experimental Procedure

After the water had been equilibrated to a constant temperature of 20 ± 0.2°C, the oxygen was purged from the system by bubbling nitrogen through the vessel. The agitator speed was adjusted to the desired value by means of a rheostat and stroboscope (Appendix B). Thereafter the reactor was spiked with a solution of the following six compounds: Freon-12, $CCl_2F_2$; chloroform, $CHCl_3$; 1,1,1-trichloroethane, $CCl_3CH_3$; carbon tetrachloride, $CCl_4$; trichloroethylene, $CHCl{=}CCl_2$; and tetrachloroethylene, $CCl_2{=}CCl_2$. Their properties are summarized in Appendix A. These six compounds were chosen because their Henry coefficients (estimated from vapor pressure and solubility data according to Eq. 15) cover a range of nearly three orders of magnitude from $3.1 \times 10^{-3}$ $[atm \cdot m^3 \cdot mol^{-1}]$ to 1.5 $[atm \cdot m^3 \cdot mol^{-1}]$; hence, they are classified as highly volatile.

The spiking solution was made up by bubbling Freon-12 gas through 5 ml methanol until about 100 mg had absorbed; then the remaining five compounds were added to the methanol with a syringe: chloroform, 45 μl; trichloroethane, 50 μl; carbon tetrachloride, 45 μl; trichloroethylene, 50 μl; and tetrachloroethylene, 40 μl. Thereafter methanol was added to make up a total amount of 10 ml. For the internal standard, 4.6 μl dibromoethane was added to 100 ml pentane.

For the experiments with chlorinated benzenes, the compounds chlorobenzene, o-, m-, and p-dichlorobenzene (DCB), were chosen because their Henry coefficients are lower than chloroform and their molecular structure is different from those of the first six compounds. The chlorinated benzene spike solution was made up by adding 217 µl chlorobenzene, 186 µl m-dichlorobenzene, 240 mg p-dichlorobenzene, and 184 µl o-dichlorobenzene to 10 ml methanol. The appropriate internal standard was prepared by adding 26.4 mg trichlorobenzene into 10 ml methanol. After 1 min of mixing following introduction of the organic compounds, an initial sample was taken. Thereafter nine additional samples were taken at regular intervals. Concurrently, the oxygen concentration in the reactor was measured with a dissolved oxygen (DO) probe (Yellow Springs Instruments, Model 5720A) and plotted on a chart recorder. The sample intervals differed: 1 hr for the lowest speed vs 1 min for the highest speed. The concentration difference between the first and the last sample normally was one order of magnitude. The sample was drawn from the reactor with a large Mohr pipette under a slight vacuum and then transferred into a 15-ml hypovial and sealed with teflon-faced rubber septum. Thereafter the vials were stored at 4°C until they were analyzed; analysis generally was performed within 1 day.

## BUBBLE COLUMN EXPERIMENTS

### Apparatus

The overall set-up is shown in Fig. 12. The apparatus was composed of a bubble column aeration device with appurtenances to supply a gas stream to the column and to sample the water in it.

The aeration device consisted of a glass column fabricated in two pieces. The column diameter, 22.5 cm (9 inches), was chosen large enough to minimize wall effects. The column is shown to scale in Fig. 13. The diffuser was a sintered glass filter (Corning 36060, porosity medium M) of 15 cm diameter, of which the upper cylinder was cut off and the bottom end adapted with a ground-glass joint. Through the bottom of the column an inlet pipe was attached to the other end of the glass joint with flanges. The column was high enough to allow variable liquid volumes: initial volumes were varied from 14 to 24 liters; the corresponding liquid depths were 35 cm to 60 cm.

The oxygen probe was attached to a supporting glass rod and was positioned inverted (membrane upward) to avoid attachment of bubbles at the sensing membrane, at 1/3 of submergence. An inverted U-tube was used to withdraw samples for organic analysis. The pressure difference was sufficient to draw the sample within less than 10 sec. The sampling point was always within 2 cm of the oxygen probe tip, and the end of the sampling tube was also inverted (upwards) to avoid excessive bubbles in the sampling line.

The air and nitrogen were supplied from cylinders. The nitrogen was used to strip the oxygen from the water. The air flow rate was measured with two rotameters (Matheson Models 602 and 603), corresponding to air flow rates of 0.05 to 0.8 ℓ/min and 0.2 to 4.6 ℓ/min at 101 kPa (14.7 psia). A pressure gauge was installed between the two rotameters. The pressure at the

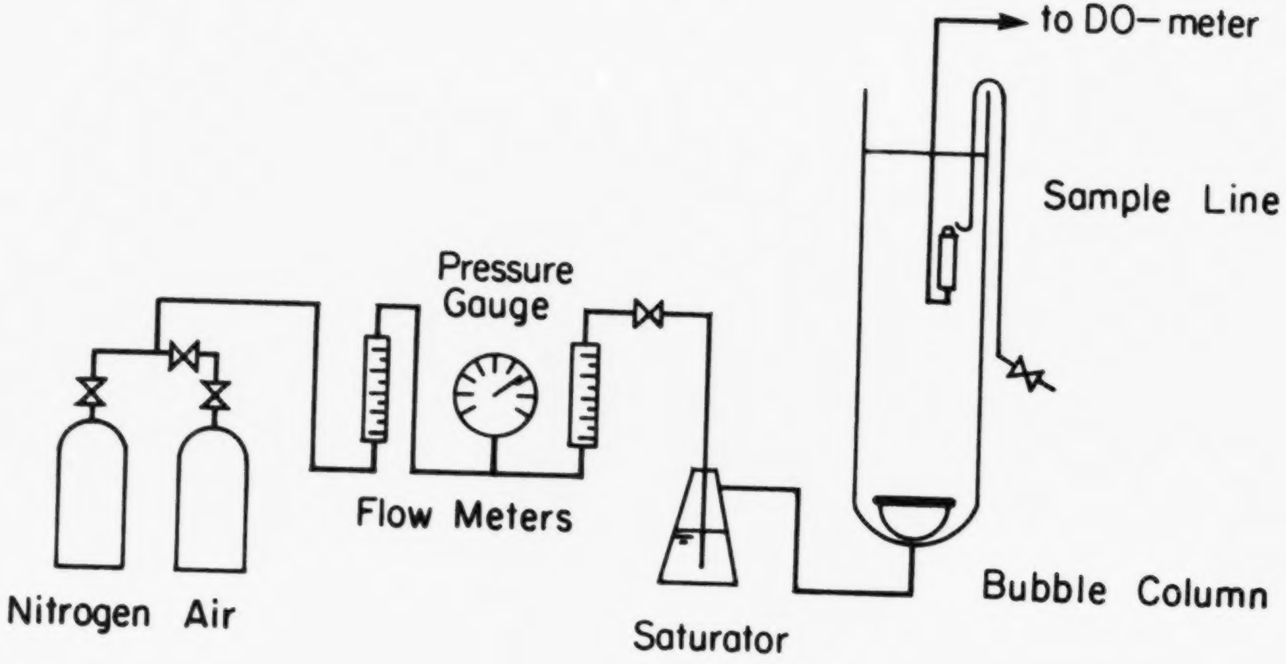
to DO– meter
Sample Line
Pressure Gauge
Flow Meters
Nitrogen
Air
Saturator
Bubble Column

Figure 12. Schematic diagram of bubble column and appurtenances.

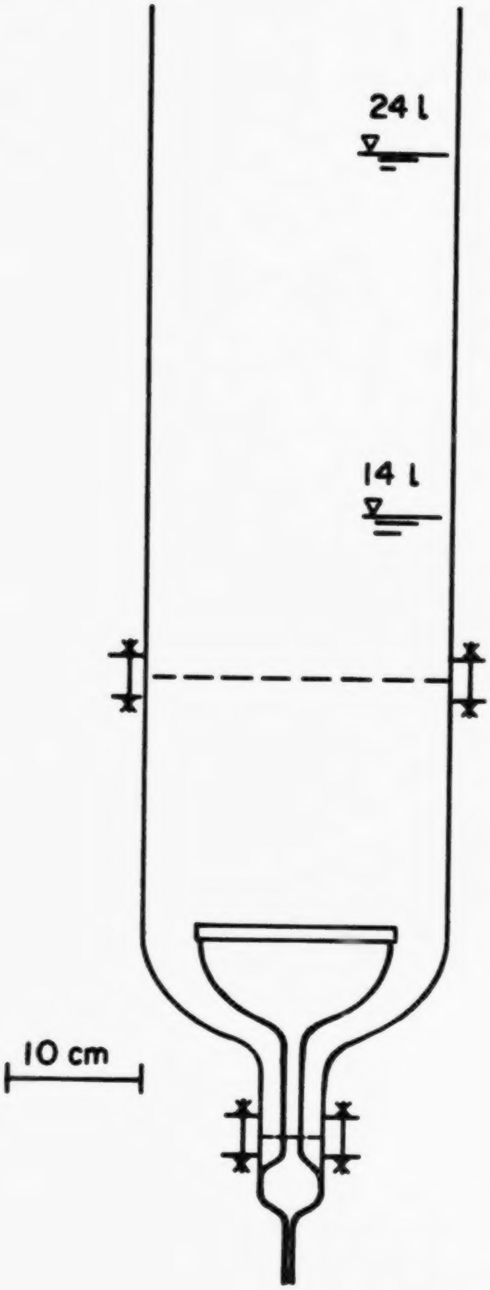
24 l
14 l
10 cm

Figure 13. Bubble column.

rotameters was always set at 142 kPa ± 0.7 (6.00 psig ± 0.1). The rotameters were calibrated at 142 kPa (6 psig) with a soap bubble meter at low flows (< 0.9 ℓ/min) and with a wet-test meter for flows > 0.8 ℓ/min. Towards the end of the study, a mass flow meter (Matheson, Model 8160-0433, range 0.6-3.0 ℓ/min, accuracy ± 1%) was used to assure the accuracy of the prior calibrations. A needle valve at the outlet of the air cylinder and a valve after the rotameters allowed regulation of pressure and flow. In order to avoid excessive evaporation, the air was passed through a saturator, after which it was directed to the diffuser at the bottom of the column.

### Experimental Design

Two sets of experiments were carried out. The first was a set of eight experiments conducted in duplicate at four differing combinations of initial liquid volume and gas flow rate. The other set consisted of three duplicate experiments at the same initial liquid volume and gas flow rate and three different concentrations of methanol. To avoid bias, the experiments within each set were conducted in random order. Initial liquid volumes were 14 ℓ, 18 ℓ, 21 ℓ, and 24 ℓ, and gas flow rates varied from 0.2 ℓ/min to 2.7 ℓ/min, thus covering a broad range of hydrodynamic conditions. When methanol concentrations were varied, the initial volume was 21 ℓ and the gas flow rate approximately 0.23 ℓ/min. The order of the experiments is given in Tables 3 and 4.

After these two sets of experiments, two more runs were conducted in which methanol at the highest concentration was added at midpoint of the experiment. All experiments were conducted in purified water: distilled water was further purified by passing through a "Milli-Q, Reagent-Grade Water System," described below. However, the addition of methanol as a solvent for the organic solutes increased the overall concentration of organic matter, measured as carbon, to an amount of approximately 10 to 15 mg/ℓ in the variable gas flow experiments, and 12 mg/ℓ and 120 mg/ℓ (mole fraction = $1.8 \times 10^{-5}$ and $1.8 \times 10^{-4}$, respectively) in the experiments with variable methanol concentration.

TABLE 3. ORDER OF BUBBLE COLUMN EXPERIMENTS WITH DIFFERING INITIAL LIQUID VOLUME AND GAS FLOW RATE

| Initial Liquid Volume [liter] | | | |
|---|---|---|---|
| 14 | 18 | 21 | 24 |
| 2 | 3 | 1 | 5 |
| 8 | 6 | 4 | 7 |
| 2.68 | 0.86 | 0.23 | 0.20 |
| Gas Flow Rate [liter/min] | | | |

TABLE 4. ORDER OF BUBBLE COLUMN EXPERIMENTS WITH DIFFERING METHANOL CONCENTRATION

| Methanol Concentration [mole fraction] | | |
|---|---|---|
| 0 | $1.8\times10^{-5}$ | $1.8\times10^{-4}$ |
| 3 | 2 | 1 |
| 4 | 6 | 5 |

## Experimental Procedure

The Milli-Q water was transferred into the column with a 2-liter graduated cylinder to the desired volume on the day prior to the experiment. Then a small gas flow (approximately 0.05 ℓ/min) was applied to equilibrate the temperature of the water as well as to avoid backflow into the air line. To assure similar conditions in all runs, the conductivity was adjusted to an ionic strength of $10^{-4}$M by adding KCl after having installed the oxygen probe and sampling line. Conductivity measurements were made with a conductivity meter (Radiometer Copenhagen CDM3, cell: type CDC 304, nominal cell constant 1.0 cm). The KCl addition of 7.87 mg/ℓ ± 0.21 resulted in the desired ionic strength, which corresponds to a conductivity of $1.5 \times 10^{-5}$ S. A thermometer was suspended in the column to measure initial and final temperatures.

First, the air flow was adjusted to the desired rate. Then the air line was closed with a valve and nitrogen was bubbled through the column until the oxygen concentration dropped to approximately 0.5 mg/ℓ. Subsequently the nitrogen supply was shut off and the air line was reopened. Approximately 1 to 2 min were allowed for equilibration of the air flow. Thereafter, the column was spiked with a solution of the following six compounds: dichlorodifluoromethane (Freon-12), $CCl_2F_2$; chloroform, $CHCl_3$; 1,1,1-trichloroethane, $CH_3CCl_3$; carbon tetrachloride, $CCl_4$; trichloroethylene, $CHCl{=}CCl_2$; and tetrachloroethylene, $CCl_2{=}CCl_2$. These compounds were chosen based on the volatility criterion described in Section 4 ($H_c > 0.12$) and because their calculated Henry coefficients cover a range of approximately 2-½ orders of magnitude from $0.13 \leq H_c \leq 62.1$; hence, they may be considered as highly volatile. The solutes were usually dissolved in methanol and approximately 0.85 ml was added with a syringe. If no methanol was used, the solutes were dissolved in oxygen-deficient Milli-Q water in a 2-ℓ flask, and this solution was added immediately after reopening the air line.

Initial concentrations ranged from 340 µg/ℓ to 2500 µg/ℓ randomly, except that for $CCl_2F_2$ the initial concentrations varied from 1350 µg/ℓ to 13,000 µg/ℓ. After one minute of mixing, the initial sample was taken. Thereafter 12 to 13 additional samples were taken. Concurrently the oxygen concentration in the column was measured with a dissolved oxygen (DO) probe (YSI, Model 5739) and plotted on a chart recorder. The run time varied from 29 min to over 6 hrs. The sampling intervals were slightly shorter at the beginning of a run due to the larger driving force for volatilization, and ranged from 2 min for short runs to 39 min for long runs. Three or four additional samples in the initial part were taken only for $CCl_2F_2$ analysis. This was necessary to obtain 8 to 9 data points before Freon-12 was completely stripped, because of the extreme volatility of the compound.

The sample volume was approximately 50 ml. Enough time was allowed for the sampling line to flush completely before taking a sample. After each sample the volume loss was recorded. The sample was collected in a 15-ml hypovial and sealed with a teflon-faced rubber septum. Thereafter, the vials were stored at 4°C and analyzed within 24 hrs. At the end of each run three samples were taken in 125-ml stoppered flasks and analyzed for DO with the Winkler method. For data analysis mean values of initial and final temperature and liquid volume were used.

## VAPOR-LIQUID EQUILIBRIUM (VLE) MEASUREMENTS

Four measurements were conducted in duplicate in an environmental chamber at 25°C. A solution spiked with the six organic compounds was transferred into 50-ml syringes. Samples were collected in 15-ml hypovials to which 1 ml pentane was added prior to sampling. The sample was withdrawn from the syringe by "injecting" the liquid below the pentane phase. The vial was filled until the pentane formed a large cap at the top. Inevitably some pentane overflowed during the closing of the vial. The initial sample was taken when the syringe was full. Then, further liquid was expelled until a desired volume remained in the syringe. Subsequently, a desired amount of air was drawn into the syringe. The needle was then closed with a rubber stopper. One day was allowed for equilibration between liquid and gas phase. The syringes were shaken 3 to 4 times during this time. Before taking the final sample the air in the syringe was expelled.

## PREPARATION OF WATER

Municipal tap water contains appreciable concentrations of suspended particulates, colloids, and dissolved organic and inorganic matter. This might alter the result of the experiment, because the compounds could adsorb and, therefore, the removal from the aqueous phase would not be due solely to volatilization. Consequently, the tap water was passed through a "Milli-Q Reagent-Grade Water System." This system (Fig. 14) essentially consists of a pump and motor, a modular series of 4 housings, a resistivity monitor, and a disposable final filtration unit.

For the reasons outlined above, the Palo Alto secondary effluent (PASE) was filtered prior to the experiments. The filter unit consisted of a dispensing pressure vessel and an in-line disk filter holder (Fig. 15). The filter diameter was 47 mm; the pore size was 0.45 µm, and the driving pressure was 350 kPa. In order to increase the length of a filter run, the PASE was prefiltered through #588 Schleicher & Schuell prepleated filters. The PASE was either used the same day or stored at 4°C overnight. A summary of the characteristics of the two waters is given in Table 5.

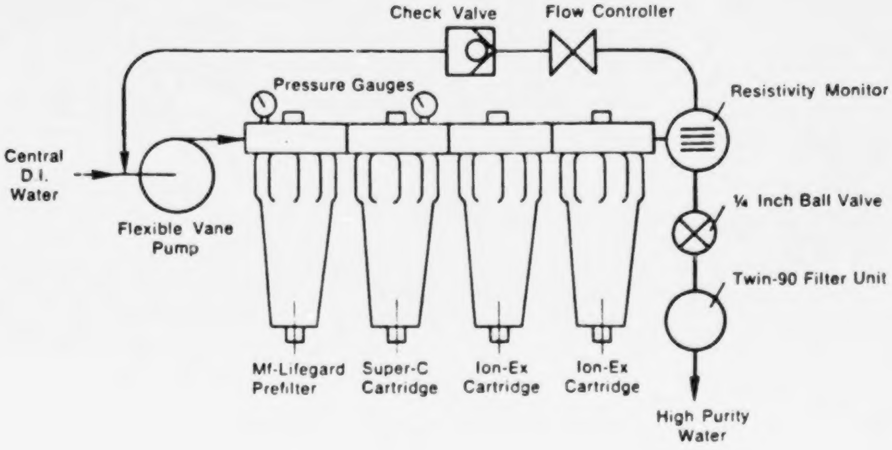
Check Valve
Flow Controller
Pressure Gauges
Resistivity Monitor
Central D.I. Water
Flexible Vane Pump
¼ Inch Ball Valve
Twin-90 Filter Unit
Mf-Lifegard Prefilter
Super-C Cartridge
Ion-Ex Cartridge
Ion-Ex Cartridge
High Purity Water

Figure 14. Milli-Q water system.

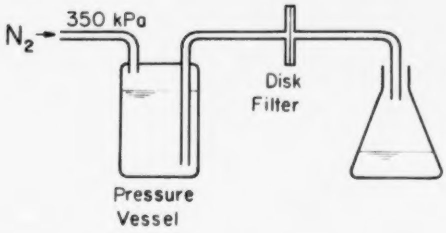
$N_2$
350 kPa
Disk Filter
Pressure Vessel

Figure 15. Filtration unit.

TABLE 5. WATER CHARACTERISTICS

| | Filtered PASE | MILLI-Q |
|---|---|---|
| TOC, mg/l C | 10 | 0.25 |
| COD, mg/l $O_2$ | 40 | 0.75 |
| Suspended solids, mg/l | < 2 | < 2 |
| Turbidity, TU | 1.5 | ~ 0.1 |
| Conductance, µS | 1300 | 0.8 |

## ANALYTICAL PROCEDURES

### Oxygen Measurements

Surface Aeration Experiments--

The dissolved oxygen (DO) concentration in the surface aeration reactor was continuously measured with an oxygen probe (type YSI 5720A). This is a self-stirring DO probe, frequently used to measure the DO concentration in BOD bottles. This type of probe was chosen to guarantee sufficient turbulence at the probe membrane at low stirring speed. The probe has a permeable membrane stretched over the sensor, isolating the sensor elements from the environment, but allowing gases to enter. When a polarizing voltage is applied across the sensor, oxygen that passes through the membrane reacts at the cathode, causing a current to flow. This current, which is proportional to the oxygen concentration in the environment, flows to an oxygen meter where the signal is displayed on a scale. In addition, a recorder was connected to the meter to measure the DO concentration continuously.

Two types of membranes are available: standard membrane (0.025 mm FEP teflon) and high-sensitivity membrane (0.013 mm FEP teflon). The advantage of the high-sensitivity membrane is its short response time.

The DO probe was tested for linearity by comparing the DO concentration measured in several samples with the probe to that determined using Winkler titration (65, Sect. 507). A typical curve is shown in Fig. 16.

Bubble Column Experiments--

The dissolved oxygen concentration in the bubble column contactor was measured continuously with an oxygen probe (type: YSI 5739). The probe was positioned inverted to avoid attachment of rising bubbles and resulting erratic readings. For this reason it was not feasible to use a self-stirring probe. Since the turbulence at the probe tip, where the sensing element is

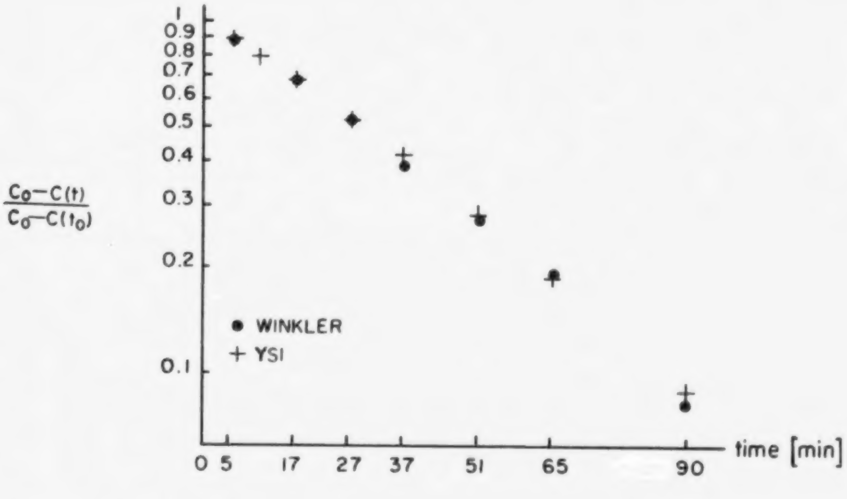

Figure 16. Calibration of oxygen probe.

located, was too low to permit accurate measurements, a small stainless steel impeller (diameter = 3 cm, width = 0.5 cm) was positioned at 0.5 cm above the probe. The stirring speed was set at approximately 50 rpm and ensured smooth oxygen absorption curves. A recorder was connected to the oxygen meter to measure the DO concentration continuously. A standard membrane (0.025 mm FEP Teflon) was used.

The mixing and DO probe linearity was tested by measuring the oxygen uptake at the top and bottom of the column simultaneously. For this purpose, the DO absorption was also measured with the Winkler method and DO probe simultaneously at the top and bottom of the column. Table 6 shows that mixing was good at low turbulence, that no significant difference between probe and Winkler measurements was observed, and that the average mass transfer coefficient, $K_{L,O_2}a'$, was similar at the top and bottom of the column.

Winkler analysis was done according to Standard Methods (65, Section 422B), with the following slight modifications. Stoppered flasks having a volume of 125 ml were used. Each was weighed for accurate volume capacity. One milliliter each of manganese sulfate solution and alkali-iodide-azide reagent was used instead of 2 ml. The samples were thoroughly shaken and allowed to settle for approximately 1 hr. Half the contents were then carefully siphoned off without disturbing the settled contents containing the fixed oxygen. Immediately thereafter 1 ml of concentrated $H_2SO_4$ was added by allowing the acid to run down the neck of the bottle. The sample was subsequently titrated in the same flask.

## Organic Analysis

### VOA Analysis--

The six compounds containing one- or two-carbon atoms were determined quantitatively by a procedure termed Volatile Organic Analysis (VOA). This procedure consists of a direct pentane extraction in the sealed hypovial in

TABLE 6. OXYGEN MASS TRANSFER RATE CONSTANTS MEASURED AT TOP AND BOTTOM OF BUBBLE COLUMN AND WITH DO-PROBE AND WINKLER TITRATION

| $K_La'$ TOP $[min^{-1}]$ | | $\frac{W-P}{W}$ | $K_La'$ BOT $[min^{-1}]$ | | $\frac{W-P}{W}$ | $\frac{P_t-P_b}{P_t}$ | $\frac{W_t-W_b}{W_t}$ |
|---|---|---|---|---|---|---|---|
| Probe $P_t$ | Winkler $W_t$ | [%] | Probe $P_b$ | Winkler $W_b$ | [%] | [%] | [%] |
| 0.0597 | 0.0605 | 1.4 | 0.0607 | 0.0592 | -2.5 | -1.7 | 2.3 |
| 0.0968 | 0.1006 | 3.7 | 0.0990 | 0.1001 | 1.1 | -2.2 | 0.5 |
| 0.204 | 0.202 | -0.6 | 0.194 | 0.206 | 5.8 | 4.7 | -1.8 |
| 0.195 | - | - | 0.198 | - | - | - | -1.7 |
| - | 0.378 | - | - | 0.377 | - | - | 0.2 |

Notes: W = Winkler; P = Probe; sub t = Top,; sub b = Bottom.
$K_La'$ = apparent $K_La$ (not corrected for gas-phase concentration).

which the sample has been stored (66,67), followed by injection of an aliquot of the pentane layer into a packed-column gas chromatograph, with automatic summation of the linearized ECD signal by a peak integrator. Quantitation is achieved by comparison of the peak area to that of a known quantity of internal standard, 1,2-dibromoethane. The peak area is converted to concentration by multiplying by a response factor. Values of the response factor were determined for each of the six compounds at concentration levels of 0.5, 5.0, 50, and 500 µg/l. The levels for $CCl_2F_2$ were chosen approximately three times higher. Five replicates were measured for each of the compounds at each of the four concentration levels; hence, the values of response factor (RF) are based on 20 measurements for each compound. The values of response factors are summarized in Table 7. The response factors are normalized to a value of 1000 for the internal standard ($BrH_2CCH_2Br$) at a concentration of 111.5 µg/l. For example, a compound having a response factor of 500 would be calculated to be present at a concentration of 55.75 µg/l in a sample in which its peak area was equal to that of the internal standard in the same chromatogram.

TABLE 7. RESPONSE FACTORS FOR VOA ANALYSIS

| Substance | Response Factor | |
|---|---|---|
| | Mean | (Std.Dev.)/Mean (n = 20) |
| $CCl_2F_2$ | 1,320 | 0.18 |
| $CHCl_3$ | 816 | 0.25 |
| $CH_3CCl_3$ | 336 | 0.21 |
| $CCl_4$ | 157 | 0.28 |
| $CHCl{=}CCl_2$ | 508 | 0.23 |
| $CCl_2{=}CCl_2$ | 188 | 0.32 |

The analytical precision (standard deviation) is considered adequate for quantitative work. The experimental standard deviations (18 to 32%) are somewhat high for that purpose, but the error seems to stem in large part from inaccuracies in preparing the standard solutions, rather than errors in concentrating and analyzing the samples. The experimental values of RF were independent of concentration, with the possible exception of $CHCl_3$ at the lowest concentration (0.5 µg/l), which was near the detection limit. The gas chromatographic conditions were as follows: 2-m packed column, 10% squalane on chromosorb W(AW), (80-100 mesh); carrier flow, 70 ml/min methane (5%) in argon; make-up gas (same composition as carrier gas), 30 ml/min; oven temperature, 67°C (isothermal); electron-capture detector (ECD) operated at 275°C; and injector temperature, 225°C.

## Chlorinated Benzene Analysis

The analytical procedure used for the chlorinated benzenes was similar to that of the highly volatile organic compounds reported in the previous section, except that a different internal standard and differing gas chromatographic conditions were used. These less volatile compounds (chlorobenzene (CBZ), o-, m-, and p-dichlorobenzene (DCB) were extracted with 1 ml of pentane in a sealed hypovial. After injection of an aliquot amount of internal standard (1,3,5-trichlorobenzene), the sample was shaken at high speed for 20 min. Each compound was quantitatively determined by glass-capillary-column gas chromatography. The chromatographic conditions are given in Table 8.

TABLE 8. RESPONSE FACTORS FOR CHLORINATED BENZENE ANALYSIS

| Substance | Abbreviation | Response Factor | |
|---|---|---|---|
| | | Mean | (Std.Dev.)/Mean (n = 10) |
| Chlorobenzene | CBZ | 0.707 | 0.05 |
| 1,3-Dichlorobenzene | m-DCB | 0.879 | 0.06 |
| 1,4-Dichlorobenzene | p-DCB | 0.812 | 0.07 |
| 1,2-Dichlorobenzene | o-DCB | 0.799 | 0.14 |

Gas chromatographic conditions:

Carlo Erba GC
Column: Glass capillary column UCON HB, 30 m, $d_c$ = 0.32 mm
Detector: FID, 49 kPa $H_2$, 78 kPa air
Carrier gas: 73 kPa He
Injection temperature: 200°C
Temperature program: 8°C/min from 40°C to 120°C
Initial oven temperatue: 40°C for 5 min.

The response factors for each of the four chlorinated benzenes have been determined at four different concentration levels to verify the analysis quantitatively in the range of 10 to 2000 μg/l. The response factors were found to be independent of the concentration within this range. The mean values of the response factors are summarized in Table 8. The experimental standard deviations are between 5% for CBZ and 14% for o-DCB, respectively.

## POWER MEASUREMENTS

The power input to the surface aeration contactor was measured with an in-line torque meter (Bex-O-Meter, Model 38, Bex Company, San Francisco). The meter was placed between the motor and the stirrer. This arrangement permitted direct measurement of the torque exerted by the stirrer. The torque was read on a calibrated scale from 0 in.oz to 25 in.oz, using a stroboscopic light while the instrument is rotating. The instrument operates in either direction, reading to an accuracy of $\frac{1}{2}$ % of the full scale. Details are given in Appendix B.

# SECTION 6

## RESULTS OF SURFACE-AERATION EXPERIMENTS

### DATA EVALUATION

The mass transfer rate expression (Eq. 33) can be rewritten as

$$\frac{d\,C_L}{dt} = K_L a \left(C_L{}^* - C_L\right) \tag{80}$$

where

$$a = A/V_L \tag{80a}$$

is the specific surface area.

For surface aeration the boundary conditions are $t = t_o$, $C_L = C_o$. Integrating Eq. 80 from $t_o$ to $t$, and $C_o$ to $C_L$ yields

$$-\ell n \left\{ \frac{C_L{}^* - C_L(t)}{C_L{}^* - C_o} \right\} = K_L a\ (t - t_o) \tag{145}$$

The equilibrium concentration for oxygen is constant and can be taken as the saturation concentration:

$$-\ell n \left\{ \frac{C^{sat}_{L,O_2} - C_{L,O_2}(t)}{C^{sat}_{L,O_2} - C_{o,O_2}} \right\} = K_L a\ (t - t_o) \tag{146}$$

In a log-linear plot of

$$\frac{C^{sat}_{L,O_2} - C_{L,O_2}}{C^{sat}_{L,O_2} - C_{o,O_2}} \text{ vs } (t - t_o)\ ,$$

the slope of the line will yield the value of $-K_L a$.

The concentration of organic compounds in the air is negligible. Therefore, according to Eq. 36, $C_L^*$ is assumed to be zero and Eq. 145 becomes

$$-\ell n \frac{C_L(t)}{C_o} = K_L a\,(t - t_o) \tag{147}$$

Hence, a semi-log plot of $[C_L(t)]/C_o$ vs $(t - t_o)$ will yield a slope of $-K_La$, as shown in Fig. 17, which represents a typical set of data. The initial and final concentrations were $C_o = 670\ [\mathrm{mg \cdot m^{-3}}]$ and $C(19) = 90\ [\mathrm{mg \cdot m^{-3}}]$, respectively. The data were analyzed by means of the regression program included in the statistical package "MINITAB" (68). Two regressions were performed. The first regression yielded estimates of $c_1$ and $(K_La)$ for the equation

$$\ell n \frac{C_L(t)}{C_o} = c_1 - K_L a\, t \tag{148}$$

In the second run the regression was forced through the origin, suppressing the constant $c_1$:

$$\ell n \frac{C_L(t)}{C_o} = -\,K_L a\, t \tag{149}$$

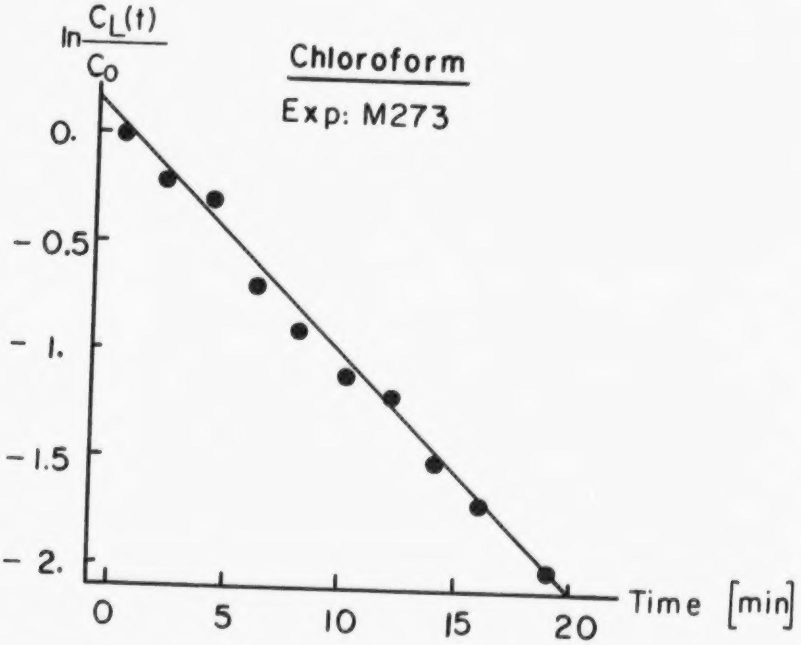

Figure 17. Sample data plot for stripping of an organic solute during surface aeration.

In most cases it could be shown that the constant $c_1$ was not significantly different at the 95% level of significance from zero. Moreover, the Ψ-values as defined by Eq. 71

$$\Psi_i = \frac{K_{L,i}a}{K_{L,O_2}a} \tag{71}$$

differed only slightly between values of $K_L$ as obtained from Eqs. 148 and 149.

Table 9 shows the "MINITAB" output for the regression analysis of the data in Fig. 17. The data correlated well with the form of Eqs. 146 and 147; the value of the square of the correlation coefficient for all experiments was $\geq$ 0.98.

The initial experiments were conducted in the reactor shown in Fig. 10. From this set of data, conclusions were drawn in order to modify the reactor to the configuration shown in Fig. 11 and to adopt a more refined experimental procedure for the main set of experiments. Details of the results are given in Appendix A of Ref. 69.

TABLE 9. SAMPLE OF MINITAB OUTPUT

```
-- REGR C17 1 C1

THE REGRESSION EQUATION IS
Y =  0.0164 - 0.108 X1


        COLUMN      COEFFICIENT        ST. DEV.     T-RATIO =
        --                             OF COEF.     COEF/S.D.
                        0.0164          0.0246          0.67
X1      TIME         -0.10773          0.00227        -47.46

THE ST. DEV. OF Y ABOUT REGRESSION LINE IS
S =      0.0424
WITH (  10- 2) =    8 DEGREES OF FREEDOM

R-SQUARED = 99.6 PERCENT
R-SQUARED = 99.6 PERCENT, ADJUSTED FOR D.F.

ANALYSIS OF VARIANCE

 DUE TO       DF          SS           MS=SS/DF
REGRESSION     1       4.04893         4.04893
RESIDUAL       8       0.01438         0.00180
TOTAL          9       4.06331

              X1           Y     PRED. Y     ST.DEV.
ROW         TIME     LNCHCL3       VALUE     PRED. Y    RESIDUAL     ST.RES.
  1          0.0         0.0       0.016       0.025      -0.016       -0.48
  2          2.0      -0.200      -0.199       0.021      -0.001       -0.03
  3          4.0      -0.324      -0.414       0.018       0.090        2.34R
  4          6.0      -0.655      -0.630       0.015      -0.025       -0.63
  5          8.0      -0.880      -0.845       0.014      -0.035       -0.87
  6         10.0      -1.116      -1.061       0.014      -0.055       -1.37
  7         12.0      -1.250      -1.276       0.015       0.026        0.67
  8         14.0      -1.500      -1.492       0.017      -0.008       -0.21
  9         16.0      -1.693      -1.707       0.021       0.014        0.37
 10         19.0      -2.020      -2.030       0.026       0.010        0.31

R DENOTES AN OBS. WITH A LARGE ST. RES.
```

Throughout this report, the criterion for statistical significance is rejection of the null hypothesis at the 95% level.

## VALUES OF THE MASS TRANSFER COEFFICIENT RATIO $\Psi$ FROM PRELIMINARY EXPERIMENTS

### One- and Two-Carbon Compounds

Values of the mass transfer coefficient ratio $\Psi$ (Eq. 71) were measured under various conditions. Initially the temperature was held constant and the values for $\Psi$ were determined for various levels of mixing intensity. Thereafter the mixing intensity was held constant in order to examine the effect of temperature on $\Psi$. In addition the influence of wastewater was investigated. Table 10 lists the average values for $\Psi$, including all the data collected under the above conditions.

TABLE 10. AVERAGE OF ALL VALUES OF $\Psi$ MEASURED IN SURFACE AERATION EXPERIMENTS

| Substance | $\Psi_{av}$ | Std. Dev. | % |
|---|---|---|---|
| $CCl_2F_2$ | 0.610 | 0.044 | 7 |
| $CHCl_3$ | 0.537 | 0.028 | 5 |
| $CH_3CCl_3$ | 0.574 | 0.039 | 7 |
| $CCl_4$ | 0.577 | 0.043 | 8 |
| $CHCl=CCl_2$ | 0.588 | 0.033 | 6 |
| $CCl_2=CCl_2$ | 0.585 | 0.042 | 7 |

n = 18 replicates.

In order to minimize a possible influence of mixing intensity, a set of values for $\Psi$ were determined at a stirrer speed of approximately 190 rpm. The results obtained for Milli-Q water at 20°C and 7°C and PASE and 20°C are listed in Table 11.

A comparison of the data in Tables 10 and 11 shows that the average values of $\Psi$ measured at different mixing intensities do not deviate appreciably from the average values obtained at 190 rpm. The value of $\Psi$ at 7°C was on the average 3% lower than at 20°C, but the difference was not statistically significant.

The average values of $\Psi$ calculated from results with Milli-Q water at 20°C, including the full range of mixing intensities, are shown in Table 12.

Evaluating Tables 10, 11, and 12 the conclusion could be drawn that the values of $\Psi$ are independent of turbulence, temperature, and water composition. However, an analysis of variance showed a slightly different picture, as illustrated in Figs. 18 through 23.

TABLE 11. AVERAGE VALUES OF Ψ MEASURED AT 190 RPM

| | Milli-Q [20°C] | | | Milli-Q [7°C] | | | PASE [20°C] | | |
|---|---|---|---|---|---|---|---|---|---|
| Substance | Ψ | $s_\Psi$ | % | Ψ | $s_\Psi$ | % | Ψ | $s_\Psi$ | % |
| $CCl_2F_2$ | 0.628 | 0.048 | 8 | 0.616 | 0.041 | 7 | 0.621 | 0.039 | 6 |
| $CHCl_3$ | 0.545 | 0.028 | 5 | 0.522 | 0.022 | 4 | 0.536 | 0.009 | 2 |
| $CH_3CCl_3$ | 0.607 | 0.033 | 5 | 0.599 | 0.018 | 3 | 0.554 | 0.019 | 4 |
| $CCl_4$ | 0.616 | 0.036 | 6 | 0.603 | 0.022 | 4 | 0.554 | 0.022 | 4 |
| $CHCl=CCl_2$ | 0.618 | 0.030 | 5 | 0.597 | 0.021 | 4 | 0.575 | 0.012 | 2 |
| $CCl_2=CCl_2$ | 0.630 | 0.032 | 5 | 0.604 | 0.021 | 3 | 0.560 | 0.011 | 2 |

n = 3 replicates; s = standard deviation.

TABLE 12. OVERALL AVERAGE VALUES OF Ψ IN MILLI-Q WATER AT 20°C

| Substance | $\Psi_{av}$ | Std. Dev. | % |
|---|---|---|---|
| $CCl_2F_2$ | 0.606 | 0.049 | 8 |
| $CHCl_3$ | 0.541 | 0.032 | 6 |
| $CH_3CCl_3$ | 0.573 | 0.044 | 8 |
| $CCl_4$ | 0.576 | 0.049 | 9 |
| $CHCl=CCl_2$ | 0.589 | 0.039 | 7 |
| $CCl_2=CCl_2$ | 0.586 | 0.048 | 8 |

n = 12 replicates.

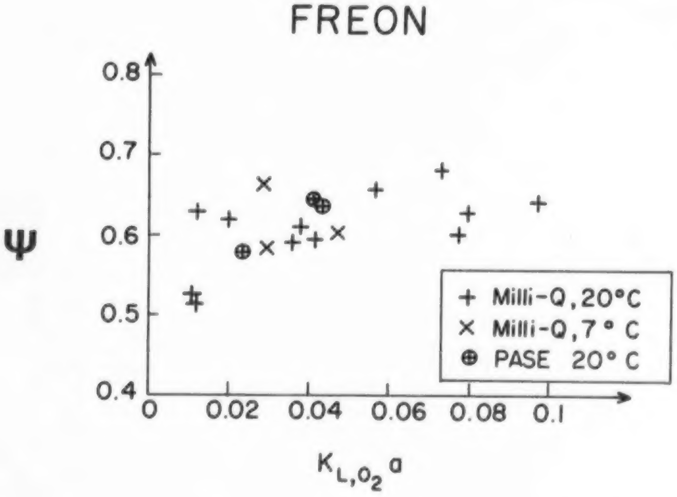

Figure 18. Ψ-values for Freon-12 from preliminary surface aeration experiments. $K_{L,O_2}a$ in $min^{-1}$.

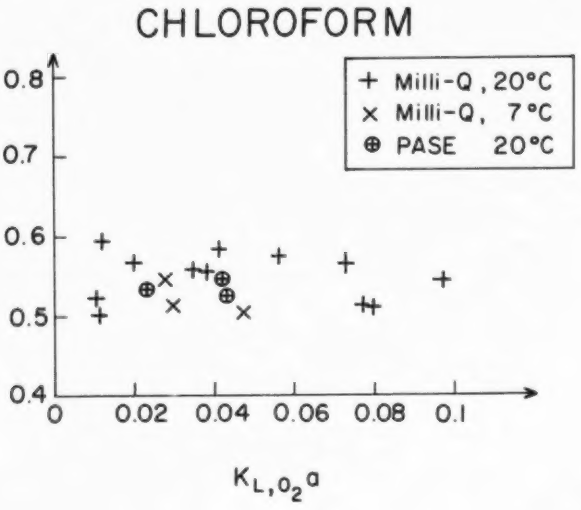

Figure 19. Ψ-values for chloroform from preliminary surface aeration experiments. $K_{L,O_2}a$ in $\min^{-1}$.

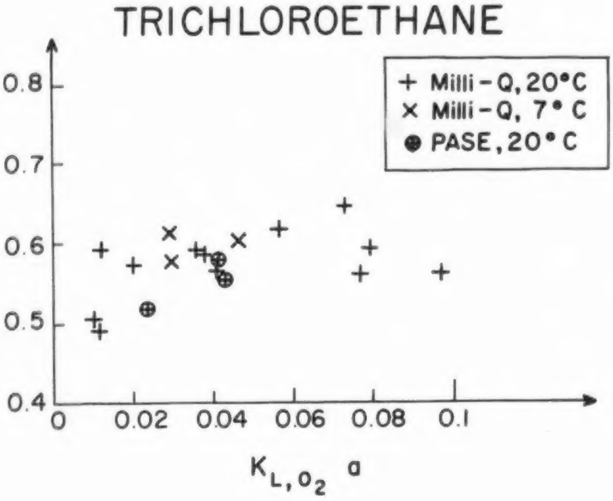

Figure 20. Ψ-values for 1,1,1-trichloroethane from preliminary surface aeration experiments. $K_{L,O_2}a$ in $\min^{-1}$.

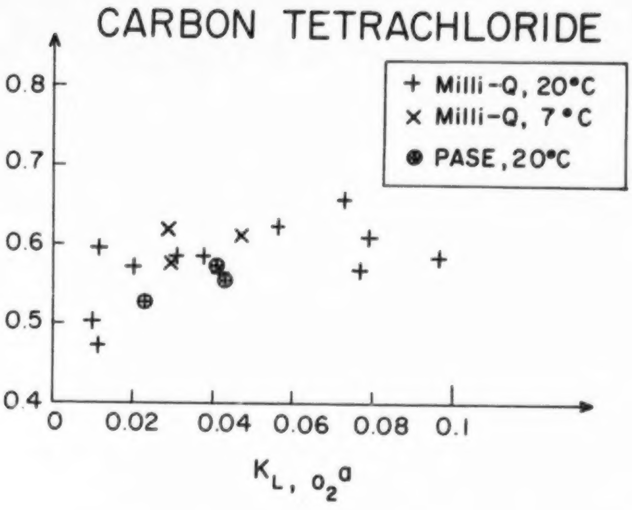

Figure 21. Ψ-values for carbon tetrachloride from preliminary surface aeration experiments. $K_{L,O_2}a$ in $min^{-1}$.

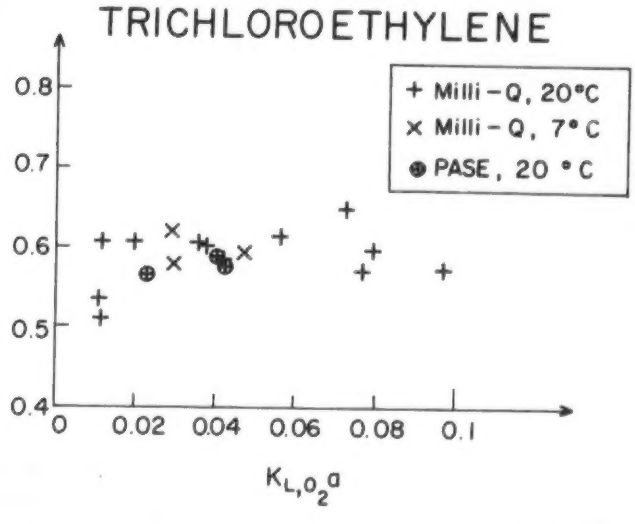

Figure 22. Ψ-values for trichloroethylene from preliminary surface aeration experiments. $K_{L,O_2}a$ in $min^{-1}$.

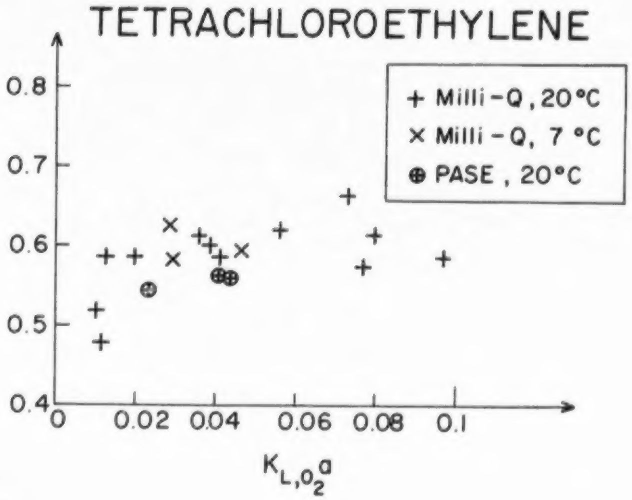

Figure 23. Ψ-values for tetrachloroethylene from preliminary surface aeration experiments. $K_{L,O_2}a$ in $min^{-1}$.

The mass transfer coefficient of oxygen was chosen as the variable for the abscissa in Figs. 18-23, because the stirring speed did not seem to describe adequately the effect of the turbulence in the reactor on mass transfer. A typical example is shown in Table 13.

TABLE 13. MASS TRANSFER RATE CONSTANT FOR OXYGEN AT 230 RPM

| | Experiment No. | | |
|---|---|---|---|
| | M231 | M232 | M233 |
| $K_{L,O_2}a$ [$min^{-1}$] | 0.0769 | 0.0566 | 0.0971 |

The wide spread of mass transfer coefficients was also observed for the six organic compounds. The correlation of Ψ against $K_{L,O_2}a$ was chosen, because the mass transfer rate constant is very sensitive to changes in turbulence. Furthermore, the oxygen-transfer rate constant was constantly monitored throughout the experimental run, whereas the stirrer speed was only controlled by rheostat setting; the power input may have changed during the course of an experiment as a result of voltage fluctuations or other perturbations. Hence, it was recognized that in subsequent experiments the mixing conditions had to be more carefully monitored and controlled; for the main set of experiments the configuration of the reactor was fixed rigorously and stirrer speed was more carefully monitored and controlled, as described in Section 5.

## Chlorinated Benzenes

The mass transfer rates of the four less volatile compounds, chlorobenzene and o-, m-, and p-dichlorobenzene, were measured and compared to the oxygen aeration rate. Duplicate experiments were conducted in Milli-Q water at a stirrer speed of 190 rpm and at 21°C. The results are summarized in Table 14.

TABLE 14. RESULTS OF SURFACE AERATION EXPERIMENTS WITH CHLORINATED BENZENES AT 190 RPM

| Compound | Expected Value* of $\Psi$ | Measured Value of $\Psi$† Mean ± Std. Dev. |
|---|---|---|
| CB | $0.39 \leq \Psi \leq 0.62$ | 0.61 ± 0.01 |
| m-DCB | $0.35 \leq \Psi \leq 0.59$ | 0.51 ± 0.02 |
| p-DCB | $0.34 \leq \Psi \leq 0.58$ | 0.49 ± 0.02 |
| o-DCB | $0.35 \leq \Psi \leq 0.59$ | 0.45 ± 0.02 |

*Calculated according to Eq. 73, assuming $-2/3 < \varepsilon < -1/3$.

†$n = 2$.

The experimental $\Psi$-values for the dichlorobenzene isomers (Table 14) are lower than the values of the highly volatile compounds containing one or two carbon atoms (Table 11), as expected. One exception is chlorobenzene (CB); the ratio of its overall mass transfer coefficient to that of oxygen was found experimentally to be 0.61. This value lies close to the upper limit of the range expected for the $\Psi_{CB}$-value, and does not differ significantly from the $\Psi$-values observed (Table 11) for Freon-12 and other 1- and 2-carbon compounds.

The $\Psi$-values of all less volatile and highly volatile compounds do not differ greatly. The reason therefore is that the diffusivity in water of oxygen and the organic compounds considered in our study are of the same magnitude ($\sim 10^{-9}$ $m^2 \cdot s^{-1}$). Values of the diffusivities of the organic compounds are rarely reported in the literature, and the equations given by Stokes-Einstein (Eq. 63) or Wilke-Chang (Eq. 64) make only an approximate estimate possible. Therefore, for each compound the estimation of the diffusivity is reflected by the range of expected $\Psi$-values. For all ten chosen organic compounds the experimental value of $\Psi$ was found to be in this range. An important implication for practice is that the volatilization rate constants are likely to be quite similar for those organic compounds in the molecular weight range characteristic of volatile organic substances. Therefore, further investigation of chlorinated benzenes would probably not yield substantial quantities of new information, so no further experiments were carried out with chlorinated benzenes.

## STATISTICAL ANALYSES OF PRELIMINARY DATA

An analysis of variance of $\Psi$ on all the preliminary data show with 95% probability that $\Psi$ is not independent of turbulence and water composition. In Fig. 24 average values for $\Psi$ with the 95% confidence interval is plotted for different stirrer speeds, Milli-Q water at 20°C and 7°C, and PASE.

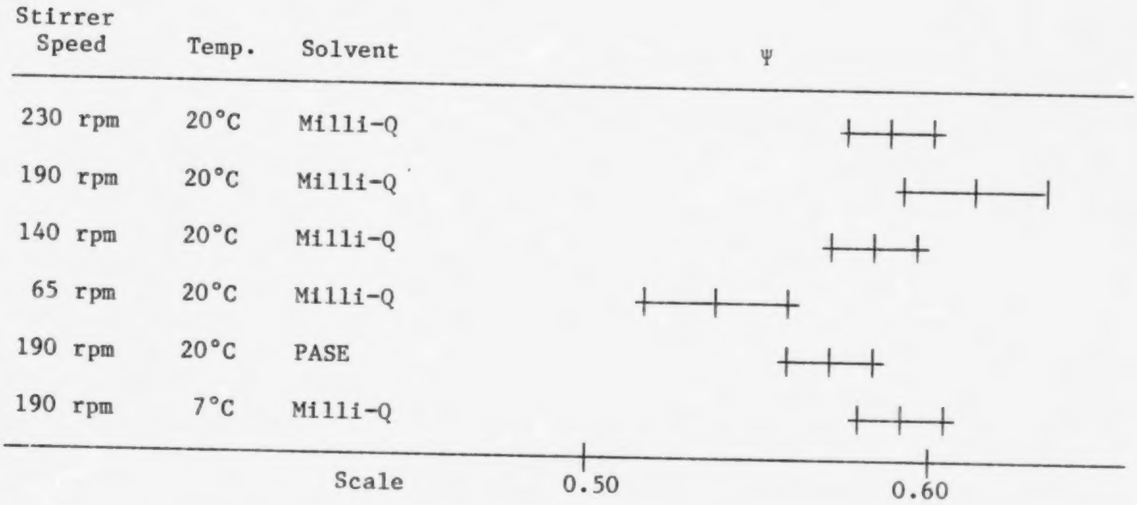

Figure 24. Average values of $\Psi$ with 95% confidence interval measured in preliminary surface aeration experiments.

The data in Fig. 24 suggest that $\Psi$ reaches a maximum at 190 rpm and decreases at lower stirrer speeds. This behavior might indicate that the flow regime changes with increasing stirrer speed, altering significantly the mass transfer conditions in the reactor. At low rpm the flow regime might be laminar or at the beginning of the transition zone, compared to high stirrer speeds, where the reactor is in the turbulent zone. Another possibility would be that at low stirring speeds, the reactor was not mixed well compared to the volatilization rate of the compounds. It is also possible that the values of $\Psi$ actually vary with turbulence, although there are no convincing arguments to support such a variation.

Table 15 shows the regression equations obtained for Milli-Q water at 20°C. For Freon-12 the slope of the regression line is significantly different from zero at the 95% level. For the remaining compounds the slope is not significantly different from zero. The low values of the square of the correlation coefficient $r^2$ in Table 15 show that the correlation is weak. This suggests a very weak dependence of $\Psi$ on $K_{L,O_2}a$, compared to the substantial scatter of data.

TABLE 15. REGRESSION OF $\Psi$ VS $K_{L,O_2}a$ FOR MILLI-Q WATER AT 20°C

| Substance | Regression Equation[†] | $r^2$ |
|---|---|---|
| $CCl_2F_2$ 12 | $\Psi = 0.573 + 0.826\ K_{L,O_2}a$ | 0.24[#] |
| $CHCl_3$ | $\Psi = 0.556 + 0.432\ K_{L,O_2}a$ | 0.15 |
| $CH_3CCl_3$ | $\Psi = 0.554 + 0.561\ K_{L,O_2}a$ | 0.14 |
| $CCl_4$ | $\Psi = 0.550 + 0.737\ K_{L,O_2}a$ | 0.20 |
| $CHCl{=}CCl_2$ | $\Psi = 0.577 + 0.334\ K_{L,O_2}a$ | 0.06 |
| $CCl_2{=}CCl_2$ | $\Psi = 0.560 + 0.702\ K_{L,O_2}a$ | 0.19 |

[†] 15 experiments; $K_{L,O_2}a$ expressed as $[\text{min}]^{-1}$.

[#] Coefficient of $K_{L,O_2}a$ significantly different from zero ($p = 0.95$).

In summary, the analysis of variance of the preliminary data indicate that the values of $\Psi$ might not be independent of turbulence. But the data do not allow any conclusion on how strong this dependence could be, because the scatter of data points is large compared to the range of measured mass transfer coefficients.

Based on the preliminary data and the statistical interpretation thereof, a second set of experiments was conducted under more tightly controlled conditions.

## DESIGN OF THE MAIN SERIES OF EXPERIMENTS

The results obtained from the preliminary experiments suggested several changes in the setup of the experiments. The poor correlation in the equations for the regression lines of $\Psi$ vs $K_{L,O_2}a$ demanded less scatter in the data measured over a larger range of $K_{L,O_2}a$-values. This goal was achieved by modifying the impeller and decreasing the reactor volume; the latter change also decreased the time of mixing. In addition to measuring wider ranges of mass transfer coefficients, the new stirrer was a more realistic model of a surface aerator used in treatment plants.

In order to monitor the flow regime more accurately the stirring speed was measured several times during the experimental run, minimizing possible unsteady agitation of the reactor. In addition, the power input of the impeller into the reactor was measured in order to estimate the characteristics of the flow regime. Especially important was to ascertain whether the contactor flow regime corresponded to turbulent mixing.

Because it had been observed in the preliminary experiments that values of $\Psi$ did not change significantly at low temperatures, study of temperature effects was terminated.

## RESULTS OF MAIN SET OF EXPERIMENTS

The main set of experiments was conducted to determine under rigorously controlled conditions the effect of mixing intensity on the Ψ-values, and to assess the effect of the wastewater matrix by comparing Ψ-values for PASE and Milli-Q at high and low mixing intensities. The main set of experiments was conducted in the reactor shown in Fig. 11. The results of these experiments are summarized in Appendix C.

### Average Values of Ψ

Table 16 and Fig. 25 summarize the average values of Ψ for Milli-Q water and for PASE. The values of Ψ measured in PASE were on the average 2% higher than those measured in Milli-Q water. However, the difference ΔΨ between Milli-Q and PASE was in all cases smaller than the standard deviation, and hence is considered insignificant.

TABLE 16. AVERAGE VALUES OF Ψ FROM THE MAIN SERIES OF SURFACE AERATION EXPERIMENTS

| Substance | Milli-Q* | % | PASE† | % | ΔΨ | % |
|---|---|---|---|---|---|---|
| $CCl_2F_2$ | 0.661 ± 0.039 | 5.8 | 0.668 ± 0.076 | 11.4 | 0.007 | 1.1 |
| $CHCl_3$ | 0.560 ± 0.036 | 6.5 | 0.584 ± 0.035 | 6.1 | 0.024 | 4.3 |
| $CH_3CCl_3$ | 0.607 ± 0.030 | 4.9 | 0.619 ± 0.029 | 4.7 | 0.012 | 2.0 |
| $CCl_4$ | 0.617 ± 0.033 | 5.4 | 0.627 ± 0.037 | 5.9 | 0.010 | 1.6 |
| $CHCl{=}CCl_2$ | 0.615 ± 0.029 | 4.6 | 0.626 ± 0.026 | 4.2 | 0.011 | 1.8 |
| $CCl_2{=}CCl_2$ | 0.608 ± 0.034 | 5.6 | 0.625 ± 0.026 | 4.5 | 0.017 | 2.8 |

*16 experiments, mean ± std. dev.

† 4 experiments, mean ± std. dev.

### Effect of Wastewater Matrix

A common way to compare the mass transfer coefficient of a compound in wastewater to that in clean water is to calculate the ratio of the respective $K_La$-values; this ratio is defined as

$$\alpha = \frac{K_La \text{ (wastewater)}}{K_La \text{ (clean water)}} \tag{150}$$

For $\alpha = 1$, there is no difference between wastewater and clean water. With decreasing $\alpha$, the resistance to mass transfer increases in wastewater. Table 17 shows the values of $\alpha$ at two different stirring speeds; the two experiments were conducted with wastewater samples from the same point (effluent from the Palo Alto secondary clarifier), but collected on different days.

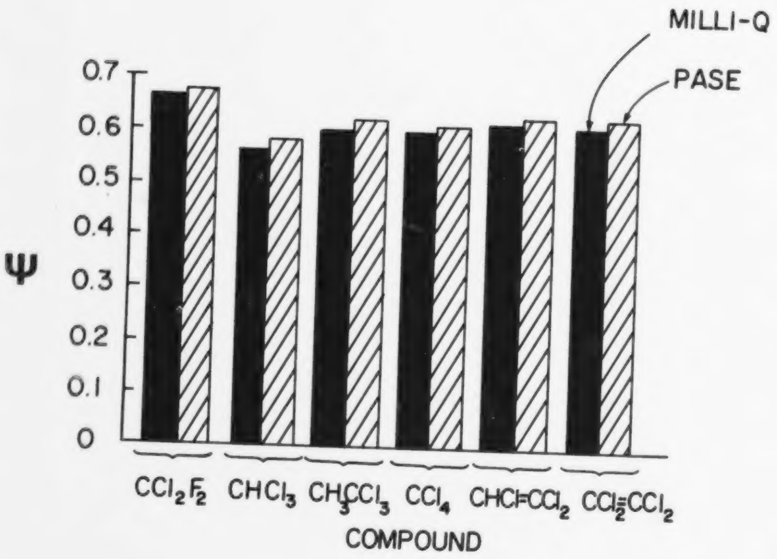

Figure 25. Comparison of values of $\Psi$ for Milli-Q and PASE.

In each case, the presence of wastewater constituents hinders mass transfer of both oxygen and the organic solutes. The data in Table 17 indicate that, for the two given sets of mixing conditions, the value of $\alpha$ is approximately 0.9 for organic compounds, apparently somewhat higher than the average value of $\alpha$ for oxygen, 0.81. However, when all data are considered, the ratio $\Psi$ is not significantly influenced by the presence of wastewater constituents, as seen from Table 16 and Fig. 25.

Dependence of $\Psi$ on the Oxygen Transfer Rate Constant

The equations of the regression lines for the $\Psi$-values as functions of $K_{L,O_2}a$ are shown in Table 18, which is based on experiments with Milli-Q water only. The slopes of the regression lines are significantly different from zero for some of the compounds: for Freon-12, chloroform, and carbon tetrachloride, the slope is different from zero at the 95% level of significance, as indicated by the t column in Table 18. The low values of $r^2$ show that the correlations are weak. The slope is not significantly different from zero at the 95% level for the remaining compounds: trichloroethane, trichloroethylene, and tetrachloroethylene. The relationships between the $\Psi$-values for the individual compounds and the value of $K_La$ for oxygen are depicted in Figs. 26 through 31. From inspection of the graphs, it is difficult to see any trends with increasing $K_{L,O_2}a$. This is due to the very weak dependence of $\Psi$ on $K_{L,O_2}a$, compared to the substantial scatter of the data.

TABLE 17. VALUES OF $K_La$ AND $\alpha$ FOR PASE AT 172 RPM AND 281 RPM

| | $K_La$ [$\text{min}^{-1}$] | | $\alpha = \frac{K_La\ (\text{PASE})}{K_La\ (\text{Milli-Q})}$ |
|---|---|---|---|
| | Milli-Q | PASE | |
| 172 ± 5 rpm | | | |
| $CCl_2F_2$ | 0.020685 | 0.018573 | 0.898 |
| $CHCl_3$ | 0.018887 | 0.016992 | 0.900 |
| $CH_3CCl_3$ | 0.019487 | 0.016992 | 0.880 |
| $CCl_4$ | 0.019704 | 0.017156 | 0.870 |
| $CHCl{=}CCl_2$ | 0.020178 | 0.017151 | 0.873 |
| $CCl_2{=}CCl_2$ | 0.019348 | 0.017172 | 0.888 |
| | | | $\alpha_{av} = 0.885 \pm 1.5\%$ |
| $O_2$ | 0.037139 | 0.028398 | 0.765 |
| 281 ± 5 rpm | | | |
| $CCl_2F_2$ | 0.143424 | 0.13487 | 0.940 |
| $CHCl_3$ | 0.114319 | 0.10449 | 0.914 |
| $CH_3CCl_3$ | 0.130138 | 0.11979 | 0.920 |
| $CCl_4$ | 0.133395 | 0.12368 | 0.927 |
| $CHCl{=}CCl_2$ | 0.130172 | 0.11864 | 0.911 |
| $CCl_2{=}CCl_2$ | 0.130688 | 0.11993 | 0.918 |
| | | | $\alpha_{av} = 0.922 \pm 11\%$ |
| $O_2$ | 0.210550 | 0.18127 | 0.861 |

TABLE 18. REGRESSION OF $\Psi$ VS $K_{L,O_2}a$

| Substance | Regression Equation[†] | $r^2$ | t |
|---|---|---|---|
| $CCl_2F_2$ | $\Psi = 0.626 + 0.206\ K_{L,O_2}a$ | 0.51 | 4.11[#] |
| $CHCl_3$ | $\Psi = 0.587 - 0.154\ K_{L,O_2}a$ | 0.30 | 2.71[#] |
| $CH_3CCl_3$ | $\Psi = 0.590 + 0.099\ K_{L,O_2}a$ | 0.15 | 1.92 |
| $CCl_4$ | $\Psi = 0.593 + 0.136\ K_{L,O_2}a$ | 0.27 | 2.57[#] |
| $CHCl{=}CCl_2$ | $\Psi = 0.616 - 0.005\ K_{L,O_2}a$ | 0.07 | 0.09 |
| $CCl_2{=}CCl_2$ | $\Psi = 0.590 + 0.104\ K_{L,O_2}a$ | 0.12 | 1.73 |

[†] 16 experiments; $K_{L,O_2}a$ expressed as $[\text{min}]^{-1}$.

[#] Coefficient of $K_{L,O_2}a$ is significantly different from zero ($t > t^*_{95\%} = 2.23$).

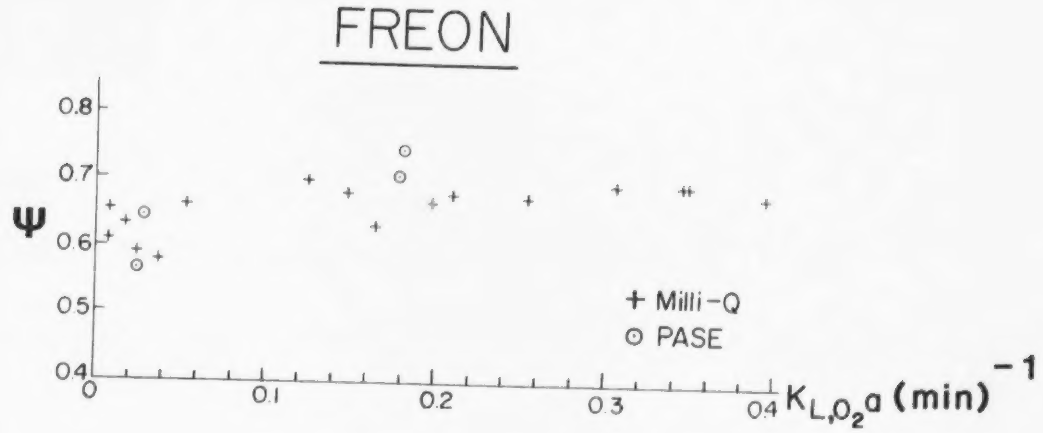

Figure 26. Relation between Ψ for Freon and the oxygen mass transfer coefficient.

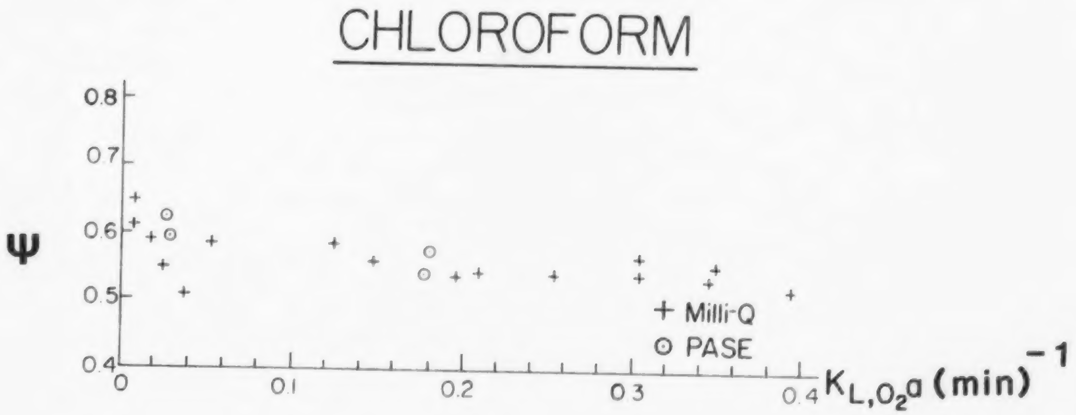

Figure 27. Relation between Ψ for chloroform and the oxygen mass transfer coefficient.

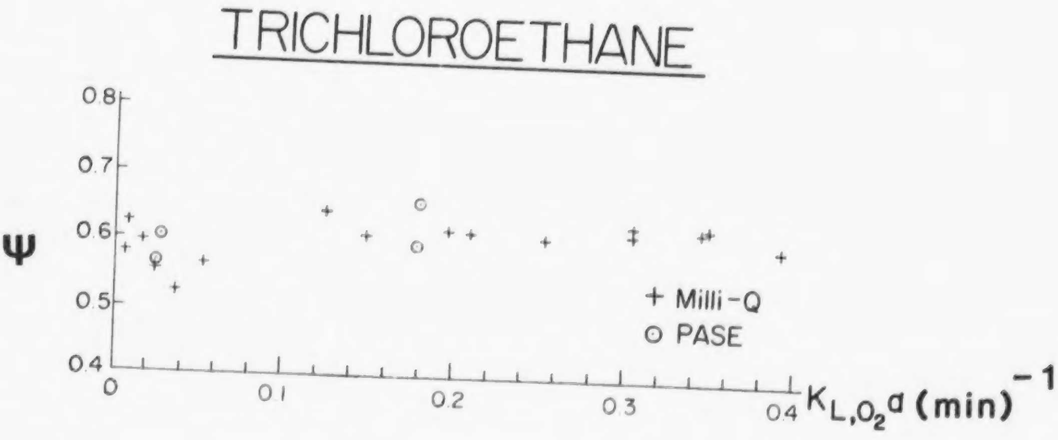

Figure 28. Relation between Ψ for trichloroethane and the oxygen mass transfer coefficient.

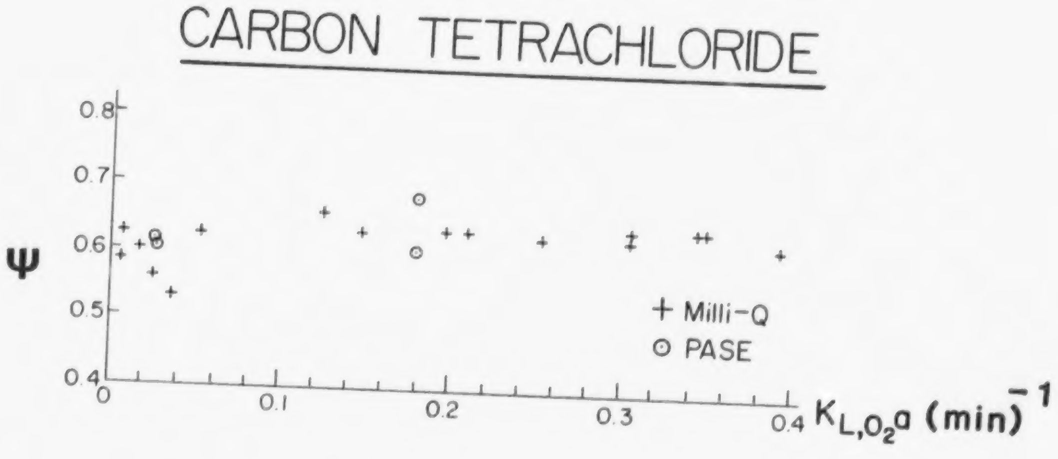

Figure 29. Relation between Ψ for carbon tetrachloride and the oxygen mass transfer coefficient.

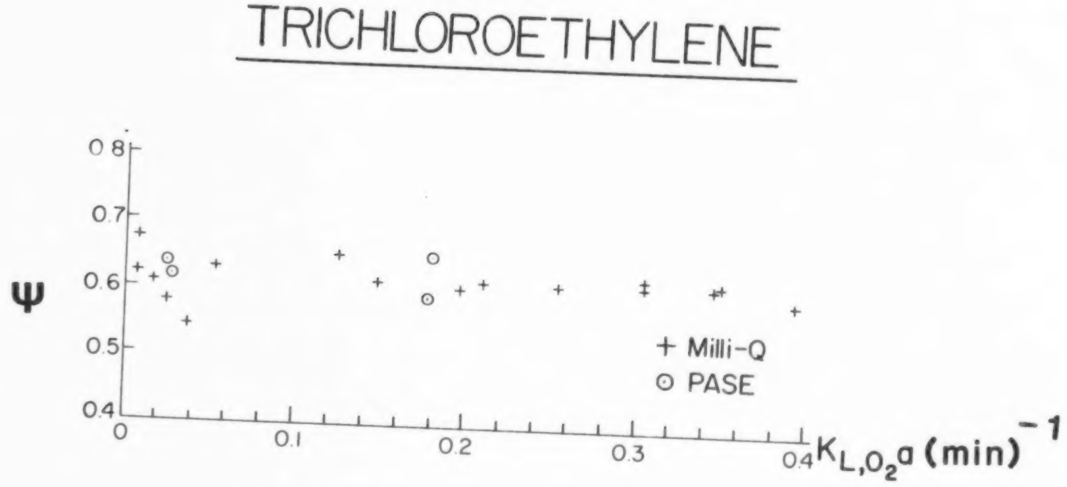

Figure 30. Relation between Ψ for trichlorothylene and the oxygen mass transfer coefficient.

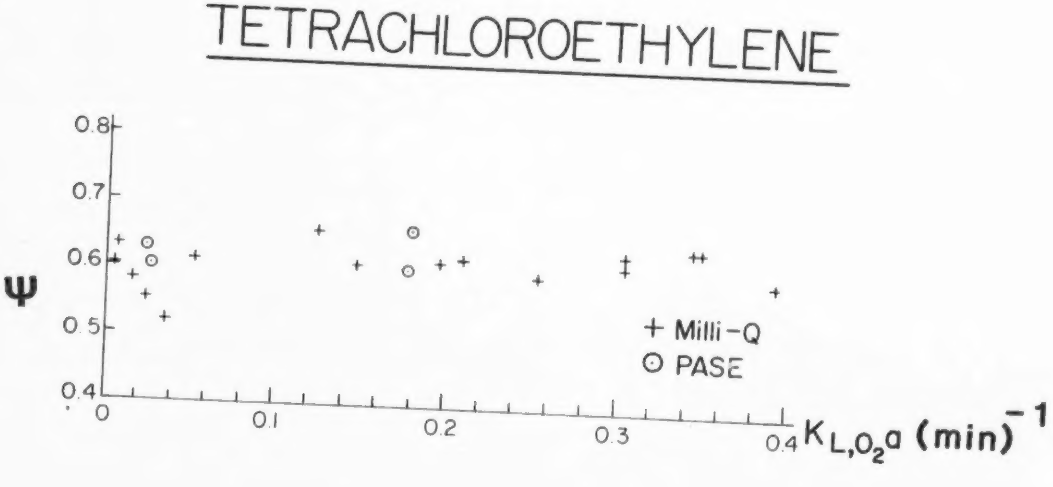

Figure 31. Relation between Ψ for tetrachloroethylene and the oxygen mass transfer coefficient.

# SECTION 7

# RESULTS OF BUBBLE-COLUMN AND EQUILIBRIUM EXPERIMENTS

In this section, data on mass transfer rate and equilibrium obtained in bubble-column and closed-system equilibrium experiments are summarized. The results of individual experiments are presented in detail elsewhere (70).

## DATA ANALYSIS

### Parameter Estimation Techniques

In Section 4 the equations describing the processes of absorption and stripping were derived. These were:

for absorption:

$$-\ell n\left(\frac{1-(C_L/C_L^*)}{1-(C_{Lo}/C_L^*)}\right)=\frac{Q_G\cdot H_c}{V_L}\cdot\left(1-\exp(-\Phi Z_s)\right)\cdot(t-t_o) \qquad (103)$$

for stripping:

$$-\ell n\left(\frac{C_L}{C_{Lo}}\right)=\frac{Q_G\cdot H_c}{V_L}\cdot\left(1-\exp(-\Phi Z_s)\right)\cdot(t-t_o) \qquad (111)$$

Both equations can be represented simply by

$$f(C)=\text{slope}\cdot(t-t_o) \qquad (104)$$

This suggests that a linear least-squares regression will yield an estimate of the slope, from which either the Henry coefficient, $H_c$, or the average mass transfer rate constant, $K_La$, can be calculated. However, the regression performed will very likely predict an intercept b, i.e. the regression equation will take the form:

$$f(C)=\text{slope}\cdot(t-t_o)+b \qquad (104a)$$

It is possible to carry out the linear regression suppressing the intercept. At first glance, this appears to be the correct approach, since it is in accordance with the theoretical equations. However, in a statistical sense, this implies that the initial concentration, $C_{Lo}$, is a "true" value, i.e., that the determination of $C_{Lo}$ entails no experimental error. Obviously this is incorrect. Therefore, the regression was not forced through the origin, even though the intercepts predicted are mostly not different from zero at the 95% confidence level.

Other possibilities to analyze the data become apparent if Eqs. 103 and 111 are transformed from logarithmic to exponential form. Equation 103 becomes

$$C_L = C_L^* - (C_L^* - C_{Lo}) \cdot \exp\left(- \frac{Q_G \cdot H_c}{V_L} \cdot \left(1 - \exp(-\Phi Z_s)\right) \cdot (t - t_o)\right) \quad (103a)$$

and Eq. 101 becomes

$$C_L = C_{Lo} \cdot \exp\left(- \frac{Q_G \cdot H_c}{V_L} \cdot \left(1 - \exp(-\Phi Z_s)\right) \cdot (t - t_o)\right) \quad (111a)$$

There are several options to fit these equations with a non-linear, least-squares regression. For Eq. 103a the choices are:

a.) estimate only the exponential term, $- \frac{Q_G \cdot H_c}{V_L} \cdot \left(1 - \exp(-\Phi Z_s)\right)$

b.) estimate the exponential term and either $C_{Lo}$ or $C_L^*$

c.) estimate the exponential term, $C_{Lo}$ and $C_L^*$ simultaneously

For Eq. 111a the possibilities reduce to (a) and the first case of (b). As discussed by Boyle et al. (71), in a statistical sense it would be best if the saturation concentration, $C_L^*$, could be estimated from actual experimental data. Since the experiments performed were long enough to measure the actual saturation concentration, we eliminate option (c) and the second case of option (b).

The arguments, whether to run a two-parameter estimate regression or a one-parameter estimate regression, are similar as with the logarithmic equations. That is, assigning to $C_{Lo}$ a fixed or "true" value, as would be the case in option (a), would weight this value disproportionately high, and hence is not appropriate.

Now we need to decide whether to use a linear regression, i.e. Eqs. 103 and 111, or a two-parameter non-linear regression. Typical plots of both methods are shown in Figs. 32 and 33 for the same experimental run and compound.

It was decided to analyze all the experimental data with both methods. The regression programs used, SYSREG and NLIN, are included in the User's Guide of SAS (72). The method of iteration used in NLIN was that of Marquardt (72). When comparing both data sets, no trends were apparent in the sense that one method would consistently yield larger or smaller estimates than the other.

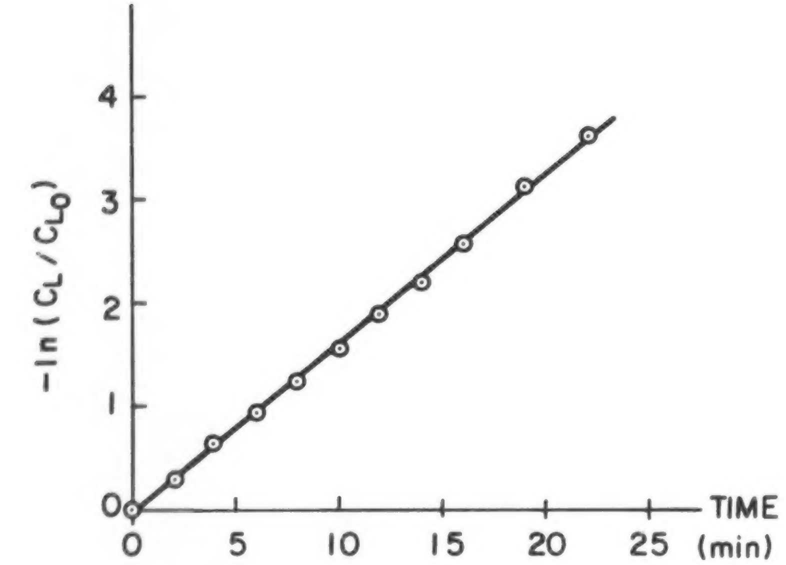

Figure 32. Linear regression of bubble-column stripping data.

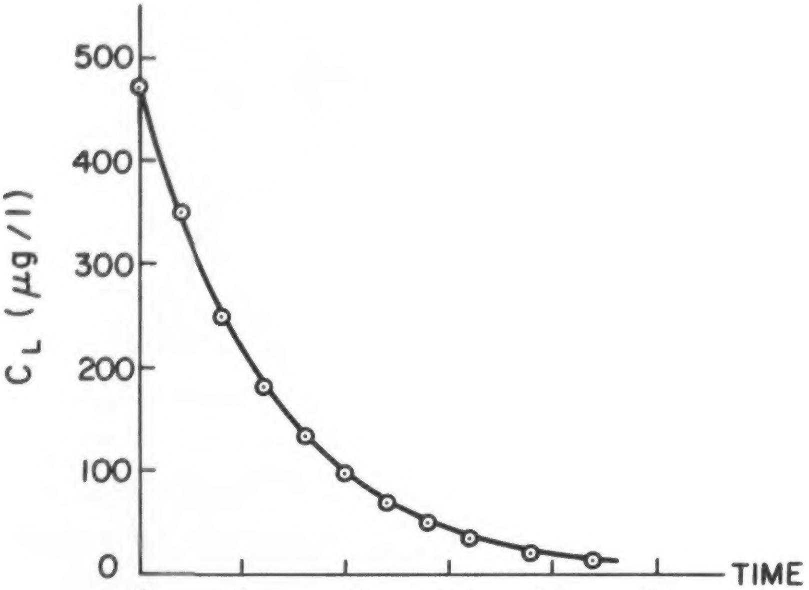

Figure 33. Non-linear regression of bubble-column stripping data.

It is important to recognize that the linear regression (log-linear) weights the observations as if the experimental error were a constant percentage of the dependent variable (71,73). For oxygen, according to Eq. 103, the dependent variable is defined as a concentration difference, whereas for stripping the variable is simply a concentration according to Eq. 111. Hence, in the case of oxygen absorption the logarithmic weighting is only correct when the larger errors are in low values of $C_L$, that is, at the beginning of an experiment. Residual plots are a useful diagnostic tool to evaluate the appropriateness of a model. Residuals should be random, normally distributed, and have a constant variance. This was observed in most cases; however, the exponential technique in several cases showed larger residuals for the initial observations. Typical residual plots are shown in Figs. 34 and 35, which correspond to the same data set as was used in Figs. 32 and 33, respectively.

After concluding that neither technique introduced any significant bias, the criterion of smaller 95% confidence intervals, expressed in percent of the estimated variable, was adopted. Surprisingly, of the 134 data sets fitted, only 11 data sets showed smaller confidence intervals for the exponential method. The calculated average values of the confidence intervals, expressed as percent of the mean value of the estimated parameter, were 10.74% for the exponential method (Eq. 111a) and 7.44% for the logarithmic method (Eq. 111). Based on this evaluation the logarithmic technique was chosen for the data analysis, i.e., Eqs. 103 and 111 were used. The analysis of the oxygen data was truncated at approximately 95% of the saturation value, $C_L^*$; however, $C_L^*$ was evaluated directly from the experimental data, i.e., read from the chart paper.

Partial Gas-Phase Saturation

As described in Section 4 the criterion for gas-phase saturation is

$$\Phi Z_s = \frac{K_L a \cdot V_L}{Q_G \cdot H_c} \geq 5 \qquad (113a)$$

Under given experimental conditions, the larger the value of $H_c$, the more difficult it is to attain complete saturation. Referring to the set of experiments with variable gas flow rates and liquid volumes (Table 3), the following approximate values of $\Phi Z_s$ were calculated (Table 19).

The cases of partial and complete gas-phase saturation are illustrated by means of concentration profiles in Fig. 36. The gas phase is only partly saturated with $CCl_4$ at high turbulence (i.e., high value of $Q_G/V_L$), but is completely saturated in the other three cases (organics) shown. The gas-phase concentrations were calculated with Eq. 98 for oxygen and Eq. 110 for the organic compounds, at conditions corresponding to $Q_G/V_L = 0.19$ and $Q_G/V_L = 0.0083\ \text{min}^{-1}$ in Table 19. Complete gas-phase saturation is indicated by a vertical slope at $(Z_s - Z)/Z_s = 1.0$.

In order to calculate the degree of saturation of an organic compound using Eq. 110, one needs to know $H_c$ as well as $K_La$ of the compound. As mentioned in Section 4, this is impossible to do with only the data of the

TABLE 19. EXPERIMENTAL GAS-PHASE SATURATION VALUES, $\Phi Z_s$

| $Q_G/V_L$ [$min^{-1}$] | Value of Gas-Phase Saturation Parameter, $\Phi Z_s$ | | | | | | |
|---|---|---|---|---|---|---|---|
| | $O_2$ | $CCl_2F_2$ | $CHCl_3$ | $CH_3CCl_3$ | $CCl_4$ | $CHCl{=}CCl_2$ | $CCl_2{=}CCl_2$ |
| 0.19 | 0.12* | 0.05 | 12.5* | 3.6 | 2.4* | 5.7 | 3.6 |
| 0.048 | 0.22 | 0.07 | 19. | 6.1 | 3.9 | 9.5 | 6.0 |
| 0.011 | 0.33 | 0.09 | 24. | 9.0 | 5.5 | 14.2 | 8.6 |
| 0.0083 | 0.37* | 0.10 | 27. * | 10.3 | 6.3* | 15.7 | 10.2 |

*Examples shown in Fig. 36.

corresponding experiment. However, there is a way to estimate approximately the $K_La$ of the compound based on the $K_La$ of oxygen from the same experiment. As discussed in Section 4, we may use Eq. 72 for this purpose

$$\Psi = \left(\frac{D_{li}}{D_{lj}}\right)^{\Omega} \qquad (73)$$

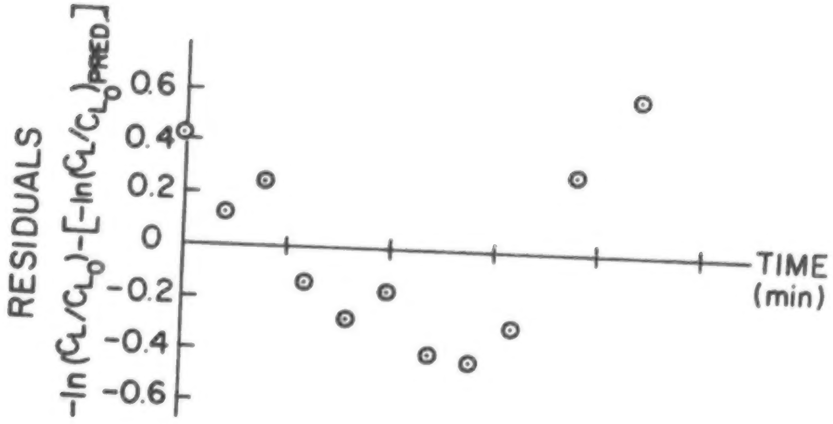

Figure 34. Residual plot of linear regression.

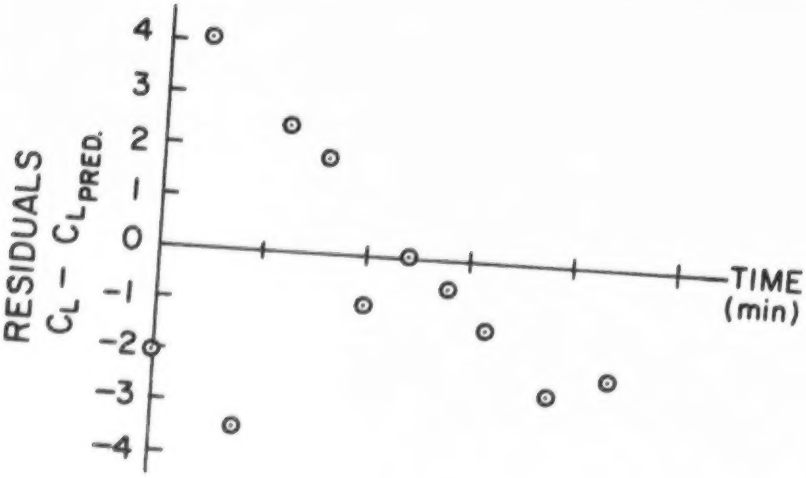

Figure 35. Residual plot of non-linear regression.

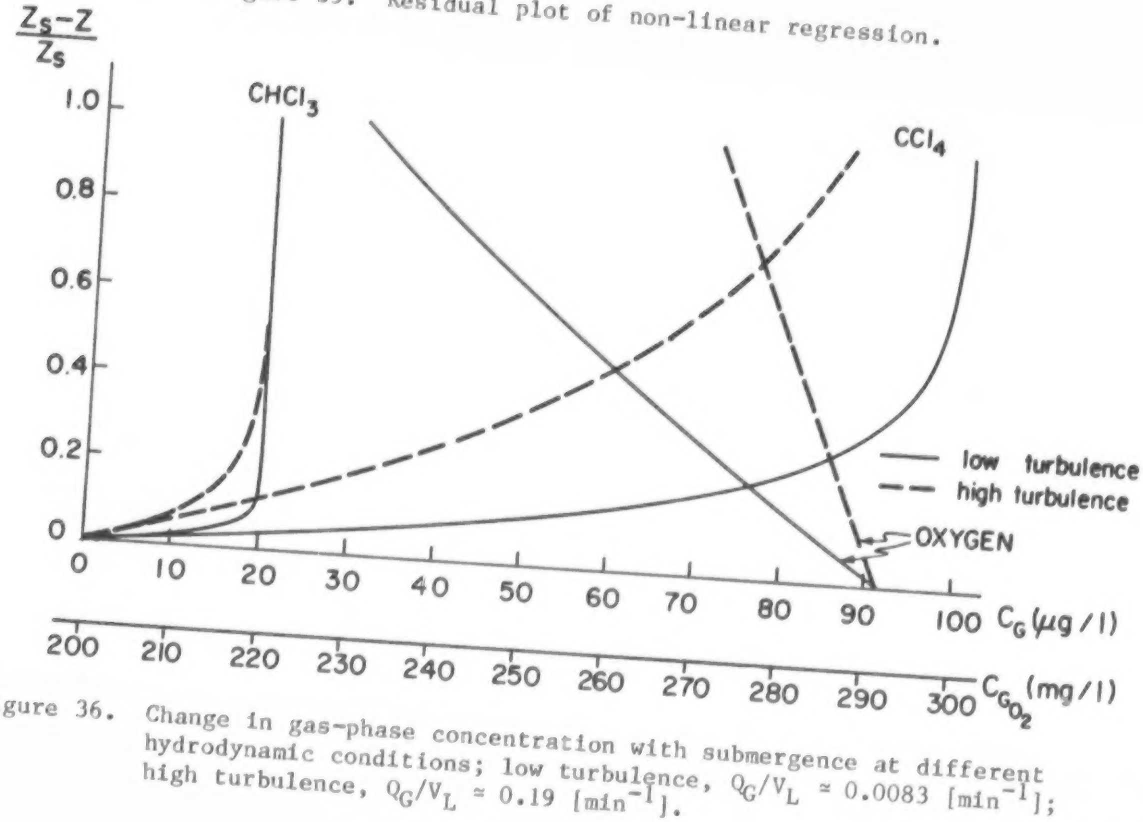

Figure 36. Change in gas-phase concentration with submergence at different hydrodynamic conditions; low turbulence, $Q_G/V_L \simeq 0.0083$ [min$^{-1}$]; high turbulence, $Q_G/V_L \simeq 0.19$ [min$^{-1}$].

Although experimental values of the critical volume are available for all compounds except $CH_3CCl_3$, we choose to use Eq. 72, expressed as a ratio of estimated diffusivities, rather than the form of Eq. 73 expressed as a ratio of measured critical volumes. The reason for doing so is that the possible values of the exponent $\Omega$ (Eq. 72) have a narrower range than those of the exponent $\Omega\varepsilon$ (Eq. 73).

Diffusion coefficients were calculated with the modified Wilke-Chang equation (Eq. 64), with the association parameter $\Phi = 2.26$ for water, as suggested by Hayduk and Laudie (74). Equation 64 was chosen because its form is closely related to the Stokes-Einstein equation, Eq. 63, whereas the Hayduk and Laudie correlation (74), although equally well suited, is more empirical.

The solute molal volume at the normal boiling point, $V_A$, to be used in Eq. 64, was estimated with the Schroeder increments (29), except for $O_2$, $CCl_2F_2$, and $CCl_4$, for which experimental data for $V_A$ are available. Schroeder increments were used, because the Le Bas additive method appears to yield values for the compounds studied which are too high. This was evaluated by comparing both additive methods with the Tyn and Calus correlation (75) as suggested by Reid et al. (29), using the available experimental values of $V_c$. A table showing the estimated liquid molar volumes with the different methods and the corresponding diffusion coefficients, also using several methods, is included in Table A-2 of Appendix A. The values of the diffusion coefficients obtained using several alternative estimating approaches are summarized in Table A-3 of Appendix A.

From Table 19 we infer that $CCl_4$ is the most critical compound in terms of attaining the lowest degree of gas-phase saturation. If we use Eq. 73 for $CCl_4$ and $O_2$ at 20°C we obtain:

$$\Psi_{CCl_4} = \left(\frac{D_{L_{CCl_4}}}{D_{L_{O_2}}}\right)^{\Omega} = \left(\frac{8.61 \cdot 10^{-6}}{20.25 \cdot 10^{-6}}\right)^{\Omega} = 0.46^{\Omega}$$

With, $1/2 \leq \Omega \leq 2/3$, $\Psi$ becomes

$$0.565 \leq \Psi_{CCl_4} \leq 0.65$$

Similarly, for the other borderline compounds, $CH_3CCl_3$ and $CCl_2{=}CCl_2$,

$$0.55 \leq \Psi_{CH_3CCl_3} \leq 0.64$$

$$0.53 \leq \Psi_{CCl_2=CCl_2} \leq 0.62$$

Having now a reasonable estimate of $\Psi_i$ for these compounds we may use Eq. 112 and solve for $H_c$ by an iterative procedure. An average value of $\Psi_i = 0.60$ was chosen for this purpose. An example of this procedure follows for $CCl_4$ as an illustration:

Compound: $CCl_4$ Conditions:

$V_L$ = 13.55 liter
$Q_G$ = 2.657 ℓ/min
T = 21.2°C

- from the linear regression of Eq. 114 we obtain the value of S needed in Eq. 115:

$$S = 0.165$$

- substituting S into Eq. 115 we obtain the first estimate of $H_c$:

$$H_c = 0.843$$

- now we take the $K_La$-value for oxygen obtained during the same experiment, $K_{L,O_2}a = 0.670$, multiply it by 0.60 and obtain:

$$K_{L,CCl_4}a = 0.402$$

- we can now estimate the saturation parameter (Eq. 113):

$$\Phi Z_s = \frac{K_{L,CCl_4} \cdot a \cdot V_L}{H_{c,CCl_4} \cdot Q_G} = \frac{0.402 \cdot 13.55}{0.843 \cdot 2.657} \simeq 2.4$$

  and the degree of gas-phase saturation (Eq. 110):

$$\frac{C_G}{C_G^*} = \frac{C_G}{C_L \cdot H_c} = \left[1 - \exp(-\Phi Z_s)\right] = \left(1 - e^{-2.4}\right) = 0.91$$

- using the value of $K_{L,CCl_4}a$ obtained above, we solve Eq. 112 iteratively until a value for $H_{c,CCl_4}$ is found which matches the experimental value of S. In this example, $H_{c,CCl_4} = 0.954$ becomes the estimated value of the Henry coefficient for $CCl_4$.

If a smaller value were chosen for $\Psi_i$, say 0.57 rather than 0.6, a larger value of $H_c$ would be estimated by the procedure described above, and conversely, a smaller value of $H_c$ would be found if the value of $\Psi_i$ is chosen larger than 0.6.

For $CCl_2F_2$, which is an extremely volatile compound, we can calculate only $\Psi$ from the bubble-column experiments in this work; $H_c$ cannot be evaluated. Values of $K_La$ were evaluated for $CCl_2F_2$ using Eq. 119, although the simpler expression of Eq. 118 could have been used because in all experiments $\Phi Z_s \leq 0.1$; an estimated Henry coefficient, $H_{c,CCl_2F_2} = 62.11$ at 20°C, was used for $CCl_2F_2$ in Eq. 119. The values of $K_La$ for oxygen, for which $0.1 < \Phi Z_s < 0.4$ in our experiments (Table 19), were calculated with Eq. 106, using a value of $H_{c,O_2} = 30.04$ at 20°C.

## Standardization of Results

In order to interpret the results properly, these must be evaluated at the same conditions. Since the temperature was not the same for all experiments and Henry coefficients vary with temperature (approximately 30% for $\Delta T = 5°C$ with $T \approx 21°C$), the results had to be standardized. The reference temperature was chosen as $T = 20°C$. Henry coefficient temperature dependence for the compounds of interest, except $CCl_2F_2$, can be found in (76). A temperature correction factor

$$f(i,T) = \frac{H_{ci}\ [T]}{H_{ci}\ [20^0C]}$$

was calculated as suggested by Kavanaugh and Trussell (76) and used to correct the experimental values of $H_c$ to 20°C.

Referring to the example on page 93, we had

$$H_{c,CCl_4}\ (21.2°C) = 0.95406 \quad \text{and} \quad f(CCl_4,\ 21.2°C) = 1.06744$$

obtaining a standardized value

$$H_{c,CCl_4} = 0.8938 \quad \text{for} \quad T = 20°C$$

Of course, the $K_La$-values for oxygen also had to be corrected to 20°C. The effect of temperature on $K_{L,O_2}a$ is commonly expressed as

$$(K_{L,O_2}a)_T = (K_{L,O_2}a)_{20} \cdot \theta^{(t-20)}$$

Although the temperature correction factor, $\theta$, has been reported to vary from 1.01 to 1.05 (43), there is wide agreement that $\theta = 1.024$ is the best value (38,77,78); the latter value was used in this work. For $CCl_2F_2$, the Henry coefficient temperature dependence was estimated from vapor pressure and solubility data (79,80). The $\Psi$-value for $CCl_2F_2$ needs no correction, since it is calculated prior to any temperature correction. Moreover, $\Psi$ should theoretically not be influenced by temperature, as shown by Eq. 73.

## EXPERIMENTS VARYING THE RATIO $Q_G/V_L$

Table 20 summarizes the average values of $H_{c,i}$ and $\Psi_{CCl_2F_2}$ obtained from the four experiments carried out in duplicate at four different combinations of liquid volume, $V_L$, and gas flow rate, $Q_G$ (Table 3). The results of the individual experiments are given in Appendix D, Table D-1. As a first approximation, the values of $H_{c,i}$ and $\Psi_i$ are expected to be independent of turbulence: $H_{c,i}$ because it is a thermodynamic property of each compound and $\Psi$ because the turbulence effect on $K_L$ or $K_La$ cancels out when computing the ratios. The value of $K_{L,O_2}a$ was taken as a measure of the effect of turbulence on mass transfer. The equations of the regression lines for $H_{c,i}$ and $\Psi_{CCl_2F_2}$ as functions of $K_{L,O_2}a$ are shown in Table 21. The high values of $r^2$ show that the correlations are significant. The slopes of the regressions are different from zero at the 95% significance level.

TABLE 20. AVERAGE VALUES OF $H_{c,i}$ AND $\Psi_i$ FROM BUBBLE-COLUMN EXPERIMENTS

| Compound | $H_c$ [20°C] or $\Psi$ Mean ± Std. Dev. | $\frac{\text{Std. Dev.}}{\text{Mean}}$ |
|---|---|---|
| $CHCl_3$ | $H_c = 0.203 \pm 0.036$ | 0.177 |
| $CH_3CCl_3$ | $H_c = 0.594 \pm 0.029$ | 0.049 |
| $CCl_4$ | $H_c = 0.977 \pm 0.041$ | 0.042 |
| $CHCl{=}CCl_2$ | $H_c = 0.388 \pm 0.033$ | 0.084 |
| $CCl_2{=}CCl_2$ | $H_c = 0.605 \pm 0.040$ | 0.066 |
| $CCl_2F_2$ | $\Psi = 0.553 \pm 0.045$ | 0.082 |

TABLE 21. REGRESSION EQUATIONS OF $H_{ci}$ and $\Psi_i$ VERSUS $K_{L,O_2}a$ FOR BUBBLE-COLUMN EXPERIMENTS

| Compound | Regression Equation* | $r^2$ |
|---|---|---|
| $CHCl_3$ | $H_c = -0.140 \cdot K_{L,O_2}a + 0.246$ | 0.93 |
| $CH_3CCl_3$ | $H_c = -0.099 \cdot K_{L,O_2}a + 0.624$ | 0.73 |
| $CCl_4$ | $H_c = -0.136 \cdot K_{L,O_2}a + 1.018$ | 0.67 |
| $CHCl{=}CCl_2$ | $H_c = -0.117 \cdot K_{L,O_2}a + 0.424$ | 0.79 |
| $CCl_2{=}CCl_2$ | $H_c = -0.130 \cdot K_{L,O_2}a + 0.645$ | 0.64 |
| $CCl_2F_2$ | $\Psi = -0.165 \cdot K_{L,O_2}a + 0.502$ | 0.82 |

*$K_{L,O_2}a$ in units of $[\text{min}^{-1}]$.

In Figs. 37 through 42 the regression lines are plotted with the individual data points and the 95% confidence intervals. The results appear to be influenced somewhat by the rate of mass transport, contrary to expectations based on theory.

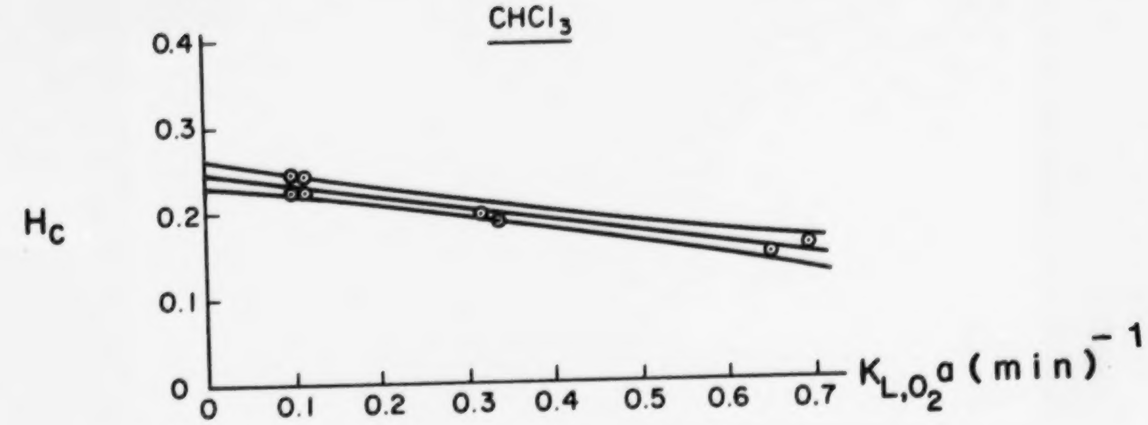

Figure 37. Regression of $H_{c,CHCl_3}$ versus $K_{L,O_2}a$ from bubble-column data.

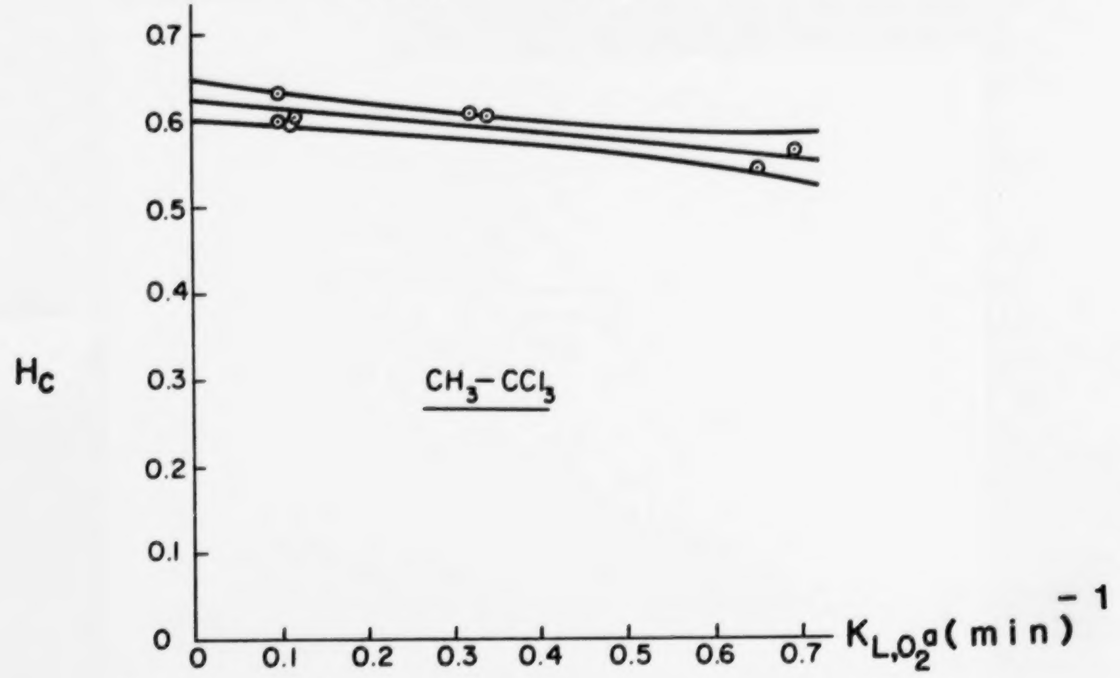

Figure 38. Regression of $H_{c,CH_3CCl_3}$ versus $K_{L,O_2}a$ from bubble-column data.

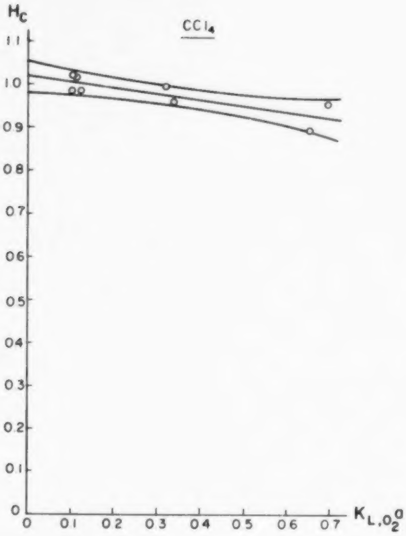

Figure 39. Regression of $H_{c,CCl_4}$ versus $K_{L,O_2}a$ from bubble-column data.

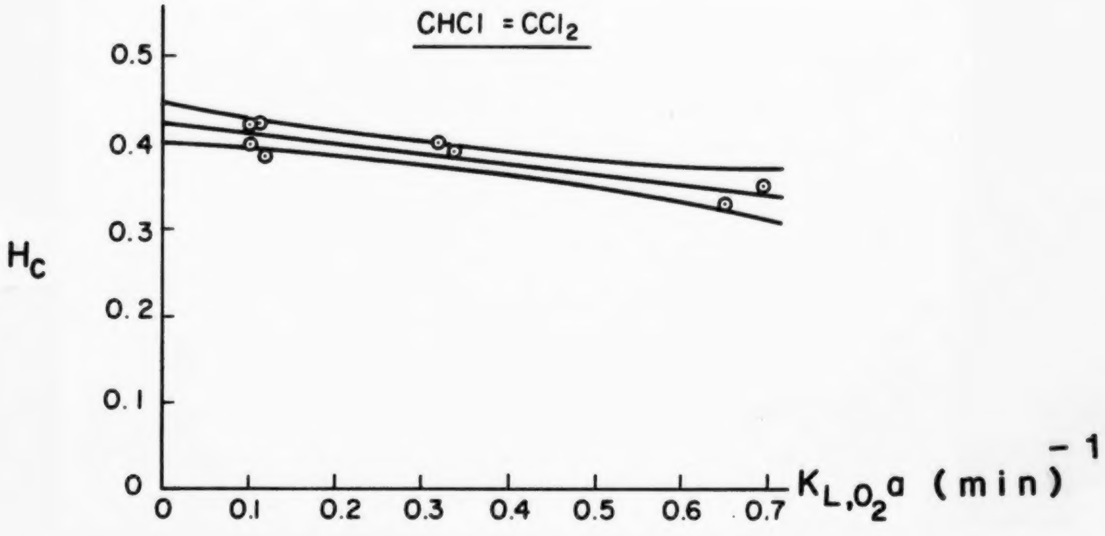

Figure 40. Regression of $H_{c,CHCl=CCl_2}$ versus $K_{L,O_2}a$ from bubble-column data.

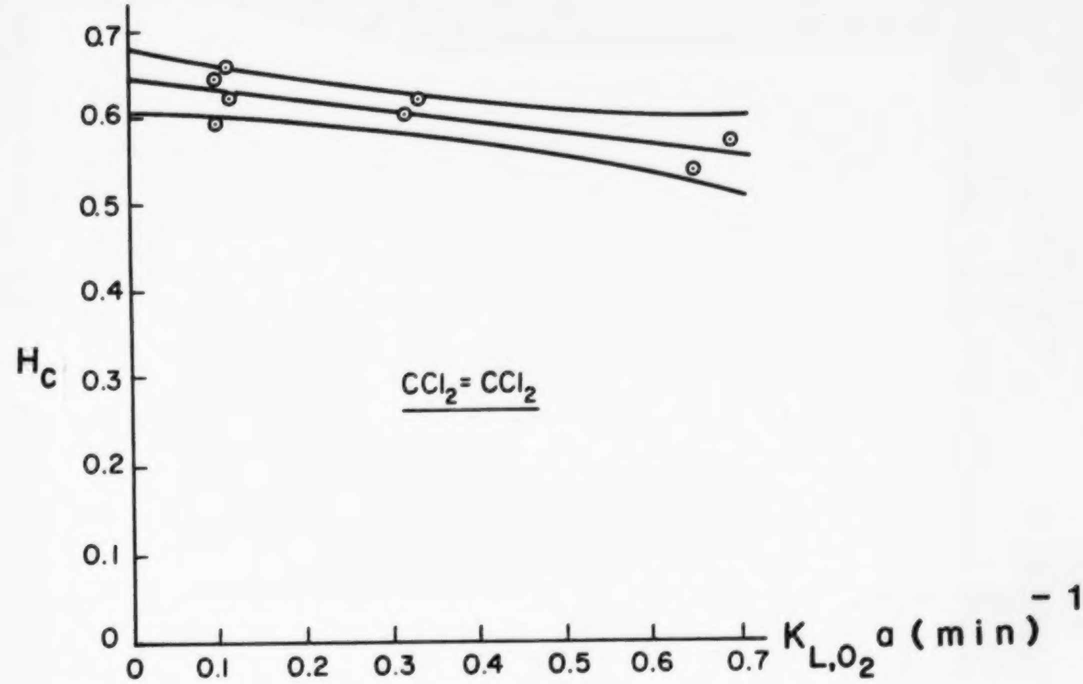

Figure 41. Regression of $H_{c,CCl_2=CCl_2}$ versus $K_{L,O_2}a$ from bubble-column data.

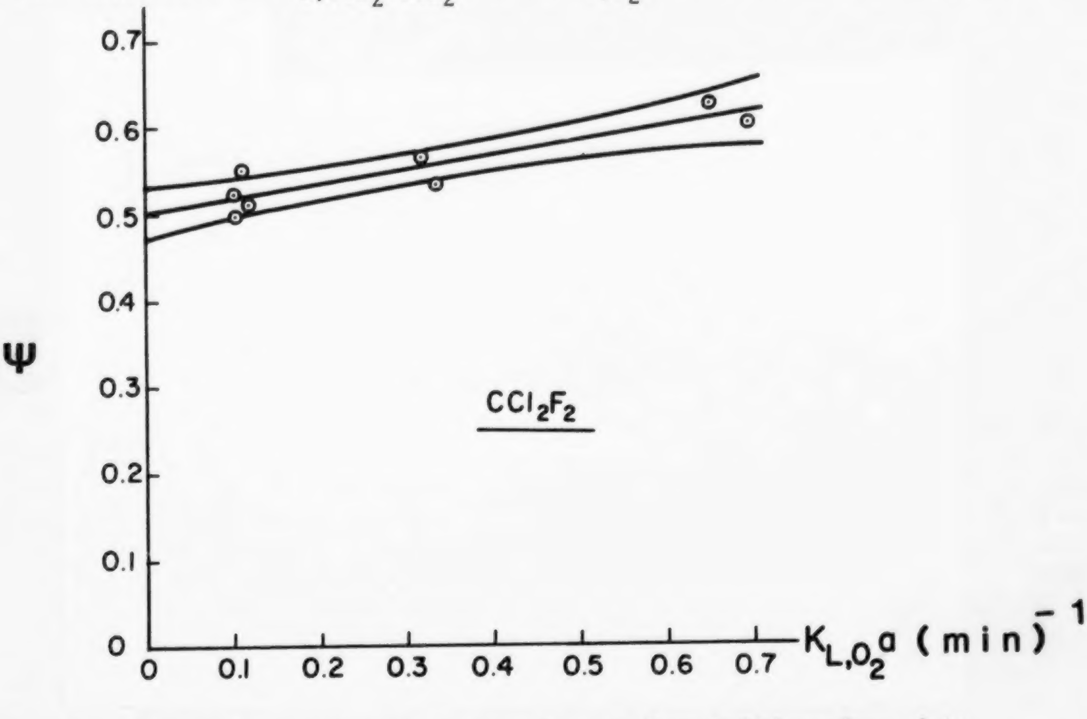

Figure 42. Regression of $\Psi_{CCl_2F_2}$ versus $K_{L,O_2}a$ from bubble-column data.

INFLUENCE OF METHANOL ON $H_{ci}$ AND $\Psi_{CCl_2F_2}$

The results of duplicate runs at three different levels of methanol concentration are shown in Fig. 43. The concentrations studied are indicated on the figure. The average values and standard deviations for the experiments are given in Table 22. The results of the individual experiments are given in Table D-2, Appendix D.

Two experiments were conducted in which the methanol was added midway through the experiment to see if any influence of increased methanol concentration would be apparent from a change in slope. The results are summarized in Table 23.

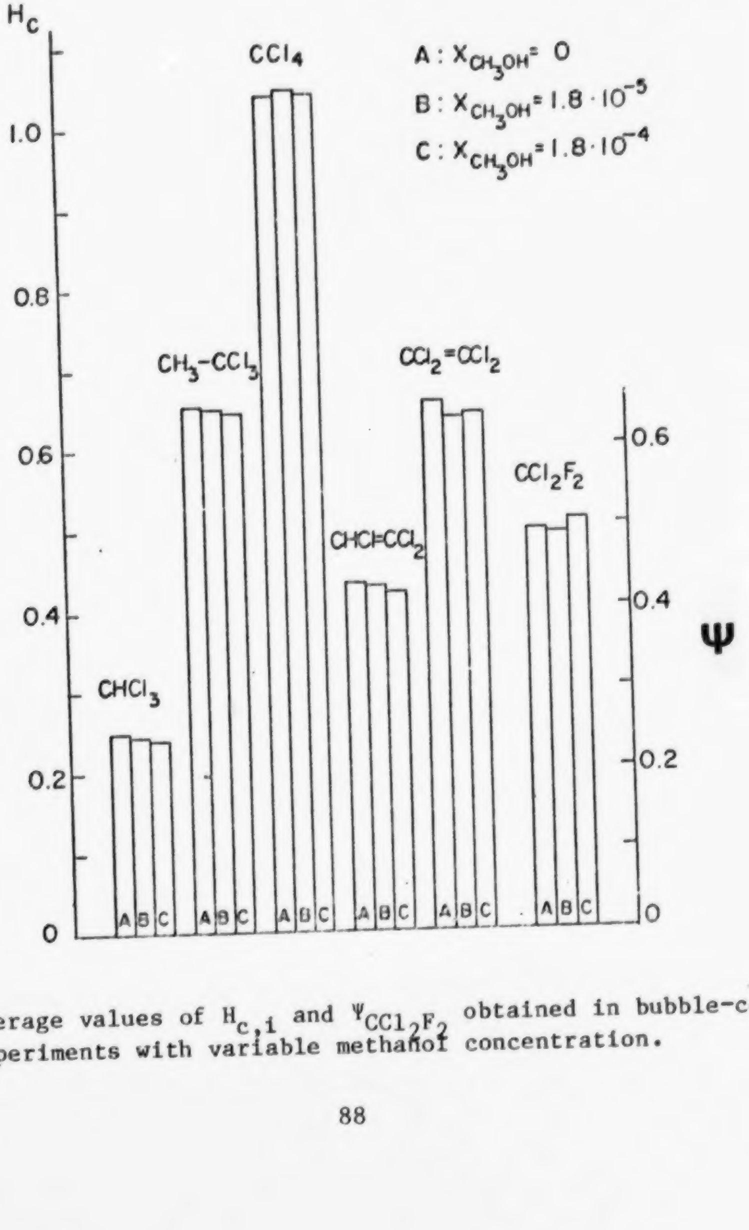

Figure 43. Average values of $H_{c,i}$ and $\Psi_{CCl_2F_2}$ obtained in bubble-column experiments with variable methanol concentration.

TABLE 22. AVERAGE VALUES OF $H_c$ and Ψ FROM BUBBLE-COLUMN EXPERIMENTS WITH VARIABLE METHANOL CONCENTRATION

| Compound | $H_c$ [20°C]<br>Mean ± Std. Dev. | Std. Dev. / Mean |
|---|---|---|
| $CHCl_3$ | 0.245 ± 0.012 | 0.049 |
| $CH_3CCl_3$ | 0.650 ± 0.013 | 0.019 |
| $CCl_4$ | 1.042 ± 0.014 | 0.014 |
| $CHCl{=}CCl_2$ | 0.427 ± 0.015 | 0.034 |
| $CCl_2{=}CCl_2$ | 0.645 ± 0.013 | 0.020 |
| $CCl_2F_2$ | Ψ = 0.498 ± 0.008 | 0.016 |

TABLE 23. RESULTS OF BUBBLE-COLUMN EXPERIMENTS WITH METHANOL ADDITION AT MIDPOINT

| Experiment | | $K_{L,O_2}a$ [$min^{-1}$] | $K_{L,CCl_2F_2}a$ [$min^{-1}$] | $\Psi_{CCl_2F_2}$ | $H_{c,i}$ [20°C]<br>$CHCl_3$ | <br>$CH_3CCl_3$ | <br>$CCl_4$ | <br>$CHCl{=}CCl_2$ | <br>$CCl_2{=}CCl_2$ |
|---|---|---|---|---|---|---|---|---|---|
| 1 | 1st-half | 0.121 | 0.0615 | 0.510 | 0.232 | 0.633 | 1.004 | 0.424 | 0.641 |
| | 2nd-half | * | 0.0685 | * | 0.230 | 0.629 | 1.037 | 0.411 | 0.641 |
| 2 | 1st-half | 0.125 | 0.0574 | 0.460 | 0.240 | 0.630 | 0.973 | 0.445 | 0.636 |
| | 2nd-half | * | 0.0649 | * | 0.232 | 0.641 | 1.051 | 0.430 | 0.666 |

*Not evaluated, because the solution was already saturated with oxygen during the second half of the experiment.

## CLOSED-SYSTEM VAPOR-LIQUID EQUILIBRIUM EXPERIMENTS

Vapor-liquid equilibria (VLE) were also measured in a closed system. The results obtained from the four duplicate experiments are shown in Table 24.

The procedure to calculate the Henry coefficient is based on a simple mass balance:

$$C_{Lo} \cdot V_L = C_L^* \cdot V_L + C_G \cdot V_G \qquad (151)$$

where $C_{Lo}$ = initial liquid concentration

$C_L^*$ = liquid concentration in equilibrium with gas phase.

TABLE 24. AVERAGE VALUES OF $H_{c,i}$ FROM CLOSED-SYSTEM VLE EXPERIMENTS

| Compound | $H_c$ [20°C]<br>Mean ± Std. Dev. | Std. Dev. / Mean |
|---|---|---|
| $CHCl_3$ | 0.111 ± 0.040 | 0.36 |
| $CH_3CCl_3$ | 0.487 ± 0.063 | 0.13 |
| $CCl_4$ | 0.831 ± 0.093 | 0.11 |
| $CHCl{=}CCl_2$ | 0.300 ± 0.053 | 0.18 |
| $CCl_2{=}CCl_2$ | 0.481 ± 0.079 | 0.16 |

Substituting the equilibrium expression

$$C_L^* = C_G/H_c \tag{35}$$

into Eq. 151 and solving for $H_c$ we obtain

$$H_c = \frac{V_L \cdot (C_{Lo} - C_L^*)}{V_G \cdot C_L^*} \tag{152}$$

The results were also standardized to 20°C as described above. The Henry coefficients from the closed-system VLE experiments (Table 24) were 20 to 50% higher than the corresponding values of $H_c$ from the bubble-column experiments (Table 20). It appears likely that equilibrium was not attained in the closed-system experiments. Hence, they are omitted in the calculations of overall averages.

## FILTERED SECONDARY EFFLUENT

To assess the effect of wastewater constituents on mass transfer and phase equilibria, four replicate experiments were carried out to compare values of $K_{L,O_2}a$, $\Psi$, and $H_c$ in Milli-Q water and filtered PASE (Table 5). The conditions chosen were $V_L$ = 21 liters and $Q_G$ = 0.23 ℓ/min. These conditions were deemed sufficient to assure $\Phi Z_s \geq 5$, which according to Eq. 110 guarantees a degree of gas-phase saturation greater than 99% for the organic solutes other than $CCl_2F_2$. The bubble-column results were analyzed to estimate $K_La$ values for $O_2$ and $CCl_2F_2$, and $H_c$ values for the other organic solutes, as discussed at the beginning of this section.

The bubble-column results for Milli-Q water and filtered PASE are compared in Table 25. The value of $H_c$ was in all cases higher in PASE than in Milli-Q water; the differences were significant for $CHCl_3$, $CH_3CCl_3$, $CHCl{=}CCl_2$, and $CCl_2{=}CCl_2$, but not for $CCl_4$. The ratio $(H_{c,PASE}/H_{c,MQ})$ ranges from 1.05 to 1.33. In contrast, $K_{L,O_2}a$ was smaller in the filtered effluent experiments than in clean water: the ratio was $(K_{L,O_2}a)_{PASE}/(K_{L,O_2}a)_{MQ} = 0.59$. The value

TABLE 25. RESULTS OF BUBBLE-COLUMN EXPERIMENTS COMPARING MILLI-Q AND PASE

| Parameter | Mean ± Std. Dev.* | |
|---|---|---|
| | Milli-Q | PASE |
| Henry Coefficient, $H_c$ | | |
| $CCl_4$ | 0.937 ± 0.020 | 0.980 ± 0.020 |
| $CH_3CCl_3$ | 0.621 ± 0.017 | 0.693 ± 0.028 |
| $CCl_2{=}CCl_2$ | 0.609 ± 0.003 | 0.698 ± 0.036 |
| $CHCl{=}CCl_2$ | 0.423 ± 0.014 | 0.507 ± 0.034 |
| $CHCl_3$ | 0.245 ± 0.016 | 0.326 ± 0.020 |
| $CHBr_2Cl$ | 0.117 ± 0.007 | 0.151 ± 0.013 |
| $CHBr_3$ | 0.083 ± 0.009 | 0.102 ± 0.016 |
| Mass Transfer | | |
| $K_{L,O_2}a$ $[s^{-1}]$ | 0.134 ± 0.009 | 0.079 ± 0.010 |
| $\Psi_{CCl_2F_2}$ | 0.489 ± 0.035 | 0.520 ± 0.068 |

of $K_La$ for $CCl_2F_2$ also was smaller in the filtered secondary effluent than in the purified water, but the ratio $\Psi_{CCl_2F_2} = K_{L,CCl_2F_2}a/K_{L,O_2}a$ did not differ significantly; the values of $\Psi_{CCl_2F_2}$ were approximately 0.5 in both Milli-Q and PASE. These values of $\Psi_{CCl_2F_2}$ are slightly smaller than the average reported for the main set of bubble-column experiments in Table 20, but are not significantly different.

## SUMMARY OF OBSERVED HENRY COEFFICIENTS

Table 26 shows the overall average results for all bubble-column experiments conducted with purified (Milli-Q) water, with and without methanol

TABLE 26. EXPERIMENTAL AND PREVIOUSLY REPORTED VALUES OF $H_c$

| Compound | n | Observed in This Work Mean ± Std. Dev. | $\frac{\text{Std. Dev.}}{\text{Mean}}$ | Ref.(81) | Ref.(82,83) | Predicted* |
|---|---|---|---|---|---|---|
| $CHCl_3$ | 18 | 0.224 ± 0.031 | 0.137 | 0.106 | 0.10 - 0.123 | 0.129 |
| $CH_3CCl_3$ | 18 | 0.621 ± 0.033 | 0.053 | 0.155 | 0.92 - 1.4 | 0.166 |
| $CCl_4$ | 18 | 1.007 ± 0.043 | 0.043 | 0.944 | 0.67 - 0.92 | 0.948 |
| $CHCl{=}CCl_2$ | 18 | 0.410 ± 0.031 | 0.075 | 0.381 | 0.365 - 0.40 | 0.398 |
| $CCl_2{=}CCl_2$ | 18 | 0.627 ± 0.034 | 0.054 | 0.883 | 0.38 - 0.90 | 0.848 |

Note: all values adjusted to 20°C.

*Calculated from vapor pressure and solubility data (Appendix A) and converted from H to $H_c$ using Eq. 16.

addition, but excluding those of the closed-system VLE experiments. Also included are predicted values for $H_{c,i}$ calculated from vapor pressure and solubility data (given in Appendix A), as well as measured values from Warner et al. (81), and a range of measured and predicted values from Dilling (82,83).

## BUBBLE CHARACTERISTICS AND FLOW REGIME

The flow conditions of the bubble swarm visually appeared quite different for the different gas flow rates used. At low flows the bubbles tended to rise towards one side of the column, while on the other side very small bubbles remained "trapped" in the liquid. This is indicative of a sort of circulatory motion. At the highest flow rate the general picture appeared more random, although a fraction of the smallest bubbles still do not rise directly to the top.

Three pictures of rising bubble swarms are shown in Figs. 44 through 46. The pictures were taken at approximately ½ of liquid depth, gas flow rates of 0.47 ℓ/min, 1.2 ℓ/min, and 2.3 ℓ/min, respectively, and liquid volume of 24 ℓ. As expected, these pictures show that the bubble size is not uniform. Also, it is apparent that the bubble diameter increases somewhat with increasing $Q_G$. It is evident that the bubble shape is spherical in the first two pictures (Figs. 44 and 45), while for $Q_G = 2.3$ ℓ/min the larger bubbles have an ellipsoidal shape (Fig. 46), which agrees quite well with Fig. 6 in Section 4 ($Eo \approx 0.85$ for $d_b = 2.5$ mm). The approximate bubble diameter ranges and estimated average diameter from these pictures are given in Table 27.

The gas holdup ratio, $\varepsilon_G$, can be roughly estimated with the correlation of Akita and Yoshida (40) using the appropriate values of the gas flow rate, $Q_G$:

$$\frac{(4 \cdot Q_G)/(\pi \cdot d_c^2)}{(g \cdot d_c)^{1/2}} = 8.887 \cdot \left(\frac{g \cdot d_c \cdot \rho}{\sigma}\right)^{-1/8} \cdot \left(\frac{g \cdot d_c^3 \cdot \rho^2}{\mu^2}\right)^{-1/12} \cdot \varepsilon_G^{10/9} \quad (153)$$

where $\varepsilon_G = (V_t - V_L)/V_t$ [dimensionless] (154)

$d_c$ = column diameter

$V_t$ = total volume

$V_L$ = liquid volume

The values of $\varepsilon_G$ corresponding to the experimental gas flow rates range from 0.04% to 0.4%. For such low values of $\varepsilon_G$ it can be safely assumed that the bubble swarm rising velocity is virtually identical to that of single bubbles. Hence, the Reynolds number can be estimated to lie in the range $40 < Re < 450$, when using the rise velocities given in Fig. 7 (Section 4). The Eotvos number can be calculated with the estimated average bubble diameters. The striped area in Fig. 6 is the result. Surprisingly good agreement is found in terms of Re and shapes: that is, the values of the estimated average bubble diameters from the pictures seem reasonable, hence confirming the assumption that the rising velocity of the bubble swarm is virtually identical to that of single bubbles.

Reproduced from
best available copy.

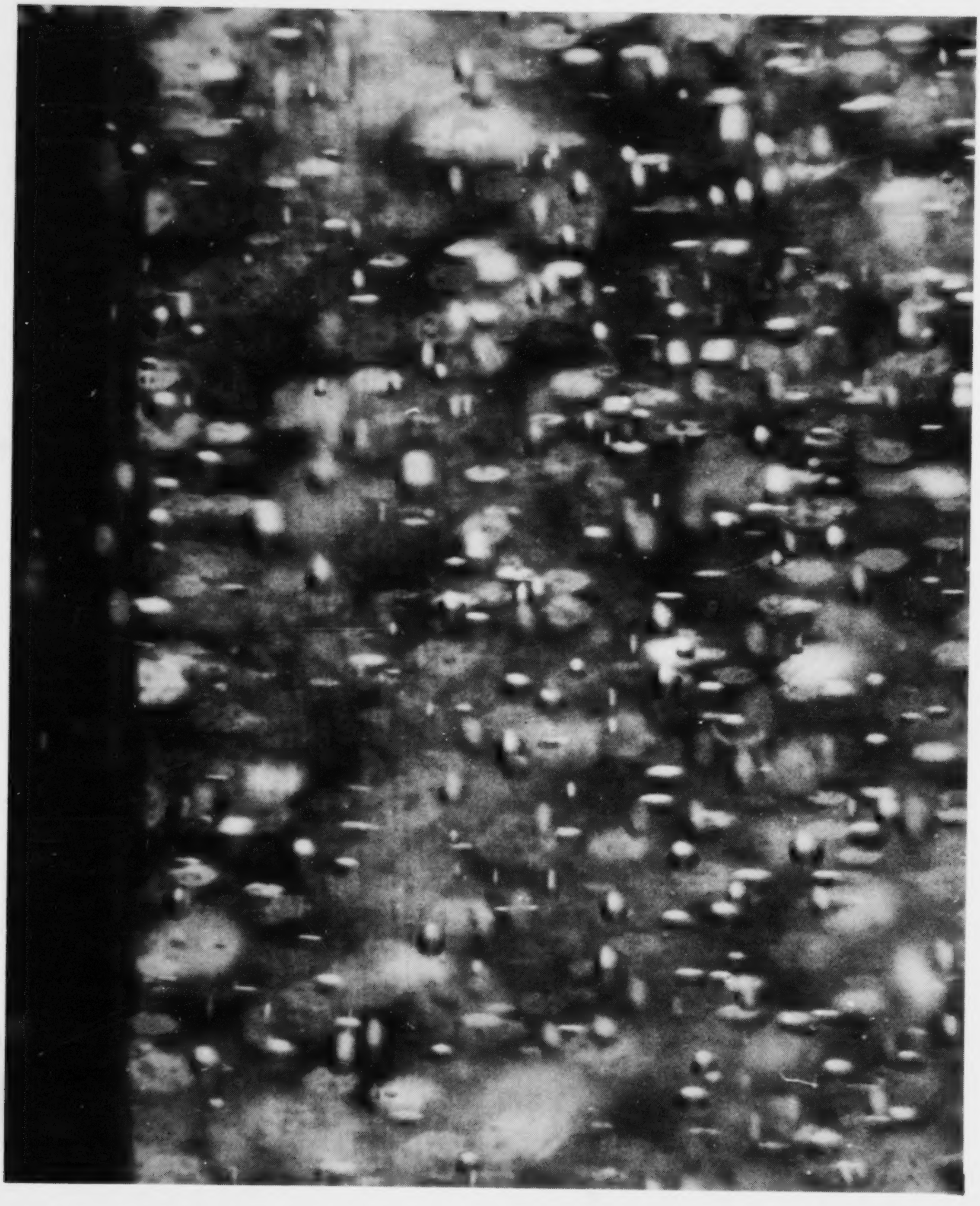

Figure 44. Rising bubble swarm at a gas flow rate of 0.47 ℓ/min.

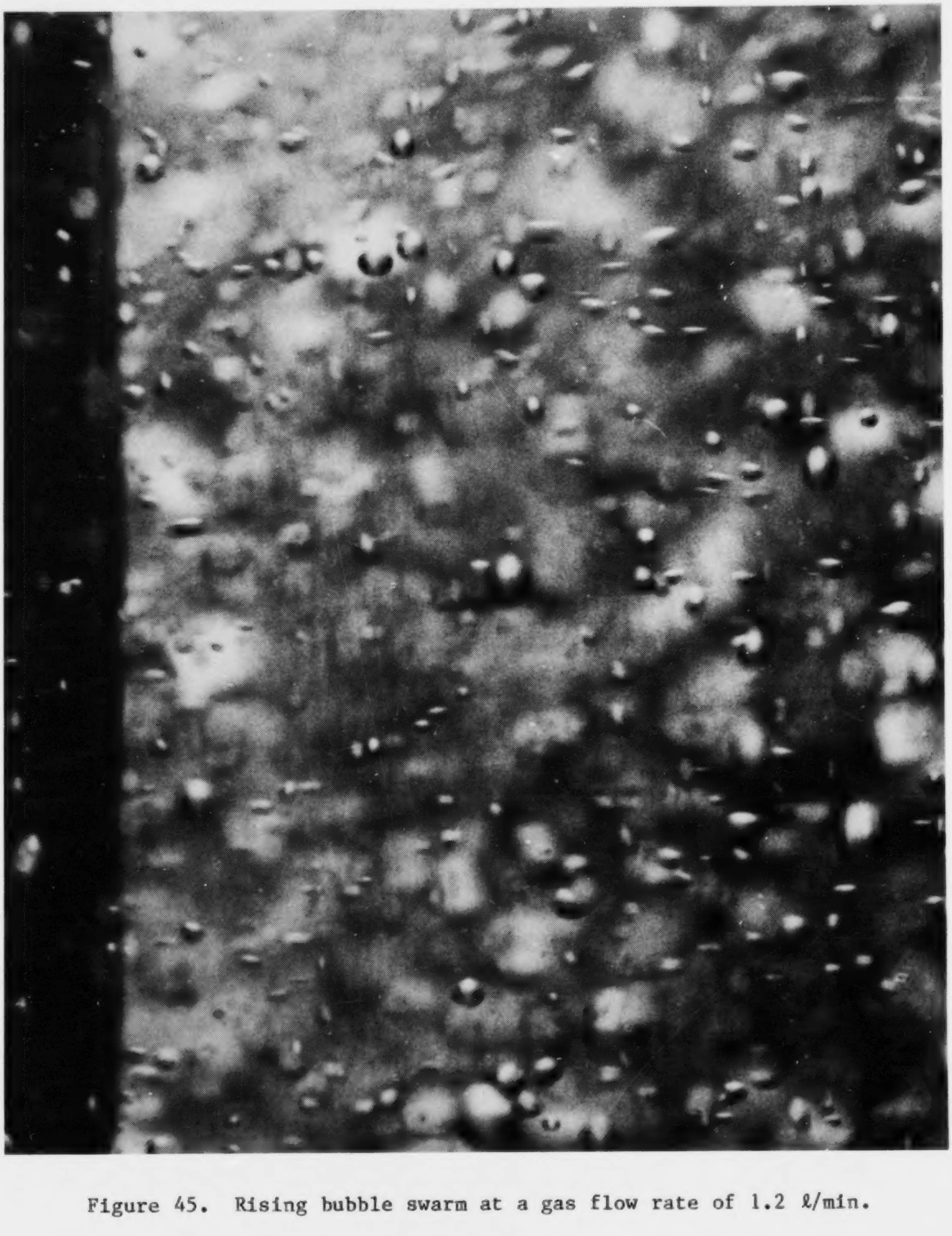

Figure 45. Rising bubble swarm at a gas flow rate of 1.2 ℓ/min.

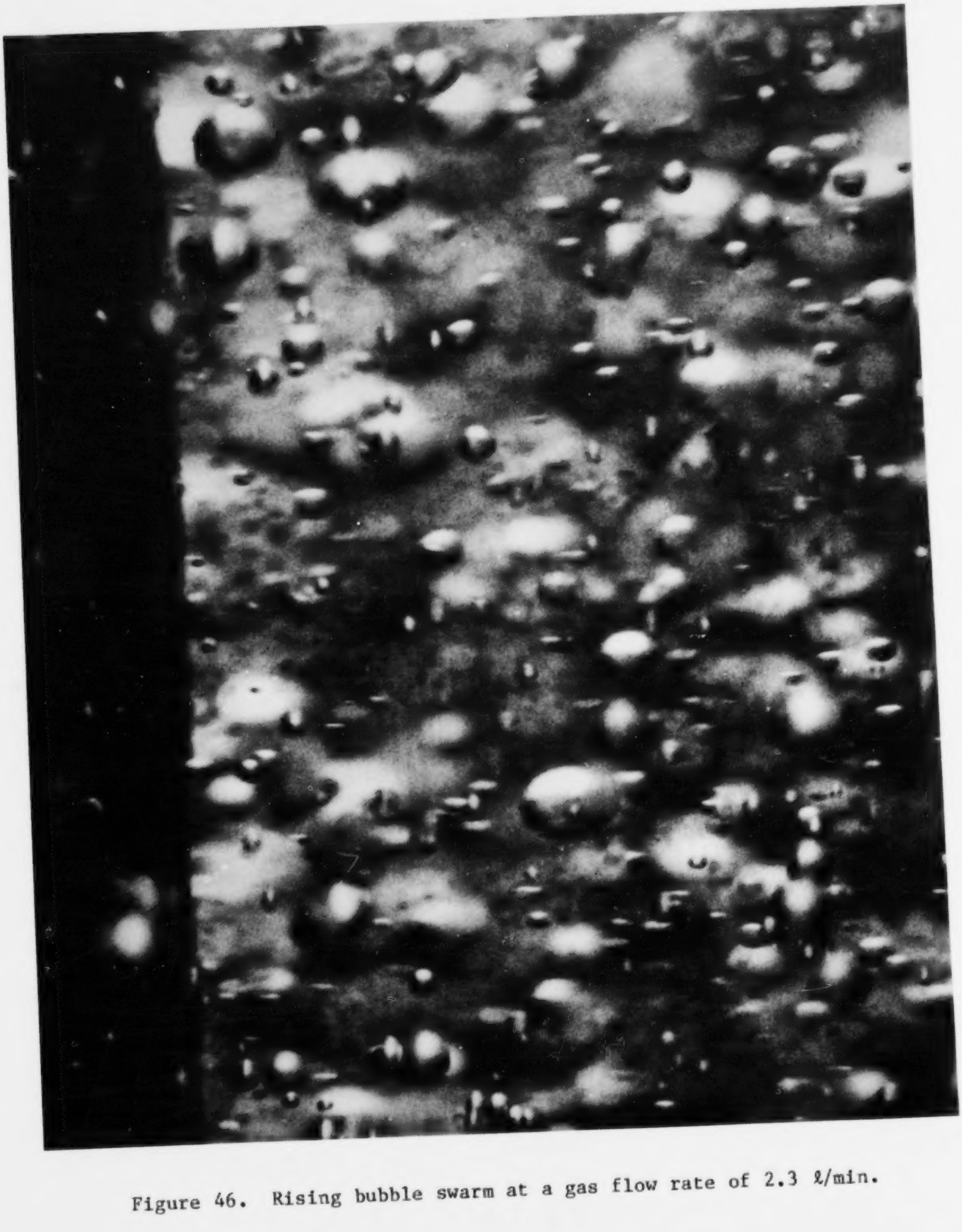

Figure 46. Rising bubble swarm at a gas flow rate of 2.3 ℓ/min.

TABLE 27. BUBBLE DIAMETERS

| Source of Estimate | Gas Flow Rate [ℓ/min] | Range of Bubble Diameter $d_b$ [mm] | Average Bubble Diameter $d_{b,av}$ [mm] |
|---|---|---|---|
| Measured (Figs. 44-46) | 0.47 | 0.5 - 1.1 | 0.7 |
| | 1.2 | 0.5 - 1.2 | 0.8 |
| | 2.3 | 0.8 - 2.5 | 1.3 |
| | ----- | ----------- | ----- |
| Interpolated from Measurements | 0.22* | - - - | 0.6 |
| | 0.86* | - - - | 0.8 |
| | 2.7 * | - - - | 1.4 |

*Conditions corresponding to the experiments reported in this work (Table 3).

# SECTION 8

# DISCUSSION

## SURFACE-AERATION EXPERIMENTS

In this section the discussion will be focused on the main set of experiments. The preliminary set of experiments was roughly analyzed in the previous section: its main purpose was to provide guidance as to the factors that most strongly influence volatilization rates. Where results of the preliminary experiments are used in this section, they will be specially designated as such.

### Experiments with Clean Water

Constancy of $K_L a$--

The graph in Fig. 17 using chloroform as an example gives some clues about the behavior of the diffusion coefficient. The slope of the line represents the $K_L a$-value, which is proportional to the diffusion coefficient. A change of slope with time (and hence, with concentration) would indicate a change of the diffusion coefficient with concentration. In Fig. 17 we clearly cannot detect any significant change in the slope of the line. This indicates that the mass transfer coefficient, and hence the diffusion coefficient, seems to remain constant over that range of concentration. Therefore, the assumption of pseudo-ideality seems to be justified for this experiment. Similarly, the data in other experiments resulted in linear relationships between $\ell n(C_L/C_o)$ and $(t - t_o)$. Hence, we infer that the diffusivity and the mass transfer coefficient were essentially independent of concentration over the concentration range studied in these experiments.

However, we cannot conclude that the activity coefficient is unity, because the term $-\ell n[C(t)/C_o)]$ from Eq. 147 actually should be expressed as

$$- \ell n[f_t/f_o] = - \ell n \left[\frac{x_t \gamma_t}{x_o \gamma_o}\right] = K_L a(t - t_o) \qquad (155)$$

where $f_o$, $x_o$, and $\gamma_o$ and $f_t$, $x_t$, and $\gamma_t$ are the fugacity, mole fraction, and activity coefficient of the solute in solution at time zero and t, respectively. This implies that our data analysis can only show changes in activities "f" with respect to changes in concentration, but will not yield any absolute values. On the other hand, $x_o \gamma_o$ is constant and therefore $-\ell n[x_t \gamma_t]$ has to be linear for constant $K_L a$. By definition C(t) has to behave the same as $x_t$, so if $\ell n$ C(t) is a linear function of t, $\ell n\ x_t$ must behave linearally too; hence we infer that $\gamma_t$ is independent of both time t and of composition x in the range studied, as predicted by theory.

The advantage of using the concentration ratio $C(t)/C_o$ as in Eq. 147 is that absolute concentrations are not necessary; as long as the concentration change over time is known, the $K_La$-value can be determined accurately. In addition, several systematic errors, such as response factors, cancel out in determining the sample concentration. While determining the response factors, the experimental standard deviation for the concentration was 18 to 32%. In contrast, Fig. 16 and corresponding Table 8 indicate a surprisingly good fit of the data for the experiment shown. The goodness of fit was equally satisfactory for the other experiments. The values of $r^2$, which denote the fraction of variance accounted for by the linear correlation, were between 0.98 and 1.00 for all experiments. With high standard deviations for concentrations, the value of $r^2$ would be expected to be lower. Hence, the accuracy of the concentration measurements is much higher than initially expected. Probably the high standard deviations for the standard concentrations stem from inaccuracies in preparing the standard solutions, rather than from the gas chromatographic analysis. This could result from volatilization while preparing the standards or from imprecise stock solutions.

A possible influence in the change of $K_La$ is the change of volume in the contactor due to sampling and evaporation. The change in volume causes a change of the specific interfacial area a (Eq. 80a) because the surface area remains constant while the liquid volume decreases. The decrease in volume due to sampling was approximately 2.5%. For short runs (30 min) the evaporation is negligible, whereas for long runs (9 hrs) the volume loss was an additional 2.5%. A decrease of 5% in total volume should have no significant effect on the calculation of $K_La$.

Changes in water temperature also affect the $K_La$-value, because the diffusion coefficient and the viscosity change with temperature. Especially for the determination of $K_{L,O_2}a$, it was essential to have the same initial and final temperature, because the oxygen saturation concentration $C_L^*$ is temperature dependent.

Utmost care was taken to keep the reactor at constant temperature during the run. For short experiments (30 min), fluctuations were less than 0.2°C, whereas for long runs (9 hrs), the temperature varied ± 0.5°C. However, the effect on the $r^2$-value of the regression was not detectable.

From the boundary conditions at $t = 0$, $C(0) = C_o$, the regression line is expected to go through the origin. Changes of temperature during the experiment have an effect on the intercept of the regression line. Also, dust particulates that are captured from the air by the water during the run may alter the $K_La$-value and therefore cause an intercept at $t = 0$. It is also likely that sampling and analytical methods introduced an error that made the regression line deviate from the origin. However, statistical analyses showed that in most cases the intercept did not differ significantly from zero, so that a regression line suppressing the intercept can be justified.

Ideality of System--

In experiments with liquid-phase data, the question arises how the system differs from ideal behavior and how such deviations affect the results. Analysis with gas chromatography yields estimates of the "true" concentration of the sample, whereas in the contactor the force driving the compound out of the liquid is governed by its fugacity. In Section 4, thermodynamic derivations led to the conclusion that for very dilute solutions the activity coefficient of the solute $\gamma$ can be expected to be constant over the range of interest. Systems with constant activity coefficients are sometimes called pseudo-ideal, in contrast to an ideal system, in which the activity coefficient by definition equals unity.

One way to check for pseudo-ideality is to investigate the behavior of the diffusion coefficient or the mass transfer coefficient, respectively. As stated in Section 4, the diffusion coefficient can change with concentration in a nonideal system. Consequently, the mass transfer coefficient may also change similarly.

Results presented in Section 6 showed that the diffusion coefficient did not change with concentration and the assumption of pseudo-ideality therefore seems reasonable. On the other hand, no distinction could be made between ideal and pseudo-ideal behavior. But from Eq. 11 ($\gamma = 1/x'$) we can estimate the order of magnitude of $\gamma$. For example, the solubility of chloroform is $x' = 1.22 \times 10^{-3}$, from which we infer, by using Eq. 11, that $\gamma \approx 800$; hence $\gamma$ is almost three orders of magnitude greater than unity. Therefore, chloroform will certainly not behave ideally. Rather, pseudo-ideal behavior could be expected with $\gamma$ equal to a constant greater than unity, as confirmed by the experiments.

Flow Regime--

Mixing conditions are very important for mass transfer. If the intensity of turbulence is insufficient, diffusion through the bulk of the liquid to the liquid film will influence the rate of mass transfer substantially. The diffusion coefficient of the bulk liquid can be written as (25, p. 126)

$$D_t = D_E + D_{AB} \tag{156}$$

where $D_t$ = overall turbulent diffusion coefficient

$D_E$ = diffusion coefficient due to eddies

$D_{AB}$ = diffusion coefficient due to molecular diffusion.

For intense turbulence $D_E$ is much larger than $D_{AB}$; therefore, $D_{AB}$ can be neglected. In analyzing our data, the diffusion through the bulk phase was totally neglected, owing to the assumption that bulk-phase mass transport is rapid and therefore not limiting. In turbulent mixing this assumption is justified, because $D_E$ is five to six orders of magnitude greater than $D_{AB}$ (25, p. 127).

The intensity of turbulence can be inferred by interpreting a power curve, as shown in Fig. 47. The power input was measured in a duplicate set of

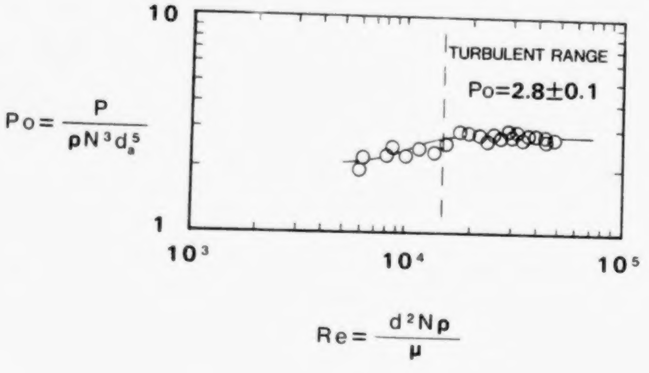

Figure 47. Power curve for impeller used in the main set of surface-aeration experiments.

experiments. The power curve in Fig. 47 can be divided into a turbulent and a transitional region, similar to the typical behavior exemplified in Fig. 4. In the range 15,000 < Re < 50,000, the power number is constant (Po ~ 2.8); therefore the reactor is assumed to be in the turbulent region (37). Below a Reynolds number of 15,000, the power number increases slightly with growing turbulence, so the reactor is expected to be in the transition zone (37). In this zone it is possible that molecular diffusion in the bulk liquid influences to some extent the rate of mass transport to the liquid boundary, e.g., some molecules are transported by eddies to the liquid film (turbulent mixing), whereas other molecules diffuse through the bulk to the liquid surface.

The portion of the data in Figs. 26 through 31 corresponding to low Reynolds numbers shows much greater variation in $\Psi$ than do the data for high Reynolds numbers. Possibly, the diffusion in the bulk phase influenced the rate of mass transfer at low degrees of turbulence in some experiments, although no definite conclusion can be drawn.

Dependence of $K_La$ on Power Input--

The values of $K_La$ for oxygen increased over nearly two orders of magnitude as the agitator speed was increased from 60 to 400 rpm. Figures 48 and 49 show how $\log_{10}P$ and $\log_{10}(K_{L,O_2}a)$ depend on the stirrer speed. The power input was calculated as in Appendix B. The power input ranged from 6 × $10^{-3}$W to 2.3 W in the main set of experiments reported here. This is equivalent to a range of 0.8 to 320 W/$m^3$ for the power input per unit volume. Paulson (84)

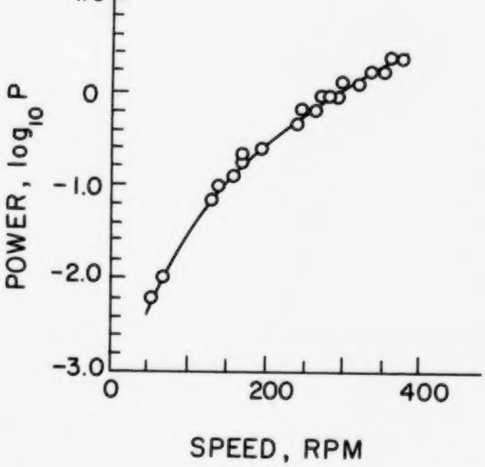

Figure 48. Effect of impeller speed on power input; units of P are [W].

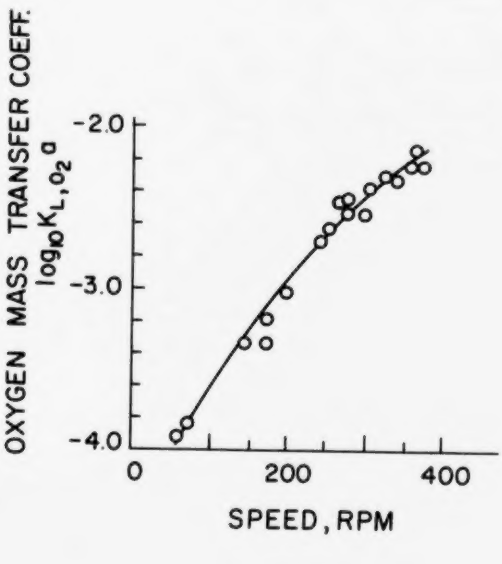

Figure 49. Effect of impeller speed on the oxygen mass transfer rate constants, $K_{L,O_2}a$ [$s^{-1}$].

reports that the power input per aeration-basin volume ranges from 8 to 60 $W/m^3$ (0.04 to 0.3 hp/1000 gal) for surface aeration in activated-sludge treatment practice. The range of power inputs studied in this work brackets the narrower range typical in practice.

Comparison of the shapes of the curves in Figs. 48 and 49 suggests a log-log correlation between the $K_{L,O_2}a$ and the power input, as shown in Fig. 50. A linear regression of $\log_{10}(K_{L,O_2}a)$ against $\log_{10}P$ yields for the fully turbulent range (Re > 15,000)

$$K_{L,O_2}a\ [s^{-1}] = 3.75 \times 10^{-3}\ P^{1.004} \tag{157}$$

The regression was calculated after excluding the two data points at 68 and 57 rpm, for which the value of Re was approximately 10,000, because the system apparently was not fully turbulent (Fig. 47). The data points included in the regression represent power input per unit volume in the range $11\ W/m^3 < (P/V_L) < 320\ W/m^3$; this range slightly exceeds the values of $8\ W/m^3 < (P/V_L) < 60\ W/m^3$ reported by Paulson (84) for typical practice in activated-sludge treatment.

For the fully turbulent flow range, Re $\geq$ 20,000 (N $\geq$ 130 rpm) in these experiments, the oxygen mass transfer coefficient was found to be proportional to the power input, according to the regression result, Eq. 157. The proportionality implied by Eq. 157 is consistent with the general consensus from

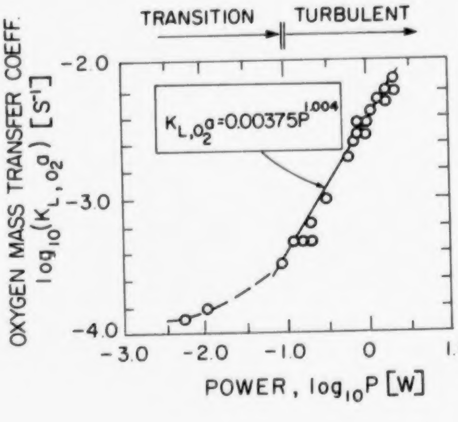

Figure 50. Dependence of $K_{L,O_2}a$ [$s^{-1}$] on power input [W] to surface aerator.

treatment practice that the oxygen transfer rate is proportional to the power input (77,84,85). The relation between $K_{L,O_2}a$ and P in Eq. 157 is equivalent to an oxygen-transfer:energy ratio of 0.78 kg $O_2$/kWh, calculated as shown in Appendix B. This value is less than the values reported for mechanical surface aerators used in wastewater treatment practice, which fall in the range from 1.2 to 2.4 kg $O_2$/kWh for clean water tests (77,86). The lesser oxygen-transfer:energy ratio of the surface aerator used in the present work probably results from its multipurpose design: the agitator was intended to ensure complete mixing of the bulk liquid as well as to promote gas transfer at the water surface, and care was taken to minimize slashing and bubble entrainment. The energy input needed to achieve rapid mixing of the water volume was necessary from the research viewpoint to provide accurate data, but was in effect partially "wasted" from the practical viewpoint of enhancing the oxygen transfer rate.

Influence of Bubbles--

With very high turbulence, entrainment of fine air bubbles may increase drastically the interfacial area a. In tests reported by Eckenfelder (88), up to 60% of oxygen transfer resulted from liquid spray and 40% from turbulence entrainment. With high air entrainment, the mass transfer model changes from pure surface aeration to a mixed model of submerged and surface aeration. The mass transfer partially occurs at the water surface with a driving force of $(C^*_{L,O_2} - C_{L,O_2})/(C^*_{L,O_2} - C_{o,O_2})$ and partially through the air bubbles with a driving force similar to submerged aeration.

For stripping of organics by submerged aeration in a batch experiment, the change in liquid-phase concentration with time is given by Eq. 111. If, in surface aeration, the mass transfer to entrained bubbles were predominant the liquid-phase concentration could be calculated using the following modified form of Eq. 111

$$\frac{C^*_L}{C_L} = \frac{V_G \cdot H_c}{\bar{t}_G \cdot V_L} \left[1 - \exp\left(\frac{K_L a\ V_L}{H_c} \cdot \left(\frac{\bar{t}_G}{V_G}\right)\right)\right] (t - t_o) \qquad (158)$$

where $(V_G/\bar{t}_G$ = ratio of the entrained air holdup volume to the average residence time of the entrained air bubbles. Equation 158 clearly differs in form from Eq. 147. Therefore, in systems with substantial air entrainment, $K_La$-values obtained with Eq. 147 are erroneous. In systems with fairly low air entrainment, the error in values of $K_La$ calculated from by Eqs. 146 and 147 is negligible.

In order to get true $K_La$-values for mixed aeration systems, a mass transfer relationship would have to be developed that accounts for simultaneous surface and submerged aeration. This would be very difficult, because the amount of bubbles formed and their pathway through the water has to be known. Presently no such relationship is known to describe this situation properly. Therefore, our experiments were not extended into that region and the complications arising from the presence of entrained air bubbles were considered to be negligible in the surface-aeration experiments in this work.

$\Psi$ as a Function of $K_{L,O_2}a$--

According to theory, $\Psi$ should depend only on the organic compound and should be independent of turbulence. In order to compare the behavior of the compounds on a unified basis, a common indicator is needed. Because the turbulence measured as a Reynolds number is dependent on the geometry of the reactor, the variable $K_{L,O_2}a$ was chosen for the common abscissa. The graphs in Figs. 26 through 31 show the data for all the compounds. The regression equations are displayed in Table 18. Figure 51 depicts the regression lines, and confirms that the observed values of the mass transfer coefficient ratios are independent of the absolute value of the reference transfer rate constant $K_{L,O_2}a$, for practical purposes.

For the following compounds, the slope is not significantly different from zero: 1,1,1-trichloroethane; trichloroethylene; and tetrachloroethylene. For the other compounds--Freon-12, chloroform, and carbon tetrachloride--the slopes differ significantly from zero.

In Table 18, the values for the t statistic for the slope of the regression lines are listed. If $t \leq t^*_{95\%}$, then the slope is not different from zero at the 95% level of significance. If $t \geq t^*_{95\%}$, the slope is statistically different from zero at the 95% level. Therefore, for the latter group of compounds, $\Psi$ does vary with $K_{L,O_2}a$ to a statistically significant extent, whereas this cannot be said of the former group.

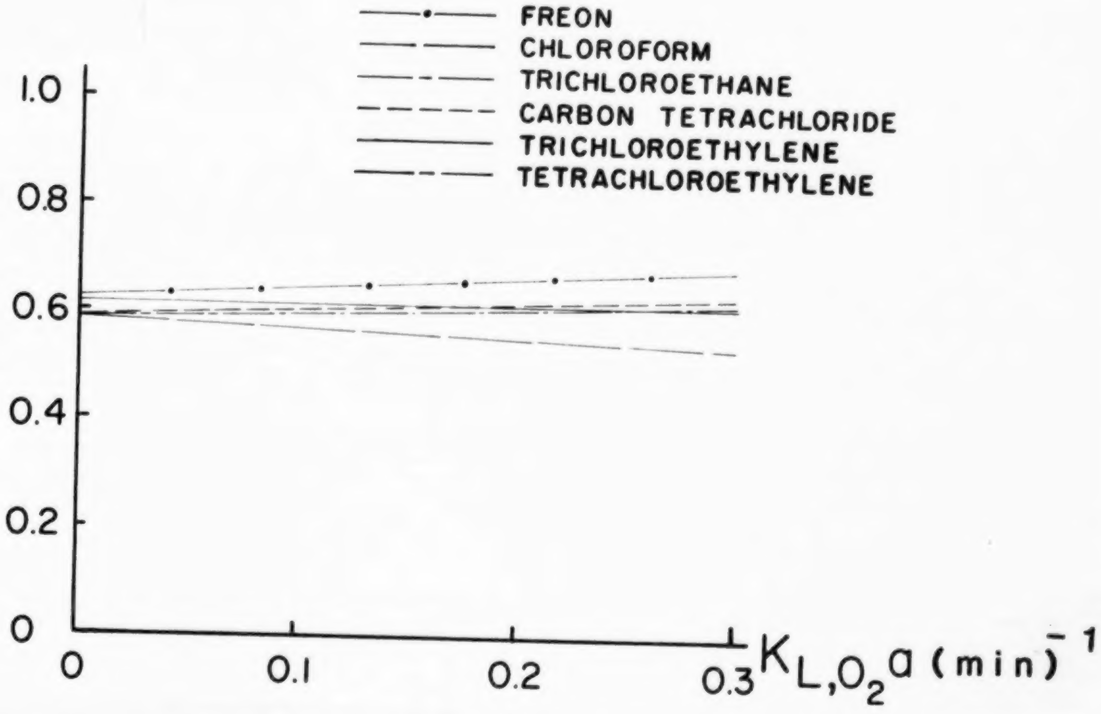

Figure 51. Summary of regressions of $\Psi$ vs $K_{L,O_2}a$ from surface-aeration experiments.

## Comparison of Preliminary and Main Data Sets

The following comparisons can be made between the preliminary set (Table 12) and the main set of data (Table 16). The average values of $\Psi$ are about 5% lower for the preliminary set, where the range and average value of $K_{L,O_2}a$ are narrower. This observation supports the notion that $\Psi$ could be slightly dependent on the turbulence of the flow regime. The differing values of $\Psi$ could also be caused by the change of impeller types.

In Tables 15 and 18 Freon-12 has the largest coefficient of $K_{L,O_2}a$; the coefficient decreases in the same order of substances in both tables. This suggests that the slope might be influenced by some solute property. The compounds ranked as follows in descending order of $\Psi$-values: first, Freon-12, next, a group consisting of carbon tetrachloride, trichloroethylene, tetrachloroethylene, and trichloroethane; and finally, chloroform. This rank order is in approximate accord with the solute's hydrophobicity as measured by the Hansch parameter (87) and also agrees with the inverse order of the solutes' Henry coefficients (Table 20 and Table A-1). However, from an engineering point of view, the change of $\Psi$ with $K_{L,O_2}a$ is not significant, and average values for $\Psi$ as shown in Table 16 are acceptable.

## Mass Transfer Models

Understanding the physical phenomena that occur in a reactor often helps to explain unexpected deviations from mathematically derived expressions. The model proposed for mass transfer was the simple film-resistance model; later the penetration, surface-renewal, and boundary-layer theories were advanced because not all phenomena observed in mass transfer experiments could be brought into accordance with the film theory.

One approach to discerning which of the alternative mass transfer theories agrees best with the experimental data is to consider the dependence of the observed mass transfer coefficient upon the solute diffusivity, as expressed in Eq. 72.

$$\Psi_i = \left(\frac{K_{L,i}}{K_{L,O_2}}\right) = \left(\frac{D_{L,i}}{D_{L,O_2}}\right)^{\Omega} \tag{72}$$

To estimate the diffusion coefficients for substitution into Eq. 72, the Wilke-Chang relation (Eq. 64) was used with $\Phi = 2.26$ (74) and the solute molal volumes estimated using Schroeder increments (29). The justification for this procedure is given in Section 7. The specific values of the diffusion coefficients used in the following analysis are those starred in Table A-3 of Appendix A.

The relation of the mass transfer coefficient ratio $\Psi$ to the ratio of diffusivities is shown in Fig. 52, using oxygen as the reference compound. The corresponding values of $\Psi$ and the diffusivity ratio are given in Table 28. The locus of points corresponding to a constant value of $\Omega$ is represented as a straight line in Fig. 52; lines are shown for the film theory ($\Omega = 1$), the boundary-layer theory ($\Omega = 2/3$ for pure water), and the

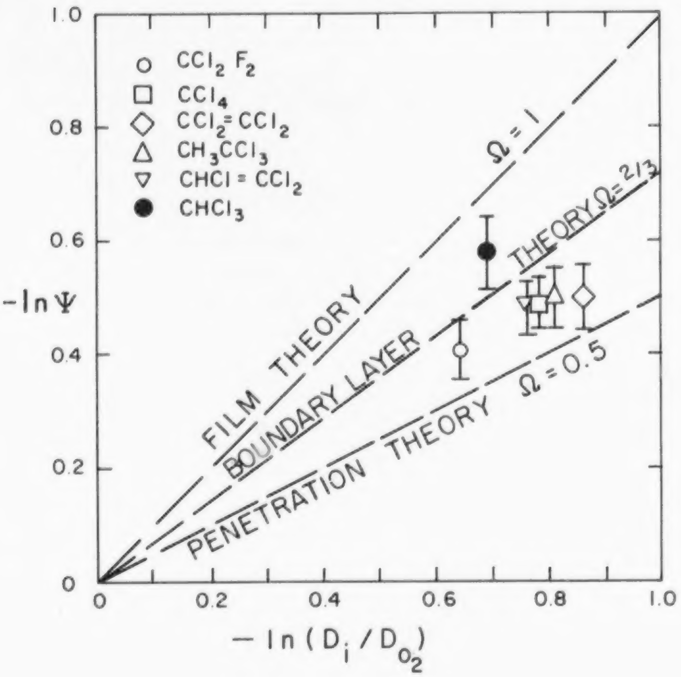

Figure 52. Comparison of mass transfer models for describing the relation between Ψ-values and diffusion coefficients. Error bars represent the mean and standard deviation of the estimate of Ψ from surface-aeration experiments with clean water.

TABLE 28. RATIOS OF MASS TRANSFER RATE CONSTANTS AND DIFFUSIVITIES

| | Ratio of Mass Transfer Rate Constants* | | Diffusivity Ratio |
|---|---|---|---|
| Substance | Ψ | ℓn Ψ | $\ln(D_i/D_{O_2})$ |
| $CCl_2F_2$ | 0.661 | -0.41 | -0.64 |
| $CHCl_3$ | 0.560 | -0.58 | -0.69 |
| $CH_3CCl_3$ | 0.607 | -0.50 | -0.81 |
| $CCl_4$ | 0.617 | -0.48 | -0.78 |
| $CHCl=CCl_2$ | 0.615 | -0.49 | -0.77 |
| $CCl_2=CCl_2$ | 0.608 | -0.50 | -0.87 |

*Average values for experiments with Milli-Q water (Table 16).

penetration theory ($\Omega = 1/2$). The data points for five of the six compounds are clustered in the zone bounded by the predictions of the penetration and boundary-layer theories. Chloroform, which appears to demonstrate a stronger dependence of the mass transfer coefficient on the diffusion coefficient than is evidenced by the other organic compounds, constitutes the exception.

It is possible that the apparently stronger dependence of the chloroform mass transfer rate upon the diffusivity in fact reflects a diminution of the transfer rate arising from a significant gas-phase mass transfer resistance. This may be inferred from the fact that chloroform is the least volatile compound of the six considered (Table 20). According to Eq. 46, the ratio of the gas to the liquid-phase resistance increases with decreasing Henry coefficient. However, the magnitude of the gas-phase resistance could not be calculated owing to lack of data on the air velocity above the liquid surface.

Hence, there is reason to believe that the correct value of $\Omega$ lies between $1/2$ and $2/3$ under the conditions of surface aeration in this work, so long as the liquid-phase resistance truly controls. The values of the exponent $\Omega$ are given as the mean ± standard deviation in Table 29 for the six compounds. For all six compounds the overall average is $\Omega_{av} = 0.66$, which agrees closely with the value of $\Omega = 2/3$ predicted by the boundary-layer theory. However, if chloroform is excluded, the average for the remaining five compounds is $\Omega_{av} = 0.62$ with 95% confidence interval equal to $0.61 < \Omega_{av} < 0.63$ ($n = 80$). The latter average value agrees closely with the value of $\Omega = 0.61 \pm 0.07$ reported by Smith et al. (36) for eleven compounds from surface aeration experiments conducted in the laboratory under conditions similar to this work.

TABLE 29. ESTIMATED VALUES OF $\Omega$

| Substance | Diffusivity $D \times 10^9$ [$m^2/s$] | Measured Values of $\Psi$ | $n^*$ | Estimated Values$^\dagger$ of $\Omega$ |
|---|---|---|---|---|
| $CCl_2F_2$ | 0.991 | 0.66 ± 0.04 | 16 | 0.65 ± 0.09 |
| $CHCl_3$ | 0.944 | 0.56 ± 0.04 | 16 | 0.84 ± 0.09 |
| $CH_3CCl_3$ | 0.830 | 0.61 ± 0.03 | 16 | 0.62 ± 0.06 |
| $CCl_4$ | 0.861 | 0.62 ± 0.03 | 16 | 0.63 ± 0.07 |
| $CHCl=CCl_2$ | 0.864 | 0.62 ± 0.03 | 16 | 0.63 ± 0.06 |
| $CCl_2=CCl_2$ | 0.785 | 0.61 ± 0.03 | 16 | 0.57 ± 0.07 |

*Main set of surface aeration experiments, Milli-Q.

†Mean ± standard deviation of the mean.

## Effect of Wastewater Matrix

### Comparison of $K_La$ and $\Psi$ in Milli-Q and PASE--

A convenient way to compare mass transfer coefficients in wastewater and clean water is the $\alpha$ factor (Eq. 150). Table 17 gives a summary of $\alpha$ for two different speeds. It should be noted that the organic compounds have nearly equal $\alpha$ factors ($\alpha = 0.885 \pm 1.5\%$ at 172 rpm), and it is significantly different from $\alpha_{O_2}$ ($\alpha_{av} = 0.765$). This suggests that the different organic compounds are influenced in the same way by wastewater constituents. Moreover, it is likely that the same constituents in the wastewater influence the organic compounds. From studies of oxygen transfer it is known that the presence of materials such as protein, detergents, oils, and other surface-active agents affect film thickness and surface tension. The effects of surfactants can be described in different ways. Mancy et al. (88) suggest two main causes:

- The surfactants form a film, which may cover partially or totally the water surface and act like an insulating film, separating the gas and the liquid phase. This interfacial film exerts resistance to gas transfer and distorts intermolecular forces between the water surface and the gas molecules.

- The surfactants increase the viscosity and depress the hydrodynamic activity of the water surface. "The increase of viscosity of the water surface results in the elimination of all random surface motion, a phenomenon called surface stagnation or quiescence" (88). Aiba et al. (89) came to the same conclusion, suggesting that surface-active agents make the interface more quiescent, and therefore "decrease the rate of surface renewal" (89, p. 452).

In both cases, the resistance to mass transfer is increased and the $K_La$-value is reduced by the surfactant. Both models describe the decrease in mass transfer in purely physical terms. This suggests that no difference should be seen between oxygen and organic compounds, and that the value of the $\Psi$-ratio for a given solute should be unaffected by impurities such as those in filtered effluent. This hypothesis is confirmed by the slightness of the differences in $\Psi$-values when the Milli-Q and PASE data are compared (Table 16 and Fig. 25).

Influence of Turbulence--

Mass transfer analogies (90, p. 527) show that the liquid-film resistance in mass transfer will decrease with higher turbulence and accordingly the mass transfer rate constant will increase. When comparing wastewater to clean water by comparing the mean of $\alpha$-factors, it must be recognized that either the diffusion coefficient or the film thickness may differ.

It is very unlikely that the film thickness $\delta_L$ will be the same in wastewater as it is in clean water, because surfactants can substantially increase the film resistance. Hence, it could be expected that the film thickness of the wastewater will change differently than that of pure water and therefore, the $\alpha$-factor will vary with turbulence. Eckenfelder et al. (91) attempted to describe the relation between the $\alpha$-factor and turbulence for oxygen transfer. They suggested that with increasing turbulence the interfacial film is broken up and mass transfer is controlled by surface renewal. The $\alpha$-values for a system in which the film resistance supposedly governed were lower than the $\alpha$-values at higher turbulence.

The effect of turbulence can be assessed by comparing values of $\alpha$ corresponding to different energy inputs. In this work, four surface-aeration experiments were conducted with filtered secondary effluents at impeller speeds from 163 to 296 rpm (Table C-1). The relation between $K_{L,O_2}a$ and power input for PASE was found to be

$$K_{L,O_2}a\ [s^{-1}] = 2.95 \times 10^{-3}\ P^{1.11} \tag{159}$$

by means of a regression of log $K_{L,O_2}a$ on log P [W], with $r^2 = 0.98$. The experiments correspond to a range of power inputs from $0.17 < P < 1.1$ W. The correlation for $K_{L,O_2}a$ in purified (Milli-Q) water for the same range of power input is

$$K_{L,O_2}a\ [s^{-1}] = 3.80 \times 10^{-3}\ P^{1.16} \tag{160}$$

based on regression ($r^2 = 0.99$) of log $K_{L,O_2}a$ $[s^{-1}]$ on log P [W] for the six Milli-Q experiments in the range $163 < N < 296$ rpm (Table C-1).

Estimating $\alpha$ as the ratio of the $K_{L,O_2}a$-values obtained from Eqs. 159 and 160, one obtains $\alpha$-values in the range 0.77 to 0.85, as shown in Table 30. We conclude, in view of the small number experiments and the consequent error of estimate, that the value of $\alpha$ did not vary significantly with power input (and hence with turbulence) over the range studied. The average value of $\alpha$ was approximately $\alpha_{av} \simeq 0.8$ for these experiments.

TABLE 30. VALUES OF $\alpha$ INFERRED FROM SURFACE-AERATION EXPERIMENTS

| Power Input | | $\alpha = \dfrac{(K_{L,O_2}a) \text{ in Filtered Effluent}}{(K_{L,O_2}a) \text{ in Clean Water}}$ |
|---|---|---|
| P [W] | P/V [W/m$^3$] | |
| 0.17 | 23 | $\dfrac{4.12 \times 10^{-4}}{4.86 \times 10^{-4}} = 0.85$ |
| 0.43 | 60 | $\dfrac{1.16 \times 10^{-3}}{1.43 \times 10^{-3}} = 0.81$ |
| 1.1 | 150 | $\dfrac{3.28 \times 10^{-3}}{4.24 \times 10^{-3}} = 0.77$ |

Statistical Significance of Differences of $\Psi$-Values Between Milli-Q and PASE--

The possible influences that change the $K_L a$-values in wastewater have been discussed previously. Due to the definition of $\Psi$, the $K_L a$-values of organic compounds are compared to oxygen. If the influence of wastewater is the same on organic compounds as it is on oxygen, no change in the Ψ-value is expected to be seen. Comparisons of the Ψ-values in Table 16 and Fig. 25 show that the differences in Ψ are slight. Nonetheless, an analysis of variance showed that Ψ differs significantly ($p = 0.95$) between wastewater and clean water. The reasons could be: differences in adsorption; different influences of surfactants in the liquid boundary layer, due to different polarities; different change in activities, due to surfactants or salts; or a combination of the above. As discussed previously in this section, it is unlikely that adsorption will occur under the present conditions. Aside from this, it does not seem possible to tell which of the above points are predominant.

Comparing the Ψ-values in Table 16, the differences ΔΨ between PASE and Milli-Q water are extremely small, i.e., in the range of 1 to 5%. For all substances the standard deviation is larger than ΔΨ. The large standard deviation is partly due to the changes of Ψ with speed. From a practical point of view there is little difference between volatilization behavior in treated, filtered wastewater and in clean water. For engineering needs an average value (Milli-Q and PASE) will suffice. Further, the compounds can be grouped as in Table 31, where the given values are viewed as suitable for use in wastewater engineering. For volatile compounds not included in Table 31, a value of $\Psi = 0.62$ probably would be an acceptable approximation, with accuracy of ± 10%. However this value should be applied only for substances at least as volatile as chloroform ($H_c = 0.245$). Unfortunately, the grouping does not strictly coincide with any physical-chemical properties of the substances. It is noteworthy that Freon-12, with the highest volatility, has the largest Ψ, whereas chloroform with its low Ψ-values is the least volatile. Differences in volatility do not necessarily imply differing Ψ-values, except insofar as the gas-phase resistance becomes increasingly significant as the Henry coefficient decreases; this may have been an important factor in the chloroform data. The other compounds, trichloroethylene, carbon tetrachloride, trichloroethylene, and tetrachloroethylene, have similar Ψ-values, despite their differing volatilities. Hence, the approach based on the analogy between stripping of volatile organic compounds from wastewater and absorption of oxygen has been demonstrated to be valid under controlled surface aeration conditions. However, caution must be observed in generalizing this conclusion to other less volatile compounds. It appears that the transfer rates of compounds whose volatility is equal to or less than that of chloroform may be influenced by a significant gas-phase resistance.

TABLE 31. RECOMMENDED VALUES OF Ψ FOR WASTEWATER ENGINEERING PURPOSES

| Compound | Ψ |
|---|---|
| Freon-12 | 0.66 |
| Chloroform | 0.56 |
| Trichloroethane | 0.62 |
| Carbon tetrachloride | 0.62 |
| Trichloroethylene | 0.62 |
| Tetrachloroethylene | 0.62 |

## BUBBLE-COLUMN EXPERIMENTS

### Influence of Methanol

Because methanol was used as a solvent to assure rapid dissolution of the organic solutes during the bubble-column experiments, it is necessary to evaluate the effect of the presence of methanol on the measured Henry coefficients. In Section 4 we showed the theoretical development to estimate the influence of a second solvent on the Henry coefficient. Wilson (92) provides some experimental data for activity coefficients at infinite dilution. Although these data are mostly for $T \approx 50°C$, they can be used to evaluate the generalized correlation of Pierotti et al. (12). The activity coefficients thus obtained are substituted into Eqs. 22c, 23c, and 24c to obtain values of $B_{ij}$; these in turn are substituted into Eq. 21 to evaluate $H_{2m}$, the Henry coefficient of solute 2 in the mixed solvent (methanol + water). This method predicts a ratio of Henry coefficients, $H_{2m}/H_{21} \approx 0.999$ (mixed solvent:pure water), which indicates virtually no influence of methanol on the Henry coefficient, $H_{21}$, at the highest concentration studied, i.e., $x_{CH_3OH} = 1.8 \times 10^{-4}$.

Such small differences are not significant compared to experimental error, as is apparent from the data in Fig. 43. Three compounds, $CHCl_3$, $CH_3CCl_3$, and $CHCl{=}CCl_2$, show a decline in $H_c$ with increasing methanol concentration as predicted, but substantially larger (0.962, 0.988, and 0.972, respectively). The other two compounds show a random behavior. Hence, rather than showing an actual influence of methanol on $H_c$, these results can be assumed to be representative of the experimental error. The standard deviations of the average values (Table 22) are small considering the relatively few data points involved. Table 23, although representing only two experiments, also confirms the above conclusion: there is no indication of the influence of methanol on $H_c$.

The $K_La$-values for $CCl_2F_2$ shown in Table 23, however, exhibit a substantial increase when methanol is added. Unfortunately, in these experiments $K_{L,O_2}a$ could not be measured in the second half and $\Psi_{CCl_2F_2}$ could not be calculated.

Summarizing, we conclude that the methanol concentrations used in this work have no effect on $H_c$ and $\Psi_{CCl_2F_2}$, and that the variations in Fig. 43 and Table 23 can be attributed to experimental inaccuracy. Dilling et al. (82) also concluded that there was no appreciable influence of methanol on the volatilization rates of chlorinated organic compounds in their work, but presented no data to support their contention. Also, the octanol-water partition coefficient for methanol is smaller than unity (87). This indicates that methanol behaves more similar to water than to an n-alcohol, which in turn supports the conclusion drawn above.

### Ideality of System

In experiments with liquid-phase data, the question may arise as to how the system differs from ideal behavior and how such deviations affect the results. The arguments here are identical to those stated earlier in regard to the surface-aeration experiments. Analyzing samples with gas chromatography yields an estimate of the mass concentration of the sample, whereas in the reactor the driving force for mass transfer is governed by the fugacity. In Section 4 thermodynamic derivations led to the conclusion that for very dilute solutions the activity coefficient of the solute, $\gamma$, can be expected to be constant. Systems with constant activity coefficients are sometimes called pseudo-ideal, in contrast to ideal systems where the activity coefficient by definition equals unity.

One way to check for pseudo-ideality is to investigate the behavior of the diffusion coefficient or the mass transfer coefficient. As mentioned in Section 4, the liquid-phase diffusion coefficient may change with concentration in a non-ideal system, but it was taken as constant since ideality was assumed. The example of bubble-column data in Fig. 32 gives some clues about the behavior of the diffusion coefficient. The slope of the curve is related to the $K_La$-value, and this in turn is proportional to the diffusion coefficient raised to a power $\Omega$. A change of slope with time and hence with concentration would indicate a change of the diffusion coefficient with concentration. In Fig. 32 there is clearly no significant change in the slope of the curve. This indicates that the overall mass transfer coefficient, $K_L$, and therefore the diffusion coefficient, seem to remain constant over that range of concentration. Similarly, the data in the rest of the experiments resulted in linear relationships between $-\ln(C_L/C_{Lo})$ and $(t - t_o)$. Hence, our assumption of pseudo-ideality is justified, and we conclude that the diffusion coefficient and the mass transfer coefficient are independent of concentration over the concentration range used in the experiments. However, we may not infer that the activity coefficient is unity, because the term $-\ln(C_L(t)/C_{Lo})$ in Eq. 111 actually should be expressed as:

$$- \ln \frac{f_t}{f_o} = - \ln\left(\frac{x_t \cdot \gamma_t \cdot P^o}{x_o \cdot \gamma_o \cdot P^o}\right) = - \ln\left(\frac{x_t \cdot \gamma_t}{x_o \cdot \gamma_o}\right) \qquad (155)$$

which implies that, unless the exit gas phase is saturated with the compound under consideration, the data analysis can only show changes in activities with respect to changes in concentration, but will not yield absolute values. On the other hand, $x_o \cdot \gamma_o$ is constant and therefore $-\ln(x_t \cdot \gamma_t)$ has to be linear for constant $K_La$. By definition $C_{L,t}$ has to behave the same as $x_t$. Hence, if $\ln(C_t)$ is linear, $\ln(x_t)$ must behave linearly too, and $\gamma_t$ is constant as predicted by theory.

## Constancy of $K_La$

This section is composed of two parts: one pertaining to the experimental methods and the other relating to theoretical considerations.

### Experimental Methods--

The concentration terms in both equations describing mass transfer, Eqs. 103 and 111, are expressed as concentration ratios. This has the advantage that absolute concentrations are not required; as long as the relative concentration ratio over time is known, the $K_La$-value can be determined accurately. In addition, several systematic errors, such as response factors, cancel out in determining the sample concentration. While determining the response factors, the experimental standard deviation for the concentration was 18% to 32%. In contrast, Fig. 32 indicates a surprisingly good fit of the data for the experiment shown. The goodness of fit was equally satisfactory for the other experiments. The values of the square of the correlation coefficient $r^2$, which describes the fraction of variance accounted for by the linear regression, are greater than 0.98 except in two experiments. In these two experiments, two correlations have a $r^2 > 0.97$ and two $r^2 > 0.93$. The reason for these less good fits is that the initial concentrations were relatively low and the sampling intervals too short to allow a sufficient volatilization of $CHCl_3$ (the least volatile compound), and therefore the analysis became less precise, causing overlapping of concentrations for subsequent samples. Nevertheless, these regressions can still be regarded as satisfactory. With high standard deviations for concentration measurements, the value $r^2$ would be expected to be lower. Accordingly, the accuracy of the concentration measurements is much better than initially expected. Probably the high standard deviations for the concentrations stem from inaccuracies in preparing standard solutions, rather than from the gas chromatographic analysis. This is consistent with the better-than-expected precision of the surface-aeration data, reported earlier in this section.

Changes in liquid volume due to sampling could also affect the constancy of $K_La$. The specific interfacial area, a, does not change with a change in volume, if, as assumed, the bubbles rise uniformly through the column. That is, since the surface area available to mass transfer is "standardized" to the liquid volume, $a = A_b/V_L$ is also constant for a given experiment. However, the liquid volume $V_L$ is an important parameter in calculating $K_La$, or for that matter $H_c$, from Eqs. 106, 115, and 119. The calculations were performed using the mean value from initial and final volume in order to minimize the error, based on error analysis. The average percent change in volume for the set of experiments with variable gas flow rates is 5.8%, the maximum 6.9%. When calculating the $K_La$-values for $O_2$ and $CCl_2F_2$, the difference between the values obtained using the initial volume and the final volume is $< 1.5\%$ for $O_2$ and $< 0.4\%$ for $CCl_2F_2$. This, plus the fact that no trend in curvature was observed on the linear regression plots, confirms that the change in volume due to sampling has a negligible effect on $K_La$.

Changes in water temperature also affect the $K_La$-value, because the diffusion coefficient and the viscosity change with temperature. Particularly the determination of $K_{L,O_2}a$ is very sensitive due to the temperature dependence of the oxygen saturation concentration, $C^*$. The average change in temperature, $T_f - T_o$, during the experiments was + 0.36°C, with a maximum of + 0.7°C. The mean value of initial and final temperature was used for the standardization of the results in each experiment.

As discussed in Section 7, Eq. 104, the regression line is expected to pass through the origin, although the correlation may indicate a non-zero intercept, Eq. 104a. Changes of temperature during an experiment have an effect on the intercept of the regression line. From statistical analysis we find that for oxygen in most cases a negative intercept is found that is different from zero at the 95% significance level. For the organic compounds most intercepts are not different from zero and random in terms of the sign of the intercept, at the same significance level. This suggests that, indeed, temperature did have an effect on $K_{L,O_2}a$. However, a sensitivity analysis done by Hunter and Ward, cited by Hunter (85), shows that a deviation of ± 0.1 mg/l from the true value of $C_s$ can cause an error of approximately 5% in the calculation of $K_{L,O_2}a$. This is confirmed when the data of Boyle et al. (71) are analyzed. A ± 0.5°C change in temperature causes a change of approximately ± 0.09 mg/l in $C^*$, which corresponds to approximately ± 2 mm on the chart paper from which the oxygen concentrations were read. Hence we conclude that the temperature change during an experiment did not affect the $K_{L,O_2}a$-value by more than ± 5%. In all experiments but one, the temperature rose during the course of the experiment. Consequently the measured saturation concentration would be smaller than the true $C^*$, implying that $K_{L,O_2}a$ would be overestimated. However, oxygen saturation was reached at approximately half run-time, which means that the average temperature used is quite appropriate for the measured $C^*$. Therefore, it might also be plausible that the initial readings, rather than $C^*$, were slightly in error. This, in turn, would have a smaller effect on the $K_{L,O_2}a$ estimate and might also explain the intercept deviations to a certain extent. Hence, it is likely that the error in the estimated value of $K_{L,O_2}a$ due to temperature changes is smaller than 5%.

Insufficient mixing could also affect the $K_La$-values. As was shown in Table 6, the mixing conditions were good even at the lowest gas flow rates, or, correspondingly, at the lowest $K_{L,O_2}a$. Since the precaution was also taken always to position the oxygen probe and sampling line at the same relative submergence (approximately 1/3), and to draw the sample for organic analysis immediately adjacent to the DO probe, substantial mixing effects can be excluded in this work.

According to Clift et al. (49), the following conditions should apply to ensure that wall effects have negligible influence:

$$\eta \leq 0.08 + 0.02 \cdot \log Re \qquad \text{for} \quad 0.1 < Re < 100$$

and

$$\eta \leq 0.12 \qquad \text{for} \quad Re \geq 100$$

where $\eta = d_b/d_c$, ratio of bubble diameter to column diameter. Taking any bubble diameter and corresponding Reynolds number as described in Section 7, we obtain $0.0022 \leq \eta \leq 0.012$, which is at least one order of magnitude smaller than required. Hence, we conclude that wall effects were insignificant in our studies.

Theoretical--

In Section 4 it was shown that the mass transfer coefficient, $k_L$, is related to the diffusivity $D_L$ raised to a power $\Omega$, where $\Omega = 2/3$ for bubbles with no internal circulation and $\Omega = 1/2$ for bubbles with strong internal circulation. For any given experiment we expect $1/2 \leq \Omega \leq 2/3$, where $\Omega$ = constant, which in turn means that $k_L$ will not vary during an experiment with constant gas flow rate. However, if we consider the ratios of mass transfer coefficients

$$\Psi = \frac{k_{L,i}}{k_{L,j}} = \left(\frac{D_{L,i}}{D_{L,j}}\right)^{\Omega} = (\text{constant})^{\Omega} \tag{72}$$

we realize that $\Psi$ may vary depending on the exponent $\Omega$.

We consider the bubble-column experiments in this work as "pure-system experiments." Methanol is a short molecule and does not act like a surface-active material. This is confirmed by Meissner et al. (93) who showed that the surface tension of water is virtually unaffected by the small concentrations of methanol used. Therefore, according to Section 4, we expect the internal circulation of the bubbles to increase with increasing bubble diameter, which in turn means that $\Psi$ increases with increasing bubble diameter (i.e., turbulence $\propto K_{L,O_2}a$) as the ratio of the diffusion coefficients is $< 1$. This agrees qualitatively with the results found for $CCl_2F_2$ as shown in Fig. 42. Equation 72 predicts a range $0.62 \leq \Psi \leq 0.70$, whereas the range found experimentally is $0.52 \leq \Psi \leq 0.62$. When using Eq. 73,

$$\Psi = \left(\frac{V_{ci}}{V_{cj}}\right)^{\Omega \cdot \varepsilon} \tag{73}$$

we also expect $\Psi \geq 0.62$, which indicates that the diffusion coefficients used in Eq. 72 appear reasonable. Also, an error of approximately 5% in $K_{L,O_2}a$ could not account for the discrepancy. Our results, therefore, predict an exponent $\Omega$ in Eq. 72 in the range $0.91 \geq \Omega \geq 0.67$ from low to high turbulence.

One cause for this discrepancy might be the uncertainty in the estimated diffusion coefficients. The data for oxygen diffusion in water compiled by St. Denis and Fell (94), on which our estimates are based, shows a substantial scatter of data points. For $CCl_2F_2$ we used an experimental value of the molar volume in the modified Wilke-Chang equation. A combined 10% error in the diffusion coefficient ratio is therefore possible. In this case Eq. 73, using the smaller ratio, would predict $0.58 \leq \Psi \leq 0.66$, which is much closer to the values found.

The fact that $\Psi$ increases with increasing turbulence is also predicted by the film-penetration theory (20), as well as an earlier version of this theory developed by Dobbins (95). The latter measured overall mass transfer coefficients, $K_L$, for He and $N_2$ simultaneously in a surface aeration system. His results clearly show an increase of $\Psi$ with increase in turbulence whether measured as agitator speed or as $K_{L,He}$. However, in the surface-aeration experiments in this work, the value of $\Psi$ increased with increasing agitator speed only for one compound, $CCl_2F_2$ (Fig. 50).

## Comparison with Surface Aeration Results

Only for $CCl_2F_2$ can the values of $\Psi$ estimated from the surface-aeration and the bubble-column experiments be compared. The corresponding average

$\Psi$-values for $CCl_2F_2$ in Milli-Q water were as follows: for surface aeration $\Psi_{av} = 0.66 \pm 0.04$ (Table 16), whereas for bubble aeration $\Psi_{av} = 0.55 \pm 0.05$ (Table 20). These average values differ at 95% significance level.

A possible reason lies in the relatively low value of the specific energy input in the bubble-aeration experiments. The specific energy input in bubble aeration can be estimated from

$$\frac{P}{V_L} = \frac{Q_G}{V_L} (\rho_L - \rho_G)\, gZ_s \tag{161}$$

For the bubble-column experiments in this work, the ratio $(Q_G/V_L) = 1.38 \times 10^{-4}$ to $3.18 \times 10^{-4}\ s^{-1}$, and the value $Z_s$ was 0.35 to 0.60 m. The resulting specific energy inputs are $1.3 < (P/V_L) < 31\ W/m^3$, appreciably lower than in the surface-aeration experiments $[11/(P/V_L) < 320\ W/m^3]$. Hence the difference between the surface-aeration experiments and the bubble-column experiments with regard to the observed $\Psi_{CCl_2F_2}$-values is consistent with argument that $\Psi$ should increase with increasing turbulence.

In activated sludge treatment, the specific energy input typically lies in the range $8 < (P/V_L) < 60\ W/m^3$. The surface-aeration experiments in this work coincide better with that range than do the bubble-column experiments. For that reason, and also because of the greater quantity of mass transfer data in the surface-aeration experiments, the $\Psi$-values inferred from the surface-aeration experiments (Table 31) are used for both aeration types in the example calculations in Section 9.

### Constancy of $H_c$

Figures 37 through 41 and Table 21 seem to indicate that the Henry coefficient decreases with increasing turbulence. In contrast to $\Psi$, $H_c$ should not vary with turbulence, as it is a thermodynamic state property of the compound. Therefore we must look for the cause of this anomalous behavior.

Experimental--

The value of $H_c$ is estimated from

$$S = \frac{Q_G \cdot H_c}{V_L} \tag{115}$$

It is evident that the Henry coefficient is very sensitive to any inaccuracies of the liquid volume and/or gas flow rate. The changes in volume due to sampling were mentioned above (approximately 5.8%), and also that the mean value was used in order to minimize the error. It must be recognized, however, that whichever value of $V_L$ is chosen it will have no effect on the regression equations, other than the slight variations in $\Delta V_L$ among the experiments. Hence, the liquid volume cannot be responsible for the behavior of $H_c$. The gas flow rate was initially measured with rotameters, which were calibrated with soap bubble meters and a wet-test meter. A mass flow meter (accuracy ± 1%) was later employed to verify the calibration curves and assure the correctness of the readings. The regressions were adjusted to correct for errors in the rotameter calibration (the highest flow rate was corrected by approximately 5%). We are therefore confident that the gas flow rates were measured as accurately as possible.

Sufficient time was allowed to flush the sampling line completely before taking a sample. This could be checked visually. When the sampling line is closed, the air in the tube collects at the top of the inverted U-tube. This collected air is the first large "bubble" to exit the sampling line when opened, later followed by bubbles drawn into the sampling line from the column, indicating complete flushing. The whole procedure, including filling the hypovial, took approximately 10 sec. Hence, there was no overlapping of samples.

To exclude the possibility that organic solutes are adsorbed onto the fritted glass diffuser, adsorption experiments were carried out with small fritted glass stones. By means of mass balances, which were surprisingly good (± 12% on the average), it was concluded that the solutes did not adsorb significantly onto the fritted glass material.

The compounds studied are unlikely to engage in chemical, biological, and/or photolytic reactions to a substantial extent during the duration of an experiment (0.5-6 hrs), as shown by Dilling et al. (82).

Influence of $K_La$--

The experimental estimates of $H_c$ and $K_La$ are interrelated according to our model, as shown by Eq. 111. Because for some compounds we had to correct the results due to partial gas-phase saturation, we might expect some inaccuracies when this procedure was used. From inspection of Figs. 37 through 41 one is tempted to argue that the data points at the highest turbulence level could be neglected, and simply draw a horizontal line across the remaining 6 data points (4 for $CCl_4$) for each compound. However, for two compounds, $CHCl_3$ and $CHCl{=}CCl_2$, the gas phase is saturated at all four experimental conditions according to Table 19. To check this, we recall from Section 7 that to calculate the degree of gas-phase saturation we assumed $\Psi = 0.6$. Using Eq. 72, we find

for $CHCl_3$ $\quad 0.60 \leq \Psi \leq 0.68$

for $CHCl{=}CCl_2$ $\quad 0.57 \leq \Psi \leq 0.65$

The range for $\Psi$ for both compounds indicates that the gas-phase saturation was not overestimated, but rather underestimated when substituted into

$$\Phi Z_s = \frac{K_La \cdot V_L}{H_c \cdot Q_G} \qquad (91)$$

Moreover, the corrections had to be made for high turbulence, where the $\Psi$-values tend to be at the upper end of the given range (i.e., $\Omega = 1/2$). Further evidence that the gas-phase saturation was appropriately estimated is given in Table 31, which gives the following average $\Psi$-values for a surface-aeration system: $CCl_2F_2$, $\Psi \approx 0.66$; $CHCl_3$, $\Psi \approx 0.56$; and $CH_3CCl_3$, $CCl_4$, $CHCl{=}CCl_2$, and $CCl_2{=}CCl_2$, $\Psi \approx 0.62$. However, Matter-Müller (28) reported $\Psi = 0.56$ for $CCl_2{=}CCl_2$.

Earlier in this section we concluded that the error in $K_{L,O_2}a$ was smaller than ± 5%. In order for $K_{L,O_2}a$ to yield erroneous estimates of the term $\Phi Z_s$, $K_{L,O_2}a$ itself would have to be in error by $> 150\%$ for $CHCl_3$ and $> 12\%$ for $CHCl{=}CCl_2$, according to Table 19. This means that $K_{L,O_2}a$ would have to be smaller by a factor of more than 2.5 and 1.14, respectively, in order to obtain values of $\Phi Z_s$ smaller than 5, and therefore require a correction for partial gas-phase saturation (assuming that all other variables represent true values). Such large deviations can confidently be excluded.

Hence, we may conclude so far, that since the degree of gas-phase saturation for these two compounds is not affected by the estimate of $K_{L,O_2}a$, the iterative procedure used to calculate the Henry coefficient of the other three compounds is useful and should yield reasonable results. In other words, the dependence of $H_c$ on turbulence is not due to gas-phase saturation corrections.

It is interesting to note the trend in the square of the correlation coefficient, $r^2$, of the regressions (Table 21), as well as that of the standard deviations of the average values of $H_c$ and $\Psi$. The results for $CHCl_3$, $CHCl{=}CCl_2$, and $CCl_2F_2$ were obtained without corrections for partial gas-phase saturation. These compounds yield the highest correlation coefficients, as well as the largest standard deviations. This gives some assurance that the possible error resulting from the correction for partial gas-phase saturation is small compared to other types of experimental error.

Influence of Concentration Change--

In Section 4, as well as earlier in this section, we showed that the Henry coefficient is a constant for very dilute solutions. Mackay (96), however, argues that: "when following the concentration decay in a volume of water which is being stripped of a pollutant, it can be shown that the slope of the log-concentration versus time gives H directly, and as the concentration falls, the dependence of H on concentration can be observed." This statement is surprising because it would question Mackay's own work published elsewhere (9). There is a possibility, however, that such behavior could be observed when high initial concentrations (approximately at the solubility limit) are used and the concentration change is observed down into the µg/l range. If H or $H_c$ were to change with concentration, it would become larger the lower the concentration for compounds with activity coefficients larger than one, as is the case for the compounds studied in this work. Unfortunately, Mackay (96) does not mention concentration ranges. In this work, initial concentrations for the compounds studied ranged from 340 µg/l to 2500 µg/l, except for $CCl_2F_2$, for which initial concentrations as high as 13,000 µg/l were chosen, owing to the compound's extreme volatility. These values are on the average 3 orders of magnitude lower than the respective solubilities. Hence, the conditions for linear equilibrium are fulfilled, and we do not expect to find any change of $H_c$ with decreasing concentration. This is confirmed by the linear regressions obtained; no curvature could be observed in the plots of experimental data.

Summarizing, it appears that no explanation can be found which would account for the dependence of the Henry coefficient on turbulence, if the model used is correct. The results obtained nevertheless give approximate values for $H_c$ and may still be considered as satisfactory in view of the small deviations obtained. Particularly when considering the large variation for $H_c$ given in the literature, the usefulness of this work is apparent (Table 26). Also, since the concentrations used are relatively low, the obtained values are probably quite applicable at environmental conditions and precise enough for engineering purposes or estimation of large-scale mass balances. However, these values are only representative of clean systems, where no competing processes occur that might be confounded with volatilization.

## Appropriateness of Model and Correlations

### Comparison of Observed and Predicted $K_La$-Values--

The purpose of this section is to evaluate the usefulness of the correlations found in the literature (Section 4) and used to predict the mass transfer rate of volatile organic compounds and oxygen. However, in order to do so, we have to combine two types of correlations: one for the specific interfacial area, a, and the other for the mass transfer coefficient, $k_L$, since the average mass transfer coefficient, $K_La$, was measured.

To estimate the specific interfacial area, we first use Eq. 153, which yields the gas holdup ratio $\varepsilon_G$, which then is substituted into Eq. 123 to obtain a. The corresponding values obtained ae shown in Table 32.

TABLE 32. ESTIMATED VALUES OF THE SPECIFIC INTERFACIAL AREA

| Gas Flow Rate $Q_G$ [ℓ/min] | Bubble Diameter $d_b$ [m] | Bubble Volume Fraction $\varepsilon_G$ [dimensionless] | Specific Area a $[m^{-1}]$ |
|---|---|---|---|
| 0.22 | $6 \cdot 10^{-4}$ | $4 \cdot 10^{-4}$ | 4.0 |
| 0.86 | $8 \cdot 10^{-4}$ | $1.41 \cdot 10^{-3}$ | 10.5 |
| 2.68 | $1.4 \cdot 10^{-3}$ | $4 \cdot 10^{-3}$ | 17.1 |

To estimate the mass transfer coefficient, $k_L$, for oxygen we may use several correlations. Akita and Yoshida's correlation (40) for values of $\varepsilon_G$ < 0.14 is:

$$k_L = 0.5 \cdot g^{5/8} \cdot D_L^{1/2} \cdot \rho_L^{3/8} \cdot \sigma^{-3/8} \cdot d_b^{1/2} \qquad (162)$$

where $g$ = gravity constant = 9.81 $[m/s^2]$

$D_L$ = liquid diffusion coefficient $[m^2/s]$

$\rho_L$ = liquid density $[kg/m^3]$

$\sigma$ = surface tension = 72.6 [kg/s$^2$]

$d_b$ = bubble diameter [m]

This correlation does not account explicitly for different levels of internal circulation, but is considered to a certain extent by introducing the surface tension $\sigma$.

The correlations of Yaron and Gal-Or (57) are:

$$Sh = 1.037 \cdot \left(\frac{1 - \varepsilon_G^{5/3}}{1 + 1.5 \cdot \varepsilon_G^{5/3}}\right)^{1/3} \cdot Pe^{1/3} \tag{163}$$

for bubbles with no internal circulation, and

$$Sh = 0.895 \cdot \left(\xi \cdot \frac{1 - \varepsilon_G^{5/3}}{Y}\right)^{1/2} \cdot Pe^{1/2} \tag{164}$$

for bubbles with strong internal circulation, where

$\xi = \mu_L/\mu_b + \gamma$ = viscosity ratio

$\gamma = -1/3 \cdot K \cdot (\partial\sigma/\partial\Gamma)$ = interfacial viscosity due to surfactants

$Y = 2 + 2\xi + \varepsilon_G^{5/3} \cdot (3 - 2\xi)$

$\mu_L$ = viscosity of continuous phase (water) = $1.002 \cdot 10^{-3}$ [kg/m$\cdot$s]

$\mu_b$ = viscosity of bubble phase (air) = $1.77 \cdot 10^{-5}$ [kg/m$\cdot$s]

As already mentioned, we consider our system as pure despite the methanol addition, since this substance causes no significant drop in the surface tension of the solution. Therefore, since $\varepsilon_G \rightarrow 0$ and $\gamma \rightarrow 0$ we may simplify Eqs. 163 and 164, and obtain respectively:

$$Sh = 1.037 \cdot Pe^{1/3} \tag{163a}$$

and

$$Sh = 0.895 \cdot \left(\frac{\mu_L/\mu_b}{2 \cdot [1 + (\mu_L/\mu_b)]}\right)^{1/2} \cdot Pe^{1/2} \tag{164a}$$

It must be noted that Eqs. 163, 163a, 164, and 164a are to be evaluated with the relative velocity between continuous and dispersed phase (≠ terminal velocity). The relative velocity is defined as (52):

$$U_{rel} = -\frac{3}{2} \cdot U_s \cdot \left(\frac{\varepsilon_G^{-1/3} - 1}{\varepsilon_G^{-2/3} - 1} - \frac{\varepsilon_G^{5/3} - 1}{W \cdot (\varepsilon_G^{-2/3} - 1)} - \frac{Y}{W}\right) \tag{165}$$

where

$$U_s = \frac{2}{9} \cdot \frac{(\rho_b - \rho_w) \cdot g \cdot d^2}{4 \cdot \mu_c} = \text{Stokes velocity}$$

$$W = 3 + 2\xi + 2\varepsilon^{5/3} \cdot (1 - \xi)$$

$\rho_b$ = density of bubble phase (air) = 1.2 [kg/m$^3$]

$\rho_w$ = density of continuous liquid phase (water) = 998 [kg/m$^3$]

The $k_L$a-values for oxygen which are obtained from Yaron and Gal-Or's (57) correlations (Eqs. 163a and 164a multiplied times the specific interfacial area, a) and from Akita and Yoshida's (40) correlation (Eq. 162 multiplied times a) are presented in Table 33 and compared with the experimental values.

From Table 33 we see that the experimental values are approximately 1.7 times larger than those predicted by Eq. 162; the experimental values are on the average 3.6 times larger than those predicted by Eq. 163a; and the experimental values are approximately 1.3 times smaller than those predicted by Eq. 164. This agreement can be regarded as very good in general, particularly if it is considered that the specific interfacial area, a, was calculated from an independent correlation. Another important point is that the experimental values fall within the extreme ranges of internal circulation (namely, Eqs. 163 and 164) in the correlations of Yaron and Gal-Or (57), which in turn supports their theoretical development and the conclusions drawn from it in Section 4.

TABLE 33. PREDICTED AND MEASURED $K_{L,O_2}$a-VALUES

| $d_b$ [cm] | a [m$^{-1}$] | $U_{rel}$ [cm/s] | $K_{L,O_2}a$ [min$^{-1}$] Eq. 163a | Eq. 164a | Eq. 162 | Measured |
|---|---|---|---|---|---|---|
| 0.06 | 4.0 | 27.01 | 0.0362 | 0.1438 | 0.0621 | 0.11 |
| 0.08 | 10.5 | 46.35 | 0.0939 | 0.4281 | 0.1882 | 0.32 |
| 0.14 | 17.1 | 136.14 | 0.1508 | 0.9032 | 0.4054 | 0.67 |

The work of Calderbank and Moo-Young (54) predicts $K_L$a-values which are smaller than the experimental values, although their correlations show similar dependencies of the mass transfer coefficient on the power of the diffusion coefficient. Most likely the gas holdup ratio, $\varepsilon_G$, which is not included as a variable in (54), accounts for this discrepancy.

Validity of the Assumption of Liquid-Phase Control--

In this section we re-evaluate the basic assumptions made in the development of the model, Section 4, Eq. 111. It is to be expected that these assumptions are valid: the same model has been used by other workers in the past (9,28) with apparent success.

The basic assumption of the model is that the liquid phase controls, virtually completely, the transfer of mass across the interface. As described in Section 4 we chose compounds with a Henry coefficient $H_c \geq 0.13$ at 20°C to ensure that $> 95\%$ of the mass transfer resistance would be in the liquid phase. The underlying assumption was that $k_G/k_L \simeq 150$ on the average, as illustrated with Eq. 47. However, it is likely that the ratio $k_G/k_L$ varies somewhat depending on the compound and probably also on the type of system and hydrodynamic conditions (i.e. turbulence). In fact, Mackay et al. (9) state that $k_G/k_L$ is of the order of 150 and should usually lie in the range of 50 to 300. The lower value is the critical one in regard to our assumption of liquid-phase-controlled transport. We also note a temperature dependence of Eq. 46:

$$\frac{R_L}{R_G} = H_c \cdot \frac{k_G}{k_L} = \frac{H}{RT} \cdot \frac{k_G}{k_L} \tag{46}$$

That is, the ratio $k_G/k_L$ is also temperature dependent. If we evaluate Eq. 46 for given $k_G/k_L$ and $R_L/R_G$ ratios, and solve for H, we find that

$$\frac{H\ [25°C]}{H\ [20°C]} \quad \frac{298.15}{293.15} = 1.017$$

However, by employing the temperature adjustment method suggested by Kavanaugh and Trussell (76) we estimate that for the compounds studied

$$\frac{H\ [25°C]}{H\ [20°C]} \simeq 1.30$$

This difference is substantially larger than any experimental error investigated. Hence, one may not just take a ratio of $k_G/k_L$ and use it with any temperature and with any compound, since $k_G$ and $k_L$ depend on the corresponding diffusivities raised to some power, and these in turn depend differently on the temperature. Due to the viscosity of water, the liquid diffusion coefficient depends more strongly on temperature than does the gas diffusion coefficient.

Liss and Slater (14), when using $k_G/k_L = 150$ for water and $CO_2$, suggest corrections for other compounds based on the square root ratios of the molecular weights. The diffusion coefficient equations probably led to this reasoning. When deriving the average value of $k_G/k_L = 150$, these authors do not specify the temperature. However, the Henry coefficient for oxygen, $\simeq 30$, used by them suggests a temperature of 20°C. Also, the work of Schooley (15), cited by Liss and Slater (14), refers to 20°C. Schooley also shows the strong dependence of the rate of water evaporation with temperature, and hence of $k_G$ with temperature.

Therefore, for $R_L/R_G = 20$, $k_G/k_L = 50$, and $T = 20°C$, $H_c \simeq 0.4$ [dimensionless], which means that $H_c$ would have to be greater than 0.4 to justify the assumption of liquid-phase control implicit in our approach. If $k_G/k_L = 150$ is assumed, then $H_c = 0.133$.

When doing these calculations it becomes apparent that the ratio of $k_G/k_L$ is crucial. Therefore, the assumption of liquid-phase-controlled mass transfer is only as precise as the assumption of $k_G/k_L$, the uncertainty of which embraces almost an order of magnitude.

It is interesting to note that $k_G/k_L \simeq 96$ for the compounds studied when calculated according to Liss and Slater (14) and also $(D_G/D_L)^{1/2} \simeq 97$. Although it is possible that $k_G$ and $k_L$ have the implied proportionality to the diffusion coefficients, other factors, such as viscosity, are also expected to influence the ratio $k_G/k_L$.

In Section 4 we discussed the possibility of using the correlations of Yaron and Gal-Or (57) (Eqs. 163a and 164a, preceding section) for the gas phase in view of the analogy of falling liquid drops and rising gas bubbles. We concluded that the boundary-layer approach is often approximately valid for systems with Schmidt numbers down to approximately unity. Hence, we may estimate the ratio $k_G/k_L$ using Eqs. 163a and 164a. From Eq. 164a we obtain: $k_G/k_L = (D_G/D_L)^{2/3} \simeq 488$ and from Eq. 164a: $k_G/k_L = [(\mu_G/\mu_L) \cdot (D_G/D_L)]^{1/2} \simeq 14$, assuming equal diameters and relative velocities in both phases. The range of $k_G/k_L$ obtained appears to indicate that the approximation used is indeed reasonable, when compared to the range of 50 to 300 suggested by Mackay et al. (9). Also, the dependence of $k_G/k_L$ on turbulence within the same system is evident. If we use the value of $k_G/k_L = 14$ (the most critical), which corresponds to high turbulence levels, and evaluate the ratio of resistances using $H_{c,CHCl_3} = 0.13$, we obtain by substituting into Eq. 46:

$$\frac{R_L}{R_G} = H_c \cdot \frac{k_G}{k_L} \simeq 0.13 \cdot 14 \simeq 1.8 \qquad (165)$$

or in other words, approximately 45% of the resistance for $CHCl_3$ transfer lies in the gas phase. The above calculation can also be interpreted as: $H_c \geq 1.43$ in order to assure $\geq$ 95% liquid-phase resistance.

The discussion of the ratio $k_G/k_L$ is most important in regard to calculation of Ψ-values. Since $CCl_2F_2$ is extremely volatile, as is oxygen, there is no doubt that both compounds are liquid-phase-controlled. When measuring Henry coefficients, the slope of the regression becomes independent of $K_La$ when the gas phase is completely saturated, as described by Eq. 115. In the case, the smaller the value $H_c$, i.e. the more important the gas-phase resistance, the faster the gas phase becomes saturated. This can be estimated using Eq. 46. Although $K_L$ decreases with decreasing $H_c$, the latter decreases much faster for volatile compounds and hence the term $\Phi Z_s$ increases rapidly.

Several mathematical simplifications used in Section 4 should have no effect on the predictions of the model. That is, the bubble volume and therefore the interfacial mass transfer area were averaged over depth. However, since the actual $K_La$ is measured, it already includes those variations and represents an "effective" average value. Also the assumption made in the mass balance, Fig. 5, namely $Q_{GI} = Q_{GE}$, has no significant effect. The resulting equations, Eqs. 103 and 111, are identical, when the pressure dependence of $Q_G$ is considered. Only the definition of the oxygen saturation concentration, Eq. 102, changes, but has no effect on the calculations.

The effect of organics volatilization on $Q_G$ was also considered. For the worst case, the gas flow due to all organics is < 0.1% of the air flow. In conclusion, we therefore may expect that the model accurately describes mass transfer for the cases considered of $H_c$, as well as $\Psi$ for $CCl_2F_2$, provided the assumption of $k_G/k_L = 150$ is correct.

## Closed-System VLE

In contrast to the bubble column, which is a dynamic system, the syringes used to measure VLE, i.e. $H_c$, are essentially a static system.

The values for $H_c$, Table 24, are substantially lower than those obtained in the bubble column, Tables 20 and 26. Although one day was allowed for equilibration and the syringes were shaken 3 to 4 times, it is believed that the time was too short. Also, the experimental technique was not well developed, and some volatilization might have occurred when filling the hypovials. This is also partially reflected in the large standard deviations. However, this technique, if refined, has great potential to measure Henry coefficients. Several advantages are that the procedure is inexpensive and simple; can be carried out in an environmental chamber at constant temperature; and affords the possibility that multiple experiments can be carried out simultaneously.

# SECTION 9

## ENGINEERING APPLICATION

The purpose of this section is to demonstrate by means of an example from wastewater treatment the application of the analogy between the transfer rates of volatile organic compounds and the oxygen transfer rate. The analogy expresses itself as a simple proportionality between the transfer rate constants of volatile organic contaminants and oxygen with coefficient of proportionality $\Psi$.

The $\Psi$-value is defined as in Eqs. 71 and 72. If the organic compounds are compared to oxygen as a reference compound

$$\Psi_i = \frac{k_{L,i}}{k_{L,O_2}} = \frac{K_{L,i}a}{K_{L,O_2}a} = \left(\frac{D_{Ai}}{D_{AO_2}}\right)^{\Omega} \qquad (72)$$

This equation suggests that $\Psi$ depends only on the diffusion coefficients of the compounds, i.e., is essentially independent of turbulence and therefore also not influenced by the geometry of the reactor. This means that $\Psi$-values obtained from bench-scale studies should be applicable for large-scale reactors if the mass transfer conditions are the same.

If the $\Psi$-value for a certain compound is known, it is easier to monitor this compound. Normally instruments to measure organic compounds are not readily available, whereas dissolved oxygen concentrations are measured easily. Once the influent concentrations to a reactor are known, the removal of volatile compounds can be estimated handily, knowing the rate of oxygen uptake. The same holds for the design of wastewater treatment facilities. After the oxygen requirements for biological treatment are determined, the removal of volatile compounds can be evaluated. Of course, these estimates are valid only if the organic compounds do not sorb.

### SURFACE AERATION IN ACTIVATED SLUDGE TREATMENT--EXAMPLE

The following example indicates how the $\Psi$-values can be used to estimate the effluent concentration of a typical volatile compound in an activated sludge aeration basin, assuming no losses of compounds by adsorption on solids and by biodegradation.

For typical wastewater (wastewater characteristics in Appendix C) with a flow $Q_L = 0.44\ m^3/s$, biological treatment requires:

Aeration basin volume: 6,460 $m^3$

Oxygen transfer rate: 3,130 kg $O_2$/day

The oxygen is supplied by three 30-Hp (22.38-kW) surface aerators, Brand OXY FLO, Model OX1958 (specifications in Appendix C). The $K_{L,O_2}a$-value for this aerator can be calculated using the performance data given by the manufacturer. From the manufacturer's definition of oxygen transfer rate $N_c$, the mass transfer coefficient for oxygen can be calculated from:

$$K_{L,O_2}a = \frac{N_c\, P}{V_L\, C^*} \qquad (167)$$

where $N_c$ = oxygen transfer rate [kg $O_2$/kW hr] = 2.13 [kg $O_2$/kW hr]

$P$ = brake power of aerator [kW]

$V_L$ = volume per aerator = (6,460 $m^3$)/3 = 2,153 $m^3$

$C^*$ = oxygen saturation concentration [kg $O_2/m^3$] for 20°C, 760 mm Hg

= $9.17 \times 10^{-3}$ [kg/$m^3$]

$$K_{L,O_2}a = \frac{2.13\ [\text{kg } O_2/\text{kW hr}] \times 22.38\ [\text{kW}]}{2{,}153\ m^3 \times 9.17 \times 10^{-3}\ [\text{kg } O_2/m^3]}$$

$$= 2.4\ [\text{hr}^{-1}] = 6.6 \times 10^{-4} s^{-1}\ .$$

In a completely mixed, flow reactor the mass balance yields

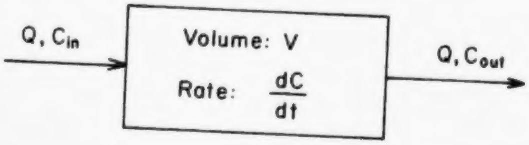

$$\frac{Q}{V} C_{LI} - \frac{Q}{V} C_{LE} - \begin{matrix}\text{Rate of}\\ \text{volatilization}\end{matrix} = \begin{matrix}\text{Rate of}\\ \text{accumulation}\end{matrix} = 0 \qquad (168)$$

$$\begin{matrix}\text{Rate of}\\ \text{volatilization}\end{matrix} = -K_{L,i}a\left(C_L^* - C_L\right) \qquad (169)$$

where $K_{L,i}a = \Psi\, K_{L,O_2}a$.

$$\begin{matrix}\text{Rate of}\\ \text{volatilization}\end{matrix} = -\Psi\, K_{L,O_2}a\left(C_L^* - C_L\right) \simeq -\Psi\, K_{L,O_2}a\left(-\, C_{LE}\right) \qquad (170)$$

$$C_{LI} - C_{LE} = (V/Q)\ \Psi\, K_{L,O_2}a\ C_{LE} \qquad (171)$$

$$\frac{C_{LE}}{C_{LI}} = \left(1 + \frac{V}{Q}\,\Psi\, K_{L,O_2}a\right)^{-1} \qquad (172)$$

Using $\Psi = 0.62$ as an average, representative value for volatile organic compounds (Table 31)),

$$\frac{C_{LE}}{C_{LI}} = (1 + \frac{6,460\ [m^3]}{0.44\ [m^3 s^{-1}]} \times 0.62 \times 6.6 \times 10^{-4}\ [s^{-1}])^{-1} = 0.14 \qquad (173)$$

In this aeration basin, 86% of the volatile organic contaminants is removed by volatilization, and only 14% is left in the effluent. For the individual compounds studied, the estimated removal by volatilization would be grouped within a very narrow range: 87% for the most volatile compound studied (Freon-12, $\Psi$ = 0.69) to 81% for the least volatile (o-dichlorobenzene, $\Psi$ = 0.45).

Under the assumptions of this example, the removal of volatile compounds in surface aeration is not greatly affected by the magnitude of the Henry's constant, which varies over three orders of magnitude for the compounds studied. However, this would not hold true for bubble aeration, where saturation of the gas phase becomes an important consideration (see below), nor for organic compounds that are insufficiently volatile to ensure that the gas-film resistance is negligible.

Similar calculations could be made for other situations, such as trickling filters, rotating biological contactors, and the like. In general, the removal of organic compounds by volatilization may be expected to increase with increasing quantity of oxygen transferred.

In the present example, the quantity of oxygen transferred (82 g oxygen per $m^3$ wastewater treated) is relatively small compared to typical cases of activated-sludge treatment. The relatively low oxygen requirement is explained by the relatively low concentration of degraded organic matter ($BOD_L$ = 159 mg/ℓ in the primary effluent). In many cases, the primary effluent contains a greater concentration of degradable organic matter; the required oxygen transfer rate and consequently the removal of organics by volatilization probably will be greater in such a case than indicated by the calculations discussed above. However, this difference may be compensated by the effect of partial saturation of the air in the atmospheric boundary layer above the aeration basin.

This example is intended only as an illustration of the importance of volatilization. In real aeration basins, complicating factors such as bubble entrainment and partial saturation of the surrounding atmosphere may significantly influence the behavior of moderately volatile compounds by reducing the concentration driving force relative to that of oxygen. Morover, sorption may play an important role in removing hydrophobic organic substances from aqueous solution by partitioning into activated-sludge solids, although not to any appreciable extent for the ten compounds studied in this work (35). Nonetheless, the proposed methodology for estimating the extent of volatilization of volatile organic compounds in surface aeration basins should prove useful in assessing the fate of such compounds in wastewater treatment.

BUBBLE AERATION--EXAMPLES

These examples illustrate how the approach described above must be modified for application to bubble aeration. The basic principle is the same: oxygen-transfer data are employed to estimate the transfer-rate constants for the volatile organic solvents. However, with bubble aeration the degree of saturation of the air bubbles must be taken into account; the method for doing so is described in Appendix C. Briefly, the method consists of estimating the required air rate $Q_G$ and the oxygen-transfer rate constant $K_{L,O_2}a$ using accepted values of the oxygen-transfer efficiency for a given type of bubble aeration. The mass transfer rate constant for the organic substances are then estimated by substituting the experimental $\Psi$-values into Eq. 72. For bubble aeration in a well-mixed, continuous-flow basin, the fractional removal is given by

$$1 - \frac{C_{LE}}{C_{LI}} = 1 - \left[1 + \frac{H_c\, Q_G}{Q_L}\left(1 - \exp(-\Phi Z_s)\right)\right] \tag{174}$$

and the fractional saturation of the air bubbles is

$$\frac{C_{GE}}{C_G^*} = \left[1 - \exp(-\Phi Z_s)\right] \tag{175}$$

Equations 174 and 175 are derived in Appendix E.

The conditions for the bubble-aeration examples are the same as those outlined above for surface aeration and described in Appendix E. The wastewater flow rate, aeration basin volume, and required oxygen-transfer rate are assumed to remain unchanged at 0.44 $m^3/s$ (10 MGD), 6,460 $m^3$, and 3,130 kg $O_2$/day, respectively. The aeration basin is assumed to be completely mixed. The modifications appropriate for bubble aeration are also described in Appendix E. Values of $H_c$ are those of PASE in Table 25.

The oxygen-transfer efficiency is assumed to be 15% in fine-bubble aeration (77, p. 497), at an assumed submergence depth of the diffuser equal to 4 m. Under these assumptions, the aeration rate is 0.86 $m^3/s$ at standard conditions of 20°C and 1 atm. The resulting estimate of $K_{L,O_2}a$ is $5.9 \times 10^{-4}$ [$s^{-1}$], approximately equal to the value of $6.6 \times 10^{-4}$ [$s^{-1}$] calculated for surface aeration in the previous example. Under this standard set of fine-bubble-aeration conditions, the fractional saturation of the air bubbles and the fractional removal of solute from the wastewater by volatilization are as summarized in Table 34.

The oxygen-transfer efficiency is lower in coarse-bubble aeration than in fine-bubble aeration, owing to the lesser specific surface area of the coarse bubbles. For coarse-bubble aeration, the oxygen-transfer efficiency is typically 6% (77, p. 497). Consequently, the required air rate is greater than in fine-bubble aeration, thus enhancing the stripping of volatile organic compounds. The removal efficiencies for the six compounds in coarse-bubble aeration range from 0.57 to 0.85 (Table 35), compared to 0.35 to 0.86

TABLE 34. FRACTIONAL REMOVAL AND FRACTIONAL BUBBLE SATURATION IN THE STANDARD CASE OF FINE-BUBBLE AERATION

| Compound | Henry's Coefficient $H_c$ | Fractional Saturation of Air Bubbles | Fractional Removal from Wastewater by Volatilization |
|---|---|---|---|
| $CCl_2F_2$ | 62. | 0.060 | 0.86 |
| $CCl_4$ | 0.98 | 0.975 | 0.61 |
| $CCl_2{=}CCl_2$ | 0.70 | 0.995 | 0.53 |
| $CH_3CCl_3$ | 0.69 | 0.995 | 0.53 |
| $CHCl{=}CCl_2$ | 0.51 | 0.999 | 0.46 |
| $CHCl_3$ | 0.33 | 1.000 | 0.35 |

Conditions: Oxygen-transfer efficiency = 15%; $Z_s$ = 4 m; $Q_G/V_L = 1.12 \times 10^{-4}$ $[s^{-1}]$; $Q_G/Q_L = 1.64$ $[m^3/m^3]$; [illegible] $K_{L,O_2}a = 5.9 \times 10^{-4}$ $[s^{-1}]$.

TABLE 35. FRACTIONAL REMOVAL AND FRACTIONAL BUBBLE SATURATION IN THE STANDARD CASE OF COARSE-BUBBLE AERATION

| Compound | Henry's Coefficient $H_c$ | Fractional Saturation of Air Bubbles | Fractional Removal from Wastewater by Volatilization |
|---|---|---|---|
| $CCl_2F_2$ | 62. | 0.023 | 0.85 |
| $CCl_4$ | 0.98 | 0.75 | 0.75 |
| $CCl_2{=}CCl_2$ | 0.70 | 0.86 | 0.71 |
| $CH_3CCl_3$ | 0.69 | 0.86 | 0.71 |
| $CHCl{=}CCl_2$ | 0.51 | 0.93 | 0.66 |
| $CHCl_3$ | 0.33 | 0.984 | 0.57 |

Conditions: Oxygen-transfer efficiency = 6%; $Z_s$ = 4 m; $Q_G/V_L = 2.28 \times 10^{-4}$ $[s^{-1}]$; $Q_G/Q_L = 4.11$ $[m^3/m^3]$; and $K_{L,O_2}a = 6.14 \times 10^{-4}$ $[s^{-1}]$.

for fine-bubble aeration (Table 34). The removal efficiency is greater in coarse-bubble aeration than in fine-bubble aeration for all five of the compounds having Henry coefficients smaller than that of oxygen ($CCl_4$, $CCl_2{=}CCl_2$, $CH_3CCl_3$, $CHCl{=}CCl_2$, and $CHCl_3$). This can be explained by the fact that air-bubble saturation constitutes a lesser constraint on mass transfer with the greater air flow rate necessitated by coarse-bubble aeration, compared to fine-bubble aeration. For the extremely volatile solute $CCl_2F_2$, air-bubble saturation is in both cases negligible, and the removal is virtually independent of oxygen-transfer efficiency. It must be remembered that the above comparisons are based on the assumption of equal quantities of oxygen transferred in the two cases.

Medium-bubble aeration, with an intermediate value of 10% for the oxygen-transfer efficiency, was chosen as the third case in the bubble-aeration analysis (Appendix E). The results for this case generally fall between those for coarse- and fine-bubble aeration.

The removal efficiencies for the six organic compounds are plotted in Fig. 53 as a function of oxygen-transfer efficiency for the three bubble-aeration cases: coarse (6%), medium (10%), and fine (15%). Also shown for comparison, but independent of the oxygen-transfer-efficiency scale, is the standard surface-aeration case discussed previously.

The calculated results shown in Fig. 53 demonstrate that removal of organics by volatilization is more complete with surface aeration than with bubble aeration, except for the most volatile compound studied, $CCl_2F_2$. Very few organic contaminants of environmental concern are as volatile as $CCl_2F_2$ ($H_c$ = 62). Hence, it can be stated as a general rule that volatilization removal efficiencies for organic contaminants are likely to be greater with surface aeration than with bubble aeration.

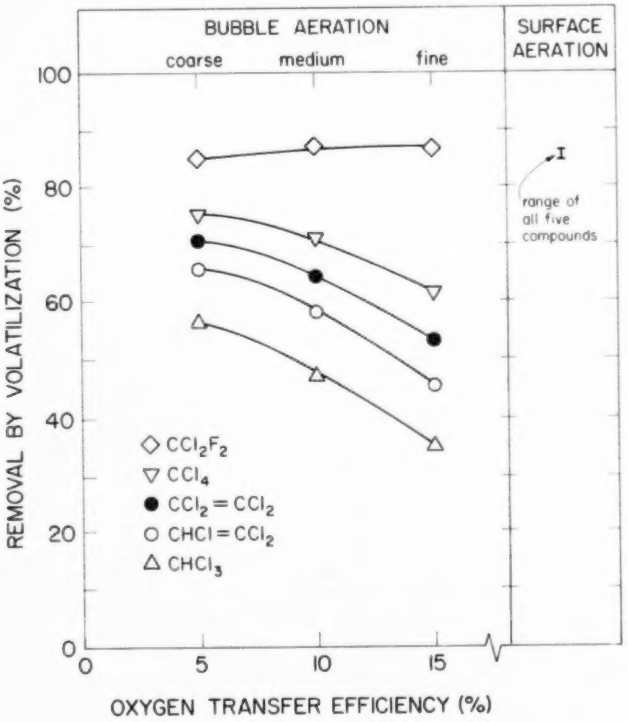

Figure 53. Removal of organic compounds by volatilization in standard cases of bubble aeration and surface aeration.

It is apparent from Fig. 53 that the volatilization removal efficiencies in bubble aeration increase with decreasing oxygen-transfer efficiency, if the oxygen mass transfer rate [kg/hr] is held constant. This seemingly anomalous result can be explained in terms of the greater air flow rate required at low oxygen-transfer efficiencies, in conjunction with the fact that the removal of moderately volatile compounds in the standard bubble-aeration case is limited by equilibrium considerations to a greater extent than by rate considerations. The dependence of removal on oxygen-transfer efficiency becomes stronger, the smaller the value of the Henry coefficient; for example the extent of removal of $CHCl_3$ ($H_c = 0.33$) is less than that of $CCl_4$ ($H_c = 0.98$), and is more strongly influenced by the oxygen-transfer efficiency.

It is emphasized that these conclusions are inferred from model calculations based upon laboratory experiments. The calculations have not been confirmed by field measurements at full-scale operating treatment plants. However, the calculations for surface aeration are consistent with observations made at a large-scale (50-100 $m^3$/day) pilot facility (28,35).

# REFERENCES

1. Maugh, T. H. Chemicals: How Many Are There? Science, 199:162, 1978.

2. Loprieno, N. L'Identitá Perduta. Scienza, 1(2):16-24, 1981.

3. Kurzel, R. The Effect of Environmental Pollutants on Human Reproduction, Including Birth Defects. Env. Sci. Tech., 15(6):626-640, 1981.

4. U.S. Environmental Protection Agency. Recommended List of Priority Pollutants. Washington, D.C., Effluent Guidelines Division, 1977.

5. Mackay, D. Finding Fugacity Feasible. Env. Sci. Tech., 13(10):1218-1223, 1979.

6. Smith, J. M., and H. C. Van Ness. Introduction to Chemical Engineering Thermodynamics, 3rd Ed. McGraw-Hill Book Company, New York, 1975. 632 pp.

7. Mackay, D., and P. J. Leinonen. Rate of Evaporation of Low-Solubility Contaminants from Water Bodies to Atmosphere. Env. Sci. Tech., 9(12): 1178-1180, 1975.

8. Mackay, D., and A. W. Wolkoff. Rate of Evaporation of Low-Solubility Contaminants from Water Bodies to Atmosphere. Env. Sci. Tech., 7(7):611-614, 1971.

9. Mackay, D., W. Y. Shiu, and R. P. Sutherland. Determination of Air-Water Henry's Law Constants for Hydrophobic Pollutants. Env. Sci. Tech., 13(3):333-337, 1979.

10. Prausnitz, J. M. Molecular Thermodynamics of Fluid-Phase Equilibria. Prentice Hall, Englewood Cliffs, New Jersey, 1969. 523 pp.

11. O'Connell, J. P., and J. M. Prausnitz. Thermodynamics of Gas Solubility in Mixed Solvents. Ind. Eng. Chem. Fund., 3(4):347-351.

12. Pierotti, G. J., C. H. Deal, and E. L. Derr. Activity Coefficients and Molecular Structure. Ind. Eng. Chem., 51(1):95-102, 1959.

13. Liss, P. S. Process of Gas Exchange Across an Air-Water Interface. Deep-Sea Research, 20:221-238, 1973.

14. Liss, P. S., and P. G. Slater. Flux of Gases Across the Air-Sea Interface. Nature, 247:181-184, 1974.

15. Schooley, A. H. Evaporation in the Laboratory and at Sea. J. Marine Res., 27:335-338, 1969.

16. Higbie, R. The Rate of Absorption of a Pure Gas into a Still Liquid During Short Periods of Exposure. Trans. Am. Inst. Chem. Engrs., 31:365-388, 1935.

17. Danckwerts, P. V. Significance of Liquid-Film Coefficients in Gas Absorption. Ind. Eng. Chem., 43(6):1460-1467, 1951.

18. Davies, J. T. Turbulence Phenomena. Academic Press, New York, 1972. 412 pp.

19. Perlmutter, D. D. Surface-Renewal Models in Mass Transfer. Chem. Eng. Sci., 16:287-296, 1961.

20. Toor, H. L., and J. M. Marchello. Film-Penetration Model for Mass and Heat Transfer. AIChE J., 4(1):97-101, 1958.

21. Skelland, A. H. P. Diffusional Mass Transfer. John Wiley & Sons, New York, 1974. 510 pp.

22. Tsao, G. T., and D. D. Lee. Oxygen Transfer in Fermentation. AIChE J., 21(5):979-985, 1975.

23. Bungay, H. R., M. Y. Huang, and W. M. Sanders. Quantitation of Eddy Diffusion Using an Oxygen Microelectrode. AIChE J., 19(2):373-375, 1973.

24. Goodgame, T. H., and T. K. Sherwood. The Additivity of Resistances Between Phases. Chem. Eng. Sci., 3(2):37-42, 1954.

25. Sherwood, T. K., P. L. Pigford, and C. R. Wilke. Mass Transfer Operations. McGraw-Hill Book Company, New York, 1975. 677 pp.

26. Wilke, C. R., and P. C. Chang. Correlation of Diffusion Coefficients in Dilute Solutions. AIChE J., 1:264-270, 1955.

27. Othmer, D. F., and M. S. Thakar. Correlating Diffusion Coefficients in Liquids. Ind. Eng. Chem., 45:589-593, 1953.

28. Matter-Müller, C. A. Sorptions- und Stoffaustauschprozesse refraktaerer organischer Leitsubstanzen in einer Belebtschlammanlage. Ph.D. Thesis, ETH No. 6403, Zürich, Switzerland, 1979. 154 pp.

29. Reid, R. C., J. M. Prausnitz, and T. K. Sherwood. The Properties of Gases and Liquids, 3rd Ed., McGraw-Hill Book Co., New York, 1977. 688 pp.

30. Lugg, G. A. Diffusion Coefficients of Some Organic and Other Vapors in Air. Anal. Chem., 40(7):1072-1077, 1968.

31. Wilke, C. R., and C. Y. Lee. Estimation of Diffusion Coefficients for Gases and Vapors. Ind. Eng. Chem., 47(6):1253-1257, 1955.

32. Chen, N. H., and D. P. Othmer. New Generalized Equation for Gas Diffusion Coefficient. J. Chem. Eng. Data, 7:37-41, 1962.

33. Elliot, R. W., and H. Watts. Diffusion of Some Hydrocarbons in Air: A Regularity in the Diffusion Coefficients of Homologous Series. Can. J. Chem., 50:31-34, 1972.

34. Bennett, C. O., and J. E. Myers. Momentum, Heat, and Mass Transfer, 2nd Ed. McGraw-Hill Book Co., 1974. 810 pp.

35. Matter-Müller, C. A., W. Gujer, W. Giger, and W. Stumm. Non-Biological Elimination Mechanisms in a Biological Sewage Treatment Plant. Prog. Wat. Tech., 12:299-314, 1980.

36. Smith, J. H., D. C. Bomberger, and D. L. Haynes. Prediction of the Volatilization Rates of High-Volatility Chemicals from Natural Water Bodies. Env. Sci. Tech., 14(11):1332-1337, 1980.

37. Holland, F. A., and F. S. Chapman. Liquid Mixing and Processing in Stirred Tanks. Reinhold Publishing Corporation, New York, 1966. 319 pp.

38. Lakin, M. B., and R. N. Salzmann. Subsurface Aeration Evaluation. J. WPCF, 51(10):2419-2428, 1979.

39. Matter-Müller, C. A., W. Gujer, and W. Giger. Transfer of Volatile Substances from Water to the Atmosphere. Internal Report, Swiss Federal Institute of Technology, 1980.

40. Akita, K., and F. Yoshida. Bubble Size, Interfacial Area and Liquid-Phase Mass Transfer Coefficient in Bubble Columns. Ind. Eng. Chem. Process Des. Dev., 13(1):84-91, 1974.

41. Barnhart, E. L. Transfer of Oxygen in Aqueous Solutions. J. San. Eng. Div. J., ASCE, 95(SA3):645-661, 1969.

42. Fair, J. R., A. J. Lambright, and J. W. Andersen. Heat Transfer and Gas Holdup in a Sparged Contactor. Ind. Eng. Chem. Process Des. Dev., 1(1):33-36, 1962.

43. Grace, J. R., T. Wairegi, and T. H. Nguyen. Shapes and Velocities of Single Drops and Bubbles Moving Freely Through Immiscible Liquids. Trans. Instn. Chem. Engrs., 54:167-173, 1976.

44. Habermann, W. L., and R. K. Morton. An Experimental Study of Bubbles Moving in Liquids. Trans. ASCE, 121:227-250, 1956.

45. Hammerton, D., and F. H. Garner. Gas Absorption from Single Bubbles. Trans. Instn. Chem. Engrs., 32:S18-S24, 1954.

46. Shulman, H. L., and M. C. Molstad. Gas-Bubble Columns for Gas-Liquid Contacting. Ind. Eng. Chem., 42(6):1058-1070, 1950.

47. Verschoor, H. Some Aspects of the Motion of a Swarm of Gas Bubbles Rising Through a Vertical Liquid Column. Trans. Instn. Chem. Engrs., 28:52-62, 1950.

48. Sideman, S., O. Hortacsu, and J. W. Fulton. Mass Transfer in Gas-Liquid Contacting Systems. Ind. Eng. Chem., 58(7):32-47, 1966.

49. Clift, R., J. R. Grace, and M. E. Weber. Bubbles, Drops and Particles. Academic Press, New York, 1978. 380 pp.

50. Garner, F. H., and D. Hammerton. Circulation Inside Gas Bubbles. Chem. Eng. Sci., 3(1):1-11, 1954.

51. Marucci, G. Rising Velocity of a Swarm of Spherical Bubbles. Ind. Eng. Chem. Fund., 4(2):224-225, 1965.

52. Gal-Or, B. On Motion of Bubbles and Drops. Can. J. Chem. Eng., 48:526-531, 1970.

53. Waslo, S., and B. Gal-Or. Boundary Layer Theory for Mass and Heat Transfer in Clouds of Moving Drops, Bubbles or Solid Particles. Chem. Eng. Sci., 26:829-838, 1971.

54. Calderbank, P. H., and M. B. Moo-Young. The Continuous Phase Heat and Mass Transfer Properties of Dispersions. Chem. Eng. Sci., 16:39-54, 1961.

55. Coppock, P. D., and G. T. Meiklejohn. The Behavior of Gas Bubbles in Relation to Mass Transfer. Trans. Instn. Chem. Engrs., 29:75-86, 1951.

56. Griffith, R. M. Mass Transfer from Drops and Bubbles. Chem. Eng. Sci., 12:198-213, 1960.

57. Yaron, I., and B. Gal-Or. Convective Mass or Heat Transfer from Size-Distributed Drops, Bubbles or Solid Particles. Int. J. Heat Mass Transfer, 14:727-737, 1971.

58. Gal-Or, B., and S. Waslo. Hydrodynamics of an Ensemble of Drops (or Bubbles) in the Presence or Absence of Surfactants. Chem. Eng. Sci., 23:1431-1445, 1968.

59. Pfeffer, R. Heat and Mass Transport in Multiparticle Systems. Ind. Eng. Chem. Fund., 3(4):380-383, 1964.

60. LeClair, B. P., and A. E. Hamielec. Viscous Flow Through Particle Assemblages at Intermediate Reynolds Numbers. Ind. Eng. Chem. Fund., 7(4):542-549, 1968.

61. Gal-Or, B., and I. Yaron. Convective Mass or Heat Transfer from Size-Distributed Ensembles of Drops, Bubbles, or Solid Particles. Prog. Heat Mass Transfer, 5:309-326, 1972.

62. Ruckenstein, E. On Mass Transfer in the Continuous Phase from Spherical Bubbles or Drops. Chem. Eng. Sci., 19:131-146, 1964.

63. Kinzer, G. D., and R. Gunn. The Evaporation, Temperature and Thermal Relaxation-Time of Freely Falling Water Drops. J. Meteorology, 8(2):71-83, 1951.

64. Stewart, M. K. Stable Isotope Fractionation Due to Evaporation and Isotopic Exchange of Falling Waterdrops: Applications to Atmospheric Processes and Evaporation of Lakes. J. Geophys. Res., 80(9):1133-1146, 1975.

65. APHA-AWWA-WPCF. Standard Methods for the Examination of Water and Wastewater, 14th Ed. American Public Health Association, Washington, D.C., 1975. 1193 pp.

66. Henderson, J. E., G. R. Peyton, and W. H. Glaze. Identification and Analysis of Organic Pollutants in Water, L. H. Keith, ed. Ann Arbor Science Publisher, Ann Arbor, Michigan, 1976. pp. 105-111.

67. Trussell, A. R., M. D. Umphres, L. Y. C. Leong, and R. R. Trussell. J. Amer. Water Works Assoc., 71:385-389, 1979.

68. Ryan, T. A., B. L. Joiner, and B. F. Ryan. Minitab Student Handbook. Wadsworth Publishing Company, Inc., Belmont, California, 1976.

69. Dändliker, P. G. Volatilization of Organic Compounds During Surface Aeration in Water. Engineer's Thesis. Stanford University, Stanford, California, 1981. 83 pp.

70. Munz, C., and P. V. Roberts. Transfer of Volatile Organic Contaminants into a Gas Phase During Bubble Aeration. Technical Report No. 262, Dept. of Civil Engineering, Stanford University, Stanford, California, 1982. 193 pp.

71. Boyle, W. C., P. M. Berthouex, and T. C. Rooney. Pitfalls in Parameter Estimation for Oxygen Transfer Data. J. San. Eng. Div., ASCE, 100(EE2):391-408, 1974.

72. SAS User's Guide, Statistical Analysis System, SAS Institute Inc., Raleigh, North Carolina, 1979. 494 pp.

73. Brown, L. C. Oxygen Transfer Parameter Estimation. In: Proceedings of the Workshop Toward an Oxygen Transfer Standard. EPA-600/9-78-021, U.S. Environmental Protection Agency, Cincinnati, Ohio, 1979. pp. 27-40.

74. Hayduk, W., and H. Laudie. Prediction of Diffusion Coefficients for Nonelectrolytes in Dilute Aqueous Solutions. AIChE J., 20(3):611-615, 1974.

75. Tyn, M. T., and W. F. Calus. Estimating Liquid Molal Volume. Processing, 21(4):16-17, 1975.

76. Kavanaugh, M. C., and R. R. Trussell. Design of Aerator Towers to Strip Volatile Contaminants from Drinking Water. J. Amer. Water Works Assoc., 72(12):684-692, 1980.

77. Metcalf and Eddy, Inc. Wastewater Engineering: Treatment, Disposal, Reuse, 2nd Ed. McGraw-Hill Book Co., New York, 1979. 920 pp.

78. Gilbert, R. G. Measurement of Alpha and Beta Factors. In: Proceedings of the Workshop Toward an Oxygen Transfer Standard. EPA-600/9-78-021, U.S. Environmental Protection Agency, Cincinnati, Ohio, 1979. pp. 147-162.

79. E. I. DuPont de Nemours and Co. Thermodyanmic Properties of Freon-12 Refrigerant. Report T-12. Wilmington, Delaware, 1971. 31 pp.

80. E. I. DuPont de Nemours and Co. Solubility Relationships Between Fluorocarbons and Water. Report B-43. Wilmington, Delaware, 1971. 13 pp.

81. Warner, H. P., J. M. Cohen, and J. C. Ireland. Determination of Henry's Law Constants of Selected Priority Pollutants. Internal Report. Municipal Environmental Research Laboratory, U.S. Environmental Protection Agency, Cincinnati, Ohio, April 1980. 14 pp.

82. Dilling, W. L., N. B. Tefertiller, and G. J. Kallos. Evaporation Rates and Reactivities of Methylene Chloride, Chloroform, 1,1,1-Trichloroethane, Trichloroethylene, Tetrachloroethylene and Other Chlorinated Compounds in Dilute Aqueous Solutions. Env. Sci. Tech., 9(9):833-838, 1975.

83. Dilling, W. L. Interphase Transport Processes. II. Evaporation Rates of Chloromethanes, Ethanes, Ethylenes, Propanes, and Propylenes from Dilute Aqueous Solutions. Comparisons with Theoretical Predictions. Env. Sci. Tech., 11(4):405-409, 1977.

84. Paulson, W. L. Review of Test Procedures. In: Proceedings of the Workshop Toward an Oxygen Transfer Standard. EPA-600/9-78-021, U.S. Environmental Protection Agency, Cincinnati, Ohio, 1979. pp. 41-54.

85. Hunter, J. S., III. Accounting for the Effects of Water Temperature in Aerator Test Procedures. In: Proceedings of the Workshop Toward an Oxygen Transfer Standard. EPA-600/9-78-021, U.S. Environmental Protection Agency, Cincinnati, Ohio, 1979. pp. 85-90.

86. Boon, A. G. Oxygen Transfer in the Activated Sludge Process. In: Proceedings of the Workshop Toward an Oxygen Transfer Standard. EPA-600/9-78-021, U.S. Environmental Protection Agency, Cincinnati, Ohio, 1979. p. 238.

87. Hansch, C., and A. Leo. Substituent Constants for Correlation Analysis in Chemistry and Biology. Wiley and Soncs, Inc., 1979. 339 pp.

88. Mancy, K. H., and W. E. Barlage, Jr. Mechanism of Interference of Surface-Active Agents with Gas Transfer in Aeration Systems. In: Advances in Water Quality Improvement. University of Texas Press, 1968. pp. 262-286.

89. Aiba, S., and K. Toda. Effects of Surface Active Agents on Oxygen Absorption in Bubble Aeration. J. Gen. and Appl. Microbiol., 9:443-453, 1963.

90. Sissom, L. E., and D. R. Pitts. Elements of Transport Phenomena. McGraw-Hill Book Co., New York, 1972. 814 pp.

91. Eckenfelder, W. W., and D. L. Ford. Engineering Aspects of Surface Aerator Design. In: Proceedings of the 22nd Industrial Waste Conference, Purdue University, 1967. pp. 279-291.

92. Wilson, G. M. Infinite Dilution Activity Coefficients Estimation of One Binary Component from the Other. AIChE Symp. Ser., 140:120-129, 1974.

93. Meissner, H. P., and A. S. Michaels. Surface Tension of Pure Liquids and Liquid Mixtures. Ind. Eng. Chem., 41(2):2782-2787, 1949.

94. St-Denis, C. E., and C. J. D. Fell. Diffusivity of Oxygen in Water. Can. J. Chem. Eng., 49:885, 1971.

95. Dobbins, W. E. Mechanism of Gas Absorption by Turbulent Liquids. In: Advances in Water Pollution Research, Vol. 2. MacMillan, New York, 1964. pp. 61-76.

96. Mackay, D. Volatilization of Pollutants from Water. In: Transformation and Biological Effects, O. Hutziger, L. H. van Lelyveld, and B. C. J. Zoetman, Eds. Pergamon Press, New York, 1978. pp. 175-185.

97. Verschueren, K. Handbook of Environmental Data on Organic Chemicals. Van Nostrand Reinhold Co., New York, 1977. 659 pp.

98. International Critical Tables of Numerical Data, Physics, Chemistry and Technology, Vol. III. McGraw-Hill Book Co., New York, 1928. 255 pp.

99. Lange's Handbook of Chemistry, 12th Ed. McGraw-Hill Book Co., New York, 1979. 1100 pp.

# APPENDIX A

## PROPERTIES OF SOLUTES STUDIED

Table A-1 lists properties of organic solutes. The following notes apply:

a Data from Verschueren (97), except as noted. Values at 20°C, except for $C_L^S$ at 25°C for $CCl_2=CCl_2$.

b Data from Reid et al. (29).

c Data from E. I. DuPont de Nemours Co. (79,80).

d Data from Dilling (83).

e Data from International Critical Tables of Numerical Data-Physics (98, Vol. III, p. 255).

TABLE A-1. PROPERTIES OF ORGANIC SOLUTES

| SUBSTANCE | M | $C_L^s$ (a) g $m^{-3}$ | P'(a) torr | $T_b$ °C | $V_c$(b) $cm^3 mol^{-1}$ | H [20°C] $atm \cdot m^3 \cdot mol^{-1}$ |
|---|---|---|---|---|---|---|
| Carbon tetrachloride, $CCl_4$ | 153.8 | 800 | 90 | 76.54 | 276 | $2.3 \times 10^{-2}$ |
| 1,1,1-Trichloroethane, $CCl_3CH_3$ | 133.4 | 4,400 | 100 | 74.1 | 283* | $4.0 \times 10^{-3}$ |
| Chloroform, $CHCl_3$ | 119.4 | 8,000 | 160 | 61.7 | 239 | $3.1 \times 10^{-3}$ |
| Dichlorodifluoromethane, $CCl_2F_2$ | 120.9 | 280(c) | 4,250(c) | -29.8 | 217 | 1.5 |
| Tetrachloroethylene, $CCl_2=CCl_2$ | 165.8 | 150(c) | 14 | 121.4 | 290 | $2.0 \times 10^{-2}$ |
| Trichloroethylene, $CHCl=CCl_2$ | 131.4 | 1,100(d) | 60 | 86.7 | 256 | $9.4 \times 10^{-3}$ |
| Chlorobenzene, $C_6H_5Cl$ | 112.6 | 500 | 8.8 | 132 | 308 | $2.6 \times 10^{-3}$ |
| 1,2-Dichlorobenzene, $C_6H_4Cl_2$ | 147.0 | 100 | 1 | 180.5 | 360 | $1.9 \times 10^{-3}$ |
| 1,3-Dichlorobenzene, $C_6H_4Cl_2$ | 147.0 | 111 | 1.49 | 173 | 359 | $2.6 \times 10^{-3}$ |
| 1,4-Dichlorobenzene, $C_6H_4Cl_2$ | 147.0 | 79 | 0.6 | 174 | 372 | $1.5 \times 10^{-3}$ |
| Oxygen, $O_2$ |  |  |  |  | 73.4 | 0.73(e) |

NOTES - see also preceding page for notes a, b, c, d, e, and f.

* calculated value.

M molecular mass.

$C_L^s$ solubility in water at 20°C.

P' vapor pressure at 20°C.

b.p. boiling point.

$V_c$ critical volume.

H $= P' M/C_L^s$

= calculated Henry coefficient.

## TABLE A-2. LIQUID MOLAR VOLUMES AT THE NORMAL BOILING POINT, $V_A$

| | | | $V_A$ [$cm^3$/mole] | | | |
|---|---|---|---|---|---|---|
| Compound | M.W. [g/mole] | $T_b$ [K] | Experimental Values | LeBas | Schroeder | T + C Correl. |
| $CHCl_3$ | 119.4 | 334.3 | - | 92.3 | 87.5 | 88.6 |
| $CH_3CCl_3$ | 133.4 | 367.3 (99) | - | 114.5 | 108.5 | - |
| $CCl_4$ | 153.8 | 349.7 | 102 | 113.2 | 105.0 | 103.0 |
| $CHCl{=}CCl_2$ | 131.4 | 360.4 | - | 107.1 | 101.5 | 95.2 |
| $CCl_2{=}CCl_2$ | 165.8 | 394.3 | - | 128.0 | 119.0 | 108.5 |
| $CCl_2F_2$ | 120.9 | 243.4 | 80.7 | 81.4 | 77.0 | 80.1 |
| $O_2$ | 32.0 | 90.2 | 27.9 (33) | 25.6 | 25.6 | 25.7 |

NOTES: $T_b$ = boiling point; T + C = Tyn and Calus (29,75) correlation; $V_A = 0.285\ V_c^{1.048}$; all values obtained from Reid et al. (29), except as otherwise referenced.

## TABLE A-3. INFINITE DILUTION DIFFUSION COEFFICIENTS IN WATER

| | $D_L \times 10^9$ [$m^2$/s] at 20°C | | | | | | | | |
|---|---|---|---|---|---|---|---|---|---|
| | Wilke-Chang (26) $\Phi = 2.6$ | | | Wilke-Chang (26) $\Phi = 2.26$ | | | Hayduk-Laudie (74) | | |
| | $V_A$ from | | | $V_A$ from | | | $V_A$ from | | |
| Compound | T + C | LeBas | Schroe. | T + C | LeBas | Schroe. | T + C | LeBas | Schroe. |
| $CHCl_3$ | 1.01 | 0.981 | 1.01 | 0.937 | 0.915 | 0.944* | 0.943 | 0.920 | 0.949 |
| $CH_3CCl_3$ | - | 0.862 | 0.890 | - | 0.804 | 0.830* | - | 0.810 | 0.836 |
| $CCl_4$ | 0.918 | 0.868 | 0.907 | 0.856 | 0.809 | 0.846 | 0.863 | 0.816 | 0.853 |
| $CHCl{=}CCl_2$ | 0.963 | 0.897 | 0.927 | 0.898 | 0.836 | 0.864* | 0.903 | 0.843 | 0.870 |
| $CCl_2{=}CCl_2$ | 0.890 | 0.806 | 0.842 | 0.830 | 0.752 | 0.785* | 0.836 | 0.759 | 0.792 |
| $CCl_2F_2$ | 1.07 | 1.06 | 1.09 | 0.996 | 0.986 | 1.02 | 1.00 | 0.991 | 1.02 |
| $O_2$ | 2.11 | 2.12 | 2.11 | 1.97 | 1.97 | 1.97 | 1.95 | 1.96 | 1.96 |
| $CCl_4$ † | | 0.924 | | | 0.861* | | | 0.867 | |
| $CCl_2F_2$† | | 1.06 | | | 0.991* | | | 0.996 | |
| $O_2$ † | | 2.01 | | | 1.875*‡ | | | 1.86 | |

*Values used in calculations.

†Calculated with the experimental values of $V_A$.

‡In the interpretation of the bubble-column experiments, the value of $D_{L,O_2} = 2.025 \times 10^{-9}$ $m^2$/s reported by St-Denis and Fell (94) was used.

## APPENDIX B

## POWER MEASUREMENT

### PROCEDURE

The torque is read on a calibrated scale from 0 in.oz. to 25 in.oz., using a stroboscopic light while the instrument is rotating. The instrument operates in either direction, reading to an accuracy of $^1/_2$% of the full scale. The specifications for the torque meter are shown in Fig. B-1.

Because the motor stirring speed fluctuated, the stroboscope (Strobotac® type 153 1A, General Radion Company) had to be triggered with a reed switch. The rotational speed of the shaft was not high enough to allow reading by eye; therefore, pictures were taken with a "Recording 2475" film at 3200 ASA; this allowed accurate reading of the torque meter.

Model 63

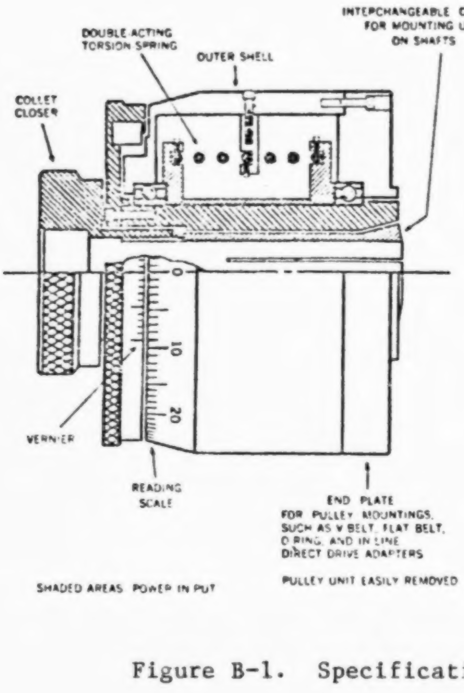
INTERCHANGEABLE COLLETS FOR MOUNTING UNIT ON SHAFTS
DOUBLE ACTING TORSION SPRING
OUTER SHELL
COLLET CLOSER
0
10
20
VERNIER
READING SCALE
END PLATE FOR PULLEY MOUNTINGS, SUCH AS V BELT, FLAT BELT, O RING, AND IN LINE DIRECT DRIVE ADAPTERS
SHADED AREAS POWER IN PUT
PULLEY UNIT EASILY REMOVED

**ACCURACY**

The extreme accuracy of the instrument is due to a double-acting torsion spring, stabilized and stress relieved in manufacture. The spring operates within its elastic limits in both directions and does not change. Internal stops prevent the spring from being overstressed.

The effect of centrifugal force on the spring system is nullified by using the double spring arrangement. One end of the spring is wound up while at the same time the other is unwound. This cancels out the effect of centrifugal force exactly. This can be demonstrated at any time by running the instrument with the belt removed and observing the zero setting.

The Bex-ometer remains accurately calibrated if the zero reading is unchanged. Further checking is not required.

Figure B-1. Specifications of Bex torque meter.

The RPM were measured with a modified algebraic pocket calculator and a stop watch. Two leads were connected to the equal sign and a reed switch. After pushing the "1" and the "+" keys, the calculator starts counting the revolutions. Figure B-2 displays a schematic setup.

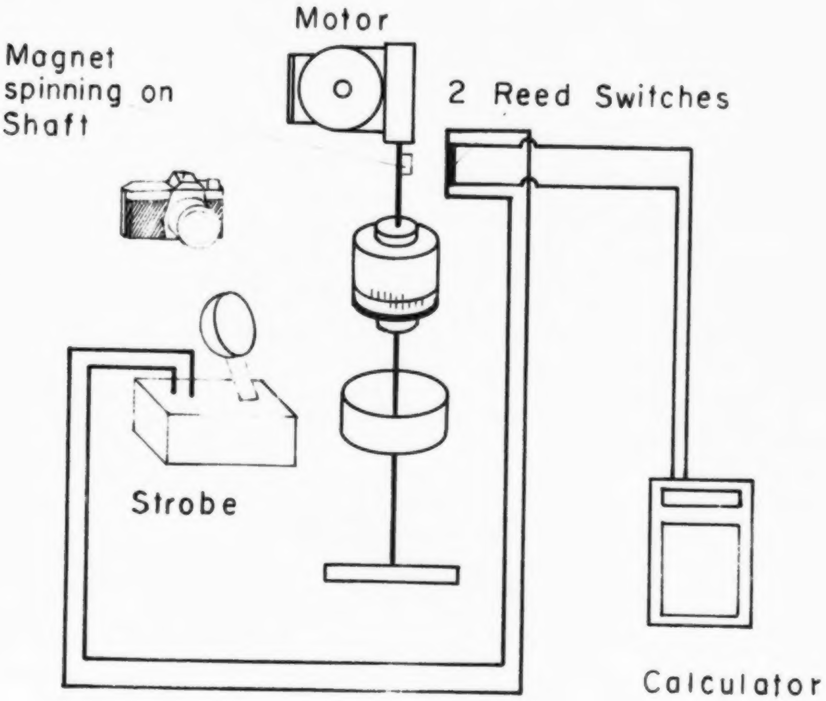

Figure B-2. Setup for torque measurements.

## RESULTS

The results of the two sets of power measurements made with the agitator used in the main set of surface-aeration experiments are shown in Tables B-1 and B-2. The results were correlated by linear regression of log P [W] against log N [Hz]. The result of the regression ($r^2 = 0.999$( after transforming was $P[W] = 0.0072\ N^{3.15}$, where N = agitator speed [Hz]. This relation was used to estimate the power inputs in the mass transfer experiments, based on the measured values of N.

TABLE B-1. POWER INPUT--DATA SET #1

| RPM | | | Torque [in•oz.] | | | Power | Power Number | Reynolds Number |
|---|---|---|---|---|---|---|---|---|
| $\overline{N}$ | $\sigma_N$ | n | $\overline{y}$ | $\sigma_y$ | n | [watts] | Po | Re |
| 58.6 | 1.5 | 3 | 0.15 | 0.003 | 3 | $6.5 \times 10^{-3}$ | 2.13 | 6,300 |
| 76.6 | 0.6 | 3 | 0.27 | 0.06 | 3 | $1.53 \times 10^{-2}$ | 2.23 | 8,200 |
| 93.7 | 0.6 | 3 | 0.4 | 0.003 | 3 | $2.77 \times 10^{-2}$ | 2.23 | 10,100 |
| 125.0 | 0 | 3 | 0.75 | 0.003 | 2 | $6.93 \times 10^{-2}$ | 2.35 | 13,500 |
| 165.3 | 0.6 | 3 | 1.65 | 0.15 | 3 | $2.02 \times 10^{-1}$ | 2.97 | 17,800 |
| 203.7 | 0.6 | 3 | 2.4 | 0.14 | 2 | $3.62 \times 10^{-1}$ | 2.82 | 21,900 |
| 238.7 | 1.2 | 3 | 3.32 | 0.18 | 3 | $5.86 \times 10^{-1}$ | 2.84 | 25,700 |
| 274.0 | 1.0 | 3 | 4.45 | 0.35 | 3 | $9.02 \times 10^{-1}$ | 2.89 | 29,500 |
| 309.0 | 1.0 | 3 | 5.61 | 0.14 | 4 | 1.28 | 2.87 | 33,300 |
| 342.3 | 0.6 | 3 | 6.70 | 0.39 | 4 | 1.7 | 2.81 | 36,900 |
| 372.0 | 1.0 | 3 | 8.05 | 0.21 | 4 | 2.21 | 2.84 | 40,000 |
| 405.3 | 0.6 | 3 | 9.28 | 0.19 | 3 | 2.78 | 2.76 | 43,700 |
| 441.0 | 1.0 | 3 | 10.75 | 0.35 | 2 | 3.51 | 2.70 | 47,500 |

TABLE B-2. POWER INPUT--DATA SET #2

| RPM | | | Torque [in•oz.] | | | Power | Power Number | Reynolds Number |
|---|---|---|---|---|---|---|---|---|
| $\overline{N}$ | $\sigma_N$ | n | $\overline{y}$ | $\sigma_y$ | n | [watts] | Po | Re |
| 57.7 | 0.6 | 3 | 0.13 | 0.03 | 3 | $5.55 \times 10^{-3}$ | 1.91 | 6,200 |
| 80.0 | 0 | 3 | 0.32 | 0.03 | 3 | $1.89 \times 10^{-2}$ | 2.46 | 8,600 |
| 108.3 | 1.5 | 3 | 0.57 | 0.03 | 3 | $4.57 \times 10^{-2}$ | 2.40 | 11,600 |
| 144.3 | 0.6 | 3 | 1.08 | 0.06 | 3 | $1.15 \times 10^{-1}$ | 2.54 | 15,500 |
| 182.3 | 1.2 | 3 | 1.93 | 0.03 | 3 | $2.60 \times 10^{-1}$ | 2.86 | 19,600 |
| 218.3 | 3.0 | 3 | 2.53 | 0.24 | 3 | $4.09 \times 10^{-1}$ | 2.61 | 23,500 |
| 251.0 | 1.0 | 3 | 3.57 | 0.13 | 3 | $6.63 \times 10^{-1}$ | 2.77 | 27,000 |
| 283.3 | 1.2 | 3 | 4.60 | 0.05 | 3 | $9.64 \times 10^{-1}$ | 2.80 | 30,500 |
| 318.3 | 1.3 | 4 | 5.59 | 0.23 | 5 | 1.32 | 2.71 | 34,300 |
| 351.3 | 1.3 | 4 | 7.06 | 0.1 | 4 | 1.83 | 2.79 | 37,800 |
| 392.5 | 1.7 | 4 | 8.72 | 0.36 | 6 | 2.53 | 2.78 | 42,200 |

## CALCULATION OF OXYGEN-TRANSFER:ENERGY RATIO

The present work resulted in a linear relation between the oxygen-transfer rate constant $K_{L,O_2}a$ and the power input P, namely

$$K_{L,O_2}a\ [s^{-1}] = 3.75 \times 10^{-3} P^{1.00} \qquad (157)$$

It is desired to translate Eq. 157 into an oxygen-transfer:energy ratio, expressed in units of kg $O_2$/kWh. The following equation is used:

$$\frac{1}{P}\frac{d\,M_{O_2}}{dt} = \frac{(K_{L,O_2}a)}{P}(C_L^* - C) \cdot V_L \cdot 3600$$

where P = power input [W]; $dM_{O_2}/dt$ = oxygen-transfer rate [kg/h]; $(K_{L,O_2}a)$ = oxygen-transfer rate constant $[s^{-1}]$; $C_L^*$ = oxygen saturation concentration $[g/m^3]$; C = dissolved oxygen concentration $[g/m^3]$; $V_L$ = aeration-basin volume; and 3600 is a factor to convert time from seconds to hours. In the present work,

$$\frac{(K_{L,O_2}a) \cdot V_L}{P} = 3.75 \times 10^{-3} \cdot 0.0073$$

Therefore

$$\frac{1}{P}\frac{d\,M_{O_2}}{dt} = 3.75 \times 10^{-3} \cdot 0.0073 \cdot 3600\ (C_L^* - C_L)$$

$$= 0.099\ (C_L^* - C_L)$$

We now substitute for $C_L^*$ and $C_L$ values typical of activated-sludge treatment. We choose $C_L^* = 8.7\ g/m^3$ and $C_L = 1\ g/m^3$. Substituting these values, we obtain

$$\frac{1}{P}\frac{d\,M_{O_2}}{dt} = 0.099(8.7 - 1.0) = 0.78\ \frac{kg\ O_2}{kWh}$$

This estimate of the oxygen-transfer efficiency is based on results with clean water rather than wastewater, and neglects energy losses in the aerator drive system. Hence, it gives only an approximate upper limit of the oxygen-transfer:energy ratio for the surface aerator used in this work.

# APPENDIX C

## RESULTS OF MAIN SET OF SURFACE-AERATION EXPERIMENTS

TABLE C-1. RESULTS OF MAIN SET OF SURFACE-AERATION EXPERIMENTS

| Type of Water | T (°C) | N (rpm) | $K_La \times 10^{-4}$ $[s^{-1}]$ | | | | | | |
|---|---|---|---|---|---|---|---|---|---|
| | | | $O_2$ | $CCl_2F_2$ | $CHCl_3$ | $CH_3CCl_3$ | $CCl_4$ | $CHCl=CCl_2$ | $CCl_2=CCl_2$ |
| Milli-Q | 20.2 | 376 | 58.3 | 40.5 | 32.0 | 36.5 | 37.5 | 36.2 | 37.2 |
| | 20.6 | 68 | 1.37 | 0.90 | 0.89 | 0.86 | 0.86 | 0.91 | 0.87 |
| | 20.1 | 245 | 21.0 | 14.6 | 12.3 | 13.5 | 13.8 | 13.7 | 13.8 |
| | 20.1 | 57 | 1.28 | 0.78 | 0.78 | 0.75 | 0.75 | 0.80 | 0.77 |
| | 20.1 | 359 | 57.5 | 39.9 | 30.7 | 35.8 | 37.0 | 35.3 | 36.8 |
| | 20.1 | 273 | 33.0 | 22.3 | 17.7 | 20.3 | 21.0 | 20.0 | 20.2 |
| | 20.0 | 131 | 2.92 | 1.84 | 1.73 | 1.73 | 1.75 | 1.78 | 1.69 |
| | 20.0 | 172 | 6.18 | 3.45 | 3.15 | 3.25 | 3.28 | 3.36 | 3.22 |
| | 20.0 | 310 | 42.3 | 28.5 | 23.0 | 25.8 | 26.5 | 25.8 | 25.3 |
| | 19.9 | 254 | 24.7 | 16.8 | 13.8 | 15.1 | 15.5 | 15.2 | 15.1 |
| | 20.1 | 198 | 8.83 | 5.83 | 5.17 | 5.43 | 5.53 | 5.58 | 5.40 |
| | 19.9 | 324 | 50.8 | 35.2 | 27.3 | 31.5 | 31.7 | 31.3 | 31.3 |
| | 19.8 | 145 | 4.18 | 2.48 | 2.30 | 2.33 | 2.34 | 2.43 | 2.32 |
| | 19.8 | 283 | 35.0 | 23.8 | 19.0 | 21.7 | 22.2 | 21.7 | 21.8 |
| | 19.8 | 343 | 51.0 | 35.3 | 28.7 | 32.0 | 32.3 | 31.8 | 32.2 |
| | 19.8 | 373 | 65.5 | 44.5 | 34.0 | 39.3 | 40.7 | 39.0 | 39.0 |
| PASE | 20.0 | 163 | 4.25 | 2.41 | 2.65 | 2.62 | 2.62 | 2.70 | 2.68 |
| | 20.1 | 173 | 4.73 | 3.10 | 2.82 | 2.86 | 2.86 | 2.93 | 2.86 |
| | 19.8 | 281 | 30.2 | 22.5 | 16.7 | 20.0 | 20.7 | 19.8 | 20.0 |
| | - | 296 | 29.8 | 21.0 | 16.2 | 17.7 | 18.0 | 17.7 | 17.8 |

# APPENDIX D

## RESULTS OF BUBBLE-COLUMN EXPERIMENTS

TABLE D-1. RESULTS OF BUBBLE-COLUMN EXPERIMENTS VARYING GAS FLOW AND LIQUID VOLUME

| $Q_G/V_L$ [$\text{min}^{-1}$] | $K_{L,O_2}a$ [$\text{min}^{-1}$] | $\Psi_{CCl_2F_2}$ | $H_c$ | | | | |
|---|---|---|---|---|---|---|---|
| | | | $CHCl_3$ | $CH_3CCl_3$ | $CCl_4$ | $CHCl{=}CCl_2$ | $CCl_2{=}CCl_2$ |
| 0.0091 | 0.101 | 0.498 | 0.242 | 0.632 | 1.022 | 0.423 | 0.645 |
| 0.0088 | 0.0998 | 0.522 | 0.224 | 0.600 | 0.985 | 0.399 | 0.590 |
| 0.0116 | 0.113 | 0.553 | 0.243 | 0.597 | 1.018 | 0.424 | 0.658 |
| 0.0115 | 0.118 | 0.512 | 0.223 | 0.607 | 0.987 | 0.387 | 0.620 |
| 0.0485 | 0.318 | 0.567 | 0.199 | 0.608 | 0.994 | 0.400 | 0.604 |
| 0.0495 | 0.336 | 0.538 | 0.188 | 0.605 | 0.959 | 0.390 | 0.620 |
| 0.196 | 0.651 | 0.627 | 0.150 | 0.543 | 0.894 | 0.331 | 0.534 |
| 0.197 | 0.694 | 0.604 | 0.159 | 0.560 | 0.956 | 0.350 | 0.571 |
| Mean | | 0.553 | 0.203 | 0.594 | 0.977 | 0.388 | 0.605 |
| ± std. dev. | | ± 0.045 | ± 0.036 | ± 0.029 | ± 0.041 | ± 0.033 | ± 0.040 |

Note: All data standardized to 20°C as described in Section 7.

TABLE D-2. RESULTS OF BUBBLE-COLUMN EXPERIMENTS WITH DIFFERING AMOUNTS OF ADDED METHANOL

| Methanol Conc. Mol/ℓ | T (°C) | $K_{L,O_2}a$ [$\text{min}^{-1}$] | $\Psi_{CCl_2F_2}$ | $H_c$ | | | | |
|---|---|---|---|---|---|---|---|---|
| | | | | $CHCl_3$ | $CH_3CCl_3$ | $CCl_4$ | $CHCl{=}CCl_2$ | $CCl_2{=}CCl_2$ |
| 0 | 19.5 | 0.128 | 0.497 | 0.264 | 0.666 | 1.048 | 0.444 | 0.667 |
| 0 | 19.6 | 0.120 | 0.492 | 0.235 | 0.641 | 1.027 | 0.420 | 0.644 |
| $1.8\times10^{-5}$ | 20.9 | 0.133 | 0.489 | 0.249 | 0.650 | 1.045 | 0.441 | 0.635 |
| $1.8\times10^{-5}$ | 18.7 | 0.129 | 0.496 | 0.239 | 0.651 | 1.046 | 0.417 | 0.640 |
| $1.8\times10^{-4}$ | 20.2 | 0.134 | 0.504 | 0.230 | 0.631 | 1.022 | 0.407 | 0.632 |
| $1.8\times10^{-4}$ | 19.5 | 0.133 | 0.510 | 0.249 | 0.660 | 1.059 | 0.432 | 0.648 |
| Mean | | 0.130 | 0.498 | 0.245 | 0.650 | 1.042 | 0.427 | 0.645 |
| ± std. dev. | | ± 0.005 | ± 0.008 | ± 0.012 | ± 0.013 | ± 0.014 | ± 0.015 | ± 0.013 |

# APPENDIX E

## ACTIVATED-SLUDGE EXAMPLES

### GENERAL APPROACH

Municipal wastewater characteristics:

| | |
|---|---|
| Total suspended solids | 200 [mg/l] |
| volatile suspended solids = $X_L°$ | 65% |
| biodegradable faction of $X_L°$ | 55% |
| $BOD_5$ (soluble + suspended) | 190 [mg/l] |
| $NH_3$-N | 19 [mg/l] |
| empirical formula for waste | $C_{10}H_{19}O_3N$ |
| oxygen demand | 0.139 [mol $O_2$/electron equiv.] |

Kinetic parameters:

$k = 22\ [d^{-1}]$

$b = 0.1\ [d^{-1}]$

$K_s = 400\ [\mathrm{mg\ BOD_L/l}]$

$Y = 0.45$

$K_1 = (0.3\ d^{-1})$

Electron donor reaction:

$$1/50\ C_{10}H_{19}O_3N + 9/25\ H_2O = 9/50\ CO_2 + 1/50\ NH_4^+ + 1/50\ HCO_3 + H^+ + e^- \qquad (E\text{-}1)$$

Design parameters:

| | |
|---|---|
| solids retention time $\Theta_c$ | 6 [d] |
| hydraulic retention time $\Theta$ | 0.17 [d] |
| suspended solids removal by primary treatment | 60% |
| waste flow | 0.44 [$m^3/s$] |

Solution:

- $BOD_L$ raw waste $= \left(\frac{BOD_5}{1-e^{-5K_1}}\right) = \frac{190[\text{mg } BOD_5/l]}{1-e^{-1.5}} = 244 \ [\text{mg } BOD_L/l]$ (E-2)

- $BOD_L$ of suspended solids:

$$1/50 \ C_{10}H_{19}O_3N = 0.02 \times 201 \ [g] = 4 \ [g/e^-]$$

$$MW = 201 \ g \tag{E-3}$$

$$1 \text{ electron equivalent} = 8 \ g \ BOD_L$$

$$\frac{8}{4} \ \frac{g \ BOD_L/e^-}{g/e^-} = 2 \ \frac{g \ BOD_L}{g} \tag{E-4}$$

- Biodegradable portion of suspended solids:

$$200 \ [mg/l] \times 0.65 \times 0.55 \times 2 \ [g \ BOD_L] = 142 \ [mg \ BOD_L/l] \tag{E-5}$$

- Soluble component of raw waste:

$$= BOD_L \text{ raw waste} - BOD_L \text{ suspended solids}$$

$$= 244 \ [mg \ BOD_L/l] - 142 \ [mg \ BOD_L/l]$$

$$= 102 \ [mg \ BOD_L/l] \tag{E-6}$$

- $BOD_L$ primary effluent $= s^o$

$$= \text{soluble portion} + \text{suspended portion}$$

$$= 102 \ [mg \ BOD_L/l] + 0.4 \times 142 \ [mg \ BOD_L/l]$$

$$= 159 \ [mg \ BOD_L/l] \tag{E-7}$$

- $BOD_L$ plant effluent $= s^e$

$$= \frac{K_s \ (1 + b\Theta_c)}{\Theta_c \ (Y \ k - b) - 1} = \frac{400 \ [mg \ BOD_L/l] \ (1 + 0.1 \ [d^{-1}] \times 6 \ [d])}{(0.45 \times 22 \ [d^{-1}] - 0.1 \ [d^{-1}] \ 6 \ [d] - 1}$$

$$= 10.9 \ [mg \ BOD_L/l] \tag{E-8}$$

- Oxygen demand:

$$= Q\ (s^{o} - s^{e})\ \frac{g\ O_2}{g\ BOD_L}$$

$$= 440\ [l/s] \times 86{,}400\ [s/d](159 - 10.9)\ [mg\ BOD_L/l]\ \frac{0.139\ \frac{mol}{e^-}\ 32\ \frac{g\ O_2}{mol}}{8\ [g\ BOD_L/e^-]}$$

$$= 3{,}130\ [kg\ O_2/d] \qquad \text{(E-9)}$$

- Basin volume:

$$V = \Theta\ Q = 0.17\ [d] \times 0.44\ [m^3/s] \times 86{,}400\ [s/d]$$

$$= 6{,}460\ [m^3] \qquad \text{(E-10)}$$

Figure E-1 illustrates the specifications of the surface aerator used in the example.

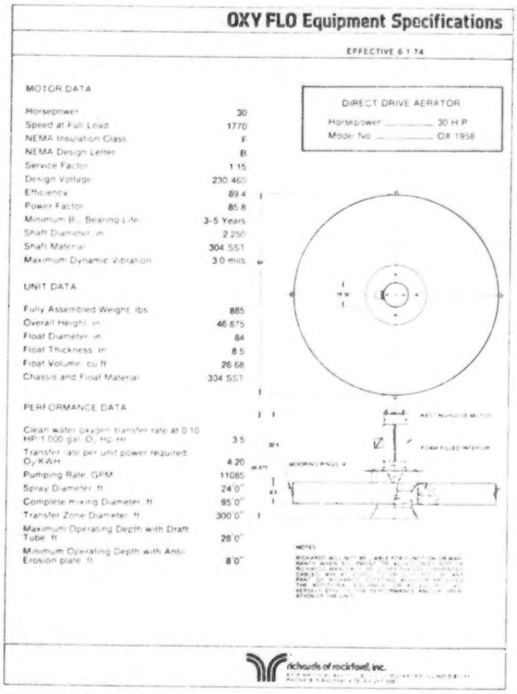

**OXY FLO Equipment Specifications**

EFFECTIVE 6 1 74

MOTOR DATA

| | |
|---|---|
| Horsepower | 30 |
| Speed at Full Load | 1770 |
| NEMA Insulation Class | F |
| NEMA Design Letter | B |
| Service Factor | 1 15 |
| Design Voltage | 230 460 |
| Efficiency | 89 4 |
| Power Factor | 85 8 |
| Minimum B... Bearing Life | 3-5 Years |
| Shaft Diameter in | 2 250 |
| Shaft Material | 304 SST |
| Maximum Dynamic Vibration | 3 0 mils |

UNIT DATA

| | |
|---|---|
| Fully Assembled Weight lbs | 885 |
| Overall Height in | 46 875 |
| Float Diameter in | 84 |
| Float Thickness in | 8 5 |
| Float Volume cu ft | 26 68 |
| Chassis and Float Material | 304 SST |

PERFORMANCE DATA

| | |
|---|---|
| Clean water oxygen transfer rate at 0 10 HP/1,000 gal O₂ Hp Hr | 3 5 |
| Transfer rate per unit power required O₂/KWH | 4 20 |
| Pumping Rate GPM | 11085 |
| Spray Diameter ft | 24'0" |
| Complete mixing Diameter ft | 95'0" |
| Transfer Zone Diameter ft | 300'0" |
| Maximum Operating Depth with Draft Tube ft | 28'0" |
| Minimum Operating Depth with Anti-Erosion plate ft | 8'0" |

DIRECT DRIVE AERATOR

Horsepower ________ 30 H P

Model No ________ OX 1958

NOTES

richards of rockford, inc.

Reproduced from best available copy.

Figure E-1. Specifications of surface aerator used in activated-sludge example.

## BUBBLE-AERATION CALCULATIONS

### Mass Balance for a Well-Mixed System

In + accumulation = out

Accumulation rate = 0 at steady state

$$Q_L C_{LI} + Q_G C_{GI} = Q_L C_{LE} + Q_G C_{GE} \tag{E-11}$$

$C_{GI} = 0$ for organic contaminants

$$(C_{LI} - C_{LE})Q_L = Q_G C_{GE} \tag{E-12}$$

Substitute from Eq. 110, evaluating $C_G = C_{GE}$ at $Z = 0$

$$C_{GE} = C_L H_c[1 - \exp(-\Phi Z_s)] \tag{110}$$

After simplifying we obtain

$$\frac{C_{LI}}{C_{LE}} = 1 + \frac{H_c\ Q_G}{Q_L}\left[1 - \exp(-\Phi Z_s)\right] \tag{E-13}$$

where

$$\Phi Z_s = \frac{K_L a \cdot V_L}{H_c \cdot Q_G} \tag{113}$$

### Conditions for the Standard Case

Oxygen demand = 3130 kg/day $O_2$

(see the example for surface aeration, Eq. E-9).

Total submergence (77, p. 505)

$$Z_s = 4 \text{ m}$$

Basin volume

$$V_L = 6460\ [\text{m}^3]$$

(see the example for surface aeration, Eq. E-10).

Oxygen solubility at 20°C

$C^s_{O_2} = 9.17$ g/m$^3$ in distilled water

Correction factor for wastewater = 0.95 (77, p. 274)

$$C_L^* \approx 9.17 \times 0.95 = 8.7 \text{ g/m}^3 \text{ O}_2$$

Henry coefficient for oxygen

$$H_c = \frac{H}{RT} = \left(\frac{0.209}{8.7/32}\right) \times \frac{1}{82.05 \times 10^{-6} \times 293} = 32 \qquad \text{(E-14)}$$

Dissolved oxygen concentration

$$C_{L,O_2} = 1 \text{ g/m}^3$$

## Oxygen Transfer

The expression for the gas-phase concentration of oxygen is given by Eq. 88

$$C_G = C_L H_c + (C_{GI} - C_L H_c) \cdot \exp[-\Phi(Z_s - Z)] \qquad (88)$$

To estimate the gas-phase concentration of oxygen in the exit air, we evaluate Eq. 88 at $Z = 0$

$$C_{GE} = C_L H_c + (C_{GI} - C_L H_c) \exp(-\Phi Z_s) \qquad \text{(E-15)}$$

where

$$\Phi Z_s = (K_L a \cdot V_L / H_c \cdot Q_G) \qquad (113)$$

For a well-mixed basin $C_L$ is uniform throughout and everywhere equal to $C_{LE}$. To find $K_L a$ given $C_{GE}$, $V_L$, $H_c$, $Q_G$, and $C_L$, simply solve Eq. E-4 for $\Phi Z_s$, substitute for $V_L$, $H_c$, and $Q_G$ in the expression (Eq. 113) for $\Phi Z_s$, and solve for $K_{L,O_2}a$.

## Fine-Bubble Aeration

Assume that the oxygen-transfer efficiency is 15% in fine-bubble aeration with a submergence $Z_s = 4$ m (77, p. 497)

$$\eta = \text{oxygen-transfer efficiency} = 0.15$$

Calculate the gas flow rate $Q_G$

$$Q_G = 3130\left[\frac{\text{kg O}_2}{\text{day}}\right] \cdot \frac{1000}{32}\left[\frac{\text{mol}}{\text{kg}}\right] \cdot \frac{1}{0.209}\left[\frac{\text{mol air}}{\text{mol O}_2}\right] \times \frac{1}{\eta} \times \frac{RT}{P_{av}} \qquad \text{(E-16)}$$

where R = gas constant = $82.06 \times 10^{-6}$ $(\mathrm{atm \cdot m^3 \cdot mol^{-1} \cdot K^{-1}})$

T = 293 K

$P_{av}$ = 1.2 atm, at mid-depth

$$Q_G = 62{,}500\ [\mathrm{m^3/day}] = 0.72\ [\mathrm{m^3/s}]$$

$$Q_G/V_L = 0.72/6460 = 1.12 \times 10^{-4}\ [\mathrm{s^{-1}}]$$

$$Q_G/Q_L = 0.72/0.44 = 1.64\ [\mathrm{dimensionless}]$$

Evaluate $C_{GI}$ and $C_{GE}$ at mid-depth condition

$$C_{GI} = \frac{P_{O_2} M_{O_2}}{RT} = \frac{1.2 \times 0.209 \times 32}{82.06 \times 10^{-6} \times 293} = 334\ [\mathrm{g/m^3}] \qquad \text{(E-17)}$$

$$C_{GE} = (1 - \eta)C_{GI} = 0.85 \times 334 = 284\ [\mathrm{g/m^3}] \qquad \text{(E-18)}$$

Substitute into Eq. E-15 to evaluate $\Phi Z_s$

$$\Phi Z_s = -\ell n\left(\frac{C_{GE} - C_{LE}H_c}{C_{GI} - C_{LE}H_c}\right) = -\ell n\left(\frac{284 - 32}{334 - 32}\right) = 0.18$$

and substitute this value into Eq. 113 to evaluate $K_{L,O_2}a$

$$K_{L,O_2}a = (\Phi Z_s)\left(\frac{Q_G}{V_L}\right)H_c = 0.18 \times 1.12 \times 10^{-4} \times 32 = 6.45 \times 10^{-4}\ [\mathrm{s^{-1}}]$$

For the organic compounds other than $CC_2F_2$

$$K_La \simeq 0.6 \times K_{L,O_2}a = 0.6 \times 6.45 \times 10^{-4} = 3.9 \times 10^{-4}\ [\mathrm{s^{-1}}]$$

Check the degree of gas saturation using Eq. 113

$$\Phi Z_s = \frac{K_La \cdot V_L}{H_c \cdot Q_G} = \frac{3.9 \times 10^{-4} \times 6460}{H_c \times 0.72} = \frac{3.5}{H_c}$$

Referring to the criterion for saturation expressed in Eq. 113, it is clear that five of the six compounds (all but $CCl_2F_2$) will be substantially saturated in the gas phase under the conditions of this example. The degree of saturation can be calculated by evaluating Eq. 110 at Z = 0

$$\frac{C_{GE}}{C_G^*} = [1 - \exp(-\Phi Z_s)] \qquad \text{(E-19)}$$

The fractional removal is calculated using Eq. E-19. Using $CCl_4$ as an example, we find by substituting into Eq. E-19

$$\frac{C_{GE}}{C_G^*} = [1 - \exp(-3.5/1.01)] = 0.97$$

that the exiting gas bubbles are 97% saturated with $CCl_4$.

To calculate the fractional removal of $CCl_4$ by volatilization under these conditions, we evaluate Eq. E-13 by substituting for $(H_c Q_G/Q_L)$ and $(\Phi Z_s)$.

$$\frac{C_{LI}}{C_{LE}} = 1 + \frac{H_c\ Q_G}{Q_L}[1 - \exp(-\Phi Z_s)] \qquad \text{(E-20)}$$

For $CCl_4$ in the fine-bubble aeration case:

$$H_c = 1.01$$

$$Q_G/Q_L = 1.64$$

$$\Phi Z_s = 3.50/H_c = 3.47$$

$$C_{LI}/C_{LE} = 1 + 1.01 \times 1.64[1 - \exp(-3.47)] = 2.60$$

$$\text{Fractional removal} = \eta_{CCl_4} = [1 - (C_{LE}/C_{LI})] = 0.616 \qquad \text{(E-21)}$$

In this example, $CCl_4$ is expected to be removed by volatilization to the extent of 61.6%. The results of similar calculations of fractional saturation and fractional removal for the other five compounds ($CCl_2F_2$, $CHCl_3$, $CH_3CCl_3$, $CHCl{=}CCl_2$, and $CCl_2{=}CCl_2$) under standard conditions of fine-bubble aeration are summarized in Table E-1.

Medium-Bubble Aeration

The oxygen transfer efficiency is 10%, intermediate between the fine-bubble and the coarse-bubble cases. Consequently, the gas flow rate is greater, the fractional saturation of the gas with organics is lower, and the fractional removal of organics is higher, compared to the fine-bubble aeration case (see Table E-1).

Coarse-Bubble Aeration

The oxygen-transfer efficiency is 6%. Consequently, the gas flow rate is the greatest of the three cases, the fractional saturation of the organics is least, and the fractional removal is greatest of the three cases.

TABLE E-1. RESULTS OF OXYGEN-TRANSFER CALCULATIONS FOR BUBBLE-AERATION CASES

| | Type of Aeration | | |
|---|---|---|---|
| | Fine-Bubble | Medium-Bubble | Coarse-Bubble |
| Oxygen-Transfer Efficiency [%] | 15 | 10 | 6.0 |
| Gas Flow Rate* [$m^3/s$] | 0.72 | 1.09 | 1.81 |
| $Q_G/V_L$ [$s^{-1}$] | $1.12 \times 10^{-4}$ | $1.68 \times 10^{-4}$ | $2.80 \times 10^{-4}$ |
| $Q_G/Q_L$ | 1.64 | 2.73 | 4.11 |
| $C_{GE}$ [$g/m^3$] | 284 | 300 | 314 |
| $K_{L,O_2}a$ [$s^{-1}$] | $6.50 \times 10^{-4}$ | $6.30 \times 10^{-4}$ | $6.14 \times 10^{-4}$ |
| Fractional Gas Saturation† | | | |
| $CCl_2F_2$ | 0.060 | 0.039 | 0.023 |
| $CCl_4$ | 0.975 | 0.898 | 0.750 |
| $CCl_2{=}CCl_2$ | 0.995 | 0.966 | 0.860 |
| $CH_3CCl_3$ | 0.995 | 0.967 | 0.864 |
| $CHCl{=}CCl_2$ | 0.999 | 0.990 | 0.930 |
| $CHCl_3$ | 1.000 | 0.998 | 0.984 |
| Fractional Removal† | | | |
| $CCl_2F_2$ | 0.86 | 0.87 | 0.85 |
| $CCl_4$ | 0.61 | 0.71 | 0.75 |
| $CCl_2{=}CCl_2$ | 0.53 | 0.65 | 0.71 |
| $CH_3CCl_3$ | 0.53 | 0.64 | 0.71 |
| $CHCl{=}CCl_2$ | 0.46 | 0.58 | 0.66 |
| $CHCl_3$ | 0.35 | 0.47 | 0.57 |

*Assuming in all three cases that the required oxygen transfer is 3130 kg/day, equivalent to 82 g $O_2$ transferred per $m^3$ wastewater treated.

†Calculated using the observed values of the Henry coefficient $H_c$ given for PASE in Table 25, and using the Ψ-values recommended in Table 31.